



THE UNIVERSITY *of* EDINBURGH

This thesis has been submitted in fulfilment of the requirements for a postgraduate degree (e.g. PhD, MPhil, DClinPsychol) at the University of Edinburgh. Please note the following terms and conditions of use:

This work is protected by copyright and other intellectual property rights, which are retained by the thesis author, unless otherwise stated.

A copy can be downloaded for personal non-commercial research or study, without prior permission or charge.

This thesis cannot be reproduced or quoted extensively from without first obtaining permission in writing from the author.

The content must not be changed in any way or sold commercially in any format or medium without the formal permission of the author.

When referring to this work, full bibliographic details including the author, title, awarding institution and date of the thesis must be given.



**The importance of axon-glia
interactions for the normal postnatal
development of the mouse peripheral
nervous system**

Sarah Louise Roche

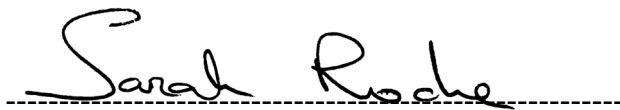
A thesis submitted for the degree of
Doctor of Philosophy

The University of Edinburgh

2014

Declaration

I declare that this thesis was composed entirely by myself and the work on which it is based is my own, unless clearly stated in the text. This work has not been submitted for any other degree or professional qualification.

A handwritten signature in black ink that reads "Sarah Roche". The signature is written in a cursive style and is positioned above a horizontal dashed line.

Sarah Louise Roche

Acknowledgements

I would first like to express my sincere gratitude to my supervisor Prof. Tom Gillingwater. His support, encouragement and guidance over the last four years never waned and I cannot thank him enough for being such an amazing supervisor and role model.

I would like to express my thanks to Derek Thomson for being a reliable source of help in the lab in my many times of need and more importantly for introducing me to the world of whisky.

Many thanks to Prof. Simon Parson for all of his interesting questions during lab meetings and Dr. Thomas Wishart for his invaluable help and support over the last four years.

Many thanks to all in the anatomy department, who made my teaching experience over the last four years an enjoyable and rewarding one.

I would like to thank all those who taught me the lab techniques of mouse dissection, immunohistochemistry and confocal microscopy (Dr. Laura Comley), PCR (Dr. Anne Desmazieres), nerve fibre teasing (Dr. Barbara Zonta), surgery (Derek Thomson), electron microscopy (Ann Wright & Steve Mitchell), Western blotting (Dr. Chantal Mutsaers), proteomic assays (Dr. Thomas Wishart) and introduced me to electrophysiology (Kosala Dissanayake & Prof. Richard Ribchester).

I would like to thank those I've worked with in Prof. Gillingwater's group for being amazing colleagues and extend that thanks to those who supported me throughout my PhD, especially Lukas Fischer, Chantal Mutsaers and Yvonne Clarkson for being such good friends. Many thanks also to my flatmate Sharon Campbell for all the delicious baked goods in times of stress.

I would like to express a very special thanks to my family for supporting me during my PhD. I couldn't have done it without the Irish imports of Barry's tea and chocolate kimberleys!

Last but not least I would like to say a very big thanks to Tadhg Landers for being by my side supporting me throughout the highs and lows of the last four years and making me smile when science failed me.

Go raibh míle maith agaibh go léir.

Abstract

The mouse nervous system undergoes a vast remodelling of synaptic connections postnatally, resulting in a reduced number of innervating axons to target cells within the first few weeks of life. This extensive loss of connections is known as synapse elimination and it plays a critical role in sculpting and refining neural connectivity throughout the nervous system, resulting in a finely tuned and well-synchronised network of innervation. This process has been well characterised at the mouse neuromuscular junction (NMJ), where synapse elimination takes place postnatally in all skeletal muscles. It has been well studied for the reasons that it is easily accessible for live imaging and post-mortem experimental analysis. Studies utilising this synapse to uncover regulators of synapse elimination have mainly focused on the importance of glial cell lysosomal activity, nerve conduction and target-derived growth factor supply. It is clear that non-axonal cell types play key roles in the success of developmental axon retraction at the NMJ, however the role of glial cells in the regulation of this process has not been fully explored, as lysosomal activity is thought of as a consequence of axon pruning rather than a molecular driver.

Previous studies have shown that signals emanating from myelinating glial cells can modulate neurofilament composition and transport within the underlying axons. We know that these changes in neurofilament composition and transport are underway during developmental synapse elimination at the NMJ, so it seems logical to predict that myelinating glial cells may play a role in the regulation of axonal pruning. Myelinating glial cells are found along the entire length of lower motor neurons and

form physical interactions with the underlying axons at regions known as paranodes. At the paranode, Neurofascin155 (Nfasc155: expressed by the myelinating glial cell) interacts with a Caspr/contactin complex (expressed by the axon). This site has been proposed as a likely site for axon-glial signalling due to the close apposition of the cell membranes.

The main focus of this PhD project was to study the potential role of myelinating glial cells in the success of synapse elimination at the NMJ, using a mouse model of paranodal disruption (*Nfasc155^{-/-}*). Chapters 3 and 4 show the results of this work. This work has revealed a novel role for glia in the modulation of synapse elimination at the mouse neuromuscular junction, mediated by Nfasc155 in the myelinating Schwann cell. Synapse elimination was profoundly delayed in *Nfasc155^{-/-}* mice and was found to be associated with a non-canonical role for Nfasc155, as synapse elimination occurred normally in mice lacking the axonal paranodal protein Caspr. Loss of Nfasc155 was sufficient to disrupt axonal proteins contributing to cytoskeletal organisation and trafficking pathways in peripheral nerve of *Nfasc155^{-/-}* mice and lower levels of neurofilament light (NF-L) protein in maturing motor axon terminals. Synapse elimination was delayed in mice lacking NF-L, suggesting that Nfasc155 influences neuronal remodelling, at least in part, by modifying cytoskeletal dynamics in motor neurons. This work provides the first clear evidence for myelinating Schwann cells acting as drivers of synapse elimination, with Nfasc155 playing a critical role in glial cell-mediated postnatal sculpting of neuronal connectivity in the peripheral nervous system.

A small section of the results within this thesis are devoted to the study of axon-glia interactions in a mouse model of childhood motor neuron disease, otherwise known as spinal muscular atrophy (SMA). In SMA, there are reduced levels of the ubiquitously expressed survival motor neuron (SMN) protein. The NMJ is a particularly vulnerable target in SMA, manifesting as a breakdown of neuromuscular connectivity and progressive motor impairment. Recent studies have begun to shed light on the role of non-neuronal cell types in the onset and progression of the disease, presenting SMA as a multi-system disease rather than a purely neuronal disorder. Recent evidence has highlighted that myelinating glial cells are significantly affected in a mouse model of SMA, manifesting as an impaired ability to produce key myelin proteins, resulting in deficient myelination. The final results chapter of this thesis (Chapter 5) is focussed on further exploring the effects that loss of SMN has in Schwann cells including their interactions with underlying axons. This work reveals a disruption to axon-glia interaction, shown by a delay in the development of paranodes, supporting the idea that non-neuronal cell types are also affected in SMA.

The results within this thesis reveal a novel role for a glial cell protein, Nfasc155, in the modulation of synapse elimination at the NMJ. Mechanistic insight in to Nfasc155's role in this process is also uncovered and likely involves axonal cytoskeletal transport systems and the filamentous protein NF-L, which have not previously been implicated in the process of synapse elimination. This work highlights an important role for axon-glia interactions during normal postnatal development of the mouse NMJ. This work also highlights a role for axon-glia

interactions in disease states of the NMJ. Using a mouse model of SMA, axon-glial interaction was assessed with the finding of a delay in paranodal maturation due to loss of SMN.

Table of Contents

Declaration	I
Acknowledgements	II
Abstract	IV
Table of Contents	VIII
Abbreviations	XIV

Chapter 1: General Introduction

1.1 The Nervous System	1
1.1.1 A brief history	1
1.1.2 Cell types in the nervous system	4
1.2 Myelin	6
1.2.1 The evolution of myelin	6
1.2.2 Myelination	7
1.2.3 Formation of molecular domains along myelinated fibres	14
1.3 Axon-glia Interactions	17
1.3.1 Formation of the paranode	17
1.3.2 Consequences of disrupted paranodes	21
1.3.3 Axon-glia interaction during the initial stages of nervous system development	21
1.3.4 Axon-glia interaction during injury/nerve regeneration	24
1.4 Axon-glia interaction between myelinating cells and axons during postnatal development/maturation of the nervous system	25
1.4.1 Axon-glia interactions for axonal cytoskeletal integrity	26
1.4.2 Axon-glia interactions for axonal transport	29
1.4.3 Axon-glia interactions for developmental remodelling of neuronal circuitry	32

1.5 The Neuromuscular Junction	33
1.5.1 Development of the NMJ	33
1.5.2 Diseases affecting the neuromuscular system	36
1.5.3 Synapse elimination at the NMJ	37
1.5.4 Regulation of synapse elimination at the NMJ	39
1.5.5 Glial cells and synapse elimination	42
1.6 Aims	45

Chapter 2: Materials and Methods

2.1 Mouse colonies and maintenance	46
2.2 Generation of <i>Nfasc155</i> ^{-/-} mice	47
2.3 Genotyping	50
2.4 Immunofluorescence on whole mount/sectioned muscle	59
2.5 Immunofluorescence on teased fibres/sectioned nerve and spinal cord ventral roots	60
2.6 Quantitative Western blots	61
2.7 Microscopy	64
2.8 Quantification of immunofluorescently -labelled muscles, nerves and ventral roots	65
2.9 Quantification of molecular domains	66
2.10 Quantification of spinal cord motor neurons	66
2.11 Electrophysiology	67
2.12 Electron microscopy	69
2.13 Proteomic analysis	70
2.14 Statistical analysis	73

Chapter 3: Nfasc155-mediated glial cell modulation of developmental synapse elimination in the peripheral nervous system

3.1 Introduction	75
3.1.1 Contribution of non-neuronal cell types to synapse elimination	75
3.1.2 The possible contribution of myelinating glial cells to the regulation of synapse elimination	77
3.1.3 <i>Neurofascin</i> structure and function	79
3.1.4 <i>Nfasc155</i> ^{-/-} mice	80
3.2 Results	82
3.2.1 <i>Nfasc155</i> ^{-/-} mice lack Nfasc155 and have disrupted paranodes	82
3.2.2 <i>Nfasc155</i> ^{-/-} mice display a severe tremor	83
3.2.3 <i>Nfasc155</i> ^{-/-} mice display normal ultrastructure of peripheral nerve	84
3.2.4 Normal NMJ formation in <i>Nfasc155</i> ^{-/-} mice	88
3.2.5 Loss of Nfasc155 is sufficient to delay synapse elimination at the NMJ	88
3.2.6 Synapse elimination is delayed in muscles of different developmental subtype, fibre type and body region	94
3.2.7 Neuromuscular transmission is normal in <i>Nfasc155</i> ^{-/-} mice	99
3.2.8 Pre- and post-synaptic maturation of the NMJ is delayed in <i>Nfasc155</i> ^{-/-} mice	102
3.2.9 Delayed synapse elimination in <i>Nfasc155</i> ^{-/-} mice is not due to the presence of <i>Cre</i> or <i>LoxP</i> sites	105
3.2.10 Terminal Schwann cells are unlikely to be contributing to the delay in synapse elimination in <i>Nfasc155</i> ^{-/-} mice	105
3.2.11 Outwith synapse elimination, the PNS develops normally in <i>Nfasc155</i> ^{-/-} mice	109
3.2.12 Synapse elimination occurs normally in mice lacking an axonal paranodal protein (Caspr)	115
3.2.13 Delayed synapse elimination in <i>Nfasc155</i> ^{-/-} mice is not due to a reduction in nerve conduction velocity	120

3.3 Discussion	123
3.3.1 Overview of results	123
3.3.2 Discovery of a novel role for Nfasc155	124
3.3.3 The role of glia in developmental remodelling of the nervous system	125
3.3.4 <i>Nfasc155</i> ^{-/-} model as useful tool to study the intricacies of synapse elimination regulation	127

Chapter 4: Mechanistic insight in to Nfasc155-dependent modulation of synapse elimination

4.1 Introduction	129
4.1.1 Nfasc155 does not act as a secreted molecule	129
4.1.2 Insights from previously published literature	130
4.1.3 Proteomic analysis	134
4.2 Results	136
4.2.1 Nfasc155 does not modulate synapse elimination through trophic mechanisms involving GDNF in skeletal muscle	136
4.2.2 iTRAQ proteomic analysis on peripheral nerve reveals a significantly more disrupted proteome in <i>Nfasc155</i> ^{-/-} compared to <i>Caspr</i> ^{-/-} mice	139
4.2.3 Pathway analysis reveals alterations in cytoskeletal organisation and assembly in <i>Nfasc155</i> ^{-/-} mice	144
4.2.4 Kinesin5A levels are significantly decreased in sciatic nerve of <i>Nfasc155</i> ^{-/-} mice	150
4.2.5 <i>Nfasc155</i> ^{-/-} mice exhibit a selective reduction in levels of NF-L in motor nerve terminals	152
4.2.6 Tubulin expression is unaltered in pre-terminal axons of <i>Nfasc155</i> ^{-/-} mice	156
4.2.7 Synapse elimination is significantly delayed in <i>NF-L</i> ^{-/-} mice, supporting a role for NF-L during this process	158
4.2.8 NF-L is abnormally distributed throughout the motor neuron in <i>Nfasc155</i> ^{-/-} mice	161

4.2.9 NF-L levels are higher during synapse elimination whereas NF-M and NF-H levels peak post-synapse elimination in C57BL6 mice	164
4.2.10 NF-L-dependent modulation of synapse elimination most likely takes place outside of the pre-terminal axon	167
4.2.11 NF-L is highly expressed in axon terminals and axon terminal protrusions extending beyond the endplate	170
4.2.12 Lysosomal activity is significantly altered in <i>Nfasc155</i> ^{-/-} mice	176
4.3 Discussion	179
4.3.1 Overview of results	179
4.3.2 Mechanistic insight in to paranodal formation	180
4.3.3 Cytoskeletal transport systems may regulate synapse elimination	180
4.3.4 NF-L is important for normal rates of synapse elimination	182
4.3.5 Glial control of synapse elimination	184

Chapter 5: Axon-glia interaction in a mouse model of spinal muscular atrophy

5.1 Introduction	186
5.1.1 SMA is a multi-system disorder	187
5.1.2 Schwann cell myelination is affected by loss of SMN	187
5.2 Results	190
5.2.1 Paranodal maturation is delayed in the sciatic nerve of pre-symptomatic SMA mice	190
5.2.2 Delayed paranodal maturation persists in the sciatic nerve of SMA mice in to late-symptomatic time points	196
5.2.3 Paranodes are unaffected in the intercostal nerve of late symptomatic SMA mice	199
5.2.4 Juxtaparanodes appear normal in the sciatic nerve of late-symptomatic SMA mice	202
5.3 Discussion	204
5.3.1 Overview of results	204

5.3.2 Disrupted axon-glia interactions in the sciatic nerve in a mouse model of spinal muscular atrophy	204
5.3.3 Normal axon-glia interactions in the intercostal nerve in a mouse model of spinal muscular atrophy	205
5.3.4 Disruption of axon-glia interaction in SMA mice could be due to lack of SMN in other cell types	207

Chapter 6: General Discussion

6.1 Overview of results	209
6.2 Insight into the regulation of synapse elimination – an important role for myelinating Schwann cells	213
6.3 A novel role for NF-L in axon plasticity/stability	215
6.4 SMN and paranodal maturation	217
6.5 Conclusion	218

Bibliography	219
---------------------	-----

Appendices	242
-------------------	-----

Appendix 1: Peer-reviewed publications	242
--	-----

Abbreviations

AAL	Abductor Auricularis Longus
ACh	Acetylcholine
ALS	Amyotrophic Lateral Sclerosis
BCA	Bicinchoninic Acid
BDNF	Brain-Derived Neurotrophic Factor
bFGF	Basic Fibroblast Growth Factor
BTX	Bungarotoxin
C1q	Complement
Caspr	Contactin-Associated Protein
CCD	Charged-Coupled device
Cdk5	Cyclin-dependent kinase 5
cGRP	Calcitonin Gene-Related Protein
CMT	Charcot Marie Tooth
CNP	2', 3'-Cyclic Nucleotide 3'-Phosphodiesterase
CNS	Central Nervous System
CNTF	Ciliary Neurotrophic Factor
CT	Computed Tomography
DAPI	4', 6-Diamidino-2-Phenylin-Dole
De-syn	Delayed Synapsing
DSHB	Developmental Studies Hybridoma Bank
DTT	Dithiothreitol
EPP	Endplate Potential

ERK	Extracellular Signal-Related Kinase
Fa-syn	Fast synapsing
FDB	Flexor Digitorum Brevis
FITC	Fluorescein Isothiocyanate
fMRI	Functional Magnetic Resonance Imaging
GDNF	Glial Cell Line-Derived Neurotrophic Factor
GFAP	Glial Fibrillary Acidic Protein
HNPP	Hereditary Neuropathy with Liability to Pressure Palsies
IGF	Insulin-like Growth Factor
IL	Interleukin
IPA	Ingenuity Pathway Analysis
iTRAQ	Isobaric Tag for Relative and Absolute Quantitation
LAL	Levator Auris Longus
LAMP	Lysosome-Associated Membrane Protein
LIF	Leukemia Inhibitory Factor
MAG	Myelin-Associated Glycoprotein
MBP	Myelin Basic Protein
mEPP	Miniature Endplate Potential
MEGF10	Multiple Epidermal Growth Factor
MERTK	Membrane Receptor Tyrosine Kinase
mgf	Mascot Generic File
MuSK	Muscle Specific Kinase
NF-H	Neurofilament-Heavy
NF-L	Neurofilament-Light

NF-M	Neurofilament-Medium
Nfasc	Neurofascin
NGF	Nerve Growth Factor
NMJ	Neuromuscular Junction
NT-3	Neurotrophin-3
P	Postnatal
P0	Myelin Protein Zero
P2	Myelin Protein 2
PCR	Polymerase Chain Reaction
PET	Positron Emission Tomography
PFA	Paraformaldehyde
PMP22	Peripheral Myelin Protein 22
PNS	Peripheral Nervous System
PVDF	Polyvinylidene Fluoride
RIPA	Radioimmunoprecipitation
SAPK	Stress-Activated Protein Kinase
SCM	Sternocleidomastoid
SMA	Spinal Muscular Atrophy
SMN	Survival Motor Neuron
SOD1	Superoxide Dismutase 1
TA	Tibialis Anterior
TEAB	Triethylamine-NH ₄ Bicarbonate
TRITC	Tetramethylrhodamine Isothiocyanate
TSC	Terminal Schwann Cell

TVA	Transversus Abdominis
UV	Ultraviolet

Chapter 1

General Introduction

1.1 The Nervous System

The nervous system is undoubtedly the most complicated system in the human body with billions of cells forming a network with even more inter-cellular connections and interactions. The complicated and intricate nature of this system baffled early researchers attempting to characterise and understand its structure and function, sparking many a debate between researchers throughout the history of neuroscience research. We have come a long way in our understanding of how the nervous system functions in health and disease, however there still remain many mysteries yet to be fully understood.

1.1.1 A brief history

The first descriptions of nerve cells have been attributed to Christian Gottfried Ehrenberg and Johann Evangelistan Purkinje between the years 1833-1837, who described nerve cells in the leech and mammalian cerebellum respectively (Ehrenberg, 1836; Purkinje, 1837). The first publication of a microscopic image of a nerve cell is credited to one of Purkinje's students, Valentin, who published a drawing of a nerve cell from cerebellar cortex in 1836, with its prominent nucleolus and cell body (Valentin, 1836). Two years later Robert Remak observed axis-

cylinders (Remak bands) and non-myelinated axons (Remak bundles) (Shepard, 1991; Fodstad, 2001). In the following decades, neuroscientists began to appreciate the diversity and specialisations within the nervous system, such as the specialised junctions found at the nerve-target interface, to be later known as the “synapse”. In 1862 Wilhelm Friedrich Kühne described the specialised synapse found between lower motor neurons and skeletal muscle in the frog, denoting the termination of motor nerves on muscle cells as the “endplate” (Kühne, 1862). The endplate has since been further defined as the post-synaptic element of the synapse ie. The accumulation of ACh receptors on the muscle fibre surface.

It was during the following century that the true complexity of the nervous system became recognised. The most influential neuroscientist of his time, Santiago Ramon y Cajal, dedicated his adult life to years of research that propelled the field of neuroscience into unknown territory. Cajal used Golgi’s established silver-chromate staining procedure to visualise what he referred to as “that masterwork of life” in small mammals (Cajal, 1923). Cajal replicated meticulously with drawings what he observed down the microscope, providing incredible detail on the interactions between cells in the cerebellar cortex and optic lobe. He established the “Neuron Doctrine”, which was based on the idea that neurons were individual units, representing a theory of contiguity but not continuity in the nervous system. This theory was strongly opposed by other neuroscientists such as Von Gerlach, Golgi and Kolliker, who believed in “the reticular theory”, whereby the nervous system was not composed of individual units but rather consisted of a meshwork of reticular protrusions that extended into other cellular protrusions instead of reaching a

terminus (Gerlach, 1871). Cajal is also credited with the first descriptions of impulse transmission along nerves, using arrows to indicate the direction of transmission in his drawings (Cajal, 1923). Cajal's immense contribution to neuroscience was recognised in 1906 when he was awarded the Nobel prize alongside Golgi for Physiology and Medicine.

The concept of the synapse emerged in the mid 19th century. It was Kühne in the 1870's who described how the nerve endings terminate on a muscle fibre, denoting the entire structure as the "neuromuscular junction" (Kühne, 1871). In 1897 Sir Charles Scott Sherrington wrote a chapter on the nervous system for the 'Textbook of Physiology', and introduced readers to the term "synapse", which literally means "joining together" (Foster, 1897). With the development of electron microscopy techniques in the mid 1950's came the conclusive proof of the Neuron Doctrine and the synapse. In 1954 and 1955 Sanford Louis Palay, George Emil Palade, Eduardo De Robertis and Henry Stanley Bennett provided ultrastructural evidence of neurons as single units of the nervous system and the presence of synapses, with their characteristic synaptic vesicle clustering at the synapse interface and synaptic cleft between the opposing membranes (Palade, 1954; De Robertis and Bennett, 1955).

The above discoveries, along with major advances in immunohistological staining and microscopic techniques, propelled neuroscience research in to an age of rapid growth and new discoveries. In the last century we have developed more effective imaging techniques to visualise structures in the nervous system in real time, such as functional magnetic resonance imaging (fMRI), positron emission tomography

(PET) and computerised tomography (CT). We have made major advances in our understanding and treatments of neurological disorders including Alzheimer's disease (Karch et al., 2014), Parkinson's disease (Schapira et al., 2014), Huntington's disease (Schapira et al., 2014), motor neuron disease (Patten et al., 2014) and multiple sclerosis (Inglese and Petracca, 2014). As we live in an age of great technological influence, we have also utilised our discoveries in this field alongside our knowledge of the human brain to develop exciting new ways to regain what is lost with neurodegenerative disorders. For example, a team of scientists and engineers have developed a wheelchair that is controlled solely by brain-waves, enabling people with motor impairments to get around independently (Vanacker et al., 2007). Although major discoveries and advances have clearly been made in neuroscience research, we are still faced with many challenges in our quest to understand how the human nervous system functions in health and disease. It is also becoming increasingly clear that nervous system function relies on an array of non-neuronal cell types, which play a far more active and regulatory role than was once thought (Freeman, 2006; Barres, 2008; Allen and Barres, 2009; Eroglu and Barres, 2010; Pfrieger, 2010). We therefore need to consider these other cell types as we attempt to understand processes within the nervous system.

1.1.2 Cell types in the nervous system

There are a variety of cell types found in the nervous system. Non-neuronal cells called glial cells support the cells responsible for impulse transmission, neurons. Glial cells include astrocytes, oligodendrocytes, microglia and Schwann cells (Allen

and Barres, 2009), and account for 50% of the nervous tissue cell types found in the brain (Azevedo et al., 2009). Glial cells were first discovered in the mid-1800's by Rudolf Virchow, Theodor Schwann and Robert Remak, with the first published drawings emerging in 1856 of glia in the retina (Muller cells) by Heinrich Muller. Glial cells provide support to the axons in the form of insulation (myelin), growth factor supply in development and regeneration and debris/neurotransmitter clearing (Bunge, 1968; Taniuchi et al., 1986; Giulian et al., 1988; Raff et al., 1988; Auld and Robitaille, 2003; Song et al., 2008). They are also believed to take part in neurotransmission by responding to signals from axons (Auld and Robitaille, 2003; Darabid et al., 2013).

Glial cells were initially thought of as the “glue” of the nervous system, holding the neurons in place, but they are now appreciated as playing a more direct and regulatory role in axon function and maintenance, forming close associations with neurons that allow for signalling between the two cell types (Nave and Trapp, 2008). One well-characterised association between glia and neurons is that found between myelinating glial cells and underlying axons. These cells make and maintain an insulative sheath around large diameter axons, which is essential for rapid conduction along the nerve (White and Kramer-Albers, 2014).

1.2 Myelin

Myelin, the dense wrapping found around large diameter axons in the central and peripheral nervous systems, is essential for rapid nerve conduction in vertebrates. Rudolf Virchow first discovered and described the dense lipid material surrounding axons in 1853, denoting the substance as “myelin”. As vertebrates, we evolved myelin to cope with our need for speed, metabolic efficiency and limited space in our nervous system. In myelinated fibres, transmembrane currents propagate between nodes of Ranvier, a movement termed ‘saltatory conduction’. The existence of saltatory conduction was first proven in 1949 (Huxley and Stampfli, 1949).

True myelin, characterised by a glial investment of dense multilamellar wrapping around the axon, evolved in vertebrates (Bullock et al., 1984; Zalc et al., 2008), although a form of less compact myelin is known to exist in some invertebrates such as copepods (Davis et al., 1999), earthworms (Gunther, 1976) and shrimp (Xu and Terakawa, 1999). This myelin appears less compact and uniform, so is thought to represent a premature, less efficient form of the highly evolved myelin we see in vertebrates.

1.2.1 The evolution of myelin

When creatures first developed a need for faster neurotransmission, their nervous systems could adapt in two ways. One way was for axons to increase conduction velocity by increasing axonal calibre, but this also requires a need for more space in

the nerve. This adaptation took place in the giant squid, resulting in its large size and speed (Hartline and Colman, 2007). The second adaptation was for the nervous system to develop a thin, insulative material to wrap around the axons, and massively increase conduction velocity without the need for more space. This latter adaptation emerged throughout the vertebrate kingdom and the insulative material became known as myelin (Hartline and Colman, 2007). True myelin is thought to have evolved 400 million years ago when the vertebrate class of *placodermi* emerged on the evolutionary tree (Zalc et al., 2008). These jawed vertebrates were the ancestors of modern day sharks and bony fish. Studies of myelinated axons in sharks reveal a characteristic concentric, multilaminar appearance of myelin, similar to that found in higher vertebrates (Long et al., 1968). With the emergence of myelinated nerves, which could send impulses up to 20 times faster than unmyelinated nerves in the invertebrates, came the potential for vertebrates to grow to enormous sizes. Myelin, amongst other features such as an internal skeleton, allowed vertebrates to rapidly and drastically increase their body size, without compromising on neurotransmission efficiency. Without the emergence of myelin, jawed vertebrates, including humans, could not have evolved.

1.2.2 Myelination

Myelin is formed by oligodendrocytes in the central nervous system (CNS) and Schwann cells in the peripheral nervous system (PNS). In the CNS, space is limited due to the constraints of the bony structures of the cranial and vertebral cavities. To overcome a need for space, oligodendrocytes associate with more than one axon and

form multiple segments of myelin (Figure 1.1A). In the PNS, where space is not as limited, each Schwann cell will only form one segment of myelin on one axon (Figure 1.1B). Schwann cells are derived from neural crest cells and their fate can be either as non-myelinating or myelinating Schwann cells (Jessen and Mirsky, 2005).

Sox10 is an essential master regulator for early Schwann cell differentiation from neural crest cells, and at later stages of myelinating Schwann cell differentiation along with Krox-20 (Egr-2) (Topilko et al., 1994; Britsch et al., 2001; Finzsch et al., 2010; Jessen and Mirsky, 2010). During the initial stages of PNS development and axon-glia contact, Schwann cells organise the axons through a process called ‘radial sorting’, whereby groups of axons are bundled together, surrounded by one Schwann cell (Jessen and Mirsky, 2005). Small diameter axons are bundled together in larger numbers than the large diameter axons. The majority of PNS nerve fibres (nociceptive axons, postganglionic sympathetic axons and some preganglionic sympathetic and parasympathetic fibres) maintain this relationship with the Schwann cells, as Remak bundles (Emery et al., 1977). For the large diameter axons the contacting Schwann cells eventually develop a 1:1 relationship with the axons and develop in to myelinating glia (Jessen and Mirsky, 2005; Nave and Salzer, 2006). Myelinating Schwann cells wrap around large diameter axons such that the Schwann cell membrane apposes itself when the axon is fully encircled, forming the inner mesaxon (Robertson, 1957; Bunge et al., 1989). The Schwann cell cytoplasm continues to encircle the axon in multiple layers and begins the formation of a multilamellar myelin sheath (Bunge et al., 1989). These layers are compacted to provide the axon with a thin but powerful insulative lining (Figure 1.2). These axons

are required for rapid impulse propagation to the target cells, such as lower motor neurons synapsing on skeletal muscle. This allows for a rapid response of skeletal muscle with high frequency contractions, for example when a person needs to outrun a threat.

Myelination is a tightly controlled process requiring the involvement of multiple proteins and pathways to assemble and maintain the dense lipid multilamellar wrapping. The need for a vast assembly of Schwann cell machinery for myelination in the PNS is not surprising considering that human internodes, the segments of myelin found between nodes of Ranvier, can be up to 1.8mm in length (Vizoso and Young, 1948; Vizoso, 1950) with up to 150 myelin lamellae tightly compacted in each segment (Schroder et al., 1988). Once the myelinating Schwann cell lineage has been established, the cell initiates the production of myelin for the associated axon. Compact myelin is found at the internode, interspersed with sites of non-compact myelin/Schwann cell cytoplasm known as Schmidt-Lantermann incisures (Schmidt, 1874; Lantermann, 1877; Robertson, 1958). These are sites of cytoplasmic channels, which could serve as lines of communication within the Schwann cell (Balice-Gordon et al., 1998; Meier et al., 2004).

The formation, compaction and maintenance of myelin involve an array of proteins. Myelin protein zero (P_0) accounts for 70% of the proteins found in myelinating cells. It functions in the maintenance of myelin, with genetic mutations in this gene resulting in disassembly of myelin and diseases such as Charcot-Marie-Tooth disease (Giese et al., 1992; Su et al., 1993; Rautenstrauss et al., 1994; Martini et al., 1995b;

Martini et al., 1995a; Marrosu et al., 1998; Mandich et al., 1999). Other key peripheral myelin proteins are peripheral myelin protein 22 (PMP22), myelin basic protein (MBP) and myelin protein 2 (P2). A summary of the key proteins for myelin production and maintenance in the PNS by Schwann cells, along with associated diseases is presented in Table 1.1.

Protein	% Myelin Protein	Appearance of myelin in KO mice	Function	Disease Associations	References
Myelin Protein Zero (P₀)	70%	Formed, compacted but not maintained	Formation of major dense lines and myelin maintenance	Charcot-Marie-Tooth (CMT)2, CMT1B, Dejerine-Sottas syndrome, congenital hypo-myelination	(Giese et al., 1992; Su et al., 1993; Rautenstrauss et al., 1994; Martini et al., 1995b; Martini et al., 1995a; Marrosu et al., 1998; Mandich et al., 1999)
Peripheral Myelin Protein 22 (PMP-22)	5%	Slow formation, compacted but hyper-myelinated, not maintained	Myelin assembly, thickness and maintenance	Hereditary neuropathy with liability to pressure palsies (HNPP), CMT1A, Dejerine-Sottas syndrome	(Roa et al., 1993a; Roa et al., 1993b; Nicholson et al., 1994; Adlkofer et al., 1995)
Myelin Basic Protein (MBP)	5%	Some formed but not compacted or maintained	Myelin formation and compaction, formation of major dense line	Multiple sclerosis, inflammatory neurological diseases, non-inflammatory neurological diseases	(Bird et al., 1978; Sternberger et al., 1978; Readhead et al., 1987; Ota et al., 1990; Martini et al., 1995b; Reindl et al., 1999)
Myelin protein 2 (P₂)	15%	Myelin formed and compacted	Formation of Schmidt-Lantermann incisures, lipid transport in myelin	Guillain Barré syndrome (GBS)	(Sheremata et al., 1975; Trapp et al., 1979; Suresh et al., 2010; Zenker et al., 2014)

Table 1.1 Summary of the key proteins essential for myelin formation, compaction and maintenance in the PNS.

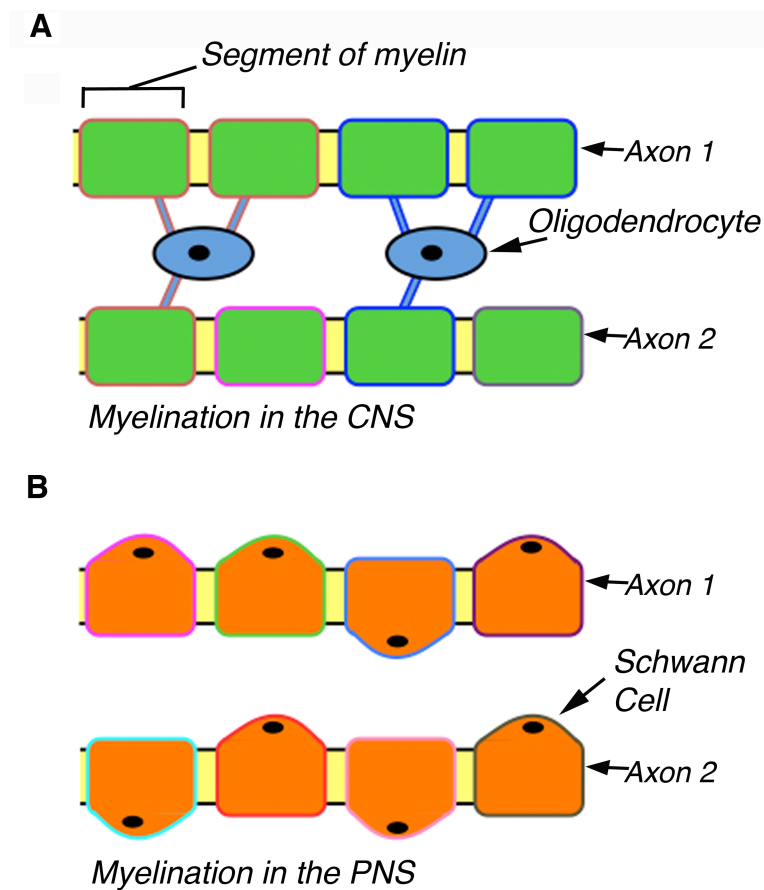


Figure 1.1. Myelination in the CNS and PNS. Simplified schematic comparing myelination in the CNS and PNS. In the CNS (**A**) each oligodendrocyte forms multiple segments of myelin on multiple axons. In the PNS (**B**) each Schwann cell forms one segment of myelin on one axon only.

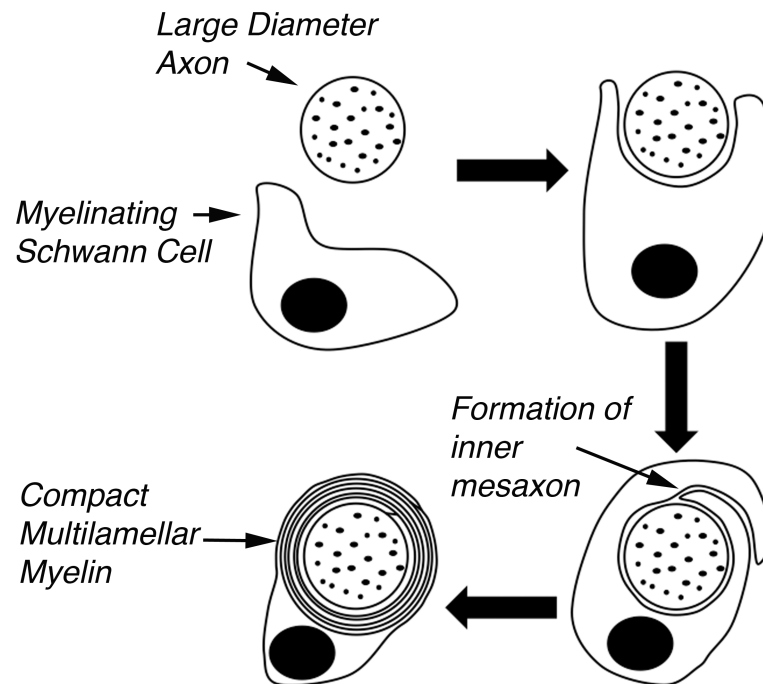


Figure 1.2. Myelination of large diameter axons by Schwann cells in the PNS.

Once the Schwann cell has differentiated into the myelinating phenotype, it associates with one large diameter axon and begins to form a segment of myelin. This myelin is compacted into a thin, dense, multilamellar insulative sheath.

1.2.3 Formation of molecular domains along myelinated fibres

The myelin sheath is closely apposed to the underlying axon, to achieve maximum insulative properties. As well as providing the axon with an insulative sheath, the formation of myelin results in the formation of nodes of Ranvier along the axon, between segments of myelin. Clusters of Na_v channels are found at the node of Ranvier. Although non-myelinated axons are known to express isoforms of Na_v channels, their clustering is less dense (Ritchie and Rogart, 1977) and more diffuse along the axon (Black et al., 2002). In contrast, myelinated axons in vertebrates display ordered and predictable nodes of Ranvier along their length (Ritchie and Rogart, 1977; Komada and Soriano, 2002; Poliak and Peles, 2003).

During the initial stages of axon-glia interaction in the PNS, Schwann cell processes extend to the axon and Na_v channels begin to cluster at these sites (Vabnick et al., 1996; Rasband et al., 1999). In the PNS, each myelinating Schwann cell forms one segment of myelin. Between these segments of myelin are the nodes of Ranvier, where Na_v channels are localised and concentrated (Figure 1.3). The nodal proteins neurofascin (Nfasc) 186 (axonal isoform of Nfasc) and ankyrin G are essential for Na_v channel anchorage (Kordeli et al., 1995; Jenkins and Bennett, 2002; Sherman et al., 2005). For the myelin sheath to have as close an apposition as possible to the underlying axon, regions of Schwann cell cytoplasm form a physical interaction with the axonal membrane, to anchor the Schwann cell to the axon. The site where this physical axon-glia interaction takes place is called the paranode, and a paranode forms on either side of each node of Ranvier (Figure 1.3). The protein accumulations

observed between the membrane of the glial cell and axon at the paranode with electron microscopy, described by Robertson in 1959 (Robertson, 1959), have become known as transverse bands. Transverse bands form after paranodal loops attach to the axon (Tao-Cheng and Rosenbluth, 1983). K_v channels are necessary for impulse propagation and they are located at the juxtaparanode (Chiu et al., 1999; Poliak et al., 2003) (Figure 1.3). The segment of axon that runs between juxtaparanodes is known as the internode (Figure 1.3). This is where the bulk of the compact myelin is found.

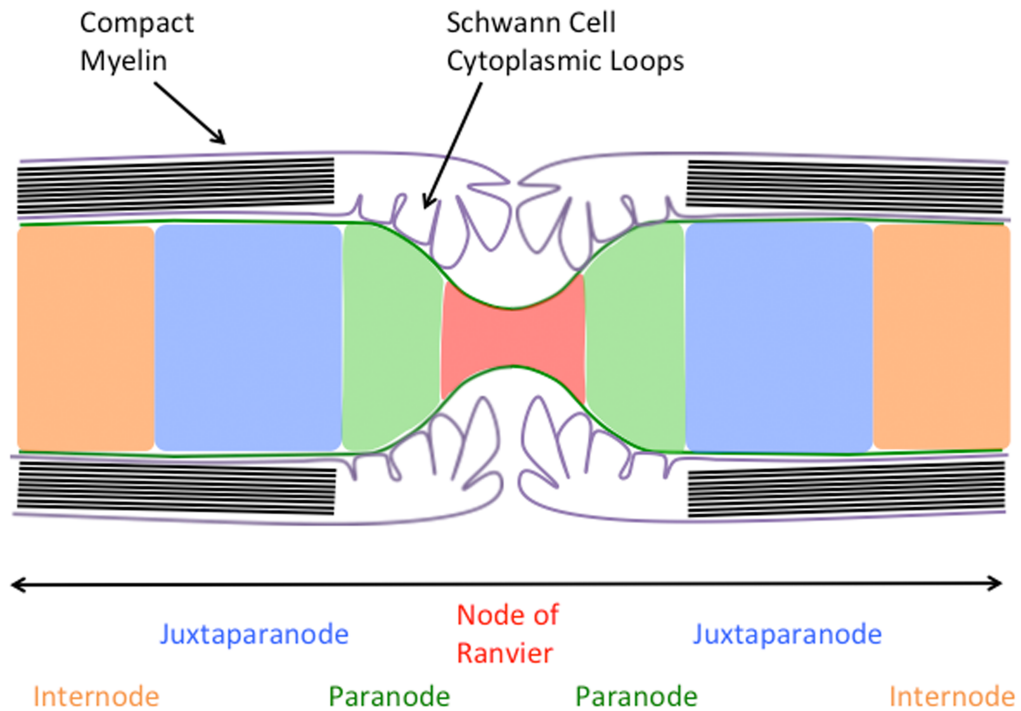


Figure 1.3. Schematic of the molecular domains found along myelinated axons. Myelination around large diameter axons results in the formation of multiple molecular domains. Na_v channels become localised to the node of Ranvier, where myelin is absent but Schwann cell processes overlay. Paranodal junctions are found between the axon membrane and cytoplasmic processes of the Schwann cell. The paranode acts as a nodal barrier by formation of a physical axon-glia interaction, restricting the Na_v channels to the node. K_v channels are found at the juxtaparanode, below layers of compact myelin. The space between juxtaparanodes at different nodes of Ranvier along the same axon is called the internode, where the majority of compact myelin is found.

1.3 Axon-glia Interactions

Axon-glia interactions are essential for normal development, maturation and maintenance of the nervous system (Freeman, 2006). Sites of axon-glia interaction are found at the paranode and internode. At the paranode, a physical interaction takes place between the two cells, forming what is known as the paranodal junction (Sugiyama et al., 2002). Sites of axon-glia interaction have also been documented along the internode. Myelin-associated glycoprotein (MAG) is one protein that has been implicated in this interaction (Trapp, 1990; Quarles, 2007). It is expressed by myelinating glial cells and localises to the adaxonal membrane at the internode. It is also present at the paranode (Marcus et al., 2002). It is not yet known what MAG interacts with on the axonal cell surface, but it likely involves lipid rafts (Vinson et al., 2003) and it has been suggested that isoforms of gangliosides on the axon membrane may serve as receptor molecules/interacting proteins (Yang et al., 1996).

1.3.1 Formation of the paranode

Axon-glia interaction at the paranode has been well studied. Three proteins interact in a complex, to form the paranodal junction. This requires the expression of proteins from the myelinating glial cell and from the axon. Nfasc 155 is expressed by myelinating glial cells and is required for physical formation of paranodes (Sherman et al., 2005). Nfasc155 has an affinity for interacting with a neuronally-expressed complex of two proteins, contactin-associated protein (Caspr) and contactin (Charles et al., 2002; Poliak and Peles, 2003).

Caspr and contactin are present in CNS and PNS axons at high levels before the onset of myelination in mice (Einheber et al., 1997). Once myelination has begun their expression levels decrease and both proteins become localised to the paranodal region (Einheber et al., 1997). Nfasc155 has been proposed to interact directly with the Caspr/contactin complex (Charles et al., 2002) (Figure 1.4). This physical interaction forms septate-like junctions, which are clearly visible with the electron microscope (Figure 1.4b) (Bhat et al., 2001; Boyle et al., 2001; Sherman et al., 2005). Paranodal junctions first develop closest to the node of Ranvier and extend away from the node (Rosenbluth, 1976) (Figure 1.5). Na_v channels can cluster at nodes of Ranvier before the formation of paranodal junctions (Jenkins and Bennett, 2002), although paranodal development is thought to provide a diffusion barrier and ensure the restriction of Na_v channels to the node (Rios et al., 2003), for efficient saltatory conduction along myelinated fibres. Due to the close proximity of glial and axonal membranes at the paranode, this molecular domain has been proposed as an ideal site for axon-glia signalling (Boyle et al., 2001; Sherman et al., 2005).

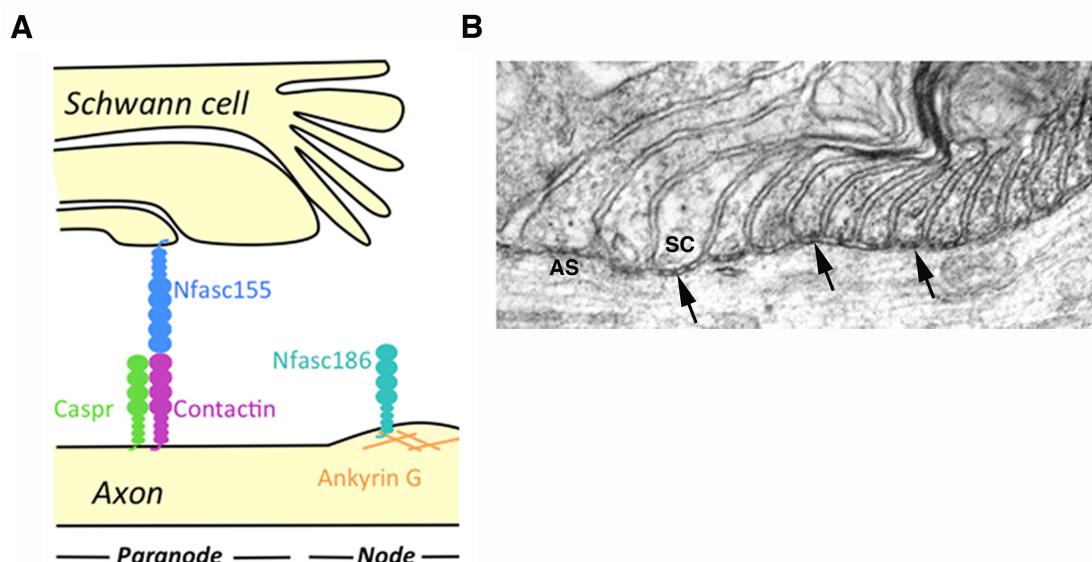


Figure 1.4. Structure of the paranode. (A) Simplified schematic of the paranode showing the localisation of the axonal isoform (Nfasc186 at the node of Ranvier) and glial isoform (Nfasc155 at the paranode) of Neurofascin (adapted from (Sherman et al., 2005)). Nfasc155 is expressed by the myelinating glial cell and localises to the paranodal region. Nfasc155 interacts with a Caspr/contactin complex on the axonal membrane to form the paranodal junction. This restricts Na_v channels to the node of Ranvier. Nfasc186 and ankyrin G are expressed by the axon and found at the node of Ranvier, where they localise and anchor Na_v channels. (B) Electron micrograph of paranode in the sciatic nerve of a P7 wild-type mouse, showing presence of septate-like junctions (arrows) between the Schwann cell microvilli (SC) and axonal surface (AS) (Image taken from Sherman et al., 2005).

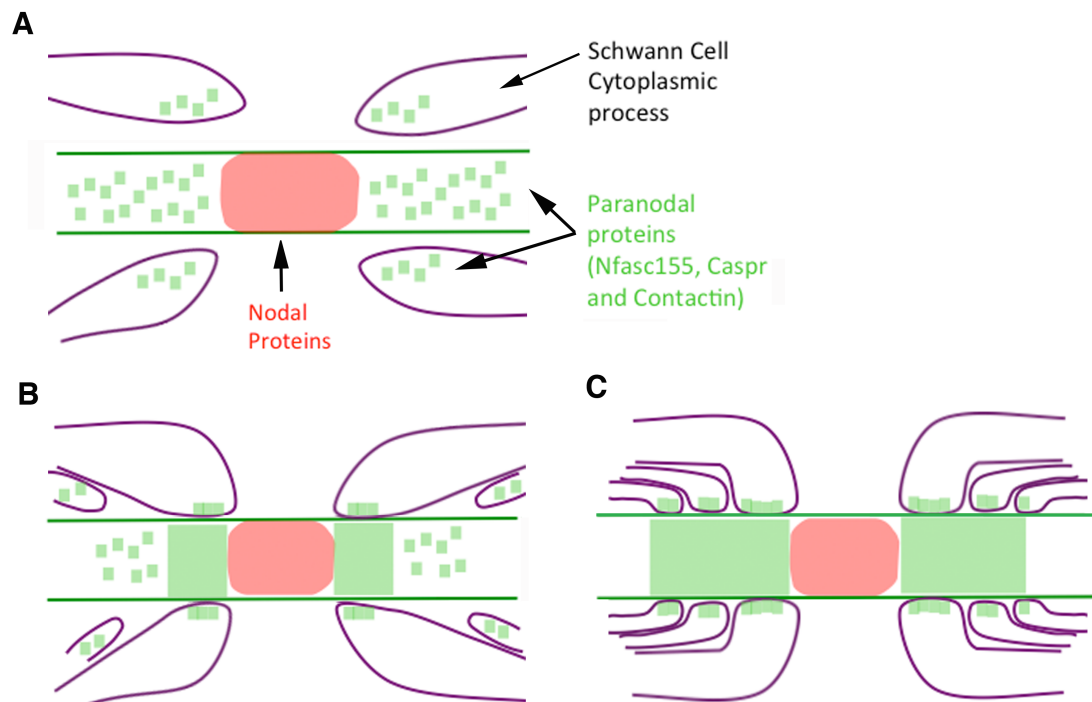


Figure 1.5. Simplified schematic illustrating paranodal development. (A) Prior to physical axon-glia interaction, paranodal proteins (green) are dispersed throughout the cell. (B) Upon contact with the Schwann cell, Na_v channels in the axon membrane (pink) become tightly localised to the nodal region. (C) Paranodes develop initially at the node of Ranvier and extend away from the node, adding more Schwann cell villi to the paranodal junction as it extends.

1.3.2 Consequences of disrupted paranodes

A disruption to paranodal integrity impacts on the conduction velocity of the axon. Conduction velocity is reduced when paranodes are disrupted by loss of Nfasc155 (Bhat et al., 2001) or Caspr (Pillai et al., 2009). The anchorage of the glial cell to the axon membrane is lost and so a gap is introduced between the two cell membranes (Bhat et al., 2001; Boyle et al., 2001; Sherman et al., 2005), possibly resulting in leakage of the impulse out of the axon. It has also been shown that a reduction in cerebral blood flow results in paranodal disintegration (Reimer et al., 2011), highlighting a close association between the vascular system and axon-glial interaction at the paranode. Paranodal abnormalities have been observed in models of multiple sclerosis (Howell et al., 2006; Pomicter et al., 2010), Guillain Barré syndrome (Yuki and Kuwabara, 2007) and spinal muscular atrophy (SMA) (Hunter et al., 2014), highlighting the importance of paranodal integrity for the normal function of peripheral nerves.

1.3.3 Axon-glial interaction during the initial stages of nervous system development

Axon-glial interactions are essential for the development and function of the nervous system. When one cell type is ablated in the PNS of *Drosophila* the development of the other cell type is dramatically hindered (Sepp and Auld, 2003). During this stage of vast growth and differentiation, communication between the Schwann cells and axons is imperative for axonal outgrowth. Schwann cells enhance the growth of the

axons by supplying the axons with essential growth factors including nerve growth factor (NGF), brain-derived neurotrophic factor (BDNF), glial cell line-derived neurotrophic factor (GDNF) and neurotrophin-3 (NT-3) (Hoke et al., 2006; Piirsoo et al., 2010). Thus, although a major role for Schwann cells is to produce myelin, it has become increasingly clear that Schwann cells also function to support the underlying axons independent of myelin formation and maintenance (Nave and Trapp, 2008). The importance of extracellular matrix components and neural cell surface molecules for the reciprocal development of Schwann cells and axons has been well studied (Martini, 1994). Just as glial scaffolds are important for nerve regeneration, so too are they required for axon growth at the transition zone from CNS to PNS (Sepp et al., 2001) and more distally in the PNS (Jacobs and Goodman, 1989). Glia and axons have a symbiotic relationship, providing instructive cues to each other to allow growth and development in unison.

Sox10 is one transcription factor identified as being involved in reciprocal communication between the two cell types during PNS development, with mutations in Sox10 resulting in disrupted migration of Schwann cells in zebrafish (Gilmour et al., 2002) and mice (Britsch et al., 2001), possibly due to downstream changes in expression which encodes the neuregulin receptor. The importance of neuregulin signalling from the axon on Schwann cell lineage and myelination has been well studied (Nave and Salzer, 2006). Mutations in a second neuregulin receptor in mice, ErbB2, revealed an important role for this receptor in Schwann cell migration from dorsal root ganglia (Morris et al., 1999). Neurotrophins have also been implicated in the complex axon-glial signalling cascades that are required for the initial stages of

myelination (Chan et al., 2001). As well as guiding axons and regulating their cytoskeletal development, Schwann cells regulate the formation of the peripheral nerve sheath by expressing *Desert Hedgehog* (Mirsky et al., 2002). It is known that Schwann cells undergo apoptosis during the initial stages of PNS development, and that this apoptosis is regulated by neuregulin signalling from the axon (Grinspan et al., 1996).

1.3.4 Axon-glia interaction during injury / nerve regeneration

Following injury in the CNS, nerves fail to successfully regenerate (Qiu et al., 2000; Yiu and He, 2006). In contrast, nerves in the PNS have the remarkable ability to regenerate following injury (Ide et al., 1983). Schwann cells have been shown to play a major role in the success of PNS regeneration. In the case of axonal damage and regeneration, myelinating Schwann cells are capable of rapidly reverting from their established myelinating phenotype back to a more immature state to allow them to remyelinate recovering axons. Following axonal transection, Schwann cells significantly downregulate expression of myelin proteins including *P₀* and *MBP* (Lemke and Chao, 1988) and upregulate activation of p38 MAPK and c-Jun to begin myelin clearance and promote axonal regeneration (Fontana et al., 2012; Yang et al., 2012). Schwann cells also upregulate expression of trophic factors and cytokines such as *NGF*, *BDNF*, *GDNF*, *interleukin (IL)-6*, *insulin-like growth factor (IGF)-1* and *leukemia inhibitory factor (LIF)* to promote axon regeneration (Hansson et al., 1986; Meyer et al., 1992; Banner and Patterson, 1994; Curtis et al., 1994; Bolin et al., 1995; Tofaris et al., 2002; Hoke et al., 2006). Glial fibrillary acidic protein (GFAP) is a cytoskeletal component of the Schwann cell, known to be upregulated following nerve damage (Garrison et al., 1991; Triolo et al., 2006). In GFAP deficient mice, axons form normally but undergo slower regeneration in the PNS following insult, compared to uninjured mice (Triolo et al., 2006).

Schwann cells only commence myelin degeneration if the axon is damaged (Glass et al., 1993). Following the initiation of myelin breakdown, the Schwann cell detaches

itself from the unwanted myelin (Stoll et al., 1989) to allow for degradation and clearance by Schwann cells and macrophages to take place (Beuche and Friede, 1984; Fernandez-Valle et al., 1995; Stoll and Muller, 1999; Hirata and Kawabuchi, 2002). Myelin clearance is an essential step in the nerve regeneration process as it reduces the risk of nerve compression during recovery. The number of glia at the site of injury exponentially increases (Sjostrand, 1965; Zhang and Guth, 1997) as they provide axons with essential neurotrophic factors to speed up the recovery process (Frostick et al., 1998; Terenghi, 1999). Schwann cells have been proposed to guide regenerating axons to their target (Son and Thompson, 1995), through attractive cues in their basal lamina (Ide et al., 1983; Nadim et al., 1990). Laminin is one such component of Schwann cell basal lamina that is essential for guiding regenerating axons (Wang et al., 1992).

1.4 Axon-glia interaction between myelinating cells and axons during postnatal development / maturation of the nervous system

Axon-glia interaction is essential for normal postnatal development of the mouse nervous system. The nervous system undergoes further development as well as vast remodelling postnatally. Myelinating Schwann cells and oligodendrocytes provide essential instructive cues for axon growth, regulating axon cytoskeletal content and transport. These cells also play an essential role in debris clearance during synaptic remodelling, recycling and degradation of unwanted axonal accumulations following withdrawal at synapses. Myelinating cells will also expend vast amounts of energy in

the postnatal period as they produce, compact and maintain myelin sheaths around underlying axons. This process has been described in detail in previous sections.

1.4.1 Axon-glia interactions for axonal cytoskeletal integrity

Signals emanating from myelinating glial cells are essential for maturation of the axonal cytoskeleton. The cytoskeleton of the axon is composed of filamentous structures that provide the axon with an internal scaffold, to support it and to also form a network on which to transport internal cargo along the length of the axon. Neurofilaments form the bulk of the cytoskeleton, along with microtubules and microfilaments, which are cross-linked to provide a stable internal scaffold (Wuerker and Palay, 1969; Yamada et al., 1970, 1971; Metzuzals and Mushynski, 1974; Metzuzals et al., 1981; Hirokawa, 1982; Schnapp and Reese, 1982; Tsukita et al., 1982). There are three neurofilament proteins expressed by axons, named by molecular weight, neurofilament-heavy (NF-H), neurofilament-medium (NF-M) and neurofilament-light (NF-L). NF-L is the most abundant and one of the earliest expressed (Willard and Simon, 1983; Carden et al., 1987). These three proteins interact to form intermediate filaments (Leung and Liem, 1996). NF-H and NF-M are always interacting with NF-L but NF-L has been shown to form homodimers (Geisler and Weber, 1981; Liem and Hutchison, 1982) as well as intermediate filaments.

NF-H and NF-M in intermediate filaments are heavily phosphorylated, and because these phosphoryl groups repel each other the intermediate filaments begin to spread

apart and increase the calibre of the axon (Cleveland et al., 1991). Kinases, including extracellular signal-related kinases 1 & 2, (Erk)1/2, cyclin-dependent kinase 5 (cdk5), p35 and stress-activated protein kinase (SAPK) phosphorylate neurofilaments (Grant and Pant, 2000). It has been shown that phosphorylation of NFs is regulated in part by MAG-dependent pathways emanating from myelinating glia (Dashiell et al., 2002). Study of neurofilaments and kinases in *MAG*^{-/-} mice revealed that loss of MAG results in reduced levels of NF-H, NF-H phospho, NF-M, NF-M phospho, cdk5 and ERK1/2 (Dashiell et al., 2002).

Signals from myelinating glial cells have been shown to be essential for increasing axon calibre, both dependent and independent of myelin formation (de Waegh and Brady, 1991; Cole et al., 1994; Sanchez et al., 1996; Brady et al., 1999). These studies showed that in mice with targeted disruption to myelin genes such as MBP (Brady et al., 1999) and P0 (Cole et al., 1994) neurofilament phosphorylation and neurofilament density in the axon were dramatically altered as a result of hypomyelinating phenotypes. Reduced axon calibre has also been reported in a mutant mouse model with a poor myelinating phenotype, the ‘Trembler’ mouse (de Waegh and Brady, 1991). When sciatic nerve grafts were taken from this mouse and transplanted into transected sciatic nerves of a healthy mouse, it was found that axon diameter in healthy axons was significantly reduced due to the presence of ‘Trembler’ Schwann cells. In all three studies, poor myelination resulted in reduced axon calibre suggesting that myelin formation in glial cells is essential for maintaining integrity of the underlying axon.

It has also been shown that myelinating glial cells can modulate axonal neurofilament dynamics independently of myelin formation (Sanchez et al., 1996). In this study, three strains of mice with different mutations that prevent myelin formation in the CNS were used to study the effect that myelinating oligodendrocytes have on the radial growth of retinal ganglion cells when myelin formation is hindered. They showed that non-myelinated axons in the mutant mice, wrapped by oligodendrocytes, increased in axon calibre and accumulated neurofilaments to the same degree as axons invested by myelinating oligodendrocytes in the control mice. This provides further support for the importance of myelinating glia for axon calibre growth and also suggests that these regulatory pathways may be distinct from those controlling myelination.

The production of cytoskeletal proteins is also an important step in the development/maturation of axons. This is also a crucial step in the regeneration process when nerves have been damaged and axons are attempting to regenerate. The importance of glia for the regulation of neurofilament synthesis in the axon has been most easily studied with crush/regeneration experiments (Liuzzi and Tedeschi, 1992). This study showed that when adult rat lumbar dorsal roots were crushed and axons allowed to regenerate, axons did so until they met the dorsal root transition zone at the peripheral nerve-spinal cord interface. This is where astrocytes are found. They measured axon regeneration by quantifying levels of NF-M and NF-L at different times post-injury. NF-M and NF-L levels in the crush group reached control levels by 14 days post-injury in the peripheral nerve, whereas axons failed to regenerate past the dorsal root transition zone. They suggest that astrocytes actively inhibit the

synthesis of neurofilaments, resulting in the poor regenerative abilities within the CNS (Liuzzi and Tedeschi, 1992).

1.4.2 Axon-glia interactions for axonal transport

In neuronal axons, microtubules form a network on which cell cargo can be transported in both anterograde and retrograde directions. Neurofilaments in lower motor neurons for example, which are synthesized in the cell body in the ventral spinal cord, are transported along this track to reach their target in the pre-terminal axons synapsing on skeletal muscle. It has been shown that neurofilaments travel in both directions, and can switch between a moving and stationary state, by hopping on and off the microtubule transport system (Monsma et al., 2014). Local signals produced by myelinating Schwann cells have been shown to alter axonal transport of neurofilaments (de Waegh and Brady, 1991; de Waegh et al., 1992; Monsma et al., 2014).

The former studies by de Waegh et al. 1991 & 1992 used a mutant mouse model with a poor myelination phenotype, the ‘Trembler’ mouse, to study the contribution of Schwann cells to the regulation of axon transport. They transplanted sciatic nerve grafts from this model into transected sciatic nerve in a healthy mouse and allowed the nerve to regenerate so that the healthy axons grew in to the graft with defective Schwann cells present. They showed that neurofilament transport was slower in the healthy axons surrounded by ‘Trembler’ Schwann cells, compared to the axons distal to the graft (de Waegh and Brady, 1991). They also showed that Schwann cells likely

modulate axonal transport through modulation of a kinase-phosphatase system in the axon (de Waegh et al., 1992). This highlights a key role for Schwann cells in modulating transport systems in the underlying axons.

Monsma et al., 2014 studied the effect of myelinating Schwann cells on transport within the underlying axons *in vitro*, using a neuron-Schwann cell co-culture. In this culture system, Schwann cells formed dispersed segments of myelin along axons. This system allowed them to visualise the transport of NF-M in myelinated and unmyelinated segments of the same axon, in real-time. They clearly showed that transport of NF-M was slower in myelinated regions, providing further evidence of a glial-based signal that is capable of modulating axon transport (Monsma et al., 2014). Molecular motor proteins such as kinesin, dynein and dynactin are responsible for interacting with cell cargo and moving it along the microtubule transport system, including the transport of neurofilaments (Shah et al., 2000; Shea and Flanagan, 2001; Xia et al., 2003; Motil et al., 2006; Uchida et al., 2009; Lee et al., 2011). A schematic of how these proteins associate with the microtubule transport system and cargo is shown in Figure 1.6.

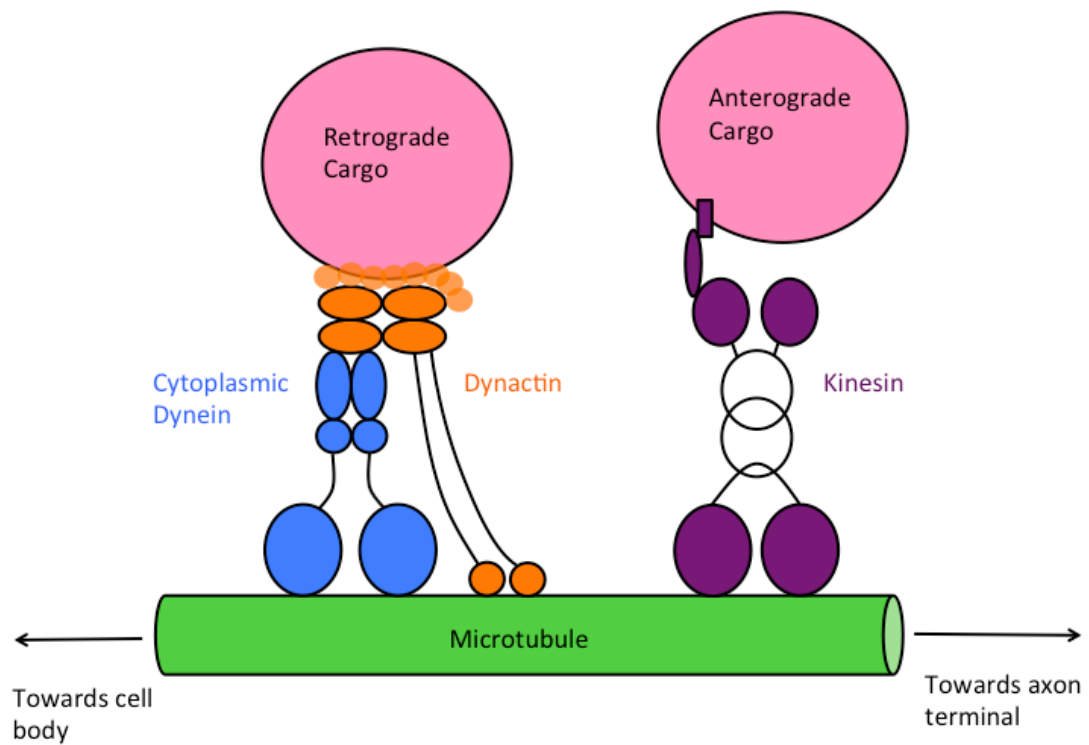


Figure 1.6. Schematic of how kinesin, dynein and dynactin associate with the microtubule cytoskeleton and cargo to perform anterograde and retrograde transport in the axon (adapted from (Duncan and Goldstein, 2006)). Kinesin, dynein and dynactin interact with the microtubule axonal network to transport cellular cargo throughout the axon. Kinesin transports cargo anterograde and dynein and dynactin interact to transport cargo in the retrograde direction.

1.4.3 Axon-glia interactions for developmental remodelling of neuronal circuitry

One of the ways in which the nervous system refines its neural connections around the time of birth is by the removal of excess synaptic inputs. At birth in the mouse there are an excess number of inputs throughout the CNS and PNS, which are pruned away by a process known as synapse elimination (Rosenthal and Taraskevich, 1977; Balice-Gordon and Lichtman, 1993). This is a fundamental and dynamic process that has been well studied at sites in the mammalian CNS (Kano and Hashimoto, 2009) such as the retina (Chen and Regehr, 2000) and cerebellum (Hashimoto and Kano, 2005). Recent research had shed light on the importance of glial cells for normal synapse elimination to occur in the CNS (Chung et al., 2013) and the PNS (Smith et al., 2013) of mice. In the CNS, it has been shown that lysosomal pathways involving multiple epidermal growth factor 10 (MEGF10) and membrane receptor tyrosine kinase (MERTK) emanating from astrocytes modulate rates of synapse elimination in the brain (Chung et al., 2013). In the PNS, it has been suggested that terminal Schwann cells (TSCs) capping the neuromuscular junction (NMJ) are involved in the regulation of synapse elimination by engulfing axonal material in axons that are still innervating the endplate (Smith et al., 2013). The most extensively studied site of synapse elimination is at the NMJ in the PNS. This is a specialised synapse formed between lower motor neurons and skeletal muscle fibres.

1.5 The Neuromuscular Junction

Research in to development of the NMJ has been extensively carried out, providing us with a detailed description of how this specialised synapse forms. The NMJ is a generally considered a tripartite structure, composed of a motor neuron axon terminal, overlying terminal Schwann cells and the muscle fibre endplate (Sanes and Lichtman, 1999), although the presence of a fourth cell type at the NMJ, the kranocyte, has also been discovered (Court et al., 2008). ACh is the neurotransmitter synthesized and exocytosed by lower motor neurons. Dense clusters of ACh receptors are present on the muscle fibre surface, forming junctional folds known as the endplate (Anderson and Cohen, 1974; Fertuck and Salpeter, 1974; Peper et al., 1974). ACh is present in vesicles in the axon terminals directly overlying the endplate, and when an impulse reaches the synapse, with the strength required for neuromuscular transmission, ACh is exocytosed and binds to the ACh receptors at the endplate. This binding results in a downstream cascade of activation in the muscle fibre and ultimately whole muscle contraction (Katz, 1966; Ali and Savarese, 1976; Standaert, 1982). Terminal Schwann cells cap the synapse and could be a source of trophic support for the NMJ (Birks et al., 1960).

1.5.1 Development of the NMJ

The organisation of the NMJ is a tightly regulated process, controlled by numerous proteins and pathways. Motor axons extend towards target muscles as myoblasts are fusing to form myotubes. Once contact has been made between the two cells,

neurotransmission begins but at a very low level. The pre- and post-synaptic components need to develop before neurotransmission can reach its full potential. Agrin is a protein expressed by the motor neuron and transported down the length of the axon to the synapse, where it is exocytosed and taken up by the basal lamina of the endplate (Cohen and Godfrey, 1992; Reist et al., 1992). Agrin is essential for post-synaptic development at the NMJ, as shown by studies in Agrin-deficient mice (Gautam et al., 1996). Agrin has been identified as an anti-dispersal agent at the post-synapse, playing an important role in preventing ACh receptors from diffusing rather than clustering them (Lin et al., 2001; Kummer et al., 2006). It counteracts the dispersal effect of neurotransmitter release from the axon terminal on ACh receptors (Misgeld et al., 2005). Muscle-specific kinase (MuSK) is a receptor expressed exclusively in muscle, and localises to the endplate (Ganju et al., 1995; Valenzuela et al., 1995). *MuSK*^{-/-} mice have an almost identical phenotype to *Agrin*^{-/-} mice, with lack of post-synaptic differentiation (DeChiara et al., 1996), which initially suggested that MuSK could be the receptor for Agrin at the NMJ. Further studies in to this hypothesis validated these claims (Gautam et al., 1996; Glass et al., 1996; Meier et al., 1996; Glass et al., 1997; Hopf and Hoch, 1998a, b). Rapsyn is a protein identified as being downstream of MuSK and another important player in organisation of the NMJ (Frail et al., 1987). Rapsyn colocalises with AChR's as they begin to cluster on the muscle fibre surface (Burden et al., 1983; Sealock et al., 1984; Noakes et al., 1993) and has been shown to orchestrate this clustering (Froehner et al., 1990; Phillips et al., 1991).

Innervation of myotubes leads to increased synthesis of ACh receptors at the endplate, in a process termed ‘synapse-specific transcription’ (Merlie and Sanes, 1985; Goldman and Staple, 1989). Calcitonin gene-related peptide (CGRP) and neuregulin have been proposed as axonally-expressed inducers of this process, which act to locally induce expression of ACh receptors on the underlying surface of the myotube (Fontaine et al., 1986; New and Mudge, 1986; Usdin and Fischbach, 1986; Fontaine et al., 1987). CGRP is synthesized in the motor neuron cell body, transported to the axon terminal and packaged in to vesicles, which are exocytosed upon arrival of a nerve impulse (Uchida et al., 1990). Neuregulin is synthesized and transported in a similar way to CRGP, but is incorporated in to the basal lamina of the muscle fibre where it acts to increase levels of ACh receptors (Goodearl et al., 1995; Loeb and Fischbach, 1995).

Innervation of muscle fibres by lower motor neurons occurs in one of two ways. When the lower motor neuron arrives at the muscle fibre to innervate it, the ACh receptors cluster either prior to or following arrival of the nerve terminal. NMJs that develop through the former process are known as fast-synapsing (fa-syn) NMJs, and the latter are known as delayed-synapsing (de-syn) NMJs (Pun et al., 2002). Muscles are composed of different fibre types, owing to varying contractile strengths. Muscle fibres are either fast-twitch or slow-twitch, determined by the myosin isoform expression (Pette and Schnez, 1977), myosin phosphorylation (Moore and Stull, 1984) and ATPase activity (Rubinstein and Kelly, 1978). Fast-twitch and slow-twitch muscles exhibit differences in their quantal content and total vesicle pool size to adapt to their differing patterns of activity (Reid et al., 1999).

1.5.2 Diseases affecting the neuromuscular system

The neuromuscular system is affected in a multitude of neurodegenerative disorders. Some disorders affect the NMJ at early developmental stages, such as spinal muscular atrophy (SMA), whilst others affect the NMJ at later stages, such as amyotrophic lateral sclerosis (ALS), Guillain Barré syndrome (GBS) and myasthenia gravis. Autoimmune disorders such as GBS and myasthenia gravis arise due to the production of antibodies that target the presynaptic nerve and postsynaptic endplate respectively. In GBS peripheral myelin breaks down, as antibodies are produced against major myelin proteins including gangliosides (Ilyas et al., 1988). In myasthenia gravis, antibodies are produced against ACh receptors on the muscle fibre surface, blocking the effect of ACh release from the lower motor neuron (Bender et al., 1975; Newsom-Davis et al., 1978). Charcot-Marie-Tooth classifies a large range of demyelinating neuropathies, however the most common cause is a genetic mutation in peripheral myelin protein 22 (PMP22) (Roa et al., 1993a), which plays a role in myelin formation and maintenance (Adlkofer et al., 1995). Major characteristics of the above disorders are altered conductive properties in the nerve and muscular weakness or atrophy, with no loss of motor neurons or a loss only in late stages of the disease.

ALS and SMA are adult and childhood forms of motor neuron disease respectively, and a major characteristic of both of these disorders is a loss of motor neurons (Jablonka et al., 2000; Fischer et al., 2004). Most cases of ALS are sporadic although a small percentage (5-10%) is familial. Mutations in the superoxide

dismutase enzyme gene, *SOD1*, have been linked to familial ALS, suggested to result in a toxic gain of antioxidant function (Rosen et al., 1993) ALS is characterised by degeneration of upper motor neurons in the cortex as well as a loss of lower motor neurons in the spinal cord (Kiernan et al., 2011). SMA is caused by a disruption in the *survival motor neuron 1 (SMN1)* gene that results in defective expression of full-length survival motor neuron (SMN) protein (Lefebvre et al., 1995; Burghes and Beattie, 2009; Lorson et al., 2010). In SMA, lower motor neurons are lost in the spinal cord (Jablonka et al., 2000) but the CNS remains unaffected. In both ALS and SMA, muscle weakness and atrophy of skeletal muscles are major features, resulting in eventual paralysis. Unlike the disorders mentioned earlier, NMJ denervation is a hallmark of ALS and SMA (Fischer et al., 2004; Murray et al., 2008).

1.5.3 Synapse elimination at the NMJ

The presence of polyinnervated endplates in the skeletal muscles of neonatal rodents was first described in 1970 by recording endplate potentials (EPPs) in individual muscle fibres (Redfern, 1970). This indicated the presence of multiple axons innervating single endplates. It was later discovered that inputs were lost at polyinnervated endplates during the postnatal life of rats (Brown et al., 1976), without any effect on neurotransmission (Rosenthal and Taraskevich, 1977), similar to what had been observed during nerve regeneration following injury at the adult NMJ (McArdle, 1975; Gorio et al., 1983; Rich and Lichtman, 1989; Costanzo et al., 1999). Postnatal synapse elimination is a fundamental part of nervous system development, facilitating removal of converging axons and driving the refinement of

neural circuits (Sanes and Lichtman, 1999; Kano and Hashimoto, 2009). It takes place throughout the central and peripheral nervous systems, and is an essential process in the refinement and fine-tuning of nerve-target innervation. The NMJ is one of the many synapses in the nervous system that develop through a process of synapse elimination, whereby excess inputs are lost following competition for innervation. Postnatal development of the mouse NMJ has been well studied due to the ease of accessibility and well-established and robust imaging protocols.

In the majority of mouse skeletal muscles, synapse elimination takes place postnatally in the first two-three weeks of life. Lower motor neurons branch extensively to weakly innervate multiple muscle fibres during the initial developmental stages of innervation, and from birth they begin to refine their targets, strengthening the strongest inputs and eliminating the weaker ones (Tapia et al., 2012). In the levator auris longus (LAL) muscle for example, each muscle fibre is innervated by multiple axons at birth and over the course of ~15 days, competition for mono-innervation of each muscle fibre takes place (Chapter 3; Figure 3.5).

In vivo studies have shown how this is a dynamic and highly active process with axons aggressively attempting to take over the synapse and force weaker inputs to die back (Walsh and Lichtman, 2003). A major feature of synapse elimination in the PNS is axonal cytoskeletal rearrangement, as terminal axons retract and expand territory as they compete for sole innervation of the synapse (Bixby, 1981; Riley, 1981; Sanes and Lichtman, 1999; Keller-Peck et al., 2001). *In vivo* visualisation of synapse elimination has shown that axon terminals are the most dynamically

changing parts of the axon during synapse elimination as they remodel and adapt to changes in innervation patterns (Keller-Peck et al., 2001; Walsh and Lichtman, 2003; Turney and Lichtman, 2012). Once an axon has left the endplate, it prunes away from the muscle fibre in the form of a retraction bulb, leaving debris behind to be engulfed for degradation or recycling by surrounding glial cells (Bishop et al., 2004; Turney et al., 2012). Interestingly, the process of synapse elimination at the NMJ can be reversed, by laser-ablating the winning axon at an endplate, where the losing axon has already started retracting (Turney and Lichtman, 2012). As synapse elimination is taking place, the post-synapse is undergoing specialisations to adapt to the pre-synaptic changes, such as eliminating ACh receptors in a newly vacated site (Balice-Gordon and Lichtman, 1993). A close correlation exists between axon withdrawal and post-synaptic changes during development (Balice-Gordon and Lichtman, 1993; Culican et al., 1998).

1.5.4 Regulation of synapse elimination at the NMJ

Although well characterised, the regulation of this dynamic process is poorly understood. There is a vast body of literature describing how innervating axons undergo dynamic changes as they compete for innervation of the muscle fibre, but few studies elucidating on the regulatory mechanisms at play. The majority of studies seeking to understand the complexity and intricacies of synapse elimination have been focused on the regulation of this process intrinsic to the innervating axons (Callaway et al., 1987, 1989; Costanzo et al., 2000; Buffelli et al., 2003; Kasthuri and Lichtman, 2003; Favero et al., 2012). Although the interaction between glial

cells and axons is known to be an essential relationship for prenatal development of the peripheral nervous system, little research has been dedicated to the potential contribution of the surrounding glial cells in the regulation of postnatal synapse elimination at the NMJ.

Studies aimed at discovering the regulators and motivators of synapse elimination at the mouse NMJ have been largely focused on the importance of nerve activity, lysosomal activity and growth factor supply for normal rates of synapse elimination to occur (Figure 1.7). It is clear that neuromuscular transmission influences synapse elimination. However, contrasting studies have made a case for inactivity (Callaway et al., 1987, 1989; Costanzo et al., 2000) and enhanced activity (Ridge and Betz, 1984; Buffelli et al., 2003) in promoting elimination of inputs. One major point to consider with these studies is that activity levels were identical in all competing inputs, either by reducing or increasing activity, which is not necessarily biologically relevant, as competing inputs will naturally have different levels of activity during competition for innervation.

The contrasting ideas in these studies have been addressed and partially resolved by studies showing that it is the firing pattern of activity between competing inputs that is important rather than the presence or absence of activity. Synchronous activity in polyinnervating axons at the rat NMJ slows down synapse elimination during postnatal development (Favero et al., 2009) and during reinnervation following a crush injury (Favero et al., 2010), whereas asynchronous activity speeds up the process (Favero et al., 2012). This provides further evidence for the competitive

nature of synapse elimination. If electrical activity is equal in innervating axons, then all inputs are equally strong and favourable winners. As soon as activity falls below, or rises above, a certain threshold in one input this allows the stronger inputs to take over the synaptic site. This competition progresses until there is only one input left, the monoinnervated state. This reasoning also explains why synapse elimination stops as soon as there is only one input left; if there is no active nerve to compete with, the last remaining input no longer needs to fight for innervation (Favero et al., 2014). It also strengthens the case for local regulation of synapse elimination at the NMJ (Keller-Peck et al., 2001), rather than a pre-encoded outcome at the beginning of the process.

Further insights in to the signals and mechanisms regulating synapse elimination at the NMJ have been presented by studies on growth factor supply from target-derived muscle cells and surrounding glial cells. The “trophic hypothesis” suggests that a limited supply of growth factor drives competition between innervating inputs (Bennett and Robinson, 1989). If this were true then an unlimited supply of growth factor would presumably delay synapse elimination, as there would not be a need for innervating axons to compete. Indeed, an unlimited injected supply of ciliary-neurotrophic factor (CNTF) and basic fibroblast growth factor (bFGF) were shown to delay synapse elimination in the lateral gastrocnemius muscle of newborn rats (English and Schwartz, 1995; Jordan, 1996). Injection of LIF from birth, which is naturally expressed in skeletal muscle, to the tensor fascia-latae muscle of the mouse prolongs developmental synapse elimination (Kwon et al., 1995). Genetically overexpressing *GDNF* in skeletal muscle also results in increased and prolonged

polyinnervation at synapses (Nguyen et al., 1998). Support for the trophic hypothesis has been extended by a study that looked at the expression profiles of various neurotrophic factors in skeletal muscle and found them to be upregulated prior to the period of synapse elimination in rat (Ip et al., 2001) with a gross downregulation post-synapse elimination. This would support the idea that a large yet limited supply of growth factor is available to innervating axons at NMJs during developmental synapse elimination.

1.5.5 Glial cells and synapse elimination

Recent studies have begun to uncover the important contributions that glial cells can make to the development and stability of the nervous system (Ullian et al., 2001; Reddy et al., 2003; Bishop et al., 2004; Fuentes-Medel et al., 2009; Eroglu and Barres, 2010; Chung and Barres, 2012). As losing axons leave the synaptic site and retract, surrounding glial cells engulf the unwanted debris for recycling/degradation (Song et al., 2008). Disruption of this process slows down synapse elimination (Song et al., 2008) highlighting an important role for glia in the success of synapse elimination. This role is largely thought of as a secondary role, following the elimination of axons, but a recent study has challenged that idea. Smith et al., 2013 suggested from ultrastructural analysis of polyinnervated NMJs, that TSCs capping the NMJs actively engulf healthy parts of innervating axons, thereby driving the process of synapse elimination and contributing to the outcome (Smith et al., 2013). They showed that TSCs project cytoplasmic protrusions into healthy axons that are still in contact with the endplate and suggested that this process would drive synapse

elimination. However, there is not enough evidence within this study to confirm a primary role for glial cells in the outcome of synapse elimination. The study is specific to TSCs, the capping glial cells at the NMJ, and is purely descriptive. Furthermore, there is no molecular insight provided as to how TSCs may drive the process. Therefore, we have yet to discover a regulatory role for glial cells in developmental synapse elimination in the PNS as well as identify the molecular drivers of this process.

The above studies provide some insight in to the key regulators at play during synapse elimination and make clear that there is unlikely to be just one key mechanism regulating this process. Glial cells, muscle fibres and axons all contribute to the outcome of the process in activity-dependent and activity-independent ways. Considering the numerous cells that regulate synapse elimination it is therefore not surprising that observing this process *in vivo* presents us with what appears to be a random and disorganised pruning of competing axons, in which the outcome of competition at each NMJ seems to be unbiased in any way (Keller-Peck et al., 2001; Walsh and Lichtman, 2003).

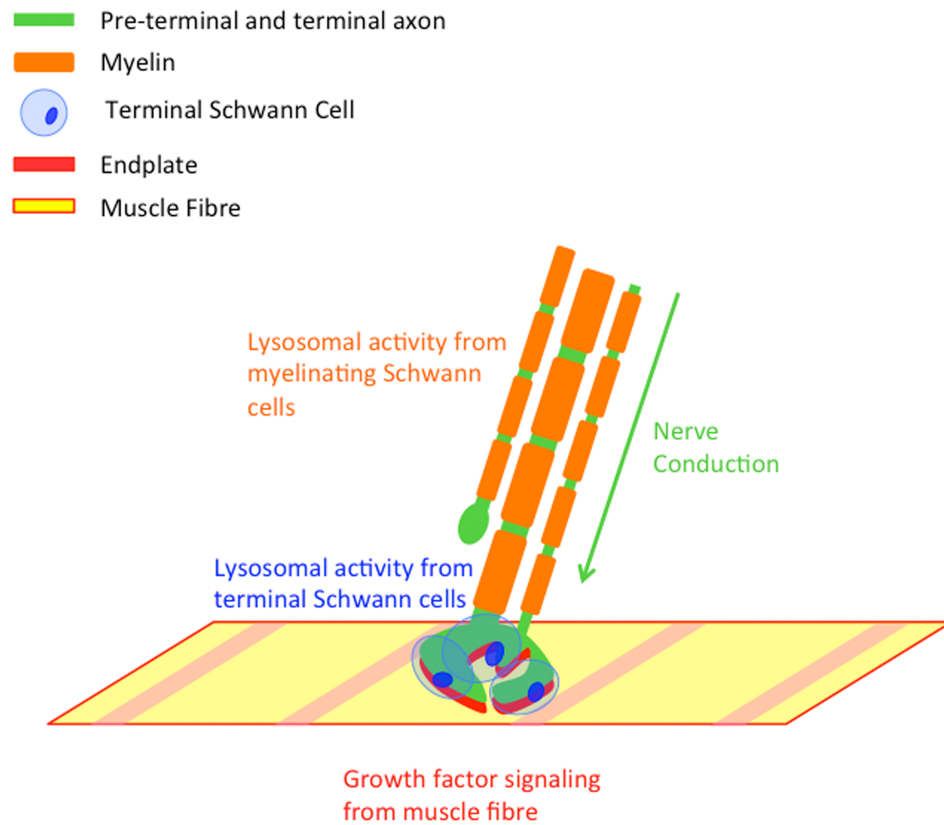


Figure 1.7. Schematic of an NMJ undergoing synapse elimination, highlighting the known factors important for normal synapse elimination to occur.

1.6 Aims

Synapse elimination at the mouse NMJ has been well characterised however we have yet to fully understand what cells and pathways are regulating this process. Previous studies have hinted at the possibility that myelinating Schwann cells could be involved in its regulation, as they have already been shown to modulate axonal cytoskeletal dynamics, which have previously been implicated in the process of axon withdrawal at the NMJ, however this field of study has been undoubtedly neglected. The paranodal junction is formed on either side of the node of Ranvier, and this site has been previously proposed as an ideal site for signalling between the two cell types, due to the close proximity of cell membranes. Nfasc155 is expressed by the myelinating glial cell at the paranode, and so is an ideal candidate protein to study the importance of axon-glial interactions for the normal postnatal development of the mouse PNS. The experiments outlined in the following results chapters were designed to study this role in detail. The following questions were the basis for the experiments designed in results chapters 3-5;

- Chapter 3: Is Nfasc155-mediated axon-glial interaction important for normal rates of synapse elimination at the mouse NMJ? If so, is this role dependent or independent of paranodal formation?
- Chapter 4: How does glial Nfasc155 modulate rates of synapse elimination?
- Chapter 5: Is paranodal development/maturation compromised in a mouse model of SMA with known Schwann cell defects?

Chapter 2

Materials and Methods

2.1 Mouse colonies and maintenance

Breeding pairs of $CNP^{Cre/+} Nfasc^{+/fl} \times CNP^{+/+} Nfasc^{fl/fl}$ and $Caspr^{+/-} \times Caspr^{+/-}$ on a C57BL6 background were established and maintained by the Brophy lab. $CNP^{Cre/+}$ mice (Lappe-Siefke et al., 2003), $Nfasc^{+/fl}$ mice (Zonta et al., 2011), $Caspr^{+/-}$ mice (Gollan et al., 2003), $NF-L^{-/-}$ mice (Zhu et al., 1997) and Taiwanese-SMA mice (Hsieh-Li et al., 2000) were generated as previously reported. Taiwanese SMA mice were maintained using a breeding strategy previously described (Riessland et al., 2010). C57BL6 litters were obtained from in-house breeding stocks at the University of Edinburgh.

The majority of analysis presented in this thesis utilised litters from $CNP^{Cre/+} Nfasc^{+/fl} \times CNP^{+/+} Nfasc^{fl/fl}$ breeding pairs, studies on which have never before been published, and for those reasons an overview of the generation of $CNP^{Cre} Nfasc^{fl/fl}$ mice ($Nfasc155^{-/-}$) along with the genotyping methods can be found in the next section. P3-P18 $CNP^{Cre/+} Nfasc^{fl/fl}$ mice were compared with $CNP^{+/+} Nfasc^{fl/fl}$ or $CNP^{+/+} Nfasc^{+/fl}$ littermate controls. P10-P12 $Caspr^{-/-}$ mice were compared with $Caspr^{+/+}$ littermate controls. Breeding pairs of $NF-L^{+/-} \times NF-L^{+/-}$ on a congenic C57BL6 background were used to generate litters of $NF-L^{+/+}$, $NF-L^{+/-}$ and $NF-L^{-/-}$ mice. These mice were maintained by Geneviève Soucy in the Julien lab, in Laval

University, Montreal. P10 *NF-L*^{-/-} mice were compared with *NF-L*^{+/+} and *NF-L*^{+/-} littermate controls. Taiwanese SMA mice express two copies of the human *SMN2* transgene without any expression of *SMN1*. This produces a mouse model of SMA in which expression of *SMN2* can partially compensate for loss of *SMN1*. These mice display pathological changes in the spinal cord and skeletal muscles typical of the SMA phenotype (Hsieh-Li et al., 2000). Breeding pairs of *SMN*^{-/-} *SMN2*^{tg/tg} X *SMN*^{+/-} on a congenic FVB/NJ background were used to generate litters of *SMN*^{-/-} *SMN2*^{tg/+} and *SMN*^{+/-} *SMN2*^{tg/+} mice. These mice were maintained and genotyped in house by Gillian Hunter in the Gillingwater lab. *SMN*^{-/-} *SMN2*^{tg/+} mice (SMA mice) were compared with *SMN*^{+/-} *SMN2*^{tg/+} mice (controls).

Mice were sacrificed either by inhalation overdose of Isoflurane (Abbott), intraperitoneal injected overdose of Euthatal (Animal Care) or cervical dislocation. All animal experiments were approved by a University of Edinburgh internal ethical review panel and were performed under the relevant personal and project licenses from the United Kingdom Home Office (Project License 60/3891, personal license 60/12972), following the guidelines set out in the Animal Scientific Procedures Act 1986 and EU legislation of 2010. Date of birth was denoted as postnatal day 0 (P0) in all litters.

2.2 Generation of *Nfasc155*^{-/-} mice

To generate mice with a conditional knock-out of Neurofascin in glia, leading to the loss of the glial isoform *Nfasc155* but retention of the axonal *Nfasc186* isoform

($CNP^{Cre/+}$ $Nfasc^{fl/fl}$; $Nfasc155^{-/-}$ mice), the *Cre* recombinase encoding sequence was inserted into the 2', 3'-cyclic nucleotide 3'-phosphodiesterase (*CNP*) locus, restricting expression of *Cre* to glial cells. These mice were generated by the Nave group (Lappe-Siefke et al., 2003). Mice expressing the *Nfasc* floxed allele were generated as previously described, by the Brophy group (Zonta et al., 2011). Breeding pairs of $CNP^{Cre/+}$ X $Nfasc^{+/fl}$ were set up to generate $CNP^{Cre/+}$ $Nfasc^{+/fl}$ mice. Breeding pairs of $CNP^{Cre/+}$ $Nfasc^{+/fl}$ X $Nfasc^{fl/fl}$ were set up to generate mice with a complete knock-out of *Nfasc155* ($CNP^{Cre/+}$ $Nfasc^{fl/fl}$). *Lox P* sites flank exon 4 of the *nfasc* gene so that when *Cre* is also expressed, exon 4 is excised and the gene is inactivated for transcription. *CNP* is expressed embryonically, as early as E12 in the PNS (Yu et al., 1994) and *Nfasc* is normally expressed postnatally at the onset of myelination (Collinson et al., 1998; Tait et al., 2000). *Nfasc155* is therefore completely absent from myelinating glia in $CNP^{Cre/+}$ $Nfasc^{fl/fl}$ mice and unlikely to be expressed in Schwann cells that have not taken up 1:1 relationships with axons. A schematic of how these mice were generated along with the genotypes of the offspring is shown in Figure 2.1A,B.

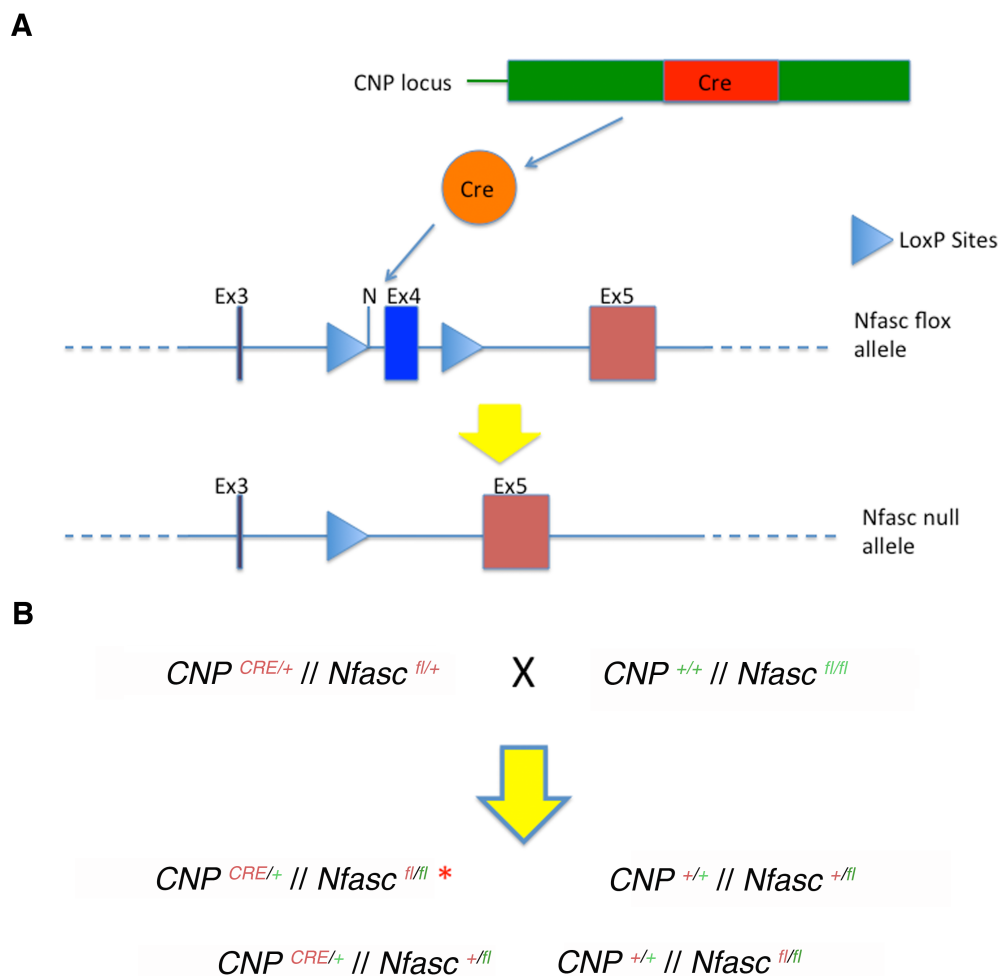


Figure 2.1. Generation of $CNP^{Cre/+} Nfasc^{fl/fl}$ mice ($Nfasc155^{-/-}$). (A) Diagram showing the insertion of *Cre* into the *CNP* locus and its enzymatic activity on the *nfasc* gene with *lox P* sites present. *Cre* cuts out exon 4 as illustrated above, inactivating the *nfasc* gene for transcription, resulting in loss of Nfasc from glial cells ($Nfasc155^{-/-}$). (B) Diagram showing the genotypes of each mouse in a breeding pair, with the resulting possible genotypes of offspring (* $Nfasc155^{-/-}$ mouse).

2.3 Genotyping

Litters from *Caspr*^{+/-} X *Caspr*^{+/-} breeding pairs were genotyped by Veronica Brivio by polymerase chain reaction (PCR). Litters from *NF-L*^{+/-} X *NF-L*^{+/-} breeding pairs were genotyped by Geneviève Soucy by Southern blot. Litters of Taiwanese-SMA mice were genotyped in house by Gillian Hunter as previously described (Hsieh-Li et al., 2000). Litters from *CNP*^{Cre/+} *Nfasc*^{+/fl} X *CNP*^{+/+} *Nfasc*^{fl/fl} breeding pairs were genotyped in house by PCR. Two PCR programs were required to genotype these mice; one PCR to determine if *Cre* was present (Cre PCR), and a second PCR followed by a digest step to determine if *lox P* sites were present in the *nfasc* gene (Nfasc PCR).

A 3mm piece of tail tip from each mouse was digested overnight in 150µl lysis buffer (50ml stock: 2.5ml Tris pH8 1M, 50µl EDTA 0.5M, 625µl SDS 20%, 46.83ml sterile H₂O) with 8µl proteinase K in a 55°C heat block. The next day the samples were centrifuged at 14,000rpm for 5min. A 1:10 unpurified DNA solution of tail tip digest: sterile H₂O was prepared. DNA levels were measured for each sample using a nanodrop (Nanodrop 2000 Spectrophotometer, Thermo Scientific) to calculate the volume required to include 30ng (Nfasc PCR) and 40ng of DNA (Nfasc PCR) per PCR reaction sample. During optimisation of the PCR programs, it was found that the PCR reactions worked best when these amounts of DNA were present in each sample.

Primers were designed for each PCR reaction by Anne Desmazieres and synthesised (by Sigma) as follows:

Cre primers

Forward (CreFW): 5' ACG AGT GAT GAG GTT CGC AA 3'

Reverse (CreRV): 5' GTT TCA CTA TCC AGG TTA CGG 3'

Nfasc primers

Forward (NFFW): 5' GTG CTG ATC CAG CCT AAA GC 3'

Reverse (NFRV): 5' TCA GCT GTT TTG AGC CAC AC 3'

Stocks of each primer were maintained as 100µM concentration and working stocks of 5µM were made. Cre PCR and Nfasc PCR reactions were ran separately. Each PCR reaction sample was prepared for the required program as shown in Table 2.1. The PCR cycles for each PCR program are shown in Table 2.2. The reason for preparing samples in duplicate for the Nfasc PCR is explained below.

Cre PCR	Nfasc PCR (each sample prepared in duplicate)
7.5µl Green Master Mix (Promega) (containing <i>Taq</i> DNA polymerase, dNTPs, MgCl ₂ and reaction buffers)	7.5µl Green Master Mix (Promega)
1.5µl 5µM CreFW	1.5µl 5µM NFFW
1.5µl 5µM CreRV	1.5µl 5µM NFRV
3.5µl sterile H ₂ O	3.5µl sterile H ₂ O

Table 2.1. Mixture of reagents used per sample for Cre and Nfasc PCRs.

Cre PCR	Nfasc PCR
94°C – 2min 55°C – 30s <i>1 cycle</i> 72°C – 1min	94°C – 2min 53°C – 30s <i>1 cycle</i> 72°C – 3min30s
94°C – 15s 55°C – 30s <i>40 cycles</i> 72°C – 1min	94°C – 30s 53°C – 30s <i>40 cycles</i> 72°C – 1min10s
94°C – 15s 55°C – 30s <i>1 cycle</i> 72°C – 10min	94°C – 40s 53°C – 30s <i>1 cycle</i> 72°C – 10min
Expected size band: ~0.8Kb	Expected size bands: 1Kb, 0.7Kb, 0.4Kb

Table 2.2. Cre and Nfasc PCR programs.

Once the PCR reaction had taken place, samples were run on a 1% agarose gel with 0.01% Sybrsafe (Invitrogen) at 120V for 30min. Two PCR reaction samples were set up for each mouse in the *Nfasc* PCR reaction but only one set was ran on a gel. Gels were imaged with ultraviolet (UV) light.

The expected PCR products for each genotype shown in Figure 2.1B are outlined in Table 2.3. Example gels from Cre and *Nfasc* PCRs imaged with UV light are shown in Figure 2.2, for one litter of 8 pups. The Cre PCR resulted in the presence or absence of a 0.8Kb size band in each sample, indicating presence or absence of *Cre* (Table 2.3; Figure 2.2A). The *Nfasc* PCR resulted in various size bands in each sample. A 1Kb size band was the product of PCR on the unaltered *nfasc* gene (ie. *nfasc* in neurons of all mice and in glia of $CNP^{Cre/+} Nfasc^{+/fl}$, $Nfasc^{+/fl}$ and $Nfasc^{fl/fl}$ mice), and 0.7Kb and 0.4Kb size bands resulted from *nfasc* floxed genes that had been cut by Cre (in $CNP^{Cre/+} Nfasc^{fl/fl}$ and $CNP^{Cre/+} Nfasc^{+/fl}$ mice) (Table 2.3; Figure 2.2B). The 1Kb size band appeared in all samples, due to the presence of *Nfasc186* in all mice, so it could not be determined from this PCR reaction alone whether or not the *nfasc* gene in each sample was *fl/fl* or *+/fl*.

NcoI sites were artificially added to the *Lox P* sites inserted in to the *Nfasc* gene. To identify the presence of *Lox P* sites in the *nfasc* gene, an overnight digest was set up on the second set of samples that were run for PCR but were not used for electrophoresis. *NcoI* enzyme (Roche) was used in the digest in a 30 μ l reaction per sample along with other reagents shown below in Table 2.4. *NcoI* enzyme recognises *NcoI* sites and cuts out the DNA between them. Samples were vortexed and

incubated in a heat block at 37°C for 2hr - overnight. The following morning, samples were run on a 1% agarose gel with 0.01% Sybrsafe at 120mV for 30min. Gels were imaged with UV light. *Nfasc*^{+/*fl*} samples showed the presence of 1Kb, 700Kb and 400Kb bands, *Nfasc*^{*fl/fl*} samples did not have the 1Kb band present (Table 2.3; Figure 2.2C).

	Four possible genotypes of offspring			
	<i>CNP^{Cre/+} Nfasc^{fl/fl}</i>	<i>CNP^{Cre/+} Nfasc^{+/fl}</i>	<i>CNP^{+/+} Nfasc^{+/fl}</i>	<i>CNP^{+/+} Nfasc^{fl/fl}</i>
<i>Cre PCR</i>	0.8 Kb band	0.8 Kb band	No band	No band
<i>Nfasc PCR</i>	1 Kb band (<i>Nfasc</i> in neurons) 0.7 Kb & 0.4 Kb bands (floxed <i>Nfasc</i> in glia)	1 Kb band (<i>Nfasc</i> in neurons & glia) 0.7 Kb & 0.4 Kb bands (floxed <i>Nfasc</i> in glia)	1 Kb band (<i>Nfasc</i> in neurons & glia)	1 Kb band (<i>Nfasc</i> in neurons & glia)
<i>NcoI Digest</i>	0.7 Kb & 0.4 Kb bands (floxed <i>Nfasc</i>)	1 Kb band (<i>Nfasc</i> in neurons & glia) 0.7 Kb & 0.4 Kb bands (floxed <i>Nfasc</i>)	1 Kb band (<i>Nfasc</i> in neurons & glia) 0.7 Kb & 0.4 Kb bands (floxed <i>Nfasc</i>)	0.7 Kb & 0.4 Kb bands (floxed <i>Nfasc</i>)
<i>Example in Figure 2</i>	M2	M4, M6	M1, M3, M7, M8	M5

Table 2.3. The expected PCR products for each genotype, following each PCR reaction and NcoI digest. Refer to Figure 2 for examples following the genotyping of one litter of 8 pups.

NcoI Digest
15µl of PCR sample
0.5µl NcoI enzyme (Roche)
3µl buffer H (Roche)
11.5µl sterile H ₂ O

Table 2.4. Reagents used per sample for NcoI digest

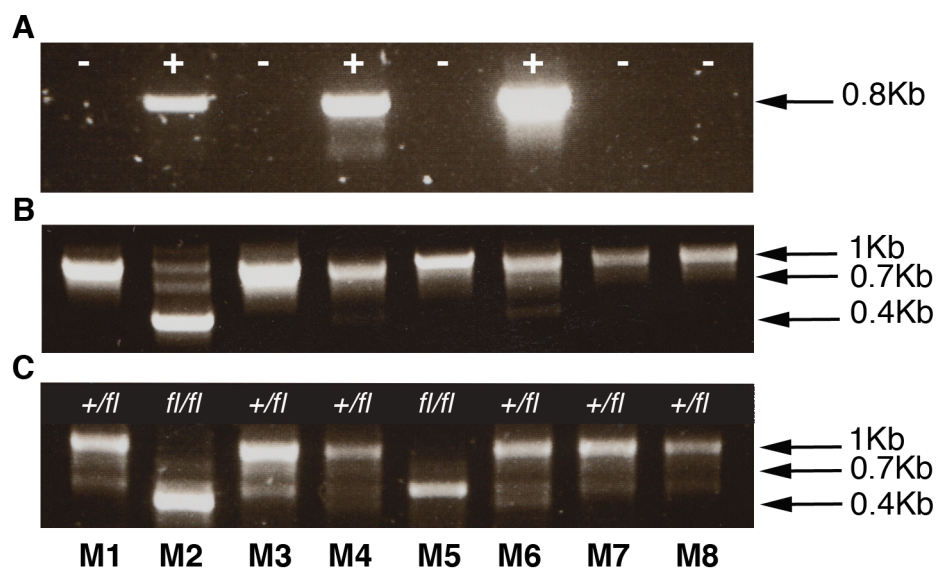


Figure 2.2. Genotyping results for one litter of 8 pups. UV exposure of gels with samples from Cre PCR, Nfasc PCR and NcoI digest. **(A)** The 0.8Kb *Cre* band can be seen in samples from M2, M4 and M6. **(B)** Nfasc PCR reveals 1Kb size bands in all samples and 0.7Kb and 0.4Kb size bands in some samples. **(C)** Digest of Nfasc PCR products with NcoI reveals that M2 and M5 are Nfasc^{fl/fl} positive. M2 is the only mouse positive for *Cre* and Nfasc^{fl/fl} identifying it as a KO (*Nfasc155*^{-/-}).

2.4 Immunofluorescence on whole mount / sectioned muscle

Levator auris longus (LAL), *abductor auricularis longus* (AAL), deep hindlimb lumbrical, tibialis anterior (TA), sternocleidomastoid (SCM) and *transversus abdominis* (TVA) muscles were dissected in 0.1M PBS. TA muscles were dissected and fixed by Geneviève Soucy in Laval University, Montreal. Muscles were fixed in 0.1M PBS 4% para-formaldehyde (PFA) (Electron Microscopy Sciences) for 10min (whole legs for TA were fixed for 30min) at room temperature. Muscles were processed as whole mount (LAL, AAL, lumbricals, TVA and SCM) or muscle sections (TA). TA muscles were sectioned at 100µm on a freezing microtome. Whole muscles/sections were incubated in 2% TritonX in 0.1M PBS for 30min, blocked in a solution of 4% bovine serum albumin (BSA) and 1% TritonX in 0.1M PBS for 30min before overnight incubation with primary antibodies raised against 200 kDa neurofilament / NF-H (rabbit, 1:1000, Abcam), 165 kDa neurofilament / NF-M (mouse, 1:200, Developmental Studies Hybridoma Bank (DSHB)), 70 kDa neurofilament / NF-L (rabbit, 1:1000, Millipore), S100 (rabbit, 1:200, DAKO) and Beta-III-Tubulin (rabbit, 1:1000, Abcam) in blocking solution.

For labelling of paranodes muscles were incubated in 4% TritonX in 0.1M PBS for 30min, blocked in a solution of 4% TritonX and 4% BSA in 0.1M PBS for 30min before overnight incubation with primary antibody against pan-Nfasc (rabbit, 1:1000, Abcam) in blocking solution. Following 3x20 min washes in 0.1M PBS, muscles were incubated in a solution of swine anti-rabbit secondary antibody conjugated to the fluorescent label fluorescein isothiocyanate (FITC) (1:40, Dako) and donkey

anti-mouse secondary antibody conjugated to the fluorescent label Cy3 (1:200; Jackson ImmunoResearch) in 0.1M PBS for 2hr. Muscles were exposed to either alpha-bungarotoxin (BTX) conjugated to tetramethylrhodamine isothiocyanate (TRITC) (TRITC-alpha-BTX; 10 µg/ml, Biotium) or alpha-BTX conjugated to CF633 (Farred-alpha-BTX; 10 µg/ml, Biotium) for 10min, washed several times in 0.1M PBS, whole-mounted in Mowiol (Calbiochem) on glass slides and cover-slipped before imaging.

2.5 Immunofluorescence on teased fibres / sectioned nerve and spinal cord ventral roots

Peripheral nerves and lumbar vertebral column were dissected in 0.1M PBS. Peripheral nerves were fixed for 30min at room temperature, pinned out on dental wax. Lumbar regions of vertebral column were fixed in 4% PFA for 2hr at room temperature. Peripheral nerves were sectioned at 10µm on a cryostat. Fixed sciatic nerve fibres were teased in 0.1M PBS on 3-amino-propyltriethoxysilane-coated slides using acupuncture needles. Peripheral nerves and lumbar spinal cords were sectioned at 10µm on a cryostat. Teased fibres, peripheral nerve sections and spinal cord sections were incubated in a solution of 0.2% TritonX and 5% BSA for 1hr before overnight incubation in primary antibodies against pan-Nfasc (either rabbit, 1:1000, Abcam or; rabbit, 1:500 dilution, Brophy lab), Caspr (rabbit, 1:100, Brophy lab), ankyrin-G (goat, 1:500, Santa Cruz Biotechnology), pan-Na_v (rabbit, 1:200, Alomone Labs), K_v1.1 (rabbit, 1:100, Alomone Labs), kinesin 5A (rabbit, 1:200, Abcam) and NF-L (rabbit, 1:1,000, Millipore). After 3x20min washes in 0.1M PBS,

peripheral nerve teased fibres and sections were incubated in a solution of swine anti-rabbit secondary antibody conjugated to the fluorescent label FITC (1:40, Dako), donkey anti-goat secondary antibody conjugated to the fluorescent label Cy3 (1:500, Jackson ImmunoResearch) and donkey anti-mouse secondary antibody conjugated to the fluorescent label Cy3 (1:200, Jackson ImmunoResearch) for 2hr. Following 3x10min washes in 0.1M PBS, tissue on glass slides was cover-slipped in Mowiol (Calbiochem) before imaging.

2.6 Quantitative Western blots

Western blotting was performed as previously described (Wishart et al., 2012). Briefly, protein was extracted in radioimmunoprecipitation (RIPA) buffer (Thermo-Scientific) with 10% protease inhibitor cocktail (Sigma). 15-30µg of protein per lane was separated by SDS/polyacrylamide gel electrophoresis on 4-12% Bis Tris gradient gels (Invitrogen) and then fast-transferred to polyvinylidene fluoride (PVDF) membrane for 8min (Invitrogen). The membranes were blocked for 30mins using Odyssey blocking buffer (Li-COR) and incubated with primary antibodies in blocking buffer and Tween20 (Beta-actin, rabbit, 1:1000 dilution, Abcam; pan-Nfasc, rabbit, 1:1000 dilution, Abcam; GDNF, rabbit, 1:200 dilution, Santa Cruz; proGDNF, rabbit, 1:200, Alomone Labs; NF-H, rabbit, 1:10,000 dilution, Abcam; NF-L, rabbit, 1:3000 dilution, Millipore; NF-M, mouse, dilution 1:2000 dilution, DSHB; kinesin 5A, rabbit, 1:2500 dilution, Abcam; cytoplasmic dynein, rabbit, 1:1000, Abcam; dynactin, rabbit, 1:1000, Abcam). Odyssey secondary antibodies were added according to manufacturers instructions (Goat anti-rabbit IRDye 680 and Goat anti-

mouse IRDye 800, Odyssey). Blots were imaged using an Odyssey Infrared Imaging System (Li-COR Biosciences). Scan resolution of the instrument ranges from 21-339 μ m and in this study blots were imaged at 169 μ m. Two independent readings were taken per blot to ensure reproducibility of measurements.

A summary of all primary antibodies used for immunofluorescence and Western blotting is shown in Table 2.5.

Antibody	Supplier	Conc.	Tissue	Technique
NF-H	Abcam	1:1000	Muscle	Immunofluor.
		1:10000	Whole Nerve	Western Blot
NF-M	DSHB	1:200	Muscle	Immunofluor.
		1:2000	Whole Nerve	Western Blot
NF-L	Millipore	1:1000	Muscle	Immunofluor.
		1:3000	Whole Nerve	Western Blot
S100	DAKO	1:200	Muscle	Immunofluor.
Beta III Tubulin	Abcam	1:1000	Muscle	Immunofluor.
Pan-Nfasc	Abcam	1:500	Spinal Cord, Sciatic Nerve,	Western Blot
		1:1000	Muscle, Teased Nerve	Immunofluor.
Pan-Nfasc	Brophy Lab	1:500	Teased Nerve	Immunofluor.
Ankyrin G	Santa Cruz	1:500	Teased nerve	Immunofluor.
K _v 1.1	Alomone Labs	1:100	Teased nerve	Immunofluor.
Pan Na _v	Alomone Labs	1:200	Teased nerve	Immunofluor.
Caspr	Brophy Lab	1:100	Teased nerve	Immunofluor.
GDNF	Santa Cruz	1:200	Muscle	Western Blot
proGDNF	Alomone Labs	1:200	Muscle	Western Blot
Kinesin 5A	Abcam	1:200	Nerve Sections	Immunofluor.
		1:2500	Whole nerve	Western Blot
Cytoplasmic Dynein	Abcam	1:1000	Nerve	Western Blot
Dynactin	Abcam	1:1000	Nerve	Western Blot
Beta-Actin	Abcam	1:1000	Muscle	Western Blot

Table 2.5. Summary of all primary antibodies used with details of supplier, concentration, tissue and techniques used.

2.7 Microscopy

Muscle, nerve and spinal cord preparations were viewed using a phase contrast microscope with a chilled charged-coupled device (CCD) camera (40x objective, for muscle fibre measurements), a standard epi-fluorescence microscope with a chilled CCD camera (20x and 40x objective, 0.8 NA, Nikon IX71 microscope, Hammamatsu C4742-95; for endplate area, endplate number and endplate maturation), an upright fluorescence microscope (40x and 60x objective, for polyinnervation and axonal input per NMJ), or a laser scanning confocal microscope (40x and 60x objective, 1.4 NA, Zeiss LSM710; number of axons innervating a muscle, polyinnervation counts, peripheral nerve axon/ pre-terminal axon/ axon terminal and spinal cord ventral root fluorescence intensity, axonal input per NMJ and imaging of nodes of Ranvier/paranodes/juxtaparanodes). On the upright and inverted fluorescent microscopes TRITC-labelled preparations were imaged using 543nm excitation and 590nm emission optics and FITC-labelled preparations utilised 488nm excitation and 520nm emission optics. For confocal microscopy, 405nm, 488nm, 543nm and 633nm laser lines were used for excitation and confocal Z-series were merged using Zen software. Identical confocal microscope settings were used between groups when imaging sciatic and tibial nerve sections, spinal cord sections and muscle preparations for fluorescence intensity measurements. Images shown are z-projections. Spinal cord sections for motor neuron cell body counts were imaged using a light microscope with a camera (Leica DMLB, DFC480 camera).

2.8 Quantification of immunofluorescently-labelled muscles, nerves and ventral roots

30-80 endplates in each LAL, 30 endplates in each AAL, 60 endplates in each TA and 30 endplates in each lumbrical muscle were assessed with the operator blind to genotype. This was achieved by carrying out the quantification before performing the PCR genotyping on each mouse. Only clearly identified, non-overlapping and en-face endplates were analysed. The number of axons innervating the LAL was quantified by taking a z-stack confocal image of the nerve to create a digital 3D reconstruction. By scanning through the axon bundle along the Z-axis individual axons were visualised in the XY plane in cross section. Individual muscle fibre diameters (>75 per muscle) were measured in ImageJ from x20 phase-contrast images from teased muscle fibre preparations. Endplate area measurements (>40 per muscle) were made in ImageJ with outlines manually traced to calculate area. Endplate maturation was assessed as previously described (Caillol et al., 2012) with 60-160 endplates analysed per muscle. Fluorescence intensity measurements (45-60 pre-terminal and terminal axons per muscle, 1000-1500 axons per nerve, 100-120 axons per ventral root) were carried out using ImageJ, by measuring ten points of intensity along terminal axons labelled for NF-H, NF-M or NF-L, from branch point to neuromuscular junction, or by drawing a small box within a transversely sectioned axon in the sciatic/tibial nerve and spinal ventral root to measure the average intensity of kinesin 5A and NF-L. The same size box was used to measure intensity in all axons. In muscles double immunolabelled for NF-M/ NF-L and NF-H/ NF-M fluorescence intensity between neurofilaments was matched in the pre-terminal

axons before fluorescence measurements were taken. A box was drawn around the endplate to measure axon terminal intensity of each neurofilament subunit. A ratio of nerve terminal/ pre-terminal axon fluorescence intensity was then calculated to accurately compare the levels of each neurofilament in axon terminals. Quantification of terminal Schwann cell (TSC) number per NMJ was carried out using single plane confocal images, acquired from Z-stacks, and counting the number of 4', 6-diamidino-2-phenylindole (DAPI) positive cells that were surrounded by S100 staining and in contact with each endplate.

2.9 Quantification of molecular domains

Paranodes, nodes and juxtaparanodes were analysed and measured using ImageJ. For paranodes, measurements were taken using the 'straight line' tool. A line was drawn from the nodal boundary of the paranode along its longitudinal length. Due to the asymmetrical development of flanking paranodes at single nodes of Ranvier (Tao-Cheng and Rosenbluth, 1982), paranodal length was not averaged at each node of Ranvier. Nodes of Ranvier were measured by using the 'straight line' tool and drawing a line across its middle longitudinal length.

2.10 Quantification of spinal cord motor neurons

Spinal cords from P11 mice were dissected, post-fixed in 4% paraformaldehyde (PFA) for 2hr, cryoprotected in 30% sucrose overnight, incubated in a 50:50 solution of OCT medium:30% sucrose before rapidly embedding and freezing on dry ice.

10µm thick horizontal sections were cut on a cryostat and stained with 0.5% cresyl violet with 0.04% acetic acid. A minimum of 30 non-adjacent sections from the lumbar region of the spinal cord were examined for large, polygonal, Nissl positive cells in the ventral horn of the spinal cord anterior to the central canal. Quantification was carried out on sections 100µm apart to avoid double counting of neurons. Quantification was carried out blinded to the genotype.

2.11 Electrophysiology

Electrophysiology of conduction velocity in the sciatic nerve was carried out in *Nfasc155^{-/-}*, *Caspr^{-/-}* and littermate controls at P11 as previously described (Court et al., 2004), in collaboration with Diane Sherman. Briefly, sciatic nerves from P10 *Nfasc155^{+/+}* and *Nfasc155^{-/-}* mice were transferred from oxygenated Krebs solution to an isolated chamber containing an array of Ag/AgCl electrodes with 1mm intervals and surrounded by liquid paraffin maintained at 37°C for periods no longer than 10min. The proximal end of the nerve was excited by a square wave (0.1ms, 0.1–1.5 V) and the conduction distance was varied from 2mm to 7mm by altering the stimulating electrode position. The voltage was adjusted to ensure exact duplication of the active population, and the compound action potential was viewed on a storage oscilloscope. Values were stored as digitised signals with the use of Chart software (MacLab System). Conduction times were measured as previously described (Gillespie et al., 2000).

Electrophysiology on nerve-muscle preparations from *Nfasc155^{-/-}* mice and littermate controls ranging from P10-P13 was carried out on *flexor digitorum brevis* (FDB) muscles as previously described (Ribchester et al., 2004), in collaboration with Richard Ribchester and Kosala Dissanayake. A minimum of 60 muscle fibres was recorded from per mouse. Briefly, mice aged P10 to P13 were sacrificed by cervical dislocation and FDB muscles with their tibial nerve supplies were dissected in mammalian physiological saline (composition in mM: NaCl, 120; KCl, 5; CaCl₂, 2; MgCl₂, 1; NaH₂PO₄, 0.4; NaHCO₃, 23.8; D-glucose, 5.6; bubbled to equilibrium with a 5% CO₂/95% O₂). After dissection, muscles were examined for evidence of sustained, tetanic muscle contraction by stimulating the tibial nerve at 30Hz for ~2s via a suction electrode connected to a Harvard Advanced Double Pass stimulator (Harvard Apparatus, Kent, UK), while observing muscle contractile responses under a dissecting microscope. Preparations were then transferred and pinned through their tendons in a Sylgard-lined recording chamber. A glass microelectrode filled with 5M potassium acetate (approximate resistance 30-40 MΩ; Sutter Instruments P87 puller; Sutter, Novato, USA) was used to impale 30 muscle fibres, selected arbitrarily. Resting membrane potentials of muscle fibres in these delicate preparations frequently depolarised from initial values of around -65mV but were discarded only if the resting potential became more positive than -25mV. The tibial nerve was then stimulated with single pulses, 0.2-1.0ms in duration and up to 10V in amplitude via a Digitimer 4030 Programmer and DS2 stimulator (Digitimer, Welwyn Garden City, UK). DC-coupled spontaneous miniature endplate potentials (MEPPs) and evoked endplate potentials (EPPs) or action potentials were recorded via an Axoclamp 2B amplifier (Molecular Devices, Sunnyville), Neurolog (Digitimer) NL106 AC-DC

amplifier and NL125 filters (low pass set at 2KHz), then digitised at 50kHz via a CED micro1401 interface (Cambridge Electronic Designs, Cambridge, UK). Mains (50Hz) interference was eliminated using a Quest Scientific Humbug filter unit (Digitimer, UK). Data capture and analysis was via WinWCP software (version 4.0, Strathclyde Electrophysiology Software, UK) running on a Dell personal computer under Windows XP. Data were statistically analysed using Graphpad Prism software and power calculations were made using an online calculator (<http://www.dssresearch.com>).

2.12 Electron microscopy

Sciatic nerves were prepared for electron microscopy and analysed for G-ratio counts as previously described (Sherman et al., 2012). Briefly, sciatic nerves were fixed for 48hr in 4% PFA: 2.5% glutaraldehyde at 4°C before incubation in 1% osmium tetroxide in 0.1M phosphate buffer for 30min. Following dehydration through an ascending series of ethanol solutions and propylene oxide, whole nerves were embedded in blocks of Durcupan resin. Ultrathin sections (60nm) were cut and collected on formvar-coated grids (TAAB), stained with uranyl acetate and lead citrate and imaged on a Philips CM12 transmission electron microscope equipped with a Gatan digital camera. Sciatic nerve fibres were analysed for G-ratio counts using ImageJ. 30-50 fibres were measured per nerve.

2.13 Proteomic analysis

Sciatic-tibial nerves from *Nfasc155*^{+/+}, *Nfasc155*^{-/-}, *Caspr*^{+/+} and *Caspr*^{-/-} mice (N=5 per genotype) were pooled into 4 groups for each genotype, for isobaric tag for relative and absolute quantitation (iTRAQ) proteomic analysis. Protein was extracted from tissues in 1ml of buffer containing 6M urea, 2M thiourea, 2% CHAPS and 0.5% SDS in dH₂O with 1% proteinase inhibitor (Roche). Tissues were homogenised in M tubes (Miltenyi Biotec Ltd. UK) using gentleMACS dissociator machine on M tube protein cycle followed by centrifugation at 300g for 2min at room temperature. Homogenates were left on ice for 15min prior to centrifugation at 20,000g for 20min at 4°C. Following extraction, protein concentrations of the soluble homogenate fractions were determined via BCA assay and used for downstream proteomic analysis as previously described (Wishart et al., 2010; Wishart et al., 2012; Wishart et al., 2014).

Douglas Lamont in the 'FingerPrints' proteomics facility carried out the following steps in the University of Dundee. Samples were precipitated with -20°C chilled acetone (1:4, vol/vol) and stored at -20°C overnight. The precipitates were spun at 4°C for 10min then washed with an acetone: water mixture (4:1, vol/vol) twice prior to air-drying. The pellets were then resuspended in iTRAQ sample buffer (25µl 500mM triethylamine-NH₄ bicarbonate (TEAB), 1µl denaturant (2% SDS) and 2µl of reducing agent (tris(2-carboxyethyl)phosphine (TCEP)). The samples were allowed to incubate for 1hr at 60°C prior to protein re-estimation in triplicate (3 x 1µl) by microBCA assay (Pierce).

20 μ l of 200Mm dithiothreitol (DTT) was added to each sample then heated at 56°C for 10min. This was then diluted with 200 μ l FASP1 (8M UREA, in 100Mm Tris/HCL pH8.5). Filters (Vivacon 500, 30Kmwco HY, Satorius Stedium Biotech) were washed 3 times with 100 μ l MilliQ then 1 in 100 μ l FASP1 (8M UREA, in 100Mm Tris/HCL pH8.5). Samples were centrifuged for 10min and added to filters. Each filter was washed with 200 μ l FASP1 five times and centrifuged for 25min at 11rpm, in a 15 degree fixed angle rotor. Flow through from the filter vials were individually decanted into 1.5ml low-bind tubes for storage. Each filter was washed twice with 200 μ l FASP2 (100Mm Tris/HCL pH8.5). 200 μ l of fresh 50Mm IAA in FASP2 was added to each filter vial then stored in the dark with gentle shaking at room temperature for 30min before spinning through the IAA for 25min at 11rpm, 15 degree. Each filter was washed three times with 200 μ l FASP3 (100Mm TEAB) and spun for 25mins at 11rpm, 15 degrees. Fresh trypsin (1 μ g each filter) was prepared with FASP3 to give a 1:100 enzyme: protein ratio and incubated for 4-6hr at 30 degrees. Samples were re-spun for 25min at 11rpm to elute the peptides into a new tube. 200 μ l 500mm NaCl was added to each vial and spun for 25min at 11rpm at 15 degree before drying by speedvac. Samples were resuspended with 25 μ l dissolution buffer. 70 μ l of ethanol was added to each reagent vial (iTRAQ 4plex), vortexed for 1min, then spun. Each tag was transferred to a separate sample (see below) before vortexing and incubating for 1hr at room temperature. The pH was checked for each sample to ensure pH was greater than 8.0 prior to incubation for 1hr at room temperature. 100 μ l of water was added to each sample to quench the reaction prior to pooling of the four iTRAQ labelled samples and subsequent drying by vacuum centrifugation as previously described (Wishart et al., 2010; Wishart et al.,

2012; Wishart et al., 2014). The iTRAQ tags were assigned to samples as follows: samples corresponding to the genotypes *Nfasc155*^{+/+}, *Nfasc155*^{-/-}, *Caspr*^{+/+} and *Caspr*^{-/-} were labelled with 117, 116, 115, and 114 respectively.

The pooled iTRAQ sample was resuspended in 120µl 5mM-Tris-HCL (pH=8) and separated with a SAX column (Dionex ion pac AS 24, 2 by 250mm) across a 0 to 100% gradient of Buffer A (5mM Tris-HCL in H₂O pH=8) to Buffer B (5mM Tris-HCL in H₂O pH=8) in 500mM NaCl pH=8 at a flow rate of 0.3 ml/min for 43 minutes. 20 fractions were collected. Each fraction was run on an LTQ Orbitrap Velos Pro with HCD fragmentation across 2hr gradients.

Raw data files were converted to mascot generic file (mgf) and searched against (IPI Mouse, version 10/02/2014) through Proteome discoverer (V 1.4) with the Mascot search engine (v 2.3.2). Database searching used the following specified parameters: precursor ion mass tolerance of 10 p.p.m., MS/MS fragment ion mass tolerance of 0.06 Da and iTRAQ fragment ion mass tolerance of 0.2 Da. The enzyme was specified as trypsin with one missed cleavage permitted, oxidation of methionine residues were allowed as variable modifications and N-terminal (iTRAQ), lysine (iTRAQ) and carbamidomethyl modification of cysteine residues were set as fixed modifications and the taxonomy was selected as Mus. The identification criterion was at least two unique peptides by MS/MS with the most stringent search settings in order to yield the most reliable data for iTRAQ quantification (peptide rank 1 and total ion score confidence intervals of at least 95%). Peptides were reported as identified iTRAQ peptides only if they met the following criteria: iTRAQ ratio of

greater than 0, all N-terminal and lysine residues were labelled and did not include tyrosine iTRAQ modification.

To obtain further insights into cellular pathways and protein interaction networks modified as a result of the *Nfasc155*^{-/-} and *Caspr*^{-/-} genotypes, Ingenuity Pathway Analysis (IPA) software (Ingenuity Systems) was used. This analysis was carried out in conjunction with Dr. Thomas Wishart in the University of Edinburgh. All proteins submitted to IPA software for bioinformatics analyses were identified by >1 unique peptide and had expression levels either increased or decreased >20% in *Nfasc155*^{-/-} or *Caspr*^{-/-} mice compared to littermate controls. IPA dynamically generates networks of gene, protein, small molecule, drug and disease associations on the basis of 'hand-curated' data held in a proprietary database. Changes in specific protein interaction networks were identified on the basis of the number and percentage of candidate proteins contributing to the entire network.

2.14 Statistical analysis

All data were collected in Microsoft Excel spreadsheets and statistical analyses were performed using GraphPad Prism software. *P* values <0.05 were considered to be statistically significant. All bar charts are shown as mean±s.e.m. The statistical tests used on the data presented in this thesis were the student t-test (including one-tailed t-test) and Mann-Whitney U-test. The student t-test was used on unpaired continuous data that was normally distributed and with homogenous variances in both groups. The one-tailed t-test was chosen when a certain outcome was expected from the

analysis. The Mann-Whitney U-test was used on non-parametric data when no assumptions about homogeneity of variances or normal distributions was required.

Chapter 3

Nfasc155-mediated glial cell modulation of developmental synapse elimination in the peripheral nervous system

3.1 Introduction

As discussed in Chapter 1, it has been known for some time that non-neuronal cell types, such as glial cells and muscle fibres, can contribute to influence the outcome of synapse elimination at the neuromuscular junction (NMJ). For example, glial cell lysosomal activity is known to play a secondary role by engulfing unwanted axonal debris, without affecting the rate of synapse elimination (Song et al., 2008), whereas limited growth factor supply in muscle is thought to play a more primary role, regulating the rate of this process (English and Schwartz, 1995; Kwon et al., 1995; Jordan, 1996; Nguyen et al., 1998). However, the possibility of a primary role for glial cells in regulating synapse elimination in the PNS has yet to be comprehensively studied, specifically the role of myelinating glial cells.

3.1.1 Contribution of non-neuronal cell types to synapse elimination

It is believed that during synapse elimination, innervating nerves at the same NMJ compete for a limited supply of muscle-derived neurotrophic factor, driving the process of synapse elimination by allowing the axons that receive more growth factor

to grow and take over territory at the endplate (Bennett and Robinson, 1989). Further evidence for this was provided by studies showing how an unlimited supply of a neurotrophic factor in skeletal muscle, either by genetic over-expression or local injection, prolonged the process of synapse elimination (English and Schwartz, 1995; Kwon et al., 1995; Jordan, 1996; Nguyen et al., 1998).

Most of our current understanding surrounding the role of glial cells during synapse elimination in the PNS has been gained from studies on the role of end-stage debris clearance by lysosomal activity (Bishop et al., 2004; Song et al., 2008; Fuentes-Medel et al., 2009; Eroglu and Barres, 2010; Chung and Barres, 2012). Lysosomes degrade macromolecules derived from the extracellular space through endocytosis or phagocytosis (Saftig and Klumperman, 2009), including the unwanted debris that retracting axons at developing NMJs leave behind (Song et al., 2008). However, the above studies do not show any evidence for glial cells acting as drivers of the elimination process; rather they suggest a secondary, passive role for them during synapse elimination. As competition for innervation of motor endplates proceeds and losing axons retract, surrounding glial cells engulf the unwanted axonal debris in lysosomes, for recycling or degradation (Song et al., 2008). This activity is prevented in a mouse model of lysosomal storage disease resulting in a high percentage of retreating axons and retraction bulbs at NMJs (Song et al., 2008). There was no significant difference in the percentage of polyinnervated endplates between the mouse model of lysosomal storage disease and control mice at the same age, suggesting that lysosomal activity is not crucial for initiating or driving the process, rather it but becomes activated to degrade the material of an axon that has already

vacated the endplate and lost the competition to the other innervating axons (Song et al., 2008).

The studies outlined above depict a secondary role for lysosomal activity, ensuing the elimination of inputs rather than driving it. However, a more recent paper has proposed the idea that lysosomal activity by non-myelinating cells at the NMJ (terminal Schwann cells (TSCs)) may also play a primary role in regulating the outcome of synapse elimination (Smith et al., 2013), by engulfing material in healthy axons that are still innervating the endplate. This study was specific to TSCs, the non-myelinating capping glial cells at the NMJ, and was purely descriptive. Furthermore, there was no molecular insight provided as to how TSCs may drive the process. Therefore, we have yet to discover a clear regulatory role for glial cells in developmental synapse elimination in the PNS as well as the molecular mediators of this process.

3.1.2 The possible contribution of myelinating glial cells to the regulation of synapse elimination

One area of research that has not been explored fully is that surrounding the possible role for myelinating glial cells in the regulation of synapse elimination. Found along the entire length of motor axons, from the cell body in the ventral horn of the spinal cord to the pre-terminal axon targeting a muscle fibre, are myelinating Schwann cells, which form segments of myelin and are closely associated with the underlying axons. As discussed in Chapter 1, the presence of myelin forms molecular domains along

axons. The paranode is one of these molecular domains, flanking the node of Ranvier, and is a site of physical axon-glia interaction (Sherman and Brophy, 2005). At the paranode, neurofascin155 (Nfasc155) expressed by the glial cell, forms a physical interaction with Caspr & contactin, both of which are expressed by the axon (Charles et al., 2002). In the absence of Nfasc155, paranodal junctions do not form, which results in loss of Schwann cell anchorage to the axon, and an increase in the distance between apposing glial and axon membranes (Sherman et al., 2005). Nfasc155 is therefore an essential protein in the formation of physical axon-glia interactions.

As discussed in detail in Chapter 1, myelinating glial cells play a fundamental role in the stages of the development, maturation and regeneration of axons in the PNS, and so it is logical to predict that they may also be playing a role during postnatal synapse elimination. In fact, previously published studies have hinted at the possibility of a role for myelinating Schwann cells in shaping neural innervation in skeletal muscle, although they did not directly study synapse elimination. During synapse elimination at the NMJ, the cytoskeleton of innervating axons is under continuous remodelling as losing axons diminish in size and form retraction bulbs and those that win take over the synapse and increase in axon diameter (Bixby, 1981; Riley, 1981; Sanes and Lichtman, 1999; Keller-Peck et al., 2001). It has already been shown that local signals emanating from myelinating Schwann cells can alter cytoskeletal dynamics in the underlying axons. A study by Cole et al. in 1994 reported on a line of transgenic mice that displayed a hypomyelinating phenotype, which resulted in increased neurofilament density and decreased neurofilament phosphorylation in the underlying axons of the sciatic nerve. From this study it was

deduced that signals from myelinating Schwann cells modulate neurofilament composition and phosphorylation (Cole et al., 1994).

More recently it has been shown that myelinating Schwann cells provide signals that modulate neurofilament composition *in vitro* (Monsma et al., 2014). This study used *in vitro* assays of neuron/Schwann cell co-cultures to study the transport of neurofilaments in myelinated versus unmyelinated segments of the same axon. They found that neurofilament transport was slower in myelinated versus unmyelinated regions, correlating with the presence or absence of a Schwann cell (Monsma et al., 2014). It is clear from the studies presented above that signals emanating from myelinating Schwann cells are essential for maintaining cytoskeletal integrity in the underlying axons. Based on this evidence it is possible that Schwann cells could be providing local signals to the axons to modulate axon cytoskeletal changes and, consequently, their pruning during developmental synapse elimination in the PNS. Due to the close proximity of glial and axonal membranes at the paranode, this molecular domain has been proposed as an ideal site for signalling between the cells (Boyle et al., 2001; Sherman et al., 2005). Nfasc155 is therefore ideally localised to play a role in signalling cascades, such as those modulating the axonal cytoskeleton, from the glial cell to the axon.

3.1.3 Neurofascin structure and function

Nfasc was first identified in 1987, as a cell-surface glycoprotein involved in neurite-neurite interactions. It was found to be primarily expressed in neurite-rich areas of

the developing chick nervous system and believed to play a role in axon growth (Rathjen et al., 1987). This study also revealed the presence of multiple Nfasc isoforms, including the Nfasc155 and Nfasc186 isoforms mentioned throughout this thesis. A later study on *Nfasc* using sequence analysis confirmed that *Nfasc* contains structural elements of proteins implicated in axonal growth, and is closely related to *neuronal cell adhesion molecule (NrCAM)* (Volkmer et al., 1992). This study also proposed that Nfasc is encoded by a single gene and its pre-mRNA undergoes alternative splicing to account for the different sized Nfasc proteins, including Nfasc186 and Nfasc155. Analysis of the expression of *Nfasc* in the mammal revealed post-natal expression of *Nfasc* (Moscoso and Sanes, 1995). The 186 isoform of Nfasc was found to be localised to axon initial segments and nodes of Ranvier, associating with ankyrin G (Davis et al., 1996) and Na_v channels (Ratcliffe et al., 2001). The Nfasc155 isoform was later found to be an essential component of axon-glia interactions at the paranode, expressed by the glial cell and interacting with the Caspr/contactin complex on the axon surface (Charles et al., 2002).

3.1.4 *Nfasc155*^{-/-} mice

Nfasc155^{-/-} mice were generated using the Cre-loxP method as discussed in Chapter 2. To generate mice with a conditional knock-out of Neurofascin in glia, leading to the loss of the glial isoform Nfasc155 but retention of the axonal Nfasc186 isoform, the *Cre* recombinase encoding sequence was inserted into the *CNP* locus, restricting expression of *Cre* to myelinating glial cells ie. Myelinating oligodendrocytes and Schwann cells (Lappe-Siefke et al., 2003). Mice expressing the *Nfasc* floxed allele

were generated as previously described, by the Brophy group (Zonta et al., 2011). *Lox P* sites flank exon 4 of the *nfasc* gene so that when *Cre* is also expressed, exon 4 is excised and the gene is inactivated for transcription. *CNP* is expressed embryonically, as early as E12 in the PNS (Yu et al., 1994) and *Nfasc* is normally expressed postnatally at the onset of myelination (Collinson et al., 1998; Tait et al., 2000). *Nfasc155* is therefore completely absent from myelinating glia in *CNP^{Cre/+} Nfasc^{fl/fl}* (*Nfasc155^{-/-}*) mice and unlikely to be expressed in Schwann cells that have not taken up 1:1 relationships with axons.

Considering the close association between myelinating Schwann cells and the underlying axons, along with a previously well-established role for these glial cells in maintaining axon stability, published literature has already hinted at the possibility of such a regulatory role for myelinating Schwann cells during development of PNS circuitry. However, this area of research has undoubtedly been neglected. To provide a comprehensive and detailed study on the potential role for myelinating glial cells in the regulation of developmental synapse elimination in the PNS, a mouse model lacking a key glial cell protein for axon-glial interaction at the paranode (*Nfasc155^{-/-}*) was used. The experiments outlined in this chapter were designed to test the hypothesis that myelinating glial cells are capable of modulating rates of developmental synapse elimination in the PNS, mediated through *Nfasc155*-dependent axon-glial signalling.

3.2 Results

3.2.1 *Nfasc155*^{-/-} mice lack *Nfasc155* and have disrupted paranodes

Nfasc155^{-/-} mice were used to study the role of myelinating glial cells during developmental synapse elimination. The generation of *Nfasc155*^{-/-} mice has been described in detail in Chapter 2. *Nfasc155*^{-/-} mice lack the glial isoform of neurofascin, which is found in Schwann cells and oligodendrocytes. As a result, you would expect paranodal junctions to be absent from these mice because the glial counterpart responsible for interacting with the Caspr/contactin complex has not been expressed (Charles et al., 2002). Paranodes are found along the entire length of myelinated nerves and so, to confirm the loss of *Nfasc155* and subsequent disruption to the paranode, teased fibres of sciatic nerve from *Nfasc155*^{-/-} mice and control littermates at P10 were immunolabelled using antibodies recognising nodal and paranodal proteins. Anti-pan-Nfasc was used to identify nodal and paranodal regions as it will recognise both the glial isoform (*Nfasc155*) and axonal isoform (*Nfasc186*) of this protein. Anti-ankyrin G was used to label the node of Ranvier, as this protein interacts with Na_v channels at the node.

Immunofluorescence on teased sciatic fibres using these antibodies confirmed a loss of *Nfasc155* at the paranodal junctions in *Nfasc155*^{-/-} mice, with *Nfasc186* (the axonal isoform of Nfasc) and ankyrin G remaining at the node of Ranvier, as expected (Figure 3.1A,B). *Nfasc155* interacts with Caspr, which is present on the axonal surface, and so without *Nfasc155* to form an interaction with, lack of Caspr

localisation at the paranode would also be expected in *Nfasc155*^{-/-} mice (Charles et al., 2002) (Figure 3.1A). This was observed when teased sciatic fibres from *Nfasc155*^{-/-} mice were also immunolabelled for Caspr (Figure 3.1B). In contrast, littermate controls displayed correct localisation of Nfasc155 and Caspr at paranodes (Figure 3.1B). A Western blot on peripheral nerve (trigeminal nerve) from *Nfasc155*^{-/-} mice and littermate controls at P6 confirmed a complete loss of glial Nfasc155 protein, with retention of the axonal Nfasc186 isoform (Figure 3.1C). The trigeminal nerve was used because the large peripheral nerves in the leg, such as the sciatic and femoral, were being used for another experiment.

3.2.2 Nfasc155^{-/-} mice display a severe tremor

Nfasc155^{-/-} mice were virtually indistinguishable from control littermates up until post-natal day 12 (Figure 3.2A), with similar body weights (Figure 3.2B), activity levels and gross patterns of behaviour. However, a notable whole body tremor was detected in *Nfasc155*^{-/-} mice from ~P12 onwards, becoming progressively worse until their premature death due to unknown causes occurring ~P18. *Nfasc155*^{-/-} mice also failed to increase their body weight from P11 onwards and declined in weight, with similar body weights recorded at P3 and P18 (P3: 2.6g, P18: 3.2g; Figure 3.2B). *Nfasc155*^{+/+} mice in contrast had reached an average weight of 10g by P18.

3.2.3 *Nfasc155*^{-/-} mice display normal ultrastructure of peripheral nerve

Although a key glial cell protein for axon-glia interaction was lacking in the *Nfasc155*^{-/-} mice, ultrastructural analysis of the sciatic nerve using transmission electron microscopy revealed normal myelin formation and compaction in *Nfasc155*^{-/-} mice (Figure 3.3A). G-ratio measurements (see methods) revealed normal thickness of myelin relative to axon diameter in *Nfasc155*^{-/-} mice (Figure 3.3B). Average axon diameter in the sciatic nerve was also similar between groups (Figure 3.3C). G-ratio plotted vs. axon diameter revealed a similar spread between groups (Figure 3.3D). These results indicate that glial *Nfasc155* is not required for formation or maintenance of myelin, consistent with previous studies elucidating on the role of neurofascin isoforms (Sherman et al., 2005).

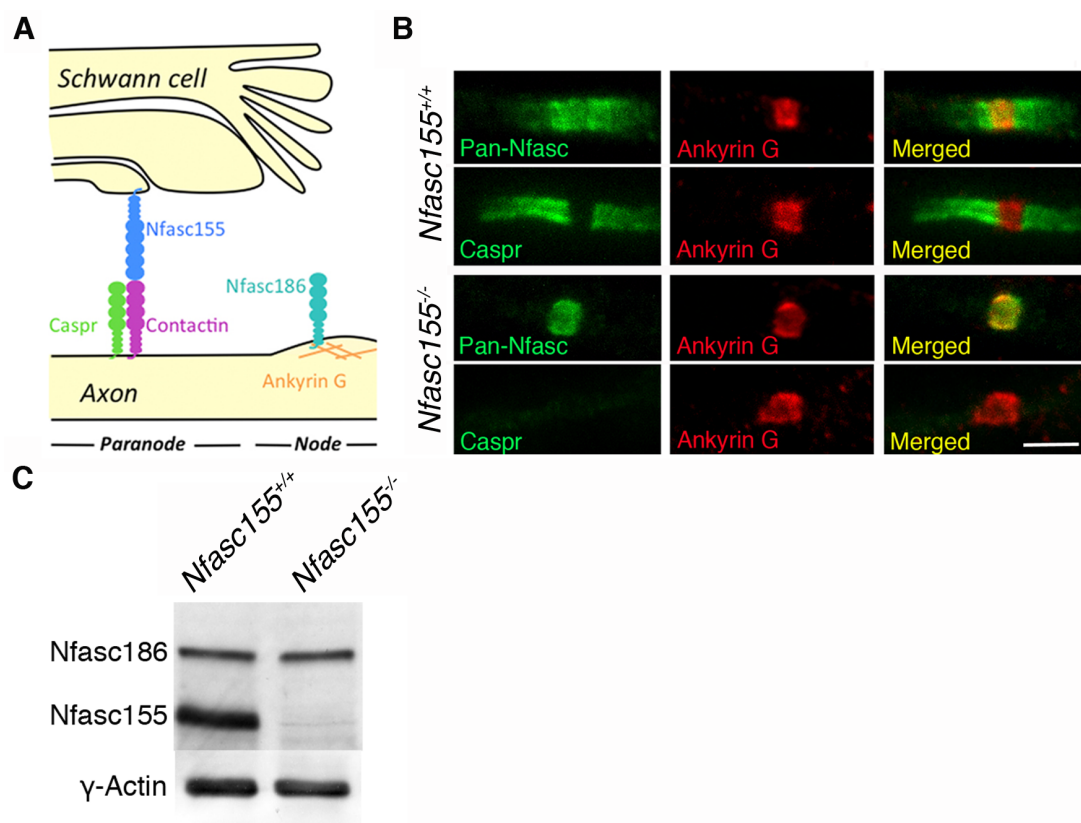


Figure 3.1. *Nfasc155^{-/-}* mice lack Nfasc155 and have disrupted paranodes*.

(A) Simplified schematic of the paranode, showing the glial (Nfasc155) and axonal (Caspr/contactin) proteins that interact to form the junction. Nfasc186 can be seen at the node of Ranvier, along with ankyrin G, which anchors Na_v channels to the node. (B) Confocal micrographs of *Nfasc155^{+/+}* and *Nfasc155^{-/-}* teased sciatic fibres displaying single nodes of Ranvier with flanking paranodes, immunolabelled for pan-Nfasc, Caspr and ankyrin G, showing loss of Nfasc155 and Caspr from paranodal regions of *Nfasc155^{-/-}* mice. Pan-Nfasc labels the node of Ranvier in *Nfasc155^{-/-}* as expected, as the Nfasc186 isoform is unaffected. Scale bar 5 μm . (C) Western blot on P6 trigeminal nerve confirming the results of the immunofluorescence assay showing absence of Nfasc155 and unchanged levels of Nfasc186 in (*Nfasc155^{-/-}*) mice (N=7 mice pooled per genotype). Gamma-actin was used as a loading control, as shown.

* *Western blot (C) carried out by Dr. Anne Desmazieres.*

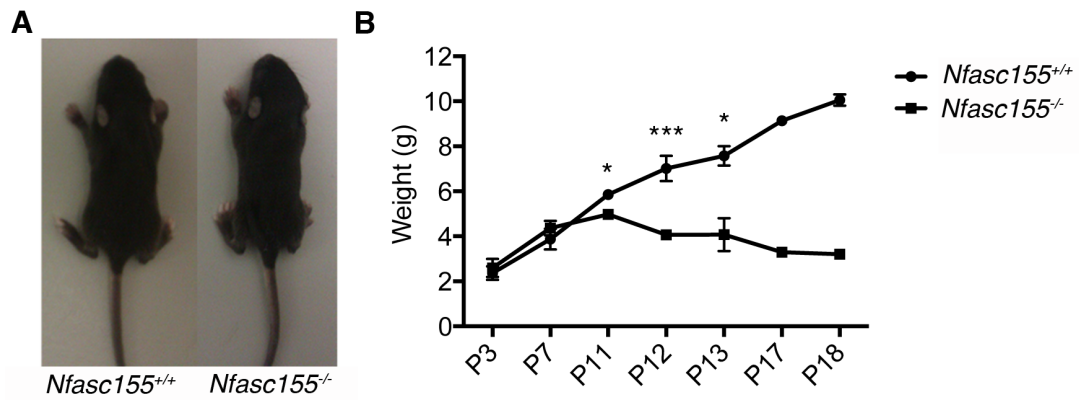


Figure 3.2. *Nfasc155^{-/-}* mice display a normal gross phenotype until ~P12. **(A)** *Nfasc155^{+/+}* and *Nfasc155^{-/-}* mice at P11 showing no obvious difference in size or gross appearance. **(B)** Weight curve of *Nfasc155^{-/-}* mice and control littermates showing no significant difference between genotypes until P11 (P3, unpaired t-test, N=5 for *Nfasc155^{+/+}*, N=3 for *Nfasc155^{-/-}*; P7, unpaired t-test, N=5, N=3; P11, p=0.0284, unpaired t-test, N=6, N=4; P12, p=0.0002, unpaired t-test, N=6, N=6; P13, p=0.006, unpaired t-test, N=4, N=4; P17, N=3, N=1; P18 N=2, N=1). *Nfasc155^{-/-}* mice began to lose weight from P11, around the time that a whole body tremor became noticeable, and displayed an average weight at P18 that was similar to that recorded at P3 (P3: 2.6g, P18: 3.2g). *Nfasc155^{+/+}* mice had reached an average weight of 10g by P18.

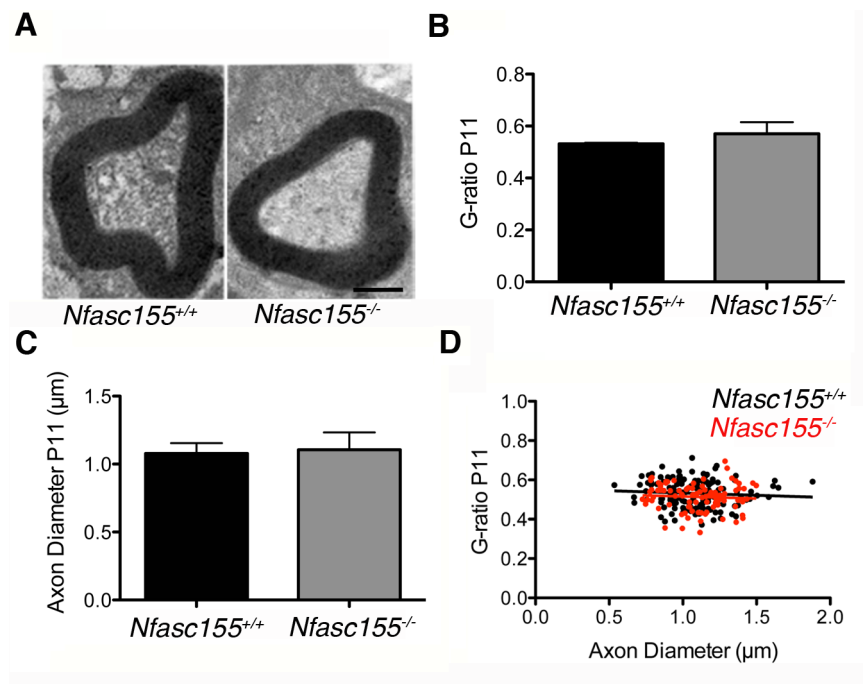


Figure 3.3. Myelination in sciatic nerve occurs normally in *Nfasc155*^{-/-} mice. (A) Electron micrographs of individual myelinated fibres in transverse section in the sciatic nerve of P11 *Nfasc155*^{+/+} and *Nfasc155*^{-/-} mice, showing normal myelin formation and compaction in *Nfasc155*^{-/-} mice. Scale bar 0.5 μm. **(B)** Average G-ratio in the sciatic nerve of *Nfasc155*^{+/+} and *Nfasc155*^{-/-} mice showing no difference (Unpaired t-test; N=3 mice per genotype). **(C)** Average axon diameter in the sciatic nerve of *Nfasc155*^{+/+} and *Nfasc155*^{-/-} mice showing no difference. **(D)** G-ratio plotted versus axon diameter in the sciatic nerve of P11 *Nfasc155*^{+/+} (black) and *Nfasc155*^{-/-} (grey) mice showing a similar spread in both genotypes.

3.2.4 Normal NMJ formation in *Nfasc155*^{-/-} mice

To assess how NMJs were forming in the *Nfasc155*^{-/-} mice, *levator auris longus* (LAL) muscles were dissected at P11 and prepared for immunofluorescence. This muscle is part of the group of cranial muscles found in the posterior neck region in mice (Murray et al., 2010) and functions in movement of the ears. It was chosen because it is a very thin muscle that can be whole mounted, and so all NMJs can be visualised and their branches traced back to the innervating nerve, in one preparation. P11 was chosen as a suitable time-point to study the formation of NMJs because the muscle has developed sufficiently to make individual endplates easily identifiable. Immunolabelling of endplates (with TRITC-alpha-BTX to label the ACh receptor clusters) and innervating axons (with anti-neurofilament-medium/NF-M) revealed the presence of fully occupied endplates on muscle fibres with just one NMJ formed on each muscle fibre in the *Nfasc155*^{-/-} mice (Figure 3.4B), similar to control littermates (Figure 3.4A).

3.2.5 Loss of *Nfasc155* is sufficient to delay synapse elimination at the NMJ

To study the role of *Nfasc155* during synapse elimination, levels of polyinnervation were qualitatively assessed in LAL muscles at P11. This time-point was chosen because synapse elimination will still be taking place in the LAL muscle with most polyinnervated endplates having two clearly distinguishable innervating axons, making it an ideal time-point to accurately assess the process of synapse elimination.

The presence of polyinnervated endplates was observed in control mice at P11 as expected, due to on-going synapse elimination. However, qualitative observations from groups of endplates suggested that the LAL had a higher percentage of NMJs innervated by more than one motor axon in *Nfasc155*^{-/-} mice (Figure 3.4B). By contrast, synapse elimination was almost complete in control littermates at this time-point, resulting in the majority of NMJs being innervated by a single motor axon, which is the mature innervation state (Figure 3.4A).

Synapse elimination takes place in the majority of skeletal muscles in mice during the first 2-3 post-natal weeks of life (Kwon et al., 1995; Nguyen et al., 1998; Personius et al., 2007). To achieve a greater understanding of how synapse elimination progressed in the *Nfasc155*^{-/-} mice, a time-course analysis was carried out in the LAL muscle using immunofluorescence, quantifying levels of polyinnervation at P3, P7, P11, P15 and P18. In the *Nfasc155*^{+/+} mice, ~85% of endplates were polyinnervated at P3 and with the advancement of synapse elimination monoinnervation was achieved at all endplates by P15 (Figure 3.5A). In the *Nfasc155*^{-/-} mice, the percentage of polyinnervated endplates was almost identical to that in the *Nfasc155*^{+/+} mice at P3 (Figure 3.5A). However, synapse elimination was significantly delayed in the *Nfasc155*^{-/-} mice thereafter, suggesting that the increased number of polyinnervated endplates was due to a delay in the removal of excess axons in the early postnatal period rather than as a result of prenatal hyperinnervation of NMJs (Figure 3.5A,D).

Although synapse elimination was taking place in the *Nfasc155*^{-/-} mice, this group had significantly more polyinnervated endplates at P7, P11 and P15 (see Figure 3.5A legend for stats) indicative of a delay in the process. Unfortunately, *Nfasc155*^{-/-} mice died prematurely at ~P19, so it could not be determined whether synapse elimination would eventually reach an end-stage in these mice. One *Nfasc155*^{-/-} mouse did survive to P18 and displayed polyinnervation levels of ~25%, which were slightly lower levels than those quantified as P15 (~30% polyinnervation) suggesting that synapse elimination may have eventually resulted in monoinnervation if the mice survived longer. These results do, however, convincingly demonstrate a clear role for *Nfasc155* in the modulation of synapse elimination at the NMJ. They also suggest that *Nfasc155* is not required for the initial stages of synapse formation and early elimination, but plays an important role as it progresses.

It is interesting to note that at P11, when *Nfasc155*^{-/-} mice are visually indistinguishable from their control littermates, there was already a significant difference of ~30% in levels of polyinnervated endplates in the LAL muscle (Figure 3.5A). It has been previously shown that reduced activity in skeletal muscles correlates with a delay in synapse elimination (Fox et al., 2011), however, this result shows that the delay in synapse elimination precedes the weight loss, making an important point that weight loss and possibly reduced activity levels in the *Nfasc155*^{-/-} mice cannot be a cause for the delay in NMJ development.

In Figure 3.5A, “a polyinnervated endplate” was defined as an endplate with more than one innervating axon. The percentage of polyinnervation does not distinguish

between the endplates with 2, 3, 4 or more innervating axons. To produce a more descriptive measure of the level of polyinnervation, the average number of axon inputs per NMJ was quantified in *Nfasc155*^{+/+} and *Nfasc155*^{-/-} mice. This showed a significant increase at P7, P11 and P15 in the *Nfasc155*^{-/-} mice compared to controls (Figure 3.5B) with the largest difference seen at P11, when the average input per NMJ in *Nfasc155*^{-/-} mice was 2-fold higher than those in controls. A detailed measure of the distribution of axonal inputs per NMJ at P11 showed a significant difference between genotypes in the percentage of NMJs with 1, 2 and 3 innervating axons (Figure 3.5C).

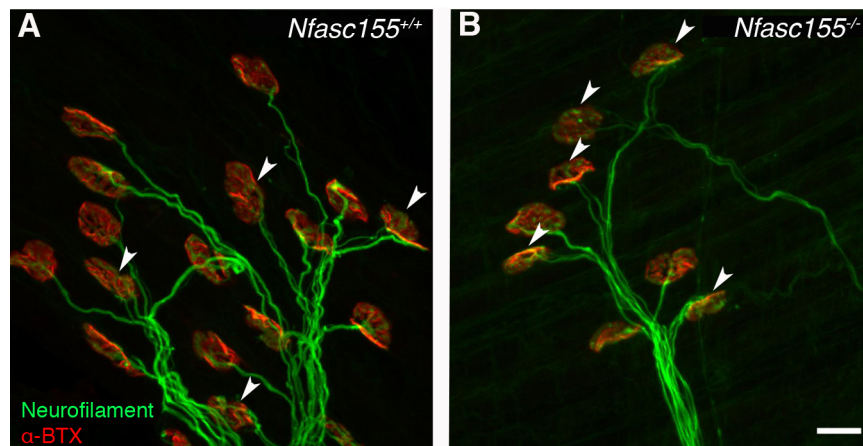


Figure 3.4. Qualitative assessment of NMJ synapse formation and elimination in *Nfasc155^{-/-}* mice reveals higher levels of polyinnervation. (A & B) Confocal micrographs of NMJs in the LAL of (A) *Nfasc155^{+/+}* and (B) *Nfasc155^{-/-}* mice at P11 immunolabelled for NF-M (green) and ACh receptors (red). NMJs were formed normally in the *Nfasc155^{-/-}* mice, with one NMJ formed per muscle fibre and each NMJ fully occupied by axon terminals. A higher percentage of polyinnervated endplates (arrowheads) was observed within groups of endplates in *Nfasc155^{-/-}* mice, indicative of a delay in synapse elimination. Scale bar 20µm.

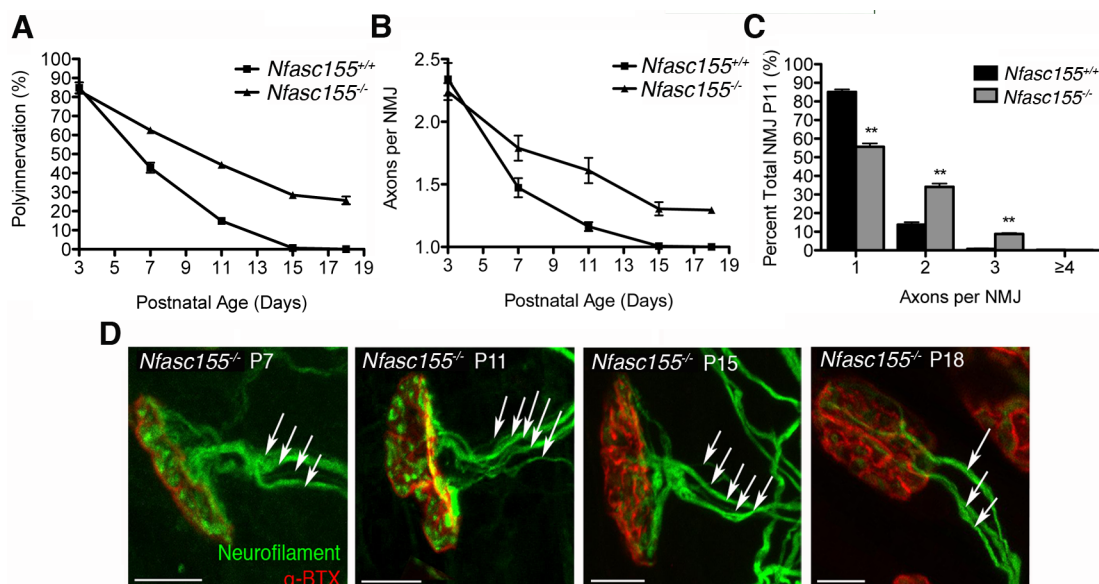


Figure 3.5. Synapse elimination is significantly delayed in the LAL muscle of *Nfasc155*^{-/-} mice. (A) Time-course of synapse elimination in the LAL muscle of *Nfasc155*^{-/-} mice and littermate controls, showing a delay in the *Nfasc155*^{-/-} mice. There was a significant difference between genotypes at P7 ($p=0.005$; Mann-Whitney U-test; $N=3$ mice per genotype, 2 muscles per mouse), P11 ($p=0.0022$; $N=3$ mice) and P15 ($p=0.0009$; $N=4$ mice) (P3; $N=3$ mice per genotype, P18; $N=1$ mouse per genotype so statistical tests were not possible). (B) Using the same data in (A) the average number of axons converging on NMJs in *Nfasc155*^{-/-} mice is shown. There was a significant difference between genotypes at P7 ($p=0.0001$; Mann-Whitney U-test; $N=3$ mice per genotype, 2 muscles per mouse), P11 ($p<0.0001$; $N=3$ mice) and P15 ($p<0.0001$; $N=4$ mice) (P3; $N=3$ mice per genotype, P18; $N=1$ mouse per genotype). (C) Distribution of axonal inputs per NMJ at P11 in *Nfasc155*^{+/+} and *Nfasc155*^{-/-} mice showing a significant increase in the numbers of polyneuronal innervated endplates in *Nfasc155*^{-/-} mice (1 axon, $p=0.0022$, Mann-Whitney U-test; 2 axons, $p=0.0022$; 3 axons, $p=0.0050$; $N=3$ mice per genotype, 2 muscles per mouse). (D) Representative confocal micrographs of polyinnervated endplates (arrows indicate individual axonal inputs) in the LAL of *Nfasc155*^{-/-} mice at P7, P11, P15 and P18. Endplates were labelled with TRITC-BTX and axons were labelled with anti-NF-M. Scale bars 20 μ m.

3.2.6 Synapse elimination is delayed in muscles of different developmental subtype, fibre type and body region

As discussed in Chapter 1, innervation of skeletal muscle varies between muscles in terms of developmental subtype and fibre type. Neuromuscular innervation can develop as fast-synapsing (fa-syn) or delayed-synapsing (de-syn), depending on whether the ACh receptors cluster on the muscle fibre before or after the arrival of the nerve terminal respectively (Pun et al., 2002). Moreover, muscles are composed of different fibre types, owing to varying contractile strengths. Muscle fibres are either fast-twitch or slow-twitch, determined by the myosin isoform expression (Pette and Schnez, 1977), myosin phosphorylation (Moore and Stull, 1984) and ATPase activity (Rubinstein and Kelly, 1978).

To determine if these variables, along with anatomical location of a target muscle, were contributory factors in the delayed synapse elimination observed in *Nfasc155*^{-/-} mice, polyinnervation levels were assessed in a variety of different skeletal muscles, including fa-syn, de-syn, slow twitch and fast twitch muscles, located in the head, neck, abdominal and lower limb regions (Table 3.1). A time-course analysis of synapse elimination in the deep lumbrical muscles of *Nfasc155*^{-/-} mice, which are predominantly composed of fast twitch muscle fibres and located in the hindpaw, revealed a similar delay to that observed in the LAL muscle compared to *Nfasc155*^{+/+} mice (Figure 3.6C,F).

The LAL muscle is composed of a caudal and rostral band, which displays fa-syn and de-syn developmental phenotypes respectively (Murray et al., 2008). To test whether synapse elimination rates varied between developmentally distinct bands within the same muscle, a time-course of synapse elimination was performed, assessing polyinnervation levels within each band. This revealed similar delays in synapse elimination in both bands (Figure 3.6A,B,D,E).

The LAL and deep lumbrical muscles are located at opposite ends of the body in the mouse. This suggests that body location is an unlikely factor in the delayed synapse elimination observed in the *Nfasc155*^{-/-} mice. To verify this result, polyinnervation levels were assessed in muscles in other regions of the body. Increased levels of polyinnervation were also observed in the sternocleidomastoid (SCM), transversus abdominis (TVA) and tibialis anterior (TA) muscles from *Nfasc155*^{-/-} mice at P12, which are found in the neck, thoracic and lower limb regions respectively (Figure 3.7A-C). The SCM, TVA and TA also differ in terms of developmental subtype and predominant fibre type. The SCM develops as de-syn. and is predominantly fast-twitch, the NMJ development of the TVA is unknown but it has been shown that it is a predominantly slow-twitch muscle, and the TA develops as fa-syn and is predominantly fast-twitch. Thus, a profound delay in synapse elimination was observed in all muscle groups examined and was not influenced by functional subtype of motor units or body location.

Muscle	NMJ development	Predominant Fibre type	Body region
LAL Caudal	Fa-syn (Murray et al., 2008)	Fast twitch (Erzen et al., 2000)	Head
LAL Rostral	De-syn (Murray et al., 2008)	Fast twitch (Erzen et al., 2000)	Head
SCM	De-syn (Pun et al., 2002)	Fast twitch (Richmond et al., 2001)	Neck
TVA	<i>unknown</i>	Slow twitch (Haggmark and Thorstensson, 1979)	Abdomen
TA	Fa-syn (Pun et al., 2002)	Fast twitch (Pette et al., 1976)	Lower limb
Lumbricals	<i>unknown</i>	Fast twitch (Yellin, 1969)	Hind-paw

Table 3.1. Summary of all skeletal muscles studied in *Nfasc155*^{-/-} and *Nfasc155*^{+/+} mice, highlighting the type of NMJ development, fibre type and body region for each.

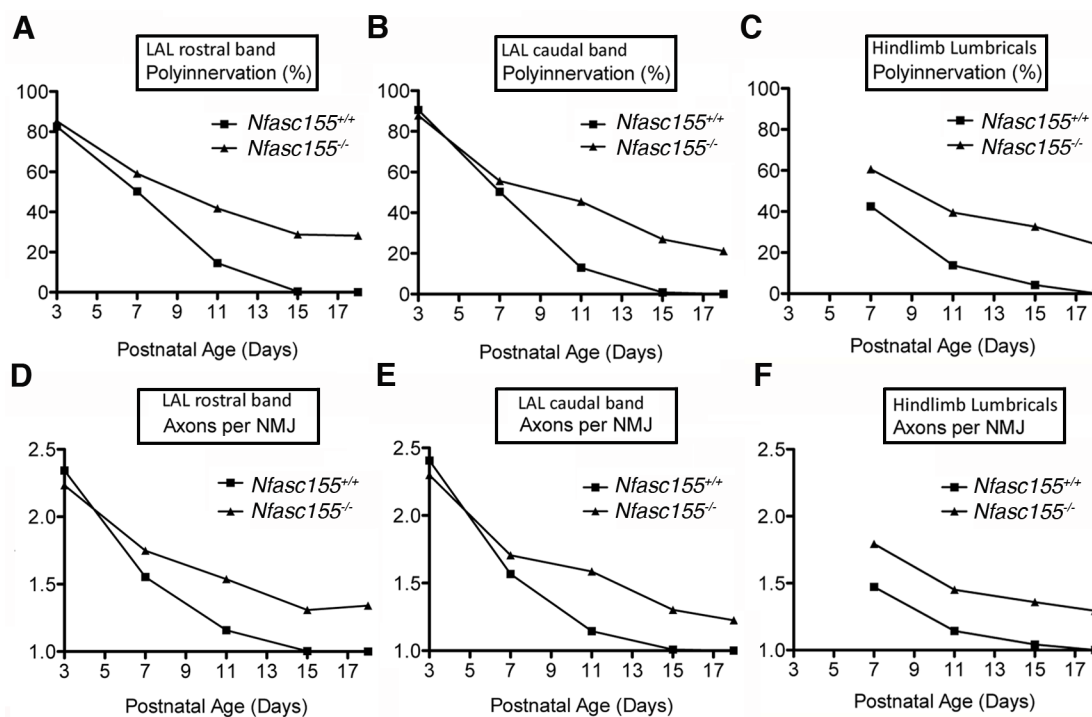


Figure 3.6. Muscles of different developmental subtypes (de-syn & fa-syn) and different body region (neck and hind-paw) show a similar delay in synapse elimination in *Nfasc155*^{-/-} mice. (A-C) Rate of synapse elimination in both the rostral (de-syn) and caudal (fa-syn) bands of the LAL and in the hindlimb lumbrical muscles of *Nfasc155*^{+/+} and *Nfasc155*^{-/-} mice, showing a consistent delay in *Nfasc155*^{-/-} mice (P3/P18, N=1 mouse per genotype, 2 LAL/3 lumbrical muscles per mouse; P7 N=3 mice per genotype for LAL, N=1 mouse per genotype for lumbrical muscles; P11 N=3 mice per genotype; P15 N=4 mice per genotype). There was a significant difference between groups in the LAL thick band at P11 ($p=0.0095$, Mann-Whitney U-test) and P15 ($p=0.0002$), in the LAL thin band at P11 ($p=0.0095$) and P15 ($p=0.0003$) and in the lumbricals at P11 ($p=0.0002$) and P15 ($p<0.0001$). (D-F) Data from the same animals shown in panels A-C, plotted as an average number of axons converging to innervate single muscle fibres as a function of postnatal age, showing higher numbers of axons per NMJ at all time-points examined. (N numbers same as A-C). There was a significant difference between groups in the LAL thick band at P11 ($p<0.0001$, unpaired t-test) and P15 ($p<0.0001$), in the LAL thin band at P11 ($p<0.0001$) and P15 ($p<0.0001$) and in the lumbricals at P7 ($p=0.0422$), P11 ($p<0.0001$) and P15 ($p<0.0001$).

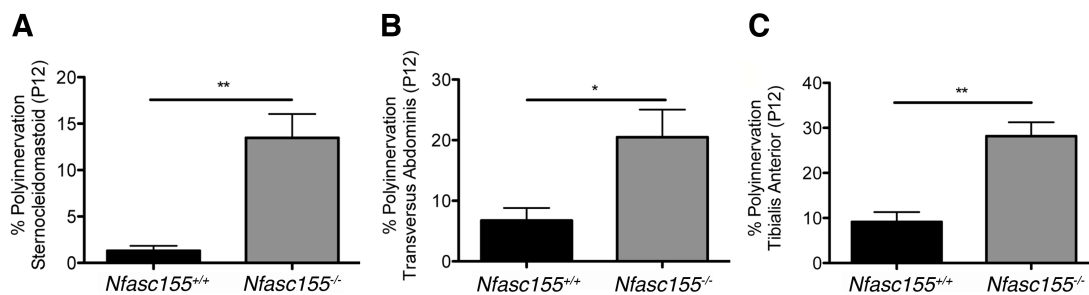


Figure 3.7. Muscles of different fibre type and body region show a similar delay in synapse elimination in *Nfasc155*^{-/-} mice. (A-C) Percentage polyinnervation in (A) SCM (fast twitch; neck), (B) TVA (slow twitch; abdomen) and (C) TA (fast twitch; lower limb) muscles at P12 showing significantly higher levels of polyinnervation in *Nfasc155*^{-/-} mice compared to *Nfasc155*^{+/+} mice in all three muscles (Mann-Whitney U-test; TVA p=0.0304; SCM p=0.0077; TA p=0.0022; N=3 mice per genotype, 2 muscles per mouse).

3.2.7 Neuromuscular transmission is normal in *Nfasc155*^{-/-} mice

It is known that increasing or decreasing neuromuscular transmission is sufficient to alter normal rates of synapse elimination at the NMJ. Contrasting studies have made a case for inactivity (Callaway et al., 1987, 1989; Costanzo et al., 2000) as well as enhanced activity (Ridge and Betz, 1984; Buffelli et al., 2003) in promoting elimination of inputs. It was therefore important to next assess neuromuscular transmission in the *Nfasc155*^{-/-} mice using electrophysiological recordings, as it remained possible that although NMJs were formed in the *Nfasc155*^{-/-} mice, they might not be functionally competent.

Flexor digitorum brevis (FDB) muscles, which are found in the hind-paw, were dissected from P10-P13 *Nfasc155*^{-/-} mice and littermate controls, along with their intact tibial nerve supply. When supramaximal nerve stimulation was applied to the tibial nerve, the FDBs from *Nfasc155*^{+/+} and *Nfasc155*^{-/-} mice responded as expected with sustained tetanic contractions. This indicated that although synapse elimination was delayed in the *Nfasc155*^{-/-} mice at this time-point, the skeletal muscles could accomplish and maintain contractions, suggesting no resulting muscle weakness from the delay.

In order to assess the responsiveness of individual muscle fibres, the tibial nerve was stimulated and responses in the muscle fibres were recorded. When a single vesicle of neurotransmitter is released by an axon terminal and taken up by receptors on the muscle fibre endplate, the muscle fibre responds in the form of a miniature endplate

potential (mEPP) (Eccles et al., 1941). When multiple mEPPs are generated simultaneously, EPPs can be generated in the muscle fibre resulting in an action potential and muscle fibre contraction. Recordings taken from individual muscle fibres of *Nfasc155*^{-/-} mice in response to tibial nerve stimulation, showed evidence for mEPPs and the production of action potentials (Figure 3.8A,B). As can be seen in Figure 3.8A, ~80% of muscle fibres responded to tibial nerve stimulation accordingly. ~20% of fibres were unresponsive in both groups due to the delicate nature of the preparation owing to the young age of the mice. Mean EPP latency was not significantly altered in *Nfasc155*^{-/-} mice (3.41±0.55 ms versus 2.74±0.15 ms in *Nfasc155*^{+/+} mice; P>0.05, unpaired two-tailed t-test) and peak EPP amplitudes were similar in both genotypes (~12 mV; P>0.05). This finding is important because it shows that nerve impulses resulted in a release of neurotransmitter at the NMJ and that the muscle fibres responded accordingly. Therefore, the delay in synapse elimination could not be attributed to gross impairment of neurotransmission at the NMJ.

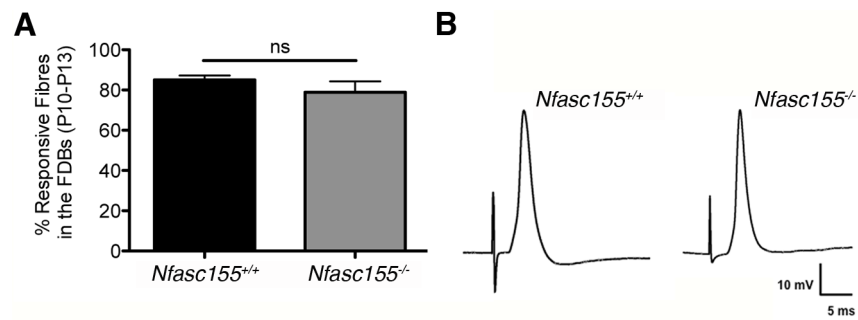


Figure 3.8. Muscle fibres in the FDBs of $Nfasc155^{-/-}$ mice respond with evoked EPPs to nerve stimulation*. (A) Percentage of responsive FDB muscle fibres in P10-P13 $Nfasc155^{+/+}$ and $Nfasc155^{-/-}$ mice showing no significant difference (Mann-Whitney U-test; N=9 $Nfasc155^{+/+}$ mice, N=3 $Nfasc155^{-/-}$ mice, 2 muscles/ 60 muscle fibres analysed per mouse). (B) Example traces of action potentials from intracellular muscle fibre recordings, generated in response to nerve stimulation, in $Nfasc155^{+/+}$ and $Nfasc155^{-/-}$ mice.

** Experiment carried out in conjunction with Prof. Richard R. Ribchester and Kosala Dissanayake. Prof. Ribchester and Kosala performed the experiments and carried out the statistical analysis in my presence.*

3.2.8 Pre- and post-synaptic maturation of the NMJ is delayed in *Nfasc155*^{-/-} mice

It is known that pre- and post-synaptic maturation are correlated at the NMJ in that ACh receptor clustering correlates with axon terminal differentiation (Balice-Gordon and Lichtman, 1993; Lichtman and Colman, 2000). To establish if delayed pruning of pre-synaptic axonal inputs in *Nfasc155*^{-/-} mice was accompanied by a comparable delay in post-synaptic maturation, motor endplate morphology was quantified in *Nfasc155*^{-/-} mice and controls at P15 using a previously established method (Caillol et al., 2012). As the endplate matures, the ACh receptor clusters become more defined and ‘pretzel’ like, mirroring the pre-synaptic axon terminals (Balice-Gordon and Lichtman, 1993). This method identifies immature endplates as ‘ovoid-plaque’, developing endplates as ‘perforated’ and mature endplates as ‘branched’ (Figure 3.9B). Interestingly, post-synaptic motor endplate maturation was significantly delayed in *Nfasc155*^{-/-} mice (Figure 3.9A), thereby confirming both a pre- and post-synaptic delay in development of the neuromuscular synapse.

It is known that as synapse elimination proceeds, the diameter of the pre-terminal axons changes (Buffelli et al., 2003). When synapse elimination is completed at an NMJ, the axon diameter of the winning innervating axon increases and the axon takes over the synaptic site (Buffelli et al., 2003). Therefore, increases in pre-terminal axon diameter are closely correlated with the rate of synapse elimination. To assess how pre-terminal axon growth at mono-innervated endplates progressed in the *Nfasc155*^{-/-} mice with delayed synapse elimination, pre-terminal axon diameters

of singly innervated NMJs were measured. The diameters of axons at polyinnervated endplates were not measured, as this would have biased the results due to a higher percentage of polyinnervated endplates in the *Nfasc155*^{-/-} mice. Rather, the pre-terminal axon diameters of monoinnervated endplates were measured providing an assessment of a pre-synaptic developmental process at NMJs that have reached the end stage of synapse elimination. This analysis showed that axon diameters at singly innervated endplates were significantly smaller in the *Nfasc155*^{-/-} mice compared to controls (Figure 3.9C,D). These results show that both post-synaptic as well as pre-synaptic maturation was delayed in a mouse model of delayed synaptic pruning at the NMJ, providing further support for the closely correlated regulation of pre- and post-synaptic development of the NMJ.

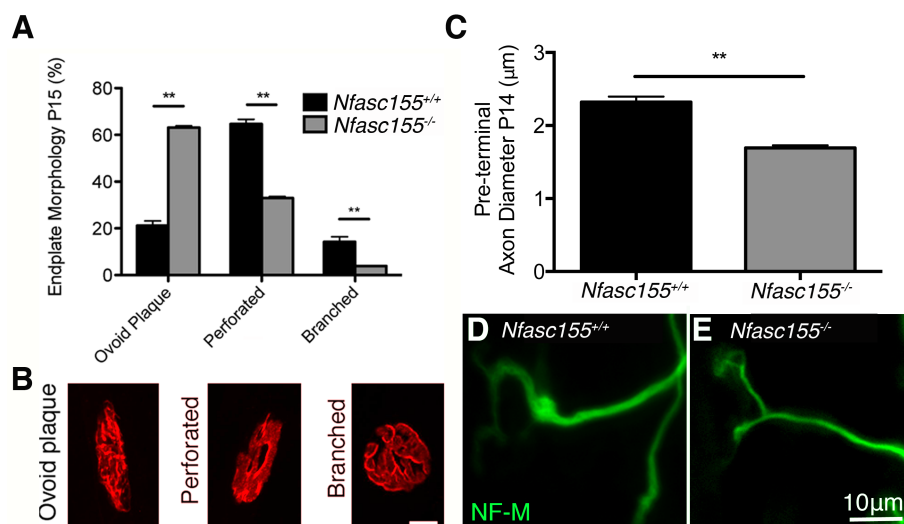


Figure 3.9. Post-synaptic endplate maturation and pre-synaptic axonal maturation are perturbed in *Nfasc155*^{-/-} mice. (A) Quantitative analysis of endplate maturation in P15 *Nfasc155*^{+/+} and *Nfasc155*^{-/-} mice. There was a significant difference in the percentage of ovoid plaque (p=0.0022, Mann-Whitney U-test; N=3 mice per genotype, 2 muscles analysed per mouse), perforated (p=0.0022), and branched (p=0.0022) endplates, revealing a significant delay in endplate maturation in *Nfasc155*^{-/-} mice. Data are represented as mean +/- SEM. (B) Example confocal micrographs of P15 ovoid plaque (immature) perforated (developing) and branched (mature) endplates in a control mouse. Endplates were labelled with TRITC-BTX. Scale bar 10µm. (C) Quantitative analysis of pre-terminal axon diameter in P14 *Nfasc155*^{+/+} and *Nfasc155*^{-/-} mice. There was a significant difference in axon diameter at singly innervated endplates between genotypes (p=0.0018; unpaired t-test; N=3 mice per genotype, 1 muscle analysed per mouse). (D&E) Example confocal micrographs of P14 pre-terminal axons in the LAL of (D) *Nfasc155*^{+/+} and (E) *Nfasc155*^{-/-} mice showing a smaller axon in the *Nfasc155*^{-/-} mice. Axons were labelled with anti-NF-M. Scale bar 10µm.

3.2.9 Delayed synapse elimination in *Nfasc155*^{-/-} mice is not due to the presence of *Cre* or *Lox P* sites

Nfasc155^{-/-} mice were generated by genetic insertion of *Cre* in to the *CNP* locus and *lox P* sites in to the *Nfasc* gene. To establish that the delayed elimination observed in *Nfasc155*^{-/-} mice was not due to the insertion of *Cre* or *lox P* sites, levels of polyinnervation in both *CNP*^{Cre/+} and *Nfasc fl/fl* mice were quantified. These mice displayed normal levels of polyinnervation in the LAL muscle at P15. Increased levels of polyinnervation were only seen in mice that were positive for both *Cre* and *Nfasc fl/fl* (*Nfasc155*^{-/-} mice) (Figure 3.10).

3.2.10 Terminal Schwann cells are unlikely to be contributing to the delay in synapse elimination in *Nfasc155*^{-/-} mice

TSCs are known to respond to changes in pre-terminal axonal activity, by increasing intracellular Ca²⁺ levels in response to neuromuscular transmission (Darabid et al., 2013). They are also known to play a secondary role in synapse elimination by cleaning up the unwanted axonal debris once axonal inputs have withdrawn from endplates (Keller-Peck et al., 2001; Song et al., 2008). It was therefore important to next address the possibility that *Nfasc155* was having an effect on synapse elimination through TSC activity. *Nfasc155* expression was examined in TSCs using immunofluorescence in the TA muscle of C57BL6 mice at P9. Endplates and axons were immunolabelled using far-red-BTX and anti-NF-M respectively. Anti-pan-*Nfasc* was used to identify the localisation of *Nfasc*. Paranodes and nodes were

identified along axons as expected (Figure 3.11), however Nfasc155 expression was not detected in areas overlying the endplate. This suggests an absence of Nfasc155 in TSCs and eliminates the possibility of TSCs playing a role in Nfasc155-dependent modulation of synapse elimination (Figure 3.11). Interestingly, pan-Nfasc labelling of P9 control muscle also revealed an absence of paranodes from pre-terminal axons entering the NMJ (Fig. 3G). This is in agreement with previous studies reporting on myelination of intramuscular axons, showing that pre-terminal axons are myelinated post-synapse elimination (Bixby, 1981; Slater, 1982), thereby eliminating paranodal development in pre-terminal axons as a determining factor in the outcome of synapse elimination. This also confirms that the delay in synapse elimination in *Nfasc155*^{-/-} mice cannot be due to the absence of paranodal junctions in pre-terminal axons, as paranodal junctions will also be absent from pre-terminal axons in control mice during the same period.

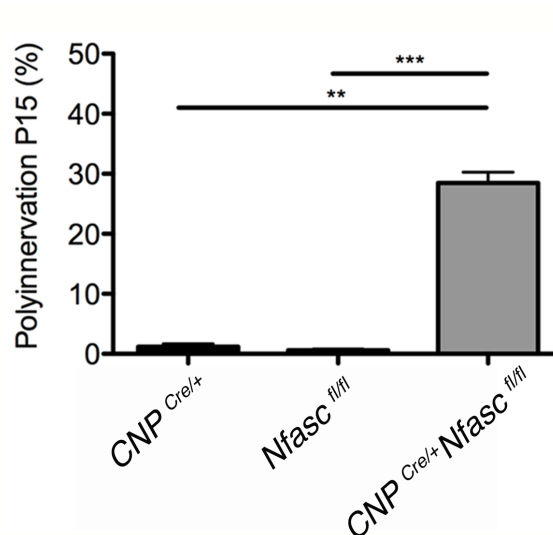


Figure 3.10. Synapse elimination is normal in $CNP^{Cre/+}$ and $Nfasc^{fl/fl}$ mice. Percentage polyinnervation in the LAL of $CNP^{Cre/+}$, $Nfasc^{fl/fl}$ and $CNP^{Cre/+} Nfasc^{fl/fl}$ ($Nfasc155^{-/-}$) mice at P15 showing a significant difference between $CNP^{Cre/+}$ and $CNP^{Cre/+} Nfasc^{fl/fl}$ mice ($p=0.0023$; Mann-Whitney U-test; $CNP^{Cre/+}$ N=3 mice, 2 muscles analysed per mouse, $CNP^{Cre/+} Nfasc^{fl/fl}$ N=4 mice) and $Nfasc^{fl/fl}$ and $CNP^{Cre/+} Nfasc^{fl/fl}$ ($p=0.0009$; Mann-Whitney U-test; N=4 mice). Data are represented as mean \pm SEM.

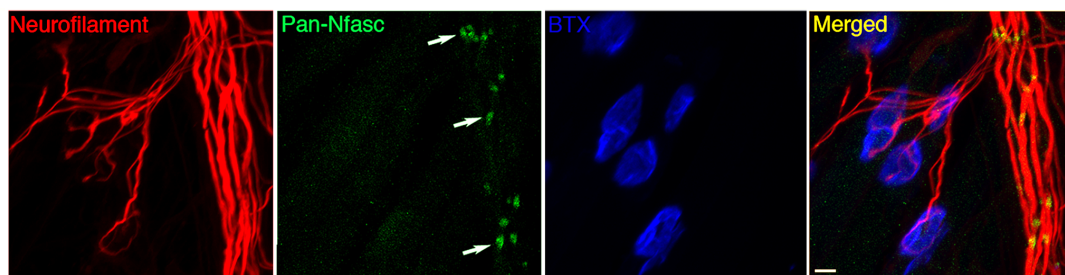


Figure 3.11. Terminal Schwann cells do not express high levels of Nfasc. Confocal micrographs of NMJs in the TA of a P9 wild-type mouse showing robust presence of Nfasc155 at paranodes formed by myelinating Schwann cells (green; arrows), alongside intramuscular axons (red) and motor endplates (blue). Labelling of Nfasc155 was not evident in terminal Schwann cells or other cell types covering motor endplates. Axons were labelled with anti-NF-M, paranodes with anti-pan-Nfasc and endplates with far-red-BTX. Scale bar 10 μ m.

3.2.11 Outwith synapse elimination, the PNS develops normally in

Nfasc155^{-/-} mice

Synapse elimination is a competitive process that takes place at the level of each neuromuscular junction between the innervating axons. The axons that innervate each NMJ have their cell bodies located in the ventral horn of the spinal cord. The number of lower motor neuron cell bodies in the ventral horn of the spinal cord does not change during the course of synapse elimination (Brown et al., 1976; Lowry et al., 2001). The axons of these cells descend in the anterior white matter tracts of the spinal cord until the point of exit, where they follow a course in a peripheral nerve to a group of skeletal muscles (Nicolopoulos-Stournaras and Iles, 1983). Each skeletal muscle receives innervation from a mixture of lower motor neuron branches (Keller-Peck et al., 2001; Kasthuri and Lichtman, 2003). In the *Nfasc155*^{-/-} mice, Nfasc155 is absent from early on in post-natal development, coinciding with the onset of myelination (Chapter 2). Therefore, it remained possible that lack of Nfasc155 resulted in aberrant postnatal organisation of the PNS, which could be attributed to the delay in synapse elimination. It was therefore important to assess the arrangement and development of other features of the PNS in *Nfasc155*^{-/-} mice.

To establish if there was a difference in the number of lower motor neurons in *Nfasc155*^{-/-} mice at a time when synapse elimination was delayed, lower motor neuron cell bodies were quantified at P11. A significantly greater pool of motor neurons in the *Nfasc155*^{-/-} mice for example, could explain the delay as this could result in increased nerve branching in the muscle. Quantification of lower motor

neuron cell bodies in the ventral horn of the spinal cord revealed no significant difference between genotypes, eliminating increased numbers of motor neurons as a contributory factor in the delayed synapse elimination observed in the *Nfasc155*^{-/-} mice (Table 3.2 & Figure 3.12a/b).

Similarly, to determine if lack of Nfasc155 resulted in increased numbers of axons in the peripheral nerve innervating the LAL, which could also be attributed to increased branching at NMJs, the number of axons innervating the LAL in *Nfasc155*^{-/-} and *Nfasc155*^{+/+} mice at P15 was also assessed. This analysis showed no significant difference between genotypes (Table 3.2 & Figure 3.12a/b). These results suggest that loss of Nfasc155 does not hinder gross development of the PNS but rather is specifically required for the fine-tuning of innervation patterns in skeletal muscle.

There is a very close apposition of cell membranes between the pre-terminal axon, the endplate and the TSCs at the NMJ (Smith et al., 2013). These latter cells overlay the axon terminals and are also closely apposed to the muscle fibre membrane (Smith et al., 2013). TSCs respond with increased intracellular Ca²⁺ to neurotransmission at the NMJ and increase in number during synapse elimination (Darabid et al., 2013). It has been suggested that signalling in the form of growth factors (Nguyen et al., 1998) or other proteins (McCann et al., 2007) from muscle fibres is essential for normal rates of synapse elimination. Therefore, to establish if the delayed developmental phenotype in *Nfasc155*^{-/-} mice included any change in the morphology of the two non-axonal cell types that constitute the NMJ, which could be attributed to the delay in synapse elimination, various aspects of muscle development along with terminal

Schwann cell number were measured. The diameter of teased muscle fibres was measured in the LAL muscle at P15. Interestingly muscle fibre growth was unaltered in the *Nfasc155*^{-/-} mice. There was also no change in endplate area, endplate number or terminal Schwann cell number per NMJ in *Nfasc155*^{-/-} mice (Table 3.2 & Figure 3.12a/b). These results suggest a highly specialised role for Nfasc155, in the later stages of developmental neuronal remodelling, rather than in the gross arrangement of the PNS.

Quantity	<i>Nfasc155</i> ^{+/+}	<i>Nfasc155</i> ^{-/-}	P-value
Number of motor neurons per ventral horn in the spinal cord (P11)	9.139 ± 0.4652 (N=3, unpaired t-test)	10.29 ± 0.5115 (N=3)	P>0.05
Number of axons innervating the LAL (P11)	40.33 ± 6.227 (N=3, 6 muscles, unpaired t-test)	44.17 ± 6.215 (N=3, 6 muscles)	P>0.05
Muscle fibre diameter of the LAL (P15) (µm)	11.57 ± 0.4220 (N=3, 6 muscles, unpaired t-test)	12.70 ± 0.4861 (N=3, 6 muscles)	P>0.05
Endplate area in the LAL (P15) (µm ²)	213.2 ± 4.499 (N=4, 6 muscles, unpaired t-test)	222.3 ± 5.903 (N=3, 6 muscles)	P>0.05
Endplate number in the LAL (P15)	556.4 ± 16.67 (N=4, 6 muscles, unpaired t-test)	539.8 ± 19.71 (N=3, 6 muscles)	P>0.05
Terminal Schwann cell number per NMJ in the LAL	5.23 ± 1.01 (N=3, 3 muscles, unpaired t-test)	3.98 ± 0.38 (N=3, 3 muscles)	P>0.05

Table 3.2. Comparison of the numbers of motor neurons, axons, endplates, endplate area, muscle fibre diameter and terminal Schwann cell number per NMJ in *Nfasc155*^{+/+} and *Nfasc155*^{-/-} mice. Motor neuron number was quantified in the ventral horns of the spinal cord. All other analyses were carried out on the LAL muscle.

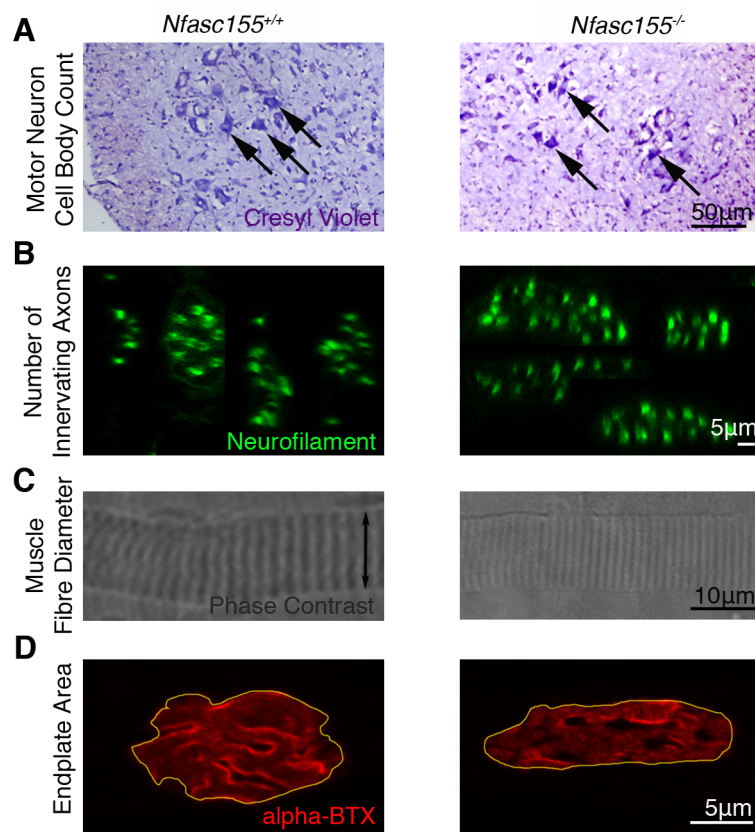


Figure 3.12a. Example confocal micrographs for the parameters in Table 3.1 (number of motor neurons and axons; muscle fibre diameter; and endplate area in *Nfasc155*^{+/+} and *Nfasc155*^{-/-} mice). (A) Example light microscope images of transverse sections of spinal cord, stained with cresyl violet to identify lower motor neurons in the ventral horn of the spinal cord. Some of the motor neurons present are indicated by arrows. (B) Example confocal transverse section of an innervating nerve to the LAL immunolabelled with anti-NF-M, generated from a 3D reconstruction of the nerve. Each green circle represents a single axon, allowing for clear distinguishing of innervating axons. (C) Example phase-contrast images of single teased LAL muscle fibres, showing how muscle fibre diameter was measured (double-headed arrow). Sarcomeres were clearly visible on each muscle fibre, indicated by the dark bands present along its length. (D) Example confocal images of single endplates labelled with TRITC-BTX, illustrating the tracing method used to calculate endplate area. The boundaries of each endplate could be clearly delineated.

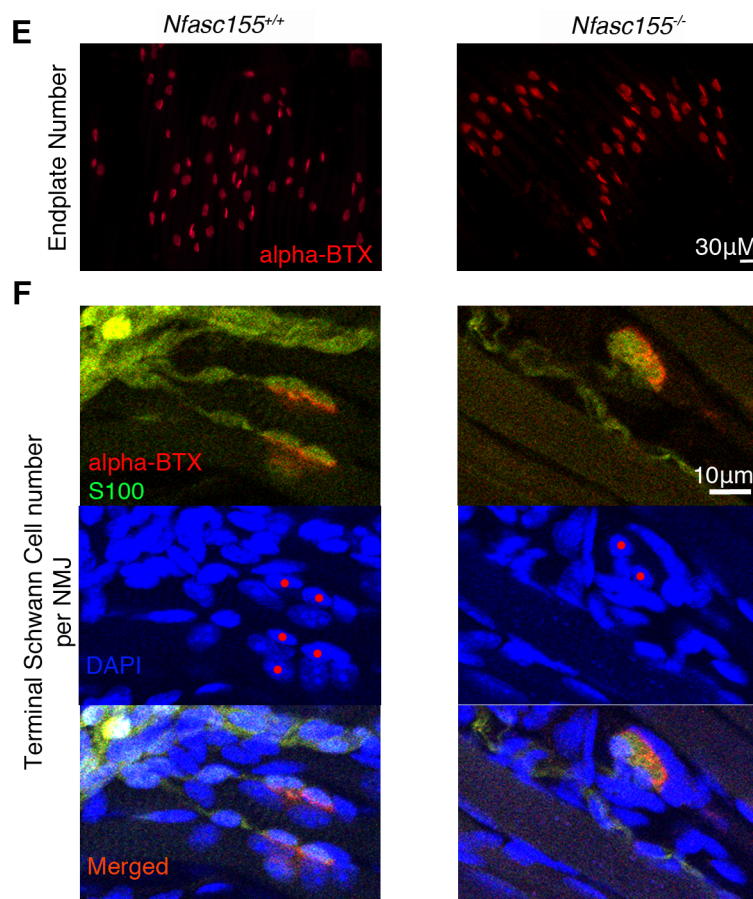


Figure 3.12b. Example confocal micrographs for the parameters in Table 3.1 (endplate number and terminal Schwann cell number per NMJ). (E) Fluorescent images of groups of endplates, as examples of the kinds of images used to count the number of endplates per muscle. (F) Example confocal images of endplates labelled for Schwann cells (S100, green), cell nuclei (DAPI, blue) and ACh receptors (TRITC-BTX, red). DAPI-positive cells that were overlapping with the S100 staining were identified as TSCs (TSCs indicated by red dots).

3.2.12 Synapse elimination occurs normally in mice lacking an axonal paranodal protein (*Caspr*)

As shown in Figure 3.1B, immunolabelling of teased fibres in *Nfasc155*^{-/-} mice revealed an absence of both glial Nfasc155 and axonal Caspr at the paranode, as expected based on previous literature (Bhat et al., 2001). To address whether delayed synapse elimination observed in *Nfasc155*^{-/-} mice was occurring as a direct result of the loss of physical axon-glia interactions at paranodal junctions (ie. Loss of Caspr as well as Nfasc155), or as a result of loss of Nfasc155 specifically, synapse elimination was assessed in mice lacking Caspr, the axonal protein required for paranodal axon-glia interactions (Bhat et al., 2001) (Figure 3.1A).

As expected, *Caspr*^{-/-} mice displayed disrupted paranodes similar to *Nfasc155*^{-/-} mice (Figure 3.13A,B), with a loss of both Caspr and Nfasc155 at paranodes. The process of synapse elimination was assessed by quantifying levels of polyinnervation in the LAL and hindlimb lumbrical muscles at P10. At this time-point in the *Nfasc155*^{-/-} mice, there was a 30% difference in the percentage of polyinnervated endplates in comparison to control mice. Interestingly the *Caspr*^{-/-} mice showed no difference in levels of polyneuronal innervation in the LAL and lumbrical muscles at P10 (Figure 3.14A,B). This suggests that in the *Nfasc155*^{-/-} mice, the absence of an intact paranode is not driving the delay in synapse elimination but rather that Nfasc155 modulates rates of synapse elimination outside of its canonical role at the paranode, highlighting a novel role for Nfasc155.

Interestingly, although Nfasc155 was not localised to paranodes of *Caspr*^{-/-} mice, these mice still expressed high levels (>70%) of Nfasc155 in the spinal cord (Figure 3.15A) and peripheral nerve (Figure 3.15B), suggesting that Nfasc155 expression was not significantly diminished in glial cells. Thus, it is unlikely that delayed synapse elimination in *Nfasc155*^{-/-} mice resulted from the loss of Nfasc155's canonical role in regulating physical axon-glial interactions at the paranode.

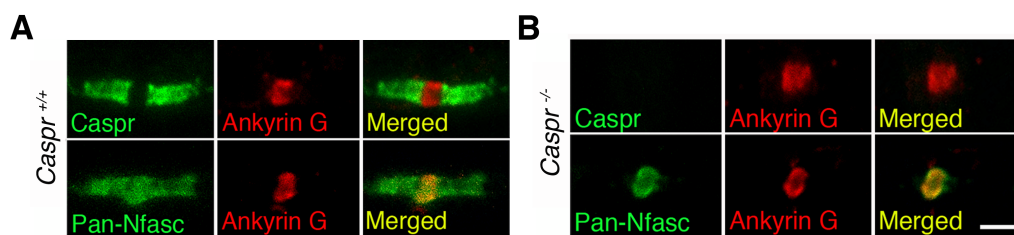


Figure 3.13. *Caspr*^{-/-} mice lack Caspr and have disrupted paranodes. (A & B) Confocal micrographs of (A) *Caspr*^{+/+} and (B) *Caspr*^{-/-} teased sciatic fibres immunolabelled for pan-Nfasc, Caspr and ankyrin G, showing loss of Nfasc155 and Caspr from paranodal regions of *Caspr*^{-/-} mice. Anti-pan-Nfasc labelled the node of Ranvier in *Caspr*^{-/-} mice as expected, as the expression of the Nfasc186 isoform is unaffected. Anti-ankyrin G labels the node of Ranvier. Scale bar 5µm.

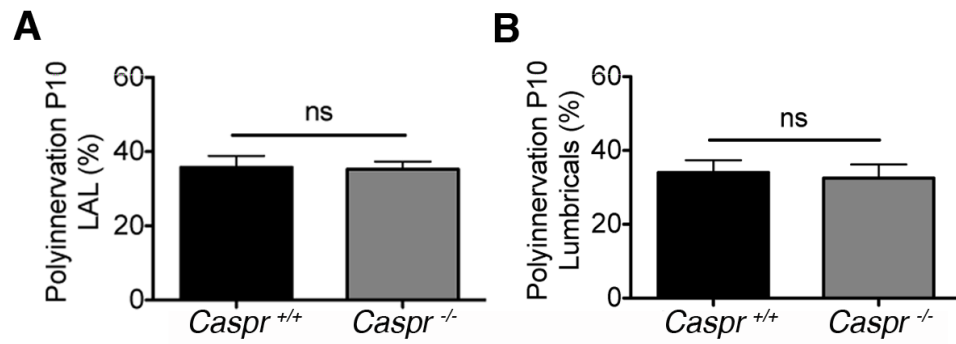


Figure 3.14. *Caspr*^{-/-} mice have normal rates of synapse elimination. (A & B) Quantitative analysis of polyinnervation levels at P10 in (A) the LAL and (B) the hindlimb lumbricals reveals no significant difference between *Caspr*^{+/+} and *Caspr*^{-/-} mice, indicative of normal rates of synapse elimination.

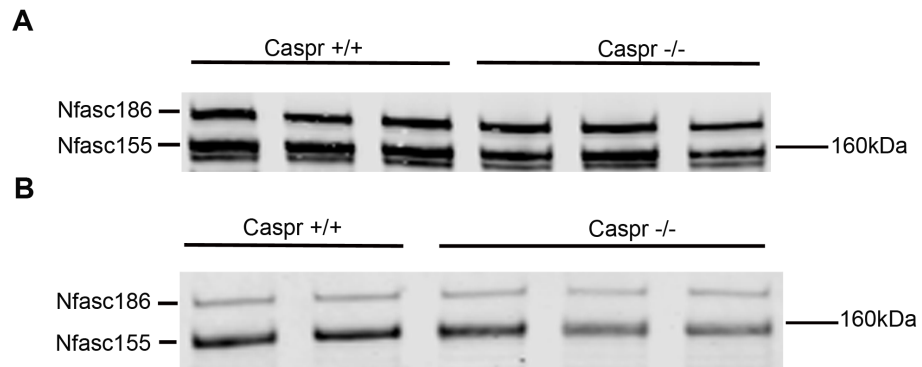


Figure 3.15. *Caspr*^{-/-} mice still express Nfasc155. (A&B) Western Blot showing persistent expression of Nfasc155 in (A) the spinal cord and (B) peripheral nerve of *Caspr*^{-/-} mice even though there is a clear lack of Nfasc155 at paranodes. The Nfasc186 isoform is present at normal levels in *Caspr*^{-/-} mice.

3.2.13 Delayed synapse elimination in *Nfasc155*^{-/-} mice is not due to a reduction in nerve conduction velocity

As highlighted in previous sections, it has been well documented that rates of synapse elimination can be altered as a result of a change in conduction velocity in the innervating nerves (Ridge and Betz, 1984; Callaway et al., 1987, 1989; Buffelli et al., 2003). It has also been shown that paranodal disruption results in reduced conduction velocity (Bhat et al., 2001; Pillai et al., 2009) likely as a result of ion leakage at the node of Ranvier and Na_v channel dispersion (Rosenbluth, 1976; Rios et al., 2003).

To address the possibility that the delay in synapse elimination observed in *Nfasc155*^{-/-} mice was due to reduced conduction velocity in peripheral nerve, conduction velocity was recorded in sciatic nerve preparations from *Nfasc155*^{-/-} mice and littermate controls at P11. *Nfasc155*^{-/-} mice exhibited a ~50% reduction in nerve conduction velocities (Figure 3.16A), consistent with previous findings from other strains of genetically modified mice lacking *Nfasc155* (Pillai et al., 2009). To establish whether reduced nerve conduction velocities caused the delayed synapse elimination observed in the *Nfasc155*^{-/-} mice, a parallel analysis of nerve conduction velocities was performed in the *Caspr*^{-/-} mice at the same age and using the same preparation. This revealed an almost identical ~50% reduction (Figure 3.16B), consistent with previous findings on *Caspr*^{-/-} mice (Bhat et al., 2001). However, no delay in synapse elimination was observed in these mice (Figure 3.14). Thus, the delay in synapse elimination observed in *Nfasc155*^{-/-} mice was unlikely to be

occurring due to perturbations in the conductive properties of peripheral nerve, as a similar reduction in conduction velocity in *Caspr*^{-/-} mice did not affect the rate of synapse elimination.

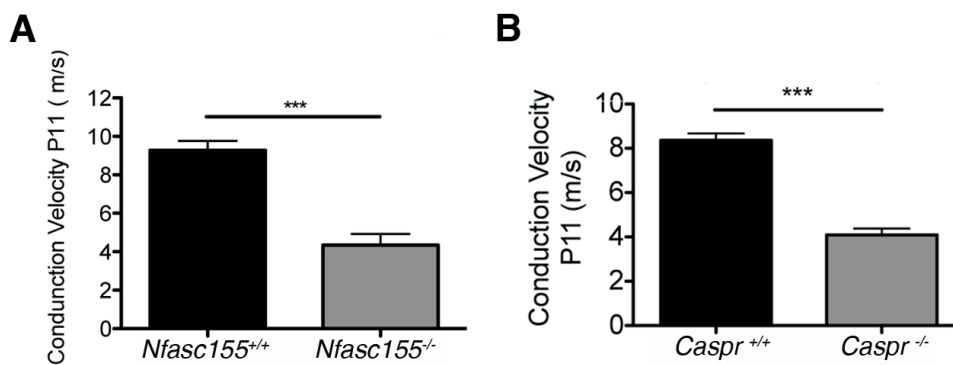


Figure 3.16. Conduction velocity is significantly reduced in both *Nfasc155*^{-/-} and *Caspr*^{-/-} mice*. (A) Significant reduction in conduction velocity of sciatic nerve in *Nfasc155*^{-/-} mice at P11 compared to *Nfasc155*^{+/+} mice (p=0.0007; unpaired t-test; N=4 mice per genotype). (B) Quantitative analysis of conduction velocity shows a significant difference between *Caspr*^{+/+} and *Caspr*^{-/-} mice (p<0.0001; unpaired t-test, N=4 mice per genotype).

* *Experiment carried out in conjunction with Dr. Diane Sherman.*

Dr. Sherman performed the dissections, recordings and statistical analysis.

3.3 Discussion

3.3.1 Overview of results

The experiments designed in this chapter sought to explore the potential role for myelinating Schwann cells in the regulation of synapse elimination at the mouse NMJ, with a particular focus on the contribution of one key Schwann cell protein: Nfasc155. Previously published evidence hints at a role for non-neuronal cell types in the regulation of this process, including a role for muscle-derived signals (Nguyen et al., 1998) and terminal Schwann cell lysosomal activity (Smith et al., 2013) in determining the outcome of synapse elimination. However, a role for myelinating Schwann cells in the control of this developmental process has never before been shown.

The results of this chapter highlight a very specific role for Nfasc155 in the development of the PNS. It is clear that Nfasc155 modulates developmental synapse elimination in a range of skeletal muscles, highlighting a global requirement for Nfasc155 in the postnatal remodelling of neuronal circuitry in the PNS. This is a very specific role, as results have shown that gross organisation in the early stages of PNS development was unaffected in *Nfasc155*^{-/-} mice. For example, the number of motor neurons along with their branch number in innervating nerves was unaffected by loss of Nfasc155. Essential features of growth and development within the non-neuronal cell types found at the NMJ, such as muscle fibre diameter, endplate number and TSC number, also developed normally in *Nfasc155*^{-/-} mice. This shows

that *Nfasc155* plays a very specific role in postnatal development of the PNS. The finding that *Caspr*^{-/-} mice, a second model of paranodal disruption, exhibit normal synapse elimination is an exciting result as it suggests a novel role for *Nfasc155* outside of its canonical duties at the paranode.

3.3.2 Discovery of a novel role for *Nfasc155*

The results of this chapter provide clear evidence of a non-canonical role for *Nfasc155*, as a key glial cell modulator in a fundamental developmental process at the NMJ. Importantly, the magnitude of delay in synapse elimination observed in *Nfasc155*^{-/-} mice was what might be expected when modulating (but not entirely blocking) a dynamic biological process, and was similar to that previously reported in other studies. For example, a study reporting on NMJ development in a mouse model lacking a key gap junction protein (connexin 40, *Cx40*^{-/-}) showed that synapse elimination was increased in this model likely due to reduced gap junctional coupling and consequential alterations in neuronal firing patterns at the NMJ (Personius et al., 2007). A second, earlier study showed that administration of leukemia inhibitory factor to the *tensor fascia latae* muscle in the mouse, led to a delay in developmental synapse elimination in multiple skeletal muscles, possibly due to an excess of growth factor supply (Kwon et al., 1995). This is in support of the “trophic hypothesis” as discussed in previous sections and chapters. These studies are in contrast to other reported experimental manipulations including over-expression of *GDNF* in muscle (Nguyen et al., 1998) where delayed synapse elimination was a secondary consequence of initial hyperinnervation of NMJs, which required more subsequent

pruning. Comparing these three studies with the results of this chapter, the change in the timing and rate of synapse elimination was within a similar range to what was observed in the *Nfasc155*^{-/-} mice.

3.3.3. *The role of glia in developmental remodelling of the nervous system*

The results of this chapter highlight a novel role for glia in developmental remodelling of neuronal circuitry. As discussed in Chapter 1, axonal arbors are vast during the early stages of nervous system development, with each target cell receiving multiple inputs from multiple neurons. Synapse elimination is a fundamental process in the fine-tuning of the nervous system, resulting in extensive pruning of inputs through competition. This process ceases when one input remains and takes over the synaptic territory.

Synapse elimination takes place throughout the nervous system. As well as at the NMJ, it has been well characterised in the CNS, particularly in the retinogeniculate system (Sretavan and Shatz, 1984; Hooks and Chen, 2006). In the mouse retinogeniculate system, geniculate cells in the lateral geniculate nucleus receive inputs from multiple retinal ganglion cells and all but one input are pruned away over a ~3 week period spanning eye opening (Sretavan and Shatz, 1984). Astrocytes have been implicated in the regulation of synapse elimination at these synapses, by releasing signals to the neurons required for synapse elimination to proceed (Stevens et al., 2007). They have been shown to induce complement (C1q) expression in neurons, which in turn stimulates lysosomal activity within astrocytes and

engulfment of C1q-positive axons. C1q expression was found to be highest during the period of synapse elimination, indicating a possible role for this protein during developmental axon pruning. In mice lacking C1q, synapse elimination in the retinogeniculate system was delayed, possibly due to loss of a signal for astrocytes to proceed with engulfment (Stevens et al., 2007). This suggests that in contrast to the PNS (Song et al., 2008), lysosomal activity in the CNS seems to play a more primary, regulatory role. Although the molecular mechanisms surrounding astrocyte-dependent synapse elimination remain largely unknown, a recent study has identified two phagocytic proteins in the astrocyte as essential components, multiple epidermal growth factor-10 (MEGF10) and membrane receptor tyrosine kinase (MERTK) (Chung et al., 2013). *MEGF10*^{-/-} and *MERTK*^{-/-} mice displayed delayed synapse elimination in the retinogeniculate system, confirming the importance of these two proteins for this process (Chung et al., 2013).

The above studies highlight essential roles for glia during developmental synapse elimination in the CNS. As of yet, a similar role has not been conclusively documented in the PNS. The results of this chapter propose that myelinating glial cells play a crucial role during developmental neuronal remodeling in the PNS, mediated through glial Nfasc155-dependent signaling pathways.

3.3.4 *Nfasc155*^{-/-} model as useful tool to study the intricacies of synapse elimination regulation

Synapse elimination at the NMJ is a very well characterised but poorly understood process. Although previous studies have described in detail what happens at the NMJ during synapse elimination (Rich and Lichtman, 1989; Balice-Gordon and Lichtman, 1993; Culican et al., 1998; Keller-Peck et al., 2001; Walsh and Lichtman, 2003), it has not yet been confirmed what the molecular drivers of competition between innervating axons are. To begin to appreciate the intricacies of this developmental process we must gain a greater understanding of the signalling pathways and proteins at play during this time of dynamic synaptic remodelling.

The *Nfasc155*^{-/-} mouse model of delayed synapse elimination provides us with a useful tool in this quest. *Nfasc155*^{-/-} mice display a selective delay in postnatal development of the NMJ, with other parameters of PNS morphology such as lower motor neuron number, myelination and muscle fibre development remaining unaffected. This is an important point as it allows us to focally tease apart the fundamental proteins and pathways regulating synapse elimination at the NMJ *in vivo*. Morphological and proteomic studies on the *Nfasc155*^{-/-} mouse model of paranodal disruption and delayed synapse elimination alongside the *Caspr*^{-/-} mouse model of paranodal disruption allows for a unique comparison, in which the proteins and pathways surrounding paranodal development can be isolated alongside those important for synapse elimination. The following chapter attempts to utilise this

comparison to provide mechanistic insight in to the possible regulators of synapse elimination at the NMJ.

Chapter 4

Mechanistic insight in to Nfasc155-dependent modulation of synapse elimination

4.1 Introduction

Following the finding that Nfasc155 modulates synapse elimination independent of its canonical role at the paranode (Chapter 3), it remained to be determined how Nfasc155 was influencing this process. Previous to the discovery of this novel role for Nfasc155, the only known role for this protein was in forming paranodal junctions by physically interacting with an axonal Caspr-contactin complex. The results of the previous chapter reveal a role for Nfasc155 outside of its paranodal duties. The experiments in this chapter were therefore designed to uncover the mechanisms through which Nfasc155 modulates synapse elimination in the PNS.

4.1.1 Nfasc155 does not act as a secreted molecule

The finding that loss of Nfasc155 led to a robust delay in synapse elimination, whereas synapse elimination occurred normally in *Caspr*^{-/-} mice (Chapter 3), suggests that Nfasc155 modulates synapse elimination by a mechanism independent of its canonical role in generating physical interactions with the axon at the paranode. One possible explanation for this is that Nfasc155 is secreted by the glial cell at the

membrane and acts as a ligand for an axonal receptor, eliciting downstream effects on axon pruning. However, this hypothesis was rejected based on a study showing that exogenous application of either the extracellular domain of Nfasc155 or anti-Neurofascin antibodies does not modulate neuronal stability or induce axonal retraction *in vitro* (Charles et al., 2002). Thus, it is unlikely that Nfasc155 modulates synapse elimination in neighbouring motor axons by acting as a secreted/soluble factor.

4.1.2 Insights from previously published literature

Published studies attempting to provide insight in to the regulators of synapse elimination have shown that changes in growth factor supply from target cells and surrounding glial cells (Kwon et al., 1995; Jordan, 1996; Nguyen et al., 1998), nerve activity (Costanzo et al., 2000; Buffelli et al., 2003) and lysosomal activity within glial cells (Song et al., 2008) are determinants in the rate and timing of synapse elimination, either by directly or indirectly modulating the process. *Nfasc155^{-/-}* mice were shown to have reduced conduction velocity in peripheral nerve (Chapter 3, Figure 3.15), however this could not have been a cause for the delay in synapse elimination in light of the *Caspr^{-/-}* mouse findings, displaying a similar reduction in conduction velocity but normal synapse elimination. *Nfasc155^{-/-}* mice were also shown to have normal neuromuscular activity (Chapter 3, Figure 3.8). These results eliminate reduced nerve activity as a cause for the delayed synapse elimination observed in the *Nfasc155^{-/-}* mice. The effect that loss of Nfasc155 has on growth

factor supply in muscle as well as on lysosomal activity is assessed as part of this chapter.

Previous studies elucidating on the importance of myelinating glial cells for maintaining axonal integrity have hinted at the possible mechanisms through which Nfasc155 could be mediating synapse elimination, although these studies have not been carried out in the context of developmental axon pruning. Studies on genetically modified lines of mice displaying hypomyelinating phenotypes have illustrated the importance of myelinating Schwann cells for maintaining cytoskeletal integrity in the axon. The ‘Trembler’ mouse displays a naturally occurring genetic mutation, resulting in poor myelination and reduced axon calibre in the PNS (Low, 1976a, b). Ultrastructural and molecular analyses on sciatic nerves in these mice showed a decrease in neurofilament phosphorylation and axonal transport of all three neurofilament subunits, which resulted in a decrease in axonal calibre and an increase in neurofilament density (de Waegh and Brady, 1991; de Waegh et al., 1992). Genetically modified mice with mutations in the *myelin protein zero (P0)* gene also display a hypomyelinating phenotype with similar reductions in neurofilament phosphorylation and axon calibre (Cole et al., 1994). These studies demonstrate the importance of signalling from myelinating Schwann cells for preserving the structural integrity of, and transport systems in, the axon.

A more recent study has strengthened the case for myelinating Schwann cells modulating transport systems in the axon, using *in vitro* assays of Schwann cell/neuron co-cultures to study the effect of myelinating Schwann cells on the

transport of NF-M in the neighbouring axons (Monsma et al., 2014). This culture system allowed for the study of myelinated versus unmyelinated regions in the same axon, as Schwann cells form dispersed segments of myelin along axons in culture. They showed that transport of NF-M is slower in myelinated versus unmyelinated segments of the same axon, resulting in higher levels of NF-M in the myelinated axon and a larger axon calibre (Monsma et al., 2014). Monsma and colleagues proposed that a signal must exist, emanating from the myelinating cell to the axon, in order to impact on cytoskeletal transport dynamics. The results of Chapter 3 suggest that Nfasc155-dependent pathways are an excellent candidate for such a signal. Although such signalling processes emanate from myelinating glial cells, the results in Chapter 3 show that it is likely to occur independent of the myelination process *per se*, as myelin formation and deposition occurs normally in *Nfasc155*^{-/-} mice (Chapter 3; Fig 3.3).

Three key essential proteins for the transport of axonal cargo are kinesin, dynein and dynactin (Shea and Flanagan, 2001). Kinesin plays a central role in anterograde transport whereas dynein and dynactin are involved in retrograde transport of cargo (Shah et al., 2000; Shea and Flanagan, 2001; Xia et al., 2003; Motil et al., 2006; Uchida et al., 2009; Lee et al., 2011). All three subunits of neurofilament, NF-H, NF-M and NF-L, which form the majority of the axon cytoskeleton, utilise this transport system to reach their targets (Shah et al., 2000; Shea and Flanagan, 2001; Shah and Cleveland, 2002; Motil et al., 2006). For example, neurofilaments that are synthesised in the cell bodies of the large motor neurons in the ventral horn, which

are destined for the pre-terminal axons at the NMJ, will be moved anterograde by kinesin and other linker proteins in the microtubule network, to reach their targets.

The above studies have shown that signals emanating from myelinating Schwann cells can modulate the axon cytoskeleton through mechanisms involving neurofilament phosphorylation and transport. It is therefore possible that myelinating Schwann cells utilise kinesin, dynein and dynactin activity to modify transport of neurofilaments in the axon. Schwann cells regulating axonal cytoskeletal dynamics could in turn impact on the remodelling of inputs during postnatal development of the NMJ, as a major feature of synapse elimination in the PNS is axonal cytoskeletal rearrangement, as terminal axons retract and expand territory as they compete for sole innervation of the synapse (Bixby, 1981; Riley, 1981; Sanes and Lichtman, 1999; Keller-Peck et al., 2001).

Interestingly, neurofilament dynamics have previously been implicated in the process of synapse elimination. It has been shown that within retraction bulbs of losing axons at polyinnervated endplates, neurofilament content diminishes (Gan and Lichtman, 1998). In this study, single motor units in the sternomastoid muscle of P0-P17 mice were visualised by lipophilic dye injection. Subsequent staining with antibodies against neurofilament allowed for the visualisation of synaptic territories of individual inputs at polyinnervated endplates. This revealed a loss of NF-H in the thin branches of terminal axons that appeared to be retracting. In a similar study, phosphorylated NF-H immunoreactivity was assessed in rat soleus muscle during the period of postnatal synapse elimination, with the finding of a correlation between

high levels of phosphorylated NF-H and winning inputs at polyinnervated NMJs (Roden et al., 1991). These studies suggest that neurofilament composition in competing pre-terminal axons is a driving factor in the outcome of synapse elimination at the NMJ.

4.1.3 Proteomic analysis

The above studies provide a tenuous yet tantalising possible link between myelinating glial cells and the regulation of synapse elimination in the PNS. This prompted the hypothesis that Nfasc155 modulates synapse elimination by modulating cytoskeletal dynamics in the underlying axons. In an attempt to uncover the mechanisms through which Nfasc155 in the myelinating Schwann cell signals to the underlying axon during axon pruning at the NMJ, and thereby test this hypothesis, a 4-way in-depth proteomic analysis was performed on sciatic-tibial nerve from *Nfasc155*^{-/-}, *Caspr*^{-/-} and littermate controls at P12. Including the *Caspr*^{-/-} mice in the analysis and comparing the results from these mice alongside the *Nfasc155*^{-/-} mice allowed for generation of a list of potential protein candidates downstream of paranodal disruption, formulated by making a list of the similarly changed proteins in both lines of knock-out mice compared to their littermate controls. By subtracting these proteins from the list of changed proteins in the *Nfasc155*^{-/-} mice, a list of potential protein candidates involved in Nfasc155-dependent modulation of synapse elimination was generated. To better understand the functional consequence of the disrupted proteome in the *Nfasc155*^{-/-} mice, pathway analysis was performed on the above dataset. Ingenuity pathway analysis (IPA) on this dataset presented a list of

networks that would be functionally altered in the *Nfasc155*^{-/-} mice based on the changes present in protein levels.

The results of the proteomic analysis were the foundation for beginning to untangle the *Nfasc155*-dependent mechanisms modulating synapse elimination. Using immunofluorescence assays to confirm and elucidate on the results of the proteomic analysis, this chapter provides a clear insight in to the proteins and pathways surrounding the modulation of synapse elimination at the NMJ, downstream of *Nfasc155* in the myelinating glial cell. The experiments outlined in this chapter were designed to tease apart the mechanisms underlying *Nfasc155*-dependent modulation of synapse elimination and provide further support for the importance of Schwann cell signalling for axon structure and function.

4.2 Results

4.2.1 *Nfasc155* does not modulate synapse elimination through trophic mechanisms involving GDNF in skeletal muscle

As discussed in Chapter 1, altered expression of target-derived signals from muscle can modulate rates of synapse elimination at the NMJ, supporting the “trophic hypothesis” of competition at the NMJ (Bennett and Robinson, 1989; English and Schwartz, 1995; Jordan, 1996). This hypothesis relies on a limited supply of growth factor that drives competition between innervating inputs. A previous study by Nguyen et al., (1998) showed how an upregulation of the growth factor GDNF can alter the rate of synapse elimination. This study looked at the effects of over-expressing *GDNF* in muscle on the rate of this developmental process. They found that in mice over-expressing *GDNF*, synapse elimination was significantly delayed (Nguyen et al., 1998). This supports the “trophic hypothesis” in that the supply of target-derived growth factor (GDNF) was increased and so competition was delayed until the supply became scarce.

To test whether GDNF levels in skeletal muscle of *Nfasc155*^{-/-} mice were altered and possibly contributing to the delay in synapse elimination, Western blot analysis was performed in gastrocnemius muscle of *Nfasc155*^{+/+} and *Nfasc155*^{-/-} mice to measure GDNF levels. The gastrocnemius muscle was chosen for its ease of dissection and large size. Levels of the precursor protein, proGDNF, were also analysed as it has been previously shown that precursor and mature forms of the growth factor, brain-

derived neurotrophic factor (BDNF), have opposite effects on the course of synapse elimination at the NMJ (Je et al., 2013). Western blot analysis revealed no significant difference between genotypes for both proGDNF and total GDNF (Figure 4.1), eliminating target-derived GDNF signalling perturbations as a contributing factor in the delayed synapse elimination observed in *Nfasc155*^{-/-} mice.

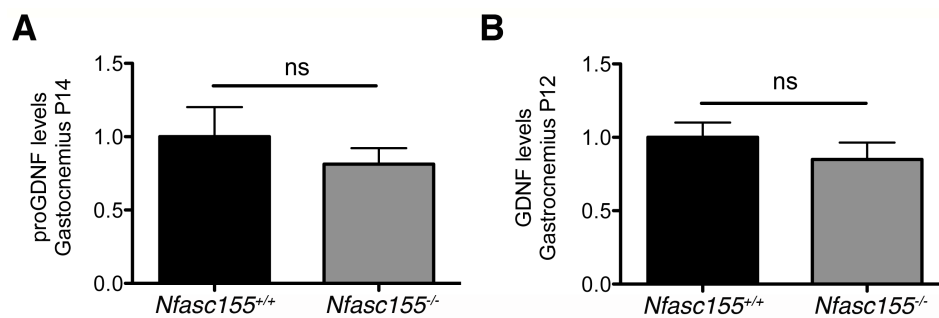


Figure 4.1. proGDNF and total GDNF levels are unchanged in gastrocnemius muscle in *Nfasc155*^{-/-} mice. (A & B) Quantitative Western blotting shows no change in (A) proGDNF levels or (B) total GDNF levels in *Nfasc155*^{-/-} mice compared to controls, eliminating GDNF signalling in muscle as part of *Nfasc155*-dependent modulation of synapse elimination (Unpaired t-test; N=3 mice per genotype; 1 muscle per mouse).

4.2.2 iTRAQ proteomic analysis on peripheral nerve reveals a significantly more disrupted proteome in *Nfasc155*^{-/-} compared to *Caspr*^{-/-} mice

In an attempt to uncover the mechanisms through which *Nfasc155* was modulating synapse elimination, independent of its paranodal functions, a 4-way comparative iTRAQ proteomic analysis of sciatic-tibial nerve was carried out using tissue harvested from P12 *Nfasc155*^{-/-} and *Caspr*^{-/-} mice, alongside littermate controls from both lines (see Chapter 2 for detailed methods), using a previously established method (Wishart et al., 2014). This in-depth analysis produced a list of >3,000 proteins whose levels were altered in *Nfasc155*^{-/-} and *Caspr*^{-/-} mice (Figure 4.2; pre-filtering). However, as can be seen in Figure 4.2, the majority of changed proteins in *Caspr*^{-/-} mice are clustered within +/- 20% ratio change, which was the cut-off for significance as explained in the next paragraph. In the *Nfasc155*^{-/-} mice on the other hand, large groups of proteins can be seen to have ratio changes greater than +/- 20%.

In order to generate a list of proteins with modified expression levels in sciatic-tibial nerves from *Nfasc155*^{-/-} and *Caspr*^{-/-} mice and be confident of the identification and measurement of individual proteins, all raw proteomics data were filtered using an established protocol (Wishart et al., 2014): only proteins identified by 2 or more unique peptides and modified greater or lesser than 20% compared to littermate controls were used for further analysis. Figure 4.2 shows the result of filtering on the dataset.

Post-filtering, 1,210 proteins had modified levels in peripheral nerve in *Nfasc155*^{-/-} mice compared to their littermate controls, whereas only 405 proteins showed modified expression levels in *Caspr*^{-/-} mice compared to their littermate controls (Figure 4.2). This result indicates that Nfasc155 has more cellular duties than Caspr, as loss of Nfasc155 resulted in a significantly more disrupted peripheral nerve proteome compared to loss of Caspr. This exciting finding also supports the results of the previous chapter, which identified a novel role for Nfasc155 outside of paranodal formation. Although Nfasc155 and Caspr both play fundamental roles in paranodal assembly, it is clear from proteomic analysis that Nfasc155 is required for many more cellular processes than was previously thought, including the modulation of synapse elimination.

Interestingly, of the 405 proteins found to have modified levels in *Caspr*^{-/-} mice, 56 proteins were commonly shared with and similarly changed in *Nfasc155*^{-/-} mice (Figure 4.3). Given that both strains of mice had disrupted paranodes, but only *Nfasc155*^{-/-} mice had delayed synapse elimination, these 56 proteins were subtracted from those modified in *Nfasc155*^{-/-} mice to establish a dataset of proteins whose expression changes directly correlated with delayed synapse elimination. This produced a list of 1,154 proteins that were distinctly changed in *Nfasc155*^{-/-} mice (Figure 4.3) and that correlated with delayed synapse elimination. The 56 proteins similarly changed were considered as a potential list of proteins downstream of paranodal disruption. For the purpose of this study, this dataset was not further studied. The 1,154 distinctly changed proteins in *Nfasc155*^{-/-} mice were further studied to identify functional networks that would be perturbed in these mice, with

the aim to untangle the regulatory pathways at play during synapse elimination, downstream of Nfasc155 in the myelinating Schwann cell.

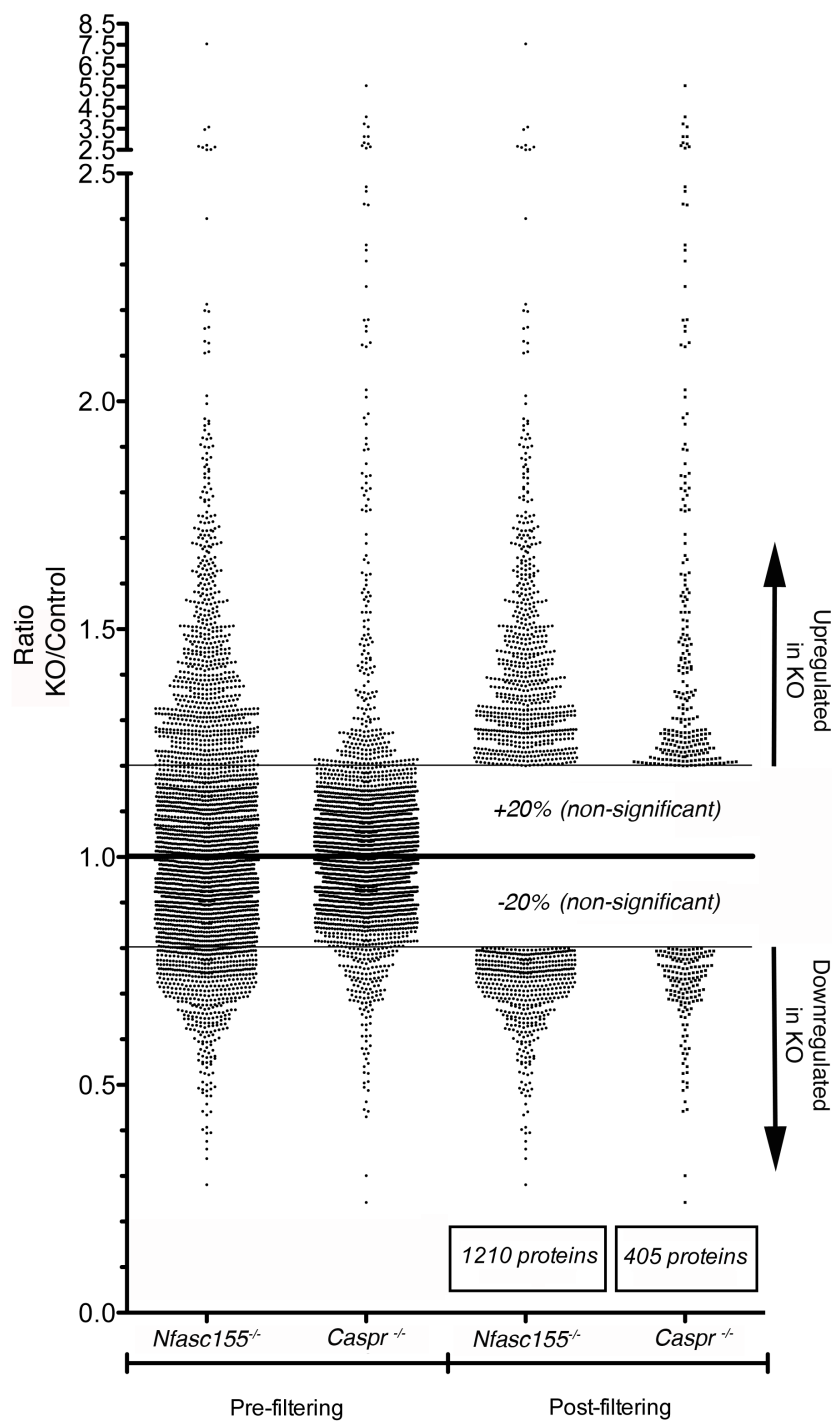


Figure 4.2. Scatter plot of proteins whose levels were changed in *Nfasc155*^{-/-} and *Caspr*^{-/-} mice compared to controls, pre-filtering and post-filtering, showing almost 3 times as many proteins changed in the *Nfasc155*^{-/-} mice than in the *Caspr*^{-/-} mice post-filtering. Each dot represents a single protein. Eliminated proteins were identified by only 1 peptide &/or had a ratio change of <20% compared to control levels.

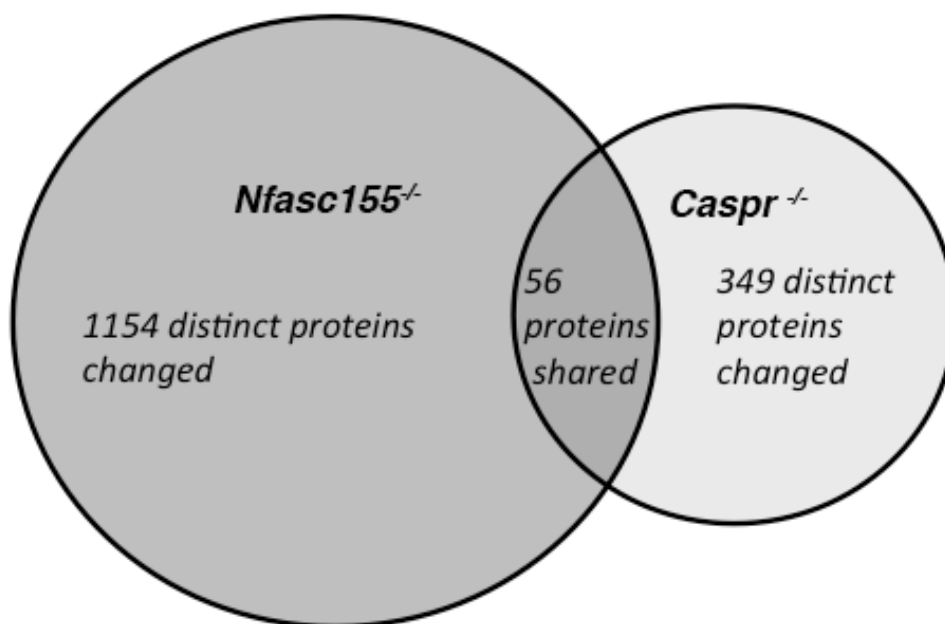


Figure 4.3. Venn diagram showing the comparison of changed proteins between *Nfasc155*^{-/-} and *Caspr*^{-/-} mice. 56 identified proteins were commonly changed between the two genotypes, considered to be downstream of paranodal disruption. 1154 distinctly changed proteins were identified in the *Nfasc155*^{-/-} mice, considered to be downstream of delayed synapse elimination, and 349 distinctly changed proteins were identified in the *Caspr*^{-/-} mice.

4.2.3 Pathway analysis reveals alterations in cytoskeletal organisation and assembly in *Nfasc155*^{-/-} mice

Proteomic analysis revealed a significantly altered peripheral nerve proteome in *Nfasc155*^{-/-} mice, indicated by 1,154 distinct proteins whose levels were altered due to loss of Nfasc155 and correlated with delayed synapse elimination. To better understand the functional consequences of proteome disruption in peripheral nerve of *Nfasc155*^{-/-} mice, and provide insight in to the pathways regulating synapse elimination, bioinformatics-based Ingenuity Pathway Analysis (IPA) software (see Chapter 2 for more details) was used to identify any functional clustering of the 1,154 modified proteins into biological networks. IPA formulates networks based on previously published associations between proteins.

IPA analyses revealed significant clustering of proteins into cellular and molecular functions surrounding ‘cellular assembly and organisation’ (Table 4.1), with 299 of the 1154 distinctly changed proteins identified in *Nfasc155*^{-/-} mice belonging to these functions. This analysis also revealed significant clustering of proteins into cellular and molecular functions known to be involved in ‘cellular function and maintenance’, ‘cell death and survival’, ‘cellular growth and proliferation’ and ‘protein synthesis’ (Table 4.1). These groups overlap in terms of proteins associated in each group and so to get a clearer indication of the individual networks that were most significantly altered as a result of loss of Nfasc155, the networks and proteins associated with ‘cellular assembly and organisation’ were studied further.

The functional cluster ‘cellular assembly and organisation’ was chosen for further analysis as it had the highest significance associated with it. It is worth noting also, that the pathways associated with each of the top 5 clusters had a significant amount of overlap in terms of proteins associated with them. Closer analysis of the functional cluster ‘cellular assembly and organisation’ revealed widespread disruption to molecular pathways and processes implicated in cytoskeletal organisation and trafficking (Table 4.2). All 299 of these proteins were either unchanged in the *Caspr*^{-/-} mice or changed in the opposite direction to *Nfasc155*^{-/-} mice. The list of pathways and processes in this table indicates that multiple networks essential for axonal transport and microtubule dynamics would be altered in the *Nfasc155*^{-/-} mice based on the protein changes identified with iTRAQ.

Study of the proteins associated with the networks in Table 4.2 presented proteins and protein isoforms, such as kinesin, dynein and dynactin, that play major roles in anterograde and retrograde transport of axonal cargo (Shea and Flanagan, 2001; Xia et al., 2003; Motil et al., 2006; Uchida et al., 2009; Lee et al., 2011). Study of the raw proteomic dataset showed that levels of all three motor proteins including several isoforms were identified in the proteomic screen as changed in *Nfasc155*^{-/-} mice (Table 4.3). Importantly, when the raw *Caspr*^{-/-} dataset was assessed, only 2/10 key transport proteins were changed in the *Caspr*^{-/-} mice. However, both of these proteins were changed in the opposite direction to the *Nfasc155*^{-/-} mice, suggesting that these changes would not have similar biological effects. These results suggest that loss of *Nfasc155*, a glial cell protein, results in targeting of axonal transport systems, which could be associated with the delayed synapse elimination observed at the NMJ. This

analysis implicates transport systems in the modulation of synapse elimination, which has never before been shown, and also provides a tangible link between Nfasc155 and the modulation of developmental pruning.

Cellular and Molecular Function	P-value	No. of Proteins
Cellular Assembly and Organisation	1.06E-25 – 3.40E-04	299
Cellular Function and Maintenance	1.06E-25 – 3.10E-04	287
Cell Death and Survival	3.22E-21 – 2.19E-04	409
Cellular Growth and Proliferation	1.04E-14 – 3.40E-04	378
Protein Synthesis	5.86E-14 – 2.17E-04	166

Table 4.1. List of top 5 changed cellular and molecular functions in the *Nfasc155*^{-/-} mice, with the largest change observed in cellular assembly and organisation. The calculated P-value for each altered function along with the number of proteins in the proteomic analysis found to be associated with each network is also shown.

Pathways and Processes	P-value	No. of Proteins	No. of Proteins	
			Upreg.	Downreg.
Organisation of cytoplasm	1.06E-25	201	123	78
Organisation of cytoskeleton	9.15E-23	183	106	77
Microtubule dynamics	1.03E-20	159	96	63
Formation of cellular protrusions	1.70E-13	110	68	42
Formation of filaments	4.11E-16	73	47	26
Growth of plasma membrane	4.90E-11	72	46	26
Growth of neurites	9.10E-11	71	45	26
Formation of plasma membrane	5.75E-08	70	45	25
Neuritogenesis	2.16E-06	60	36	24
Formation of cytoskeleton	2.80E-11	59	39	20
Organisation of filaments	4.78E-09	34	18	16
Organisation of actin cytoskeleton	2.68E-07	34	12	22
Quantity of filaments	1.18E-11	31	19	12
Quantity of cellular protrusions	1.77E-09	31	21	10
Extension of cellular protrusions	1.40E-06	30	19	11
Synaptogenesis	5.93E-06	26	21	5
Extension of neurites	8.72E-06	24	14	10
Transport of vesicles	3.30E-07	22	9	13
Polymerisation of filaments	1.12E-05	19	14	5
Stabilisation of filaments	1.36E-04	17	10	7
Stabilisation of microtubules	2.78E-04	15	9	6
Formation of microtubules	4.75E-05	14	9	5
Quantity of neurites	1.04E-04	14	11	3
Rearrangement of cytoskeleton	1.23E-04	13	9	4
Transport of synaptic vesicles	1.88E-04	11	7	4
Polymerisation of microtubules	4.34E-05	10	8	2
Quantity of axons	5.54E-05	10	8	2
Elongation of axons	2.94E-04	8	5	3

Table 4.2. List of functional pathways and processes involved in cellular assembly and organisation pathways significantly changed in the *Nfasc155*^{-/-} mice. The calculated P-value for each altered pathway and process, the number of proteins in the proteomic analysis found to be associated with each function and the direction in which those proteins were changed are shown.

Protein	<i>Nfasc155</i> ^{-/-}		<i>Caspr</i> ^{-/-}	
	Change	KO/Control	Change	KO/Control
Dynein light chain roadblock-type 1	Upreg.	1.343	NC	
Kinesin light chain 1 isoform 1A	Downreg.	0.779	NC	
Kinesin heavy chain isoform 5C	Downreg.	0.786	NC	
Kinesin heavy chain isoform 5A	Downreg.	0.675	NC	
Kinesin-like protein KIF1A isoform B	Downreg.	0.689	NC	
Dynein light chain Tctex-type 3	Downreg.	0.595	Upreg.	1.964
Cytoplasmic dynein 1 light intermediate chain	Downreg.	0.727	NC	
Cytoplasmic dynein 1 light intermediate chain	Downreg.	0.733	NC	
Dynactin subunit 5	Downreg.	0.610	Upreg.	1.759
Dynactin subunit 1 isoform 3	Downreg.	0.772	NC	

Table 4.3. Levels of core proteins involved in cytoskeletal organisation and trafficking pathways in peripheral nerve from *Nfasc155*^{-/-} and *Caspr*^{-/-} mice.

NC = not changed. Only 2/10 proteins were changed in the *Caspr*^{-/-} mice and in the opposite direction.

4.2.4 Kinesin5A levels are significantly decreased in sciatic nerve of *Nfasc155*^{-/-} mice

The proteomic analysis was carried out on whole sciatic-tibial nerve, which will include a high population of myelinating Schwann cells. Glial cells are known to express isoforms of transport proteins, including kinesin light chain (Kamal et al., 2001) and kinesin heavy chain (Schmidt et al., 2012). To validate the changes in cytoskeletal transport and organisation proteins identified in the proteomic screen, and to confirm that these changes were occurring in axonal processes of neurons, transverse sciatic nerve sections from *Nfasc155*^{-/-} mice and littermate controls were immunolabelled for kinesin 5A, which is predominantly expressed in axons (Xia et al., 1998) and the proteomics data suggested was down-regulated in *Nfasc155*^{-/-} mice (Table 4.3). Kinesin 5A is part of a multi-subunit complex that functions in anterograde transport in the axon, along with 13 other isoforms (Lawrence et al., 2004). Kinesin associates with the microtubule system and interacts with axonal cargo to transport it anterograde (Shea and Flanagan, 2001). Quantitative fluorescence intensity measurements confirmed a statistically significant reduction in levels of kinesin 5A in axons from *Nfasc155*^{-/-} mice compared to littermate controls (Figure 4.4A,B), confirming that loss of *Nfasc155* results in decreased levels of kinesin in the axon, which could be contributing to the delayed synapse elimination observed in these mice.

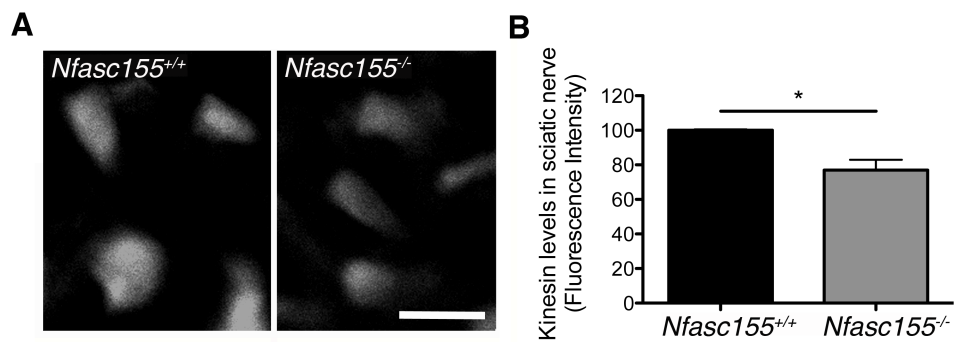


Figure 4.4. Levels of kinesin 5A are reduced in the sciatic nerve of *Nfasc155^{-/-}* mice. (A) Example confocal micrographs of transversely sectioned axons in the sciatic nerve of *Nfasc155^{+/+}* and *Nfasc155^{-/-}* mice, showing a reduction of kinesin 5A in *Nfasc155^{-/-}* mice. Scale bar 5 μ m. (B) Quantification of fluorescence intensity of kinesin 5A levels in sciatic nerve shows a significant decrease in axons of *Nfasc155^{-/-}* mice (p=0.0191; unpaired t-test; N=3 mice per genotype, 1 nerve per mouse).

4.2.5 *Nfasc155*^{-/-} mice exhibit a selective reduction in levels of NF-L in motor nerve terminals

Although proteomic analysis produced a correlation between delayed synapse elimination and altered transport systems, it remained to be determined how defective transport systems could result in delayed synapse elimination in *Nfasc155*^{-/-} mice. Kinesin, dynein and dynactin are essential components for the axonal transport of various types of cargo, including transport of neurofilaments throughout the entire length of neuronal axons (Shah et al., 2000; Shea and Flanagan, 2001; Motil et al., 2006; Lee et al., 2011). It was therefore hypothesized that, if cytoskeletal transport was disrupted in *Nfasc155*^{-/-} mice, corresponding changes in the composition and/or sub-cellular arrangement of the neurofilament cytoskeleton may also be present in peripheral nerve, which could be contributing to the delay in synapse elimination. Neurofilament dynamics have previously been proposed to influence synapse elimination with a correlation present between phosphorylated NF-H levels and winning inputs at NMJs (Roden et al., 1991) and between retreating/losing axons and neurofilament depletion (Gan and Lichtman, 1998). The suggestion of a possible local regulation of neurofilament dynamics by myelinating Schwann cells is not so intangible considering the finding that myelinating glial cells can modulate the neurofilament content and organisation of axons via local modulation of transport pathways (Monsma et al., 2014). This provides some evidence for a local signal emanating from myelinating Schwann cells in regulating transport in the underlying axon, which could involve *Nfasc155*.

To address the possibility that perturbed transport systems in the *Nfasc155*^{-/-} mice would result in altered neurofilament levels or distribution, levels of neurofilament heavy (NF-H), neurofilament medium (NF-M) and neurofilament light (NF-L) proteins were examined in the distal portions of motor axons in LAL pre-terminal axons from P11 *Nfasc155*^{-/-} and *Caspr*^{-/-} mice, by immunolabelling muscles for each of the three neurofilament subunits. This analysis was carried out in muscle to allow for a direct comparison between neurofilament composition and synapse elimination. Fluorescence intensity measurements of pre-terminal axons revealed similar levels of NF-M and NF-H in *Nfasc155*^{-/-} mice, *Caspr*^{-/-} mice and their littermate controls (Figure 4.5A,B). This is in support of the finding that axon calibre was unaffected in peripheral nerve of *Nfasc155*^{-/-} mice (Chapter 3; Figure 3.3), as phosphorylation of NF-M and NF-H subunits is believed to play a crucial role in the radial growth of axons (de Waegh et al., 1992; Sanchez et al., 2000) with NF-L believed to be dispensable for axon radial growth (Monteiro et al., 1990). However, motor axons, their terminal collateral branches and axon terminals had significantly lower levels of NF-L in *Nfasc155*^{-/-} mice compared to controls (~20% less NF-L in pre-terminal axons of *Nfasc155*^{-/-} mice compared to controls; Figure 4.6A,B). In contrast, NF-L levels remained unchanged in *Caspr*^{-/-} mice (Figure 4.6A,B). The reduced levels of NF-L in *Nfasc155*^{-/-} mice therefore correlated with delayed synapse elimination, potentially implicating NF-L in the *Nfasc155*-dependent modulation of postnatal development of the PNS and providing a credible mechanism through which *Nfasc155* monitors and alters this process.

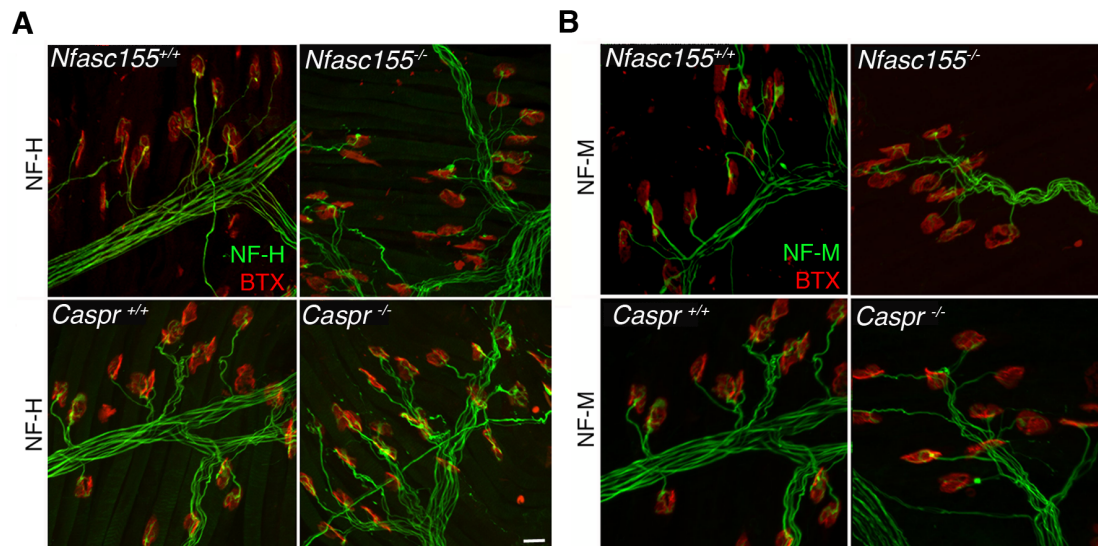


Figure 4.5. NF-M and NF-H levels are unchanged in axon terminals of *Nfasc155*^{-/-} and *Caspr*^{-/-} mice. (A & B) Confocal micrographs (taken with identical microscope settings) of NMJs in the LAL of *Nfasc155*^{+/+}, *Nfasc155*^{-/-}, *Caspr*^{+/+} and *Caspr*^{-/-} mice at P11 with axons immunolabelled for (A) NF-H and (B) NF-M. Endplates were labelled with TRITC-BTX. Fluorescence intensity of intramuscular axons and axon bundles immunolabelled for NF-H and NF-M appeared similar between groups. Scale bar 20 μ m.

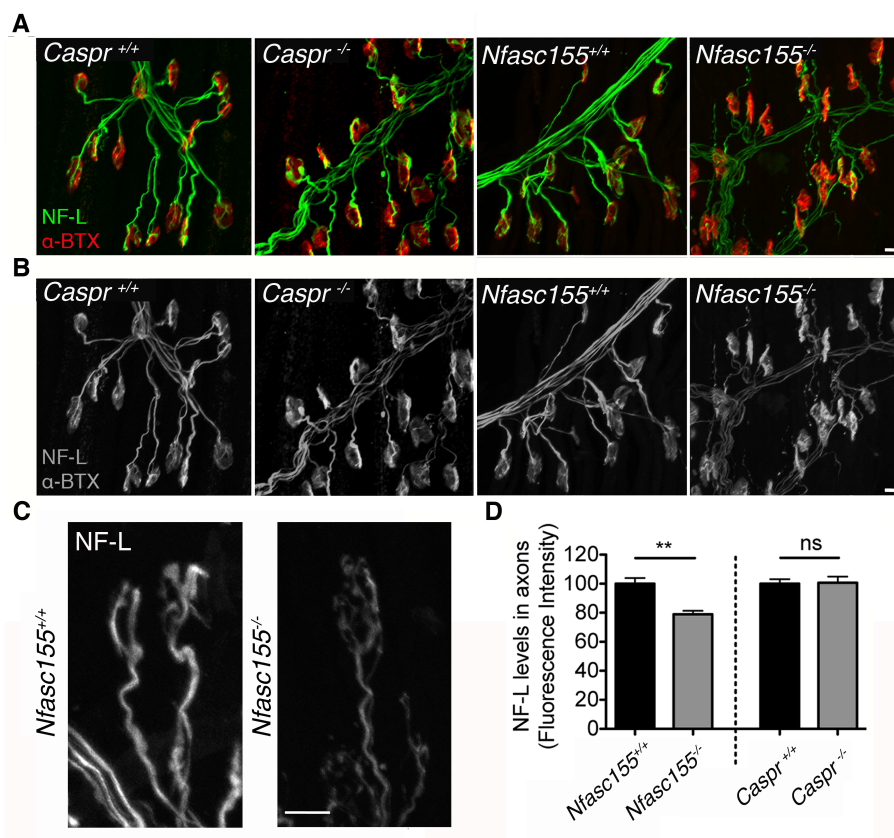


Figure 4.6. NF-L levels are significantly downregulated in pre-terminal axons of *Nfasc155*^{-/-} mice. (A) Representative confocal micrographs (taken with identical microscope settings) of NMJs in the LAL of P11 *Nfasc155*^{+/+}, *Nfasc155*^{-/-}, *Caspr*^{+/+} and *Caspr*^{-/-} mice with axons immunolabelled for NF-L. Endplates were labelled with TRITC-BTX. The labelling intensity of intramuscular axons bundles, pre-terminal axons and axon terminals was noticeably lower in *Nfasc155*^{-/-} mice. Scale bars 20 μ m. (B) Same confocal micrographs as those shown in (A) but in grayscale, to emphasize the noticeable reduction in NF-L levels in pre-terminal axons and axon terminals in *Nfasc155*^{-/-} mice. (C) High magnification confocal micrographs of single endplates in *Nfasc155*^{-/-} and *Nfasc155*^{+/+} mice immunolabelled for NF-L only, showing reduced levels of NF-L in pre-terminal axons as well as axon terminals overlying the endplate. (D) Quantification of NF-L levels using fluorescence intensity measurements revealed significantly lower levels in pre-terminal axons from *Nfasc155*^{-/-} mice (p=0.0018; unpaired t-test; N=3 mice per genotype, 2 muscles per mouse) but not from *Caspr*^{-/-} mice (N=3 mice per genotype).

4.2.6 Tubulin expression is unaltered in pre-terminal axons of *Nfasc155*^{-/-} mice

The cytoskeleton of axons is composed of proteins other than neurofilaments, such as microtubules (Wuerker and Palay, 1969; Yamada et al., 1970, 1971; Schnapp and Reese, 1982; Tsukita et al., 1982). β -III tubulin forms part of the network of microtubules in the axon and has been shown to be upregulated during the period of postnatal synapse elimination (Jiang and Oblinger, 1992). To determine if levels of microtubule components in the cytoskeleton were altered at the NMJ, LAL muscles in *Nfasc155*^{+/+} and *Nfasc155*^{-/-} mice were immunolabelled for β -III tubulin. Qualitative analysis revealed similar levels in pre-terminal axons of both genotypes (Figure 4.7A). Quantitative analysis confirmed that β -III tubulin levels were unchanged in the pre-terminal axons of *Nfasc155*^{-/-} mice (Figure 4.7B) indicating that cytoskeletal alterations were specific to NF-L in *Nfasc155*^{-/-} mice.

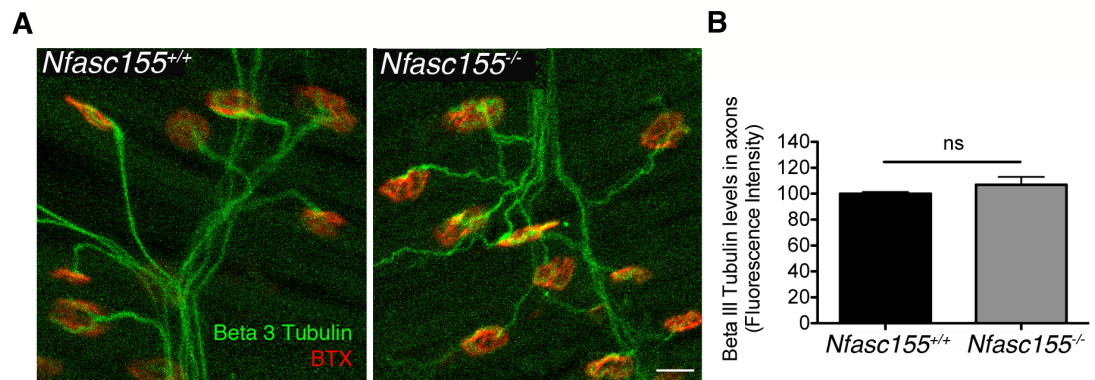


Figure 4.7. β -III tubulin levels are unchanged in pre-terminal axons of *Nfasc155^{-/-}* mice. (A) Example confocal micrographs showing similar levels of β -III tubulin in *Nfasc155^{+/+}* and *Nfasc155^{-/-}* mice. **(B)** Quantitative analysis of β -III tubulin in pre-terminal axons shows no significant difference between genotypes (Unpaired t-test; N=3 mice per genotype; 1 muscle per mouse).

4.2.7 Synapse elimination is significantly delayed in $NF-L^{-/-}$ mice, supporting a role for NF-L during this process

The above results suggested that Nfasc155 could be modulating synapse elimination through modulation of axonal transport systems, with loss of Nfasc155 resulting in selective defects in cytoskeletal transport and loss of NF-L specifically, from distal regions of motor neurons. However, NF-L specifically had never before been implicated in the regulation of synapse elimination and so, to determine whether the selective reduction in NF-L levels was contributing directly to the delay in synapse elimination, the rate of synapse elimination in mice lacking NF-L was examined (Zhu et al., 1997).

The *tibialis anterior* (TA) muscle was used in this analysis due to the ease of fixation with minimal dissection, as these muscles were transported to Edinburgh from Laval University in Canada. Tissue was harvested at P10, when synapse elimination is ongoing in the TA of mice. $NF-L^{+/-}$ and $NF-L^{+/+}$ littermates were used as controls because they had comparable levels of polyinnervation. The absence of NF-L from motor axons in $NF-L^{-/-}$ mice was confirmed using immunofluorescence on the TA with an NF-L specific antibody (Figure 4.8A). To assess the rate of synapse elimination in $NF-L^{-/-}$ mice, TA muscles from P11 mice were immunolabelled with anti- β -III-Tubulin and TRITC-BTX, and polyinnervation levels quantified. Antibodies recognising neurofilaments could not be used to label axons as both NF-M and NF-H levels are significantly reduced in peripheral nerve of $NF-L^{-/-}$ mice (Zhu et al., 1997).

In support of the hypothesis that NF-L is an essential cytoskeletal component for driving normal rates of synapse elimination, this analysis revealed almost twice as many polyinnervated motor endplates in *NF-L*^{-/-} mice compared to control mice (21% polyinnervated in *NF-L*^{-/-} mice versus 12% polyinnervation in controls), indicative of a delay in synapse elimination (Figure 4.8B,C). Interestingly, the magnitude of the delay in synapse elimination observed in *NF-L*^{-/-} mice did not reach those levels previously observed in *Nfasc155*^{-/-} mice at the same age (increase of 79% in *NF-L*^{-/-} mice versus increase of 198% in *Nfasc155*^{-/-} mice compared to control littermates). This suggests that Nfasc155 may modulate synapse elimination through NF-L-dependent as well as NF-L-independent mechanisms, with delayed synapse elimination caused by loss of glial Nfasc155 likely to be mediated, at least in part, through modulation of the axonal cytoskeleton.

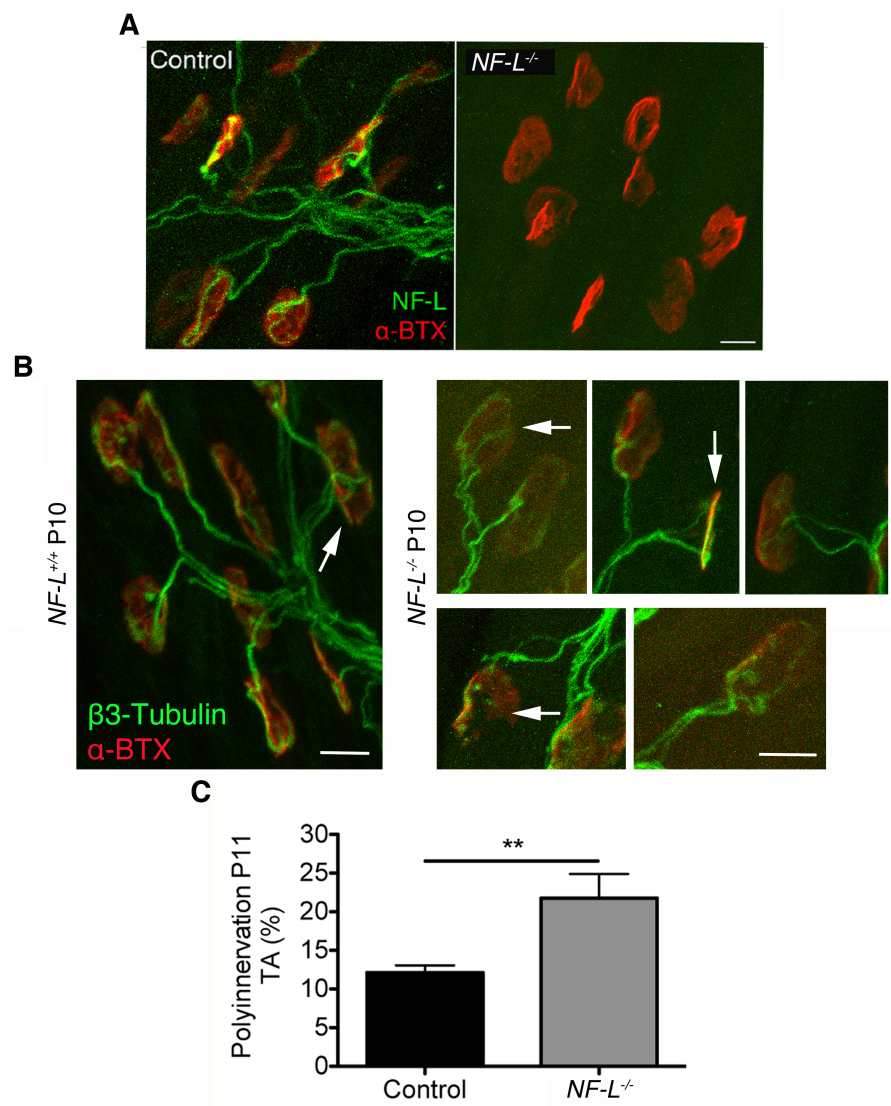


Figure 4.8. Synapse elimination is significantly delayed in $NF-L^{-/-}$ mice. (A) Confocal micrographs showing presence of NF-L in axons and motor nerve terminals (identified by neighbouring motor endplates; red) from a TA muscle in a control mouse at P11, but absence in comparable $NF-L^{-/-}$ mouse tissue. Endplates were labelled with TRITC-BTX. Scale bar 20 μ m. (B) Confocal micrographs showing NMJs in the TA muscle of control and $NF-L^{-/-}$ mice labelled with β -III-Tubulin, including examples of polyinnervated endplates (indicated by arrows). Endplates were labelled with TRITC-BTX. Scale bars 20 μ m. (C) There was a significant delay in synapse elimination in $NF-L^{-/-}$ mice compared to littermate controls (p=0.0046; Mann Whitney U-test; N=16 control mice, N=8 $NF-L^{-/-}$ mice, 2 muscles per mouse).

4.2.8 NF-L is abnormally distributed throughout the motor neuron in *Nfasc155*^{-/-} mice

The results presented above provide clear mechanistic insight into *Nfasc155*-dependent modulation of synapse elimination. An in-depth proteomic analysis on peripheral nerve in *Nfasc155*^{-/-} mice revealed alterations to transport systems, which resulted in a selective depletion of NF-L in the most distal regions of motor neurons. This suggested a role for NF-L during synapse elimination and a mechanism through which *Nfasc155* modulates this process. Indeed, *NF-L*^{-/-} mice recapitulated the delayed synapse elimination observed in *Nfasc155*^{-/-} mice, verifying the importance of this neurofilament subunit in the outcome of developmental pruning at the NMJ. The proteomic analysis suggests that reduced NF-L levels at pre-terminal axons is likely due to abnormal distribution of NF-L throughout the nerve rather than defects in expression levels. In an attempt to provide further support for this hypothesis, NF-L levels were assessed in more proximal regions of motor neurons, in tibial nerve and spinal cord ventral roots. If *Nfasc155* was locally modulating transport systems in the underlying axons then you would predict that NF-L would be abnormally distributed in more proximal regions of the motor neurons as well as distally, because myelinating Schwann cells will be found along the entire length of lower motor neurons.

Transversely sectioned tibial nerve from P14 *Nfasc155*^{-/-} and *Nfasc155*^{+/+} mice immunolabelled for NF-L indicated lower levels of NF-L in *Nfasc155*^{-/-} compared to controls (Figure 4.9C). This was confirmed quantitatively revealing significantly

lower levels in *Nfasc155*^{-/-} mice (Figure 4.9D). Interestingly, transversely sectioned spinal cord from P14 *Nfasc155*^{-/-} and *Nfasc155*^{+/+} mice immunolabelled for NF-L revealed significantly higher levels of NF-L in the ventral roots of *Nfasc155*^{-/-} mice (Figure 4.9A,B). This data is in keeping with the presence of a defect in the axonal transport systems in *Nfasc155*^{-/-} mice. It appears that due to defective axonal transport, NF-L levels are significantly reduced in the more distal regions, such as axon terminals and peripheral nerve, whereas NF-L appears to be accumulating in the more proximal parts of the nerve, such as the ventral roots of the spinal cord. This finding is summarised in Figure 4.9E.

Proteomic analysis on sciatic-tibial nerve revealed no difference in levels of NF-L in *Caspr*^{-/-} mice, but a small increase in levels in *Nfasc155*^{-/-} mice (25%; 5% above the cut-off for significance). This is most likely due to the fact that whole sciatic-tibial nerve was used in the analysis, with more proximal regions contributing a greater proportion of tissue than distal parts, thus biasing the results in favour of the regions where NF-L was accumulating. Interestingly, the proteomic screen also revealed significant changes in levels of α -internexin (upregulated 25%) and peripherin (downregulated 40%) in *Nfasc155*^{-/-} mice, two intermediate filament proteins expressed earlier than or at the same time as NF-L in the nervous system (Portier et al., 1983; Escurat et al., 1990; Kaplan et al., 1990). It is known that NF-L is the most abundant out of the three neurofilament subunits and one of the earliest expressed in the embryo (Willard and Simon, 1983; Carden et al., 1987). Thus, the significant disruption to transport systems in the axons of *Nfasc155*^{-/-} mice appears to have the most notable effects on levels of the earliest expressed filamentous proteins.

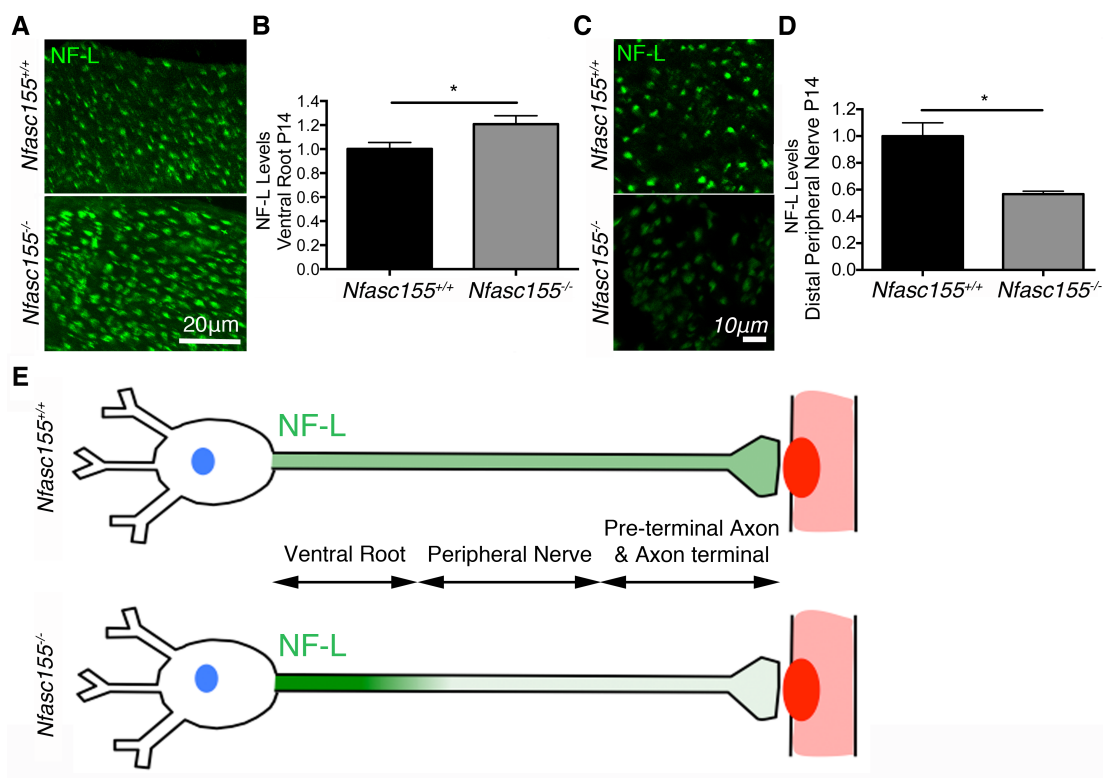


Figure 4.9. Disrupted cytoskeletal transport networks in *Nfasc155*^{-/-} mice results in increased levels of NF-L in spinal cord ventral roots and reduced levels in tibial nerve. (A) Example confocal micrographs of transverse spinal cord sections immunolabelled for NF-L, showing increased levels in the ventral roots of P14 *Nfasc155*^{-/-} mice. Scale bar 20µm. (B) Fluorescence intensity measurements showing a significant increase in NF-L levels in spinal cord ventral roots of P14 *Nfasc155*^{-/-} mice (p=0.0239; unpaired t-test; N=3 mice per genotype, 2-9 ventral horns analysed per mouse). (C) Example confocal micrographs of transverse tibial nerve sections immunolabelled for NF-L, showing reduced levels in P14 *Nfasc155*^{-/-} mice. Scale bar 10µm. (D) Fluorescence intensity measurements showing a significant reduction in NF-L levels in tibial nerve of P14 *Nfasc155*^{-/-} mice (p=0.0132; unpaired t-test; N=3 mice per genotype, 1 nerve per mouse). (E) Simplified schematic of a motor neuron summarising the disruption to NF-L levels in *Nfasc155*^{-/-} mice. Green shading indicates NF-L. *Nfasc155*^{+/+} motor neurons display a uniform distribution of NF-L throughout the motor neuron whereas NF-L appears to be accumulating in proximal ventral roots and decreased in more distal regions, in peripheral nerve and axon terminals.

4.2.9 NF-L levels are higher during synapse elimination whereas NF-M and NF-H levels peak post-synapse elimination in C57BL6 mice

The above results suggest that Nfasc155 modulates synapse elimination rates by modulating axonal transport systems and trafficking of NF-L, without affecting levels of NF-M and NF-H. In an attempt to discover why NF-L specifically could be playing a role during synapse elimination, experiments were performed in C57BL6 mice to study the expression and localisation of NF-L during normal synapse elimination. The sciatic nerve was used to analyse total protein levels by Western blotting. Cranial muscles were used to analyse both protein level in pre-terminal axons and localisation of individual neurofilament subunits at the NMJ by immunofluorescence.

It is known that NF-L is the most abundant out of the three neurofilament subunits and one of the earliest expressed in the embryo (Willard and Simon, 1983; Carden et al., 1987) but it has not been shown how levels of the three neurofilament proteins differ between a time when synapse elimination is occurring and when it has been completed. Based on the previous results implicating NF-L specifically in the process of synapse elimination, one might expect to find a difference between the expression profiles or localisation of NF-H, NF-M and NF-L during normal synapse elimination, that could explain its role during this time. The following experiments were designed to test these hypotheses using C57BL6 mice.

Levels of NF-H, NF-M and NF-L were assessed by Western blot on sciatic nerve from C57BL6 mice at P10, when synapse elimination was still occurring, and P19, when synapse elimination had been completed. To eliminate litter-litter variability, a single litter was used in this analysis, harvesting tissue from four mice at P10 and four littermates at P19. This revealed significantly higher levels of NF-H and NF-M at P19 compared to P10 (normalised to β -actin) (Figure 4.10A,B). There was no difference in levels of NF-L between P10 and P19 (Figure 4.10C). This suggests that higher levels of NF-H and NF-M are required post-synapse elimination, possibly for axon growth and maturation (Cleveland et al., 1991), whereas peak NF-L levels are required earlier, during the time when synapse elimination is taking place. This provides further support for a role for NF-L in postnatal development of the NMJ.

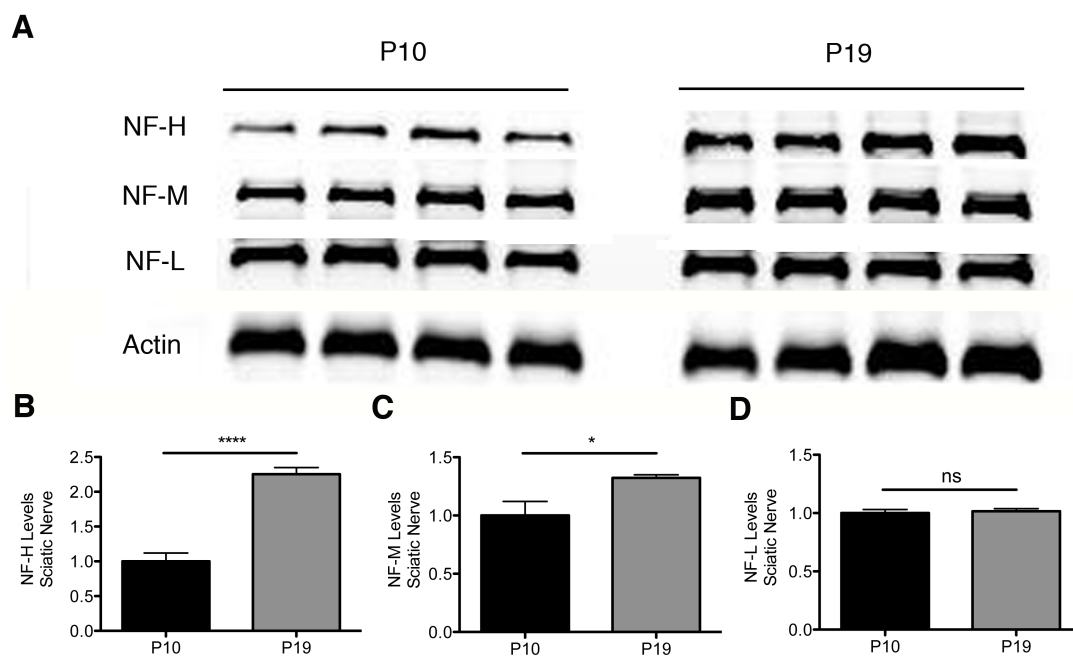


Figure 4.10. NF-L protein levels in peripheral nerve are high during synapse elimination whereas NF-M and NF-H levels increase post-synapse elimination. (A) Scans of blots used for quantification of NF-H, NF-M and NF-L levels in P10 and P19 sciatic nerve. (B-D) Quantification from Western blots on sciatic nerve for (B) NF-H, (C) NF-M and (D) NF-L at P10 and P19. There was a significant difference between levels of (B) NF-H ($p < 0.0001$; unpaired t-test; $N = 4$, 2 nerves per mouse) and (C) NF-M ($p = 0.0208$; unpaired t-test; $N = 4$, 2 nerves per mouse) correlating high levels of NF-L with ongoing synapse elimination. β -actin was used as a loading control.

4.2.10 NF-L-dependent modulation of synapse elimination most likely takes place outside of the pre-terminal axon

To further examine neurofilament localisation during synapse elimination, and determine whether the expression profile of NF-L at poly-innervated endplates could explain its role during synapse elimination, a detailed analysis of poly-innervated endplates was carried out at P10, on muscles double immunolabelled for NF-M/NF-L and NF-H/NF-M. P10 was chosen as a suitable time-point to study synapse elimination, as the majority of poly-innervated endplates had only two innervating axons, making them easier to study for differences in neurofilament levels between competing inputs. The hypothesis behind this experiment was that NF-L levels would vary between competing inputs, conferring the axons with higher levels of NF-L with an advantage during synapse elimination, whereas NF-M and NF-H levels in competing inputs would be similar.

Fluorescence intensity measurements were taken along pre-terminal axons for each neurofilament subunit at endplates with two innervating axons, averaged per axon, and a ratio calculated as a measure of the expression profile (Input 1/Input 2). This analysis revealed similar expression profiles of each neurofilament subunit at poly-innervated endplates (ie. NF-L versus NF-M, NF-M versus NF-H) (Figure 4.11A-C), suggesting that increased levels of NF-L in competing pre-terminal axons approaching the endplate do not drive the outcome of synapse elimination. However, it remained possible that NF-L was driving synapse elimination through mechanisms in the most distal part of the motor neuron, the axon terminal, which actively adapts

to compete for synaptic territory (Keller-Peck et al., 2001; Walsh and Lichtman, 2003; Turney and Lichtman, 2012). Indeed, reduced NF-L levels were observed in both the pre-terminal axons and axon terminals in *Nfasc155*^{-/-} mice (Figure 4.6). It is thought that the reduced NF-L levels observed in the *Nfasc155*^{-/-} mice are a cause of delayed synapse elimination, as the above results suggest that NF-L in axon terminals may provide the axon with plasticity/stability required for developmental pruning.

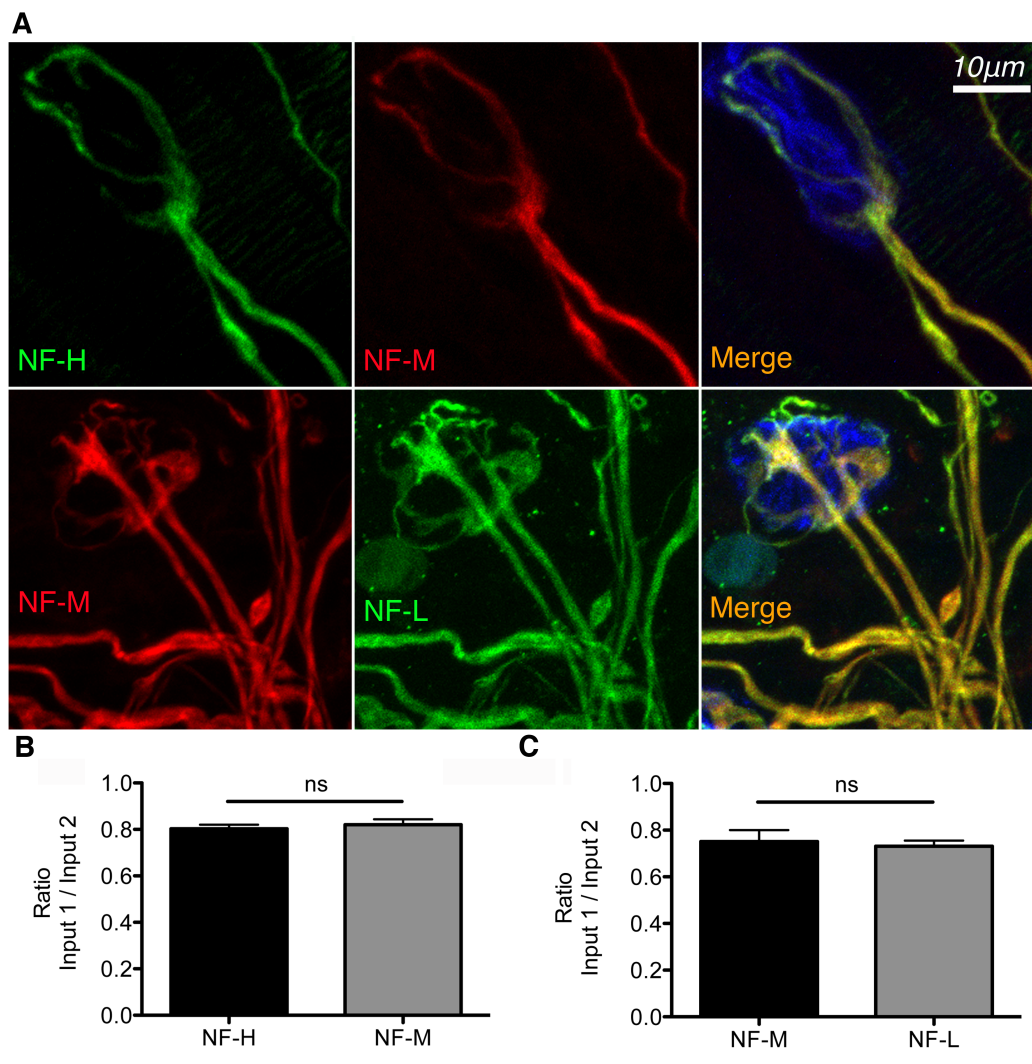


Figure 4.11. Expression profiles of NF-H, NF-M and NF-L are similar between competing pre-terminal axons at polyinnervated endplates at P10. (A) Qualitative images of single endplates at P10 double-immunolabelled for NF-H/NF-M and NF-M/NF-L, showing similar expression profiles of neurofilaments in pre-terminal axons at polyinnervated endplates. Scale bar 10 μ m. (B & C) Quantification of the expression profile of each neurofilament at competing inputs, by measuring a ratio of fluorescence intensity of input 1/input 2, for muscles immunolabelled for (B) NF-H and NF-M and (C) NF-M and NF-L. There was no significant difference in ratio found between neurofilament proteins indicating similar expression profiles of neurofilament subunits in pre-terminal axons at poly-innervated NMJs (Unpaired t-test; N=4, 1 muscle per mouse).

4.2.11 NF-L is highly expressed in axon terminals and axon terminal protrusions extending beyond the endplate

During quantitative assessment of neurofilament expression in pre-terminal axons, it was observed that NF-L was the most predominant out the three neurofilaments in nerve terminals overlying the endplate (Figure 4.11A). Fluorescence intensity of NF-L appeared as intense in the axon terminals as it did in the pre-terminal axons. In contrast, NF-H and NF-M levels were relatively low in axon terminals compared to the pre-terminal axon (Figure 4.11A).

This interesting observation prompted a quantitative analysis that revealed significantly greater expression of NF-L in axon terminals at P10, compared to NF-M, when expressed as a ratio of nerve terminal fluorescence intensity/pre-terminal axon fluorescence intensity (36% more NF-L than NF-M in axon terminals) (Figure 4.12A,C). Interestingly, this analysis also revealed significantly greater expression of NF-H in axon terminals, compared to NF-M (16% more NF-H than NF-M in axon terminals) (Figure 4.13A,B). This is perhaps not surprising, as NF-H has previously been implicated in the success of synapse elimination at the NMJ (Roden et al., 1991). NF-M co-localised with NF-H at the NMJ, which was observed when the exposure was increased for NF-M (Figure 4.13A, inset).

Higher levels of NF-L in terminal axons were also observed at P19 NMJs, double immunolabelled for NF-M and NF-L (Figure 4.12D). Similarly to P10, NF-M co-localised with NF-L in axon terminals (Figure 4.12D, inset) but was observed at

much lower levels, when fluorescence intensity levels of NF-M and NF-L were identical in pre-terminal axons. NF-L could therefore be associated with increased axon plasticity/stability throughout life rather than during postnatal development alone. This is supported by a study showing that in mice lacking NF-L, regeneration of peripheral nerve was delayed following a crush injury (Zhu et al., 1997), possibly through reduced axon plasticity/stability as the above results suggest.

A second interesting observation was that NF-L was present at high levels in axon terminal protrusions extending beyond the boundaries of the endplate (Figure 4.12A,B), dynamic regions of the motor nerve terminal that contribute to remodelling during synapse elimination (Keller-Peck et al., 2001; Walsh and Lichtman, 2003; Turney and Lichtman, 2012). Such NF-L-rich protrusions were observed at 16% of endplates (42/269 NMJs across 4 mice). These results therefore provide a plausible explanation for why NF-L specifically was playing a key role during synapse elimination, as it is present at higher levels than NF-M and NF-H in axon terminals, the region of the motor neuron that undergoes dramatic remodelling and adaptations during the competition for territory alongside other inputs (Keller-Peck et al., 2001; Walsh and Lichtman, 2003; Turney and Lichtman, 2012). These results suggest that NF-L specifically is associated with the most dynamic and terminal parts of the motor neuron, thereby able to directly influence plasticity/stability of the motor nerve terminals that is required for synapse elimination to take place.

The above results provide a detailed mechanistic insight in to Nfasc155-dependent modulation of synapse elimination. Proteomic analysis of peripheral nerve revealed significant alterations to transport systems in the *Nfasc155*^{-/-} mice, which is believed to result in abnormal distribution of NF-L throughout the motor neurons. It has clearly been shown the NF-L is required for normal rates of synapse elimination, by studies in the *NF-L*^{-/-} mouse, and that NF-L likely acquires this role by altering stability/plasticity at axon terminals competing for synaptic territory, where it is highly expressed. These results provide a convincing and robust mechanistic link between Nfasc155 in the myelinating glial cell and the regulation of synapse elimination in the PNS.

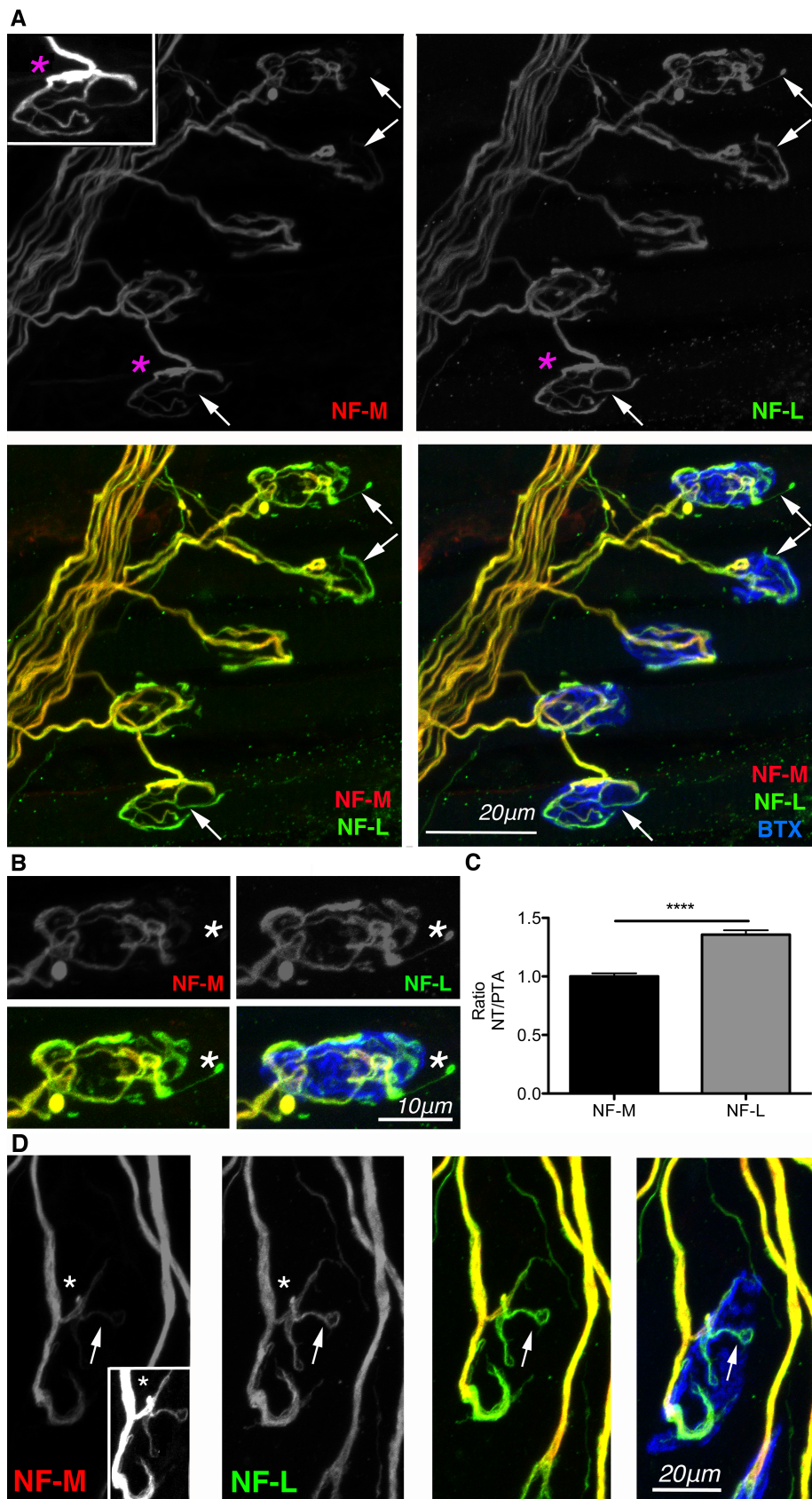


Figure 4.12. NF-L is present at high levels in terminal axons and axon protrusions extending beyond the endplate. (A) Example confocal micrographs of NMJs showing higher levels of NF-L in terminal axons (arrows) in the LAL of a C57BL6 P10 mouse. Inset shows an exposed image of an endplate labelled for NF-M (*) showing co-localisation with NF-L. Muscles were double immunolabelled for NF-M (red) and NF-L (green). Endplates were labelled with far-red-BTX (blue). Scale bar 20 μ m. **(B)** Example confocal image of a single endplate with terminal protrusion present (arrow) in a P10 muscle. High levels of NF-L are observed in the protrusion in comparison to a lack of NF-M. Scale bar 20 μ m. **(C)** Quantification of pre-terminal axon intensity/nerve terminal intensity for NF-M and NF-L at P10, showing a significant difference between ratio's (nerve terminal intensity/pre-terminal axon intensity) indicative of higher levels of NF-L in axon terminals than NF-M ($p < 0.0001$; unpaired t-test, $N=4$, 1 muscle per mouse). **(D)** Example confocal micrographs of NMJs showing higher levels of NF-L in terminal axons (arrows) in the LAL of a C57BL6 mouse at P19. Inset shows exposed image of endplate labelled for NF-M (*) showing co-localisation with NF-L. Scale bar 20 μ m.

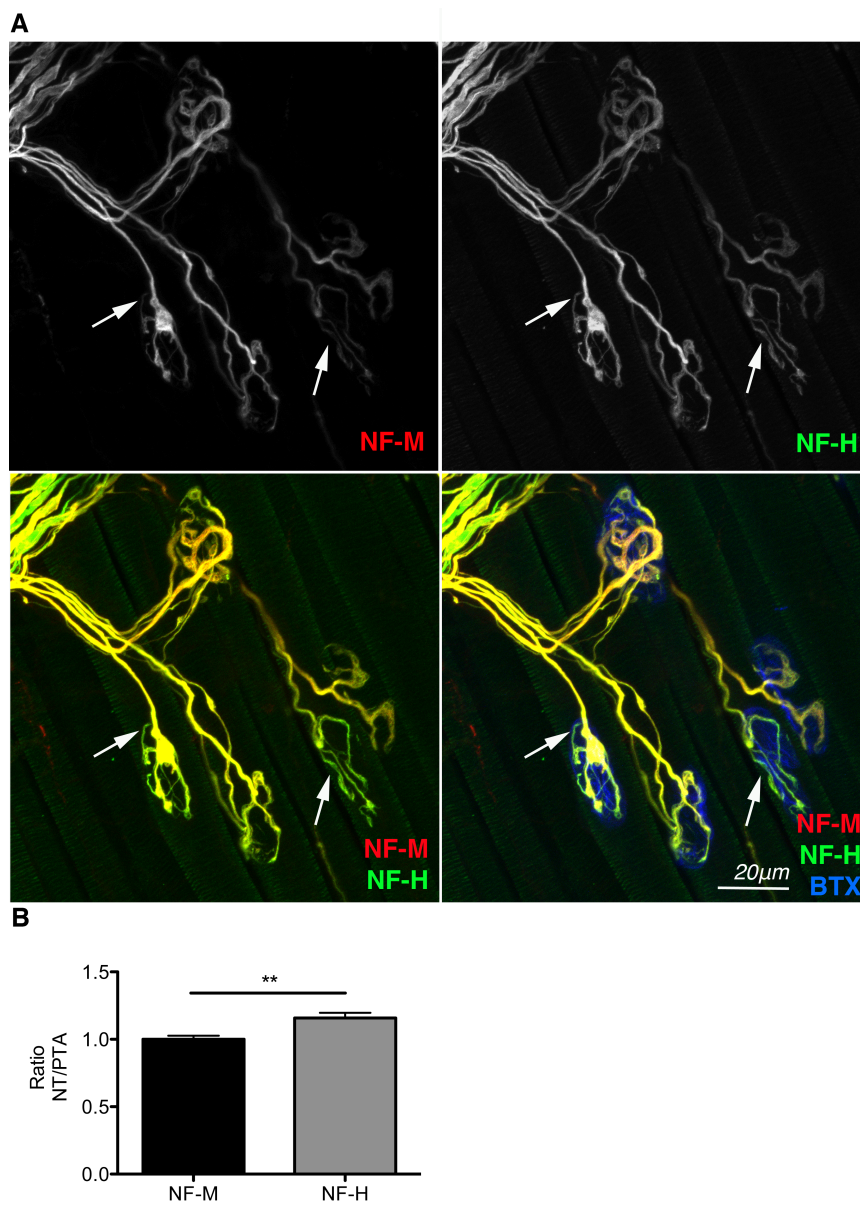


Figure 4.13. NF-H is present at high levels in terminal axons at P10. (A) Example confocal micrographs of NMJs showing higher levels of NF-H in terminal axons (arrows) in the AAL of a C57BL6 mouse. Inset shows exposed image of endplate labelled for NF-M (*) showing co-localisation with NF-H. Muscles were double immunolabelled for NF-M (red) and NF-H (green). Endplates were labelled with far-red-BTX (blue). Scale bar 20µm. **(B)** Quantification of pre-terminal axon intensity/nerve terminal intensity for NF-M and NF-H at P10, showing a significant difference between ratio's indicative of higher levels of NF-H in axon terminals than NF-M (p=0.0071; unpaired t-test, N=4, 1 muscle per mouse).

4.2.12 Lysosomal activity is significantly altered in *Nfasc155*^{-/-} mice

It has been discussed in detail in previous sections how the process of synapse elimination can be altered by changes in neurotransmission, growth factor supply and lysosomal activity by surrounding glial cells. The results of this chapter have already shown that neurotransmission and growth factor supply from target-derived muscle are unlikely to be playing any role in *Nfasc155*-dependent modulation of synapse elimination, however, the possibility that lysosomal activity is involved in this process remained to be determined.

It is known that lysosomal activity is essential for the normal process of synapse elimination at the NMJ (Song et al., 2008). Lysosomes degrade macromolecules derived from the extracellular space through endocytosis or phagocytosis (Saftig and Klumperman, 2009), including the unwanted debris that retracting axons at NMJs leave behind during synapse elimination (Song et al., 2008). Degradation within lysosomes involves an array of proteins and pathways (Lubke et al., 2009; Saftig and Klumperman, 2009). Included in the lysosomal protein arena are lysosome-associated membrane proteins (LAMPs), which are thought to protect the lysosomal membrane from hydrolytic enzymes, and support mitochondrial turnover (Eskelinen, 2006). Lysosomal α -glucosidase and lysosomal α -mannosidase are examples of catabolic enzymes found in the lysosome (Lubke et al., 2009).

Proteomic analysis in *Nfasc155*^{-/-} mice revealed an interesting finding that lysosomal activity would be significantly altered based on the protein changes identified with iTRAQ, in what appears to be a compensatory mechanism to counteract the delay in

synapse elimination. IPA network analysis on the proteomics data revealed a significant disruption to pathways and processes including ‘lysosomal storage disorder’ and ‘morphology of the lysosome’. Study of the raw dataset of changed proteins in the *Nfasc155*^{-/-} mice revealed changes to levels of proteins essential for lysosomal activity, including LAMP-2, lysosomal α -glucosidase and lysosomal α -mannosidase (Table 4.4). These proteins were upregulated, which could be a compensatory reaction to the delayed synapse elimination, in an attempt to prune away the excess inputs. Interestingly, 5/6 proteins were unchanged in the *Caspr*^{-/-} mice, and the one protein that was changed was changed in the opposite direction, correlating increased lysosomal activity with a delay in synapse elimination in *Nfasc155*^{-/-} mice (Table 4.4).

Protein	<i>Nfasc155</i> ^{-/-}		<i>Caspr</i> ^{-/-}	
	Change	Ratio	Change	Ratio
Lysozyme C-2	Upreg.	2.519	Downreg.	0.775
Lysosome membrane protein 2	Upreg.	1.937	NC	
Isoform LAMP-2A of Lysosome-associated membrane glycoprotein 2	Upreg.	1.784	NC	
Lysosomal protective protein	Upreg.	1.706	NC	
Lysosomal α -glucosidase	Upreg.	1.357	NC	
Lysosomal α -mannosidase	Upreg.	1.270	NC	

Table 4.4. Levels of core proteins involved in lysosomal morphology and activity pathways in peripheral nerve from *Nfasc155*^{-/-} and *Caspr*^{-/-} mice. NC = not changed. Only 1 out the 5 lysosomal proteins was also changed in *Caspr*^{-/-} mice but changed in the opposite direction. Ratio = KO/Control. Upregulation of lysosomal activity therefore correlated with delayed synapse elimination in the *Nfasc155*^{-/-} mice.

4.3 Discussion

4.3.1 Overview of results

The results of this chapter provide mechanistic insight into Nfasc155-dependent modulation of synapse elimination in the mouse PNS, summarised with five major, novel findings. A 4-way proteomic analysis on peripheral nerve from *Nfasc155*^{-/-}, *Caspr*^{-/-} and littermate control mice revealed changes in 1,210 proteins in the *Nfasc155*^{-/-} mice versus 405 proteins in the *Caspr*^{-/-} mice, making a clear indication that Nfasc155 is essential for many more cellular processes than Caspr, the first major finding. This is not surprising, as the two mouse models are both models of paranodal disruption, with immunofluorescence analyses on peripheral nerve revealing an almost identical appearance of nodal and paranodal molecular domains (Chapter 3, Figure 3.1 & 3.12), and an almost identical resulting reduction in conduction velocity along the sciatic nerve (Chapter 3, Figure 3.15), but a far more severe phenotype observed in the *Nfasc155*^{-/-} mice. These mice die prematurely at ~P19, exhibiting a progressively worsening tremor from P12 onwards, and have a clear developmental delay in NMJ development. In contrast, *Caspr*^{-/-} mice are indistinguishable from control littermates up until ~P30 when they display a slight weakness of hindlimbs, but do not die prematurely.

It cannot be denied that the phenotype of the *Nfasc155*^{-/-} mice alongside the proteomic analysis, compared with the *Caspr*^{-/-} mice, indicates a more global regulatory and developmental role for Nfasc155, independent of its previously

known role at the paranode. It is not yet known what proteins on the axon membrane Nfasc155 interacts with to elicit downstream changes in the rate of synapse elimination, as investigation of the axon-glia protein interactions responsible for Nfasc155's non-canonical role was beyond the constraints of the current study. However, future studies will hopefully provide some insight in to these novel protein interactions.

4.3.2 Mechanistic insight in to paranodal formation

The main goal of the proteomic analysis was to tease apart the downstream pathways influenced by Nfasc155 and generate a resulting list of potential synapse elimination regulators. This analysis also unveiled a second exciting dataset of pathways downstream of paranodal disruption. By comparing the results of the *Nfasc155*^{-/-} mice with the *Caspr*^{-/-} mice, it was predicted that the similarly changed proteins were due to the loss of paranodal integrity. 56 similarly changed proteins were identified in *Nfasc155*^{-/-} and *Caspr*^{-/-} mice. Such a dataset has never before been generated and provides an excellent tool to study the importance of axon-glia interactions at the paranode in more detail. For the purpose of this study, this dataset was not studied further.

4.3.3 Cytoskeletal transport systems may regulate synapse elimination

It has been known for some time that changes in nerve activity (Costanzo et al., 2000; Buffelli et al., 2003), glial lysosomal activity (Song et al., 2008) and target-

derived growth factor supply (Kwon et al., 1995; Jordan, 1996; Nguyen et al., 1998) can directly or indirectly modulate synapse elimination at the NMJ. The results of this chapter also present an essential role for axonal cytoskeletal transport systems in the control of synapse elimination. iTRAQ proteomic analysis revealed altered cytoskeletal transport systems in the *Nfasc155*^{-/-} mice, which correlated with delayed synapse elimination, as these changes were absent in the *Caspr*^{-/-} mice. This exciting and second major finding provides a plausible mechanism through which *Nfasc155* modulates synapse elimination at the NMJ. It has already been shown *in vitro* (Monsma et al., 2014) and *in vivo* (de Waegh et al., 1992) that the presence of myelinating Schwann cells has a local effect on the transport of cytoskeletal cargo in the underlying axon and the results of this proteomic dataset suggest that *Nfasc155* may be involved in the process of glial regulation of axonal dynamics.

It was interesting and perhaps surprising to find that disruption of axonal transport in *Nfasc155*^{-/-} mice appeared to affect NF-L levels at the NMJ specifically, as the transport systems and proteins described are known to interact and transport all three neurofilament subunits. Mice lacking glial *Nfasc155* displayed a selective loss of neurofilament light (NF-L) protein from distal axons and peripheral nerve, and accumulations of NF-L in the proximal ventral roots of the spinal cord, the third major finding in this chapter. NF-L is the most abundant neurofilament subunit and one of the earliest expressed (Willard and Simon, 1983; Carden et al., 1987). Thus, one parsimonious explanation for the apparent selective disruption of NF-L levels in motor nerve terminals of *Nfasc155*^{-/-} mice is that perturbations in cytoskeletal transport pathways had the most overt effects on the NF subunit (NF-L) that was

most abundant and was required at the earliest stages of cytoskeletal development and maturation.

4.3.4 *NF-L is important for normal rates of synapse elimination*

Our finding from knockout mouse experiments that loss of NF-L was sufficient to delay the process of synapse elimination confirms that NF-L is an important neurofilament subunit for processes of neuronal remodelling, the fourth major finding. Interestingly, the magnitude of the delay in synapse elimination observed in *NF-L*^{-/-} mice did not reach those levels previously observed in *Nfasc155*^{-/-} mice at the same age (increase of 79% in *NF-L*^{-/-} mice versus increase of 198% in *Nfasc155*^{-/-} mice). Thus, whilst it is unlikely that low levels of NF-L in motor axons are solely responsible for the delay in synapse elimination observed in *Nfasc155*^{-/-} mice, these experiments suggest that *Nfasc155* expression in Schwann cells is required for the normal development and maturation of the cytoskeleton in neighbouring motor axons, with disruption to NF-L contributing to delayed synapse elimination when *Nfasc155* is no longer present.

An important point to consider when comparing the *Nfasc155*^{-/-} and *NF-L*^{-/-} mouse models is that although *Nfasc155*^{-/-} and *NF-L*^{-/-} mice both display reduced levels/absence of NF-L from axon terminals, they must not be considered as similar models. The principal difference is that NF-L has always been absent from motor neurons in *NF-L*^{-/-} mice, with previous work showing that this leads to compensatory changes in both NF-M and NF-H (Zhang et al., 2002) whereas NF-L appears to be

expressed at normal levels in *Nfasc155*^{-/-} mice but is mislocalised due to defects in transport, with no apparent compensation from NF-M or NF-H. This suggests that, given the lack of compensatory responses to ameliorate the loss of NF-L from distal motor axons in *Nfasc155* mice, these actually represent the more ‘severe’ model with respect to an influence on synapse elimination.

It is clear from the results showing reduced levels of NF-L in the pre-terminal axons and axon terminals of the *Nfasc155*^{-/-} mice, along with the delayed synapse elimination observed in the *NF-L*^{-/-} mice that NF-L is essential for normal rates of synapse elimination to occur in skeletal muscle, whereas NF-M and NF-H levels appear to be less critical. You would expect based on these results that NF-L levels would differ from NF-M and NF-H in terms of localisation &/or expression at the NMJ during synapse elimination. In support of this hypothesis, it appears that NF-L may be modulating rates of synapse elimination through its activity at axon terminals, where it is highly expressed, the fifth major finding in this results chapter. *Nfasc155*^{-/-} mice displayed reduced NF-L levels in pre-terminal axons and axon terminals, and it is therefore possible that the reduced levels of NF-L in the pre-terminal axons did not directly affect rates of synapse elimination but rather the reduction of NF-L in axon terminals is what had consequential effects on the process. The finding that NF-L is expressed at higher levels in the axon terminals compared to NF-M and NF-H suggests that it is not always associated with NF-M and NF-H in intermediate filaments. This is not a surprising result as it has been previously shown that NF-L not only interacts with NF-H and NF-M to form intermediate filaments (Leung and Liem, 1996) but can also form homodimers (Geisler and Weber, 1981; Liem and

Hutchison, 1982). These results suggest that NF-L confers the axon terminals with plasticity/stability, which is essential during synapse elimination as inputs compete to takeover synaptic territory (Keller-Peck et al., 2001; Walsh and Lichtman, 2003; Turney et al., 2012).

These findings propose that NF-L specifically plays an important role during developmental synaptic remodeling at the NMJ, possibly by increasing stability/plasticity of axon terminals. Indeed, it has already been shown that NF-L is an important neurofilament subunit for growth and stability of motor neurons from studies showing that reduced levels of NF-L are associated with reduced motor neuron dendritic arborisation (Zhang et al., 2002) and increased motor neuron degeneration (Chen et al., 2014). Our data showing high levels of NF-L compared to NF-M & NF-H in axon terminals during synapse elimination, suggests that NF-L may be regulating this process by altering the structural integrity of competing axon terminals. This provides a plausible explanation for why reduced levels of NF-L in *Nfasc155*^{-/-} mice could be driving the delay in synapse elimination.

4.3.5 Glial control of synapse elimination

The results from this chapter corroborate with previous studies suggesting that myelinating Schwann cells closely monitor and modulate axonal cytoskeletal dynamics (de Waegh et al., 1992; Cole et al., 1994; Monsma et al., 2014), by demonstrating a role for glial *Nfasc155* in the modulation of axonal cytoskeletal transport. These results also propose a close association between glial regulation of

axonal cytoskeletal dynamics and synapse elimination at the mouse NMJ. It is proposed that *Nfasc155* in the myelinating glial cell modulates synapse elimination by utilising axonal transport systems to modulate NF-L levels in the underlying axons. These findings illustrate an active role for myelinating glial cells in the regulation of postnatal neuronal remodelling in the PNS. This depicts a relationship between Schwann cells and underlying axons whereby communication from the Schwann cell is crucial for axonal stability and plasticity, with the Schwann cell overseeing and manipulating cellular processes in the axon to guide developmental remodelling.

Equipped with this insight and new findings, future work in this field can begin to piece together the intricacies of a developmental process that takes place throughout the nervous system. The loss and gain of connections between axons and their targets underlies the basis for normal and pathological processes throughout the nervous system, from memory consolidation to motor neuron disease. An understanding of how these connections are made and lost is essential before we can fully appreciate the massively complex workings of the mammalian nervous system. The *Nfasc155*^{-/-} mouse model of delayed synapse elimination at the NMJ is an extremely powerful tool as we endeavour to unravel the key cells, proteins and networks at play during a time when such connections are undergoing vast remodelling and refinement.

Chapter 5

Axon-glia interaction in a mouse model of spinal muscular atrophy

5.1 Introduction

Previous results chapters have demonstrated a clear role for axon-glia interactions in normal development of the PNS, mediated by the glial isoform of Nfasc: Nfasc155. To determine if axon-glia interactions could be contributing to/affected by disease states of the PNS, interactions at the paranode were studied in a mouse model of spinal muscular atrophy (SMA), a motor neuron disease with known Schwann cell defects.

SMA, also known as floppy baby syndrome, is an autosomal recessive disease and childhood form of motor neuron disease. It is caused by a disruption in the *survival motor neuron 1 (SMN1)* gene that results in defective expression of full-length survival motor neuron (SMN) protein (Lefebvre et al., 1995; Burghes and Beattie, 2009; Lorson et al., 2010). This protein is ubiquitously expressed, and so, defective expression results in global body system defects (Hamilton and Gillingwater, 2013). The peripheral nervous system is particularly vulnerable to loss of SMN, manifesting as a severe breakdown of the neuromuscular system (Mutsaers et al., 2011; Ling et al., 2012). Lower motor neurons originating in the ventral spinal cord are lost

(Jablonka et al., 2000) and neuromuscular connectivity is weakened (Murray et al., 2008), resulting in skeletal muscle paralysis and atrophy. There are different forms of SMA based on severity and age of onset. The copy number of the almost identical *SMN2* gene impacts on the severity of the disease, with a higher copy number correlating with a milder phenotype (Swoboda et al., 2005).

5.1.1 SMA is a multi-system disorder

It has been known for some time that connectivity between lower motor neurons and skeletal muscle is severely affected. However, we are now only beginning to uncover and appreciate the contribution of other cell types in the body, to the onset and progression of the disease. Recent reports, using both mouse and human studies, have highlighted the various cell types and tissue types that are affected by loss of SMN, including skeletal muscle and vasculature (Mutsaers et al., 2011; Somers et al., 2012; Schreml et al., 2013), musculature of the heart (Menke et al., 2008; Rudnik-Schoneborn et al., 2008), pulmonary function (Robinson et al., 1995; Schreml et al., 2013), pancreas metabolism (Bowerman et al., 2012), brain development (Wishart et al., 2010) and morphology of the intestine (Schreml et al., 2013).

5.1.2 Schwann cell myelination is affected by loss of SMN

Schwann cells for example, the myelinating glial cells of the peripheral nervous system, are affected in SMA human patients (Farrar et al., 2011) and mouse models (Hunter et al., 2014). In two mouse models of SMA, it was shown that the

myelination process was perturbed in peripheral nerve *in vivo*, resulting in thinner myelin and unmyelinated large diameter axons. Levels of key myelin proteins were studied using quantitative fluorescent western blotting and these results showed that myelin protein zero (P₀) and peripheral myelin protein 22 (PMP22) levels were significantly decreased in the intercostal nerves of SMA mice, with a significant increase observed in myelin basic protein (MBP) levels. *In vitro* work using isolated SMA derived Schwann cells showed that these cells were intrinsically different from cultured control Schwann cells. Using quantitative fluorescence intensity measurements, a significant reduction in SMN levels was found in SMA Schwann cells. When SMA Schwann cells were co-cultured with healthy control axons, a significant and striking myelination defect was observed. The SMA Schwann cells failed to form myelin as effectively as the healthy control Schwann cells.

This work clearly shows that Schwann cells lacking SMN are intrinsically different from healthy Schwann cells. *In vitro* work has shown that these cells respond abnormally to myelination cues and this data is supported by the *in vivo* observations that myelin sheaths are thinner and sometimes lacking around large diameter axons, and that the expression of key myelin proteins is perturbed (Hunter et al., 2014).

As has been described in previous chapters, Schwann cells *in vivo* associate closely with the axons that they myelinate. As well as forming and maintaining the myelin sheath, Schwann cells express specific proteins that form axon-glia interactions with proteins in the underlying axon. Formation of the myelin sheath results in the division of the axon into molecular domains (Salzer et al., 2008). Sites of physical

axon-glia interaction are present throughout the length of the axon, at the paranode (Brophy, 2001; Brophy, 2003; Schnaar and Lopez, 2009). Paranodes are thought to provide a diffusion barrier and ensure the restriction of Na_v channels to the node (Rios et al., 2003), for efficient saltatory conduction along myelinated fibres. Paranodal junctions are known to first appear closest to the node of Ranvier and develop towards the juxtaparanode (Tao-Cheng and Rosenbluth, 1982). To further explore the effects that loss of SMN has in Schwann cells as well as their interactions with underlying axons, sites of axon-glia interaction in peripheral nerve were studied in the Taiwanese SMA mouse model. The generation of these mice has been described in Chapter 2. Teased fibre preparations from sciatic and intercostal nerves of SMA mice and control littermates were immunolabelled with various markers of nodal, paranodal and juxtaparanodal domains to study the various molecular domains of myelinated fibres, with a particular emphasis on paranodal maturation.

5.2 Results

5.2.1 Paranodal maturation is delayed in the sciatic nerve of pre-symptomatic SMA mice

Taiwanese SMA mice first show signs of a disease phenotype ~P7, when their body weight begins to drop and they show signs of motor impairment (Riessland et al., 2010). This phenotype becomes progressively worse up until their premature death ~P11. Before the age of P7 the Taiwanese SMA mice are known as pre/early symptomatic and after this time-point they are known as late symptomatic (Hunter et al., 2014). Hunter et al. 2014 performed morphological and molecular studies in both the intercostal and sciatic nerves of Taiwanese SMA mice. Defects were found in both nerves although they were more profound in the intercostal nerve. Teased fibres are more easily prepared from sciatic nerve, and for this reason paranodes and nodes were first assessed in this nerve.

Teased fibres from the sciatic nerves of P8-P10 (late symptomatic) and P6 (pre/early symptomatic) Taiwanese SMA mice and control littermates were immunolabelled with a panel of antibodies against juxtaparanodal, paranodal and nodal proteins, to study the development of axon-glia interactions in an SMA mouse model. Nfasc155 and Caspr are two proteins that are essential in the formation of the physical axon-glia interaction at the paranode (Bhat et al., 2001; Sherman and Brophy, 2005). The Schwann cell expresses Nfasc155 and Caspr is an axonally expressed protein. A second axonally expressed protein, contactin, localises with Caspr at the paranode

(Rios et al., 2000) and is also essential for normal paranodal development (Boyle et al., 2001). Nfasc155 binds to the Caspr-contactin complex to form a physical interaction with Nfasc155 on the Schwann cell adaxolemmal membrane (Charles et al., 2002).

Paranodes were studied by immunolabelling teased fibres for pan-Nfasc (nodal and paranodal), Caspr (paranodal) and ankyrin G (nodal). Qualitative observations of P6 paranodes immunolabelled for pan-Nfasc revealed that paranodes were shorter in the SMA mice (Figure 5.1A), indicating a delay in maturation. Caspr and Nfasc155, expressed by the axon and myelinating glial cell respectively, colocalise at the paranode (Bhat et al., 2001; Sherman et al., 2005). It was therefore important to determine if Caspr immunolabelling also revealed shorter paranodes in the SMA mice. Teased sciatic nerve fibres immunolabelled for Caspr were prepared and studied. Paranodes identified by the presence of Caspr also appeared shorter (Figure 5.1B), indicative of a general paranodal maturation defect in the SMA mice. Quantitative analysis on the length of paranodal and nodal domains revealed that although nodal length was unaffected, paranodal length was significantly shorter in the SMA mice at a pre-symptomatic time-point ($3.59\mu\text{m}$ in controls vs. $3.15\mu\text{m}$ in SMA mice, ie. 12% shorter in SMA mice; Figure 5.2). Quantification was carried out on teased fibres immunolabelled for pan-Nfasc and ankyrin G as both pan-Nfasc and Caspr immunolabelling revealed a similar appearance of paranodes in the SMA mice.

Nodal length was measured at both time-points by immunolabelling for ankyrin G. Although ankyrin G is known to anchor Na_v channels to the node of Ranvier, they do

not always co-localise entirely (Jenkins and Bennett, 2002), so it could only be suggested from this result that Na_v channel clustering was unaffected. To confirm that nodal length was unaffected, a second nodal marker was used to measure nodal length. Immunolabelling of nodes of Ranvier using an anti-pan Na_v channel antibody confirmed that nodal length was unaffected in the SMA mice and that Na_v channels clustered normally (Figure 5.3).

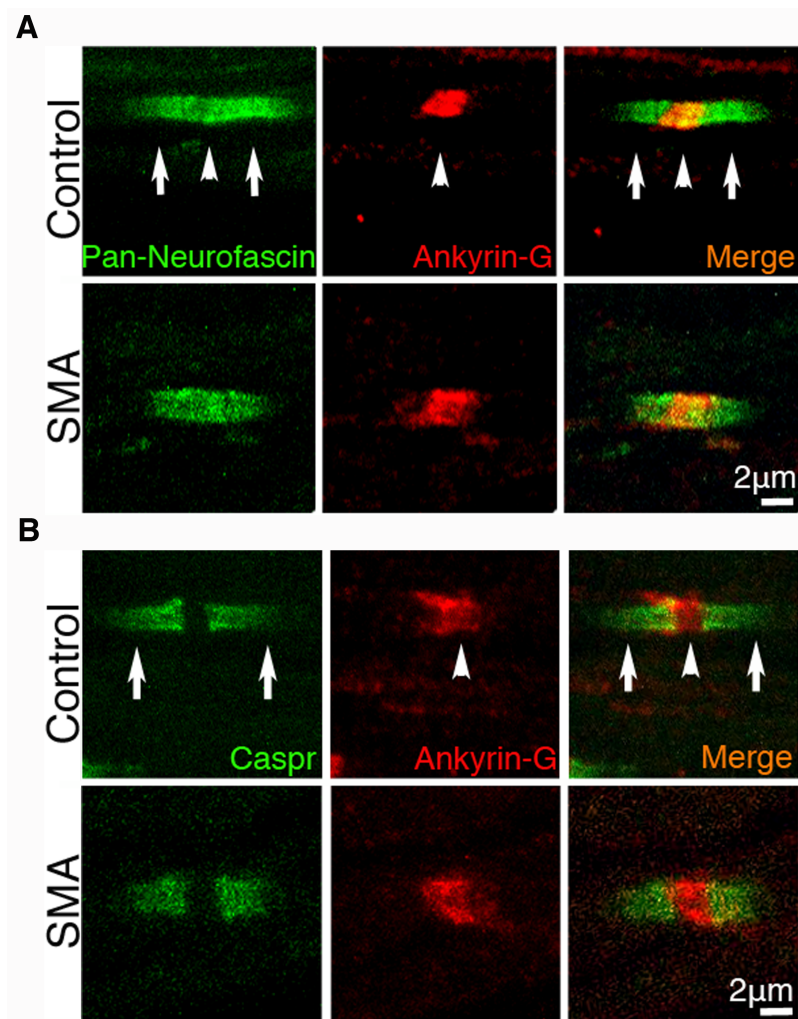


Figure 5.1. Paranodes are shorter in sciatic fibres of pre/early symptomatic SMA mice. (A) Confocal images of teased sciatic fibres of P6 SMA and control mice, showing single nodes of Ranvier. Pan-Nfasc (green) labels paranodes (Nfasc155) and nodes of Ranvier (Nfasc186). Ankyrin G (red) labels nodes of Ranvier. Paranodes and nodes are highlighted by arrows and arrowheads respectively. (B) Confocal images of teased sciatic fibres of P6 SMA and control mice, showing single nodes of Ranvier. Caspr (green) labels paranodes. Ankyrin G (red) labels nodes of Ranvier. Paranodes and nodes are highlighted by arrows and arrowheads respectively.

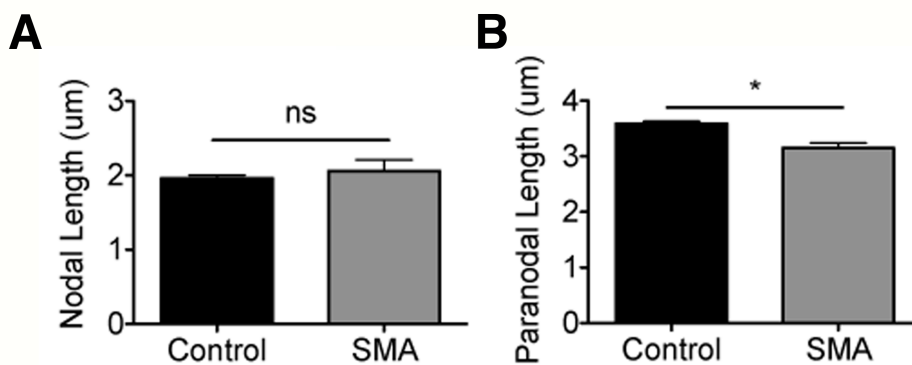


Figure 5.2. Quantitative analysis of paranodal length reveals a significant difference in the sciatic nerve between control and SMA mice at P6. (A) Bar graph of nodal length (measured from ankyrin G labelling) showing no difference between groups (Unpaired t-test, N=3 mice per genotype, n=2 nerves per mouse). **(B)** Bar graph of paranodal length (measured from neurofascin labelling) showing a significant reduction in SMA mice compared to control littermates (p=0.018; unpaired t-test; N=3 mice per genotype, n=2 nerves per mouse).

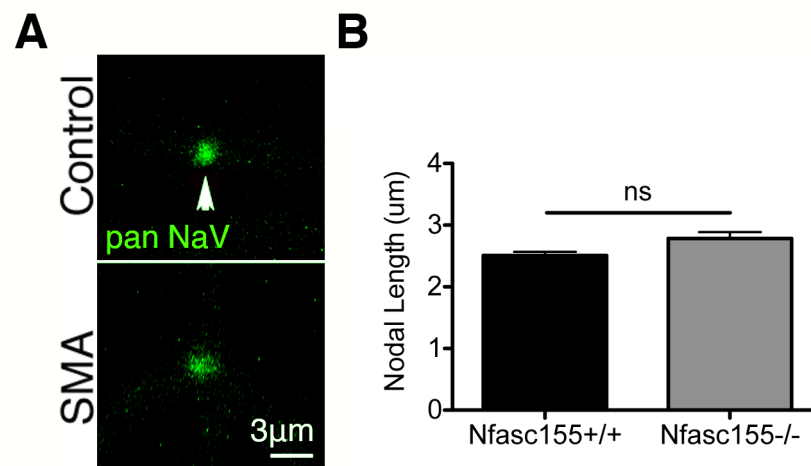


Figure 5.3. Nodes of Ranvier labelled for Na_v channels are a similar length in the sciatic nerve of SMA and control mice. (A) Confocal images of teased sciatic fibres of P8 SMA and control mice, showing single nodes of Ranvier. Pan Na_v (green) labels nodes of Ranvier, highlighted with an arrow. **(B)** Quantitative analysis of nodal length showing no significant difference between groups (Unpaired t-test; N=3 mice per genotype, n=2 nerves per mouse).

5.2.2 Delayed paranodal maturation persists in the sciatic nerve of SMA mice in to late-symptomatic time points

To determine if the observed paranodal defect worsened with disease progression, analysis was repeated at P10 when the SMA mice showed more obvious disease symptoms (Riessland et al., 2010). Qualitative analysis revealed notably shorter paranodes in teased fibres from sciatic nerves of SMA mice, when immunolabelled for both Nfasc155 and Caspr (Figures 5.4A & 5.4B). Quantitative analysis confirmed this observation with the finding of a significant difference in paranodal length between control and SMA mice (5.72 μ m in controls vs. 3.65 μ m in SMA mice; Figure 5.5). Paranodes were 12% shorter in P6 SMA mice and 36% shorter in P10 SMA mice compared to littermate controls, indicative of a progressive delay in paranodal maturation. Nodal length remained unaffected at P10.

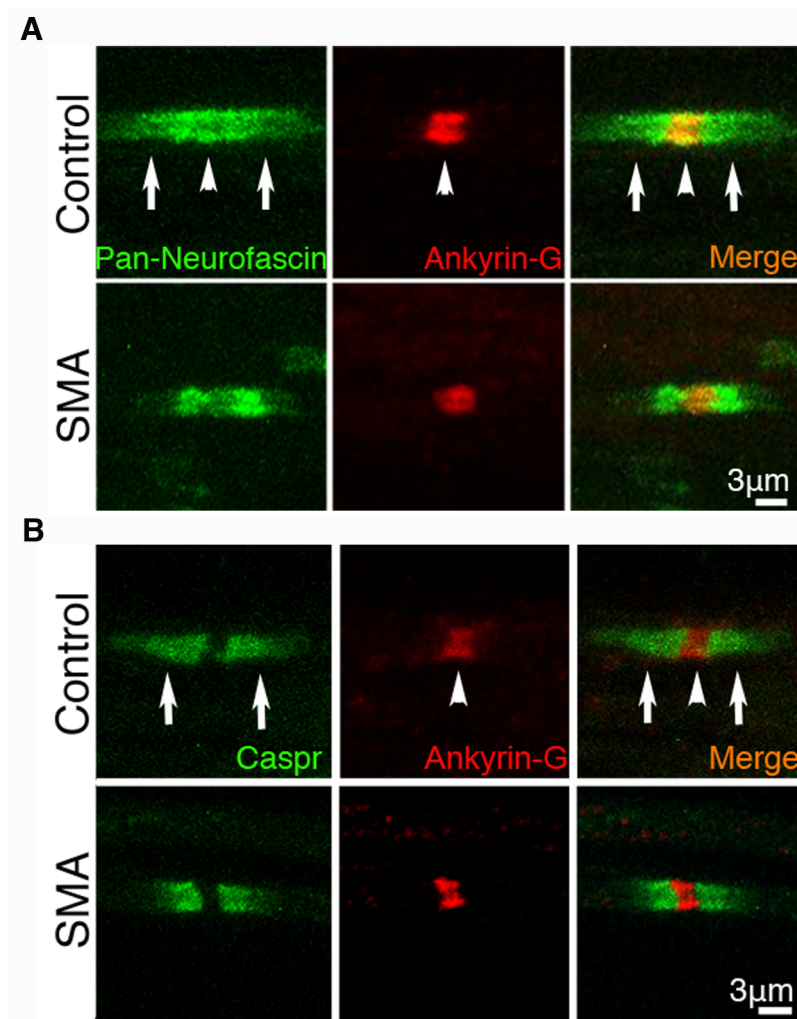


Figure 5.4. Paranodes are shorter in sciatic fibres of late symptomatic SMA mice. (A) Confocal images of teased sciatic fibres of P10 SMA and control mice, showing single nodes of Ranvier. Pan-Nfasc (green) labels paranodes (Nfasc155) and nodes of Ranvier (Nfasc186). Ankyrin G (red) labels nodes of Ranvier. Paranodes and nodes are highlighted by arrows and arrowheads respectively. (B) Confocal images of teased sciatic fibres of P10 SMA and control mice, showing single nodes of Ranvier. Caspr (green) labels paranodes. Ankyrin G (red) labels nodes of Ranvier. Paranodes and nodes are highlighted by arrows and arrowheads respectively.

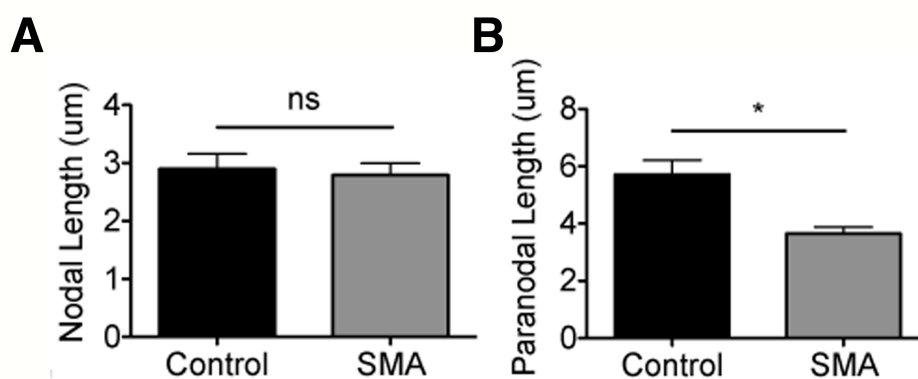


Figure 5.5. Quantitative analysis of paranodal length in the sciatic nerve reveals a significant difference between control and SMA mice at P10. (A) Bar graph of nodal length (measured from ankyrin G labelling) showing no difference between groups (Unpaired t-test; N=3 mice per genotype, n=2 nerves per mouse). (B) Bar graph of paranodal length (measured from Nfasc labelling) showing a significant reduction in SMA mice compared to control littermates (p=0.0190; unpaired t-test; N=3 mice per genotype, n=2 nerves per mouse).

5.2.3 Paranodes are unaffected in the intercostal nerve of late symptomatic SMA mice

Hunter et al., 2014 examined myelination and key myelin protein levels in both intercostal and sciatic nerves in SMA and control mice. Molecular and ultrastructural analysis identified the intercostal nerve as being more affected in SMA. Axons with thinner myelin were more numerous in the intercostal nerve, and there was a greater reduction in P₀ and PMP22 protein levels. Although teased fibre preparation can be difficult from intercostal nerves due to their small size, P9 proved to be a suitable time-point for which to dissect and tease fibres from this nerve. Paranodes were firstly qualitatively assessed in the intercostal nerve and surprisingly, appeared normal in the SMA mice (Figures 5.6A & B), in comparison to the observed difference seen at a similar time-point in the sciatic nerve. Quantitative analysis confirmed that paranodal maturation was occurring normally in the intercostal nerve of SMA mice (4.44µm in controls vs. 4.36µm in SMA mice; Figure 5.7).

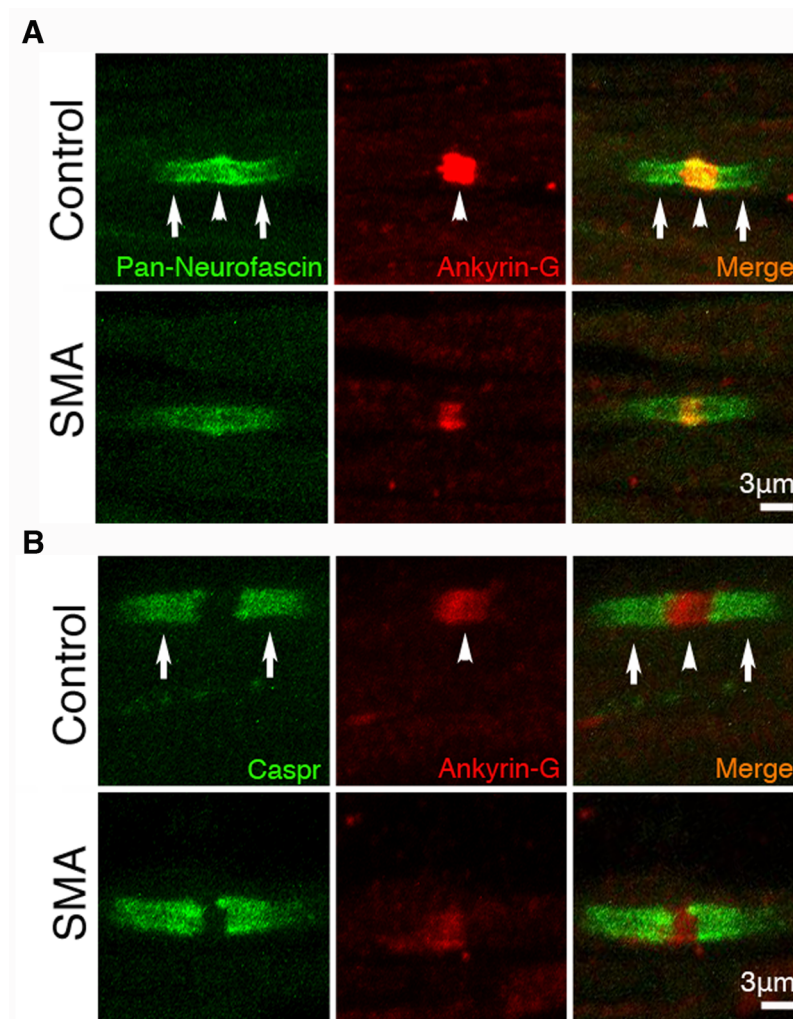


Figure 5.6. Paranodal length is unaffected in intercostal fibres of late symptomatic SMA mice. (A) Confocal images of teased sciatic fibres of P9 SMA and control mice, showing single nodes of Ranvier. Pan-Nfasc (green) labels paranodes (Nfasc155) and nodes of Ranvier (Nfasc186). Ankyrin G (red) labels nodes of Ranvier. Paranodes and nodes are highlighted by arrows and arrowheads respectively. **(B)** Confocal images of teased sciatic fibres of P9 SMA and control mice. Caspr (green) labels paranodes. Ankyrin G (red) labels nodes of Ranvier. Paranodes and nodes are highlighted by arrows and arrowheads respectively.

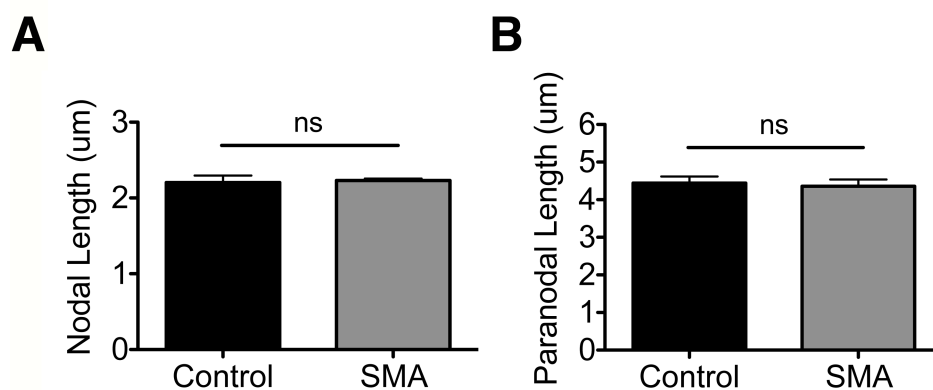


Figure 5.7. Quantitative analysis of paranodal length shows no significant difference in the intercostal nerve between control and SMA mice at P9. (A) Bar graph of nodal length (measured from ankyrin G labelling) showing no difference between groups (Unpaired t-test; N=3 mice per genotype, n=2 nerves per mouse). **(B)** Bar graph of paranodal length (measured from Nfasc labelling) showing no significant difference between groups (Unpaired t-test; N=3 mice per genotype, n=2 nerves per mouse).

5.2.4 Juxtaparanodes appear normal in the sciatic nerve of late-symptomatic SMA mice

Paranodal junctions are essential for proper localisation of ion channels at the juxtaparanode and node of Ranvier (Rios et al., 2003). If paranodal junctions are severely disrupted, K_v channels from the juxtaparanode, and/or Na_v channels from the node of Ranvier may leak out into flanking regions (Bhat et al., 2001; Rios et al., 2003; Pillai et al., 2009). This mislocalisation of ion channels can in turn affect the conductive properties of the axon, as impulses are not propagated effectively (Bhat et al., 2001; Pillai et al., 2009). Although paranodal junctions are formed in the SMA mice, it is clear that there is a delay in their maturation in the sciatic nerve. To examine the effects of this delay on juxtaparanodal development, a K_v channel marker was used to label this molecular domain. $K_v1.1$ is expressed in axons at P8 but at very low levels (Grosse et al., 2000). Immunolabelling of teased sciatic fibres for $K_v1.1$ channels revealed only ~10 sites of juxtaparanodal development in each preparation of SMA and control teased fibres. Therefore, only qualitative analysis was possible on juxtaparanodal development. This analysis indicated that juxtaparanodes were being formed normally in both control and SMA axons (Figure 5.8).

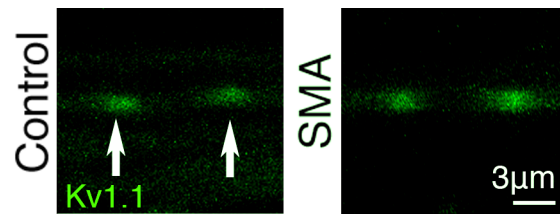


Figure 5.8. Juxtaparanodes appear to be formed normally in SMA mice. Confocal images of teased sciatic fibres of P8 SMA and control mice. Kv_v1.1 (green) labels juxtaparanodes, highlighted by arrows.

5.3 Discussion

5.3.1 Overview of results

Recent research in the field of SMA, surrounding the contribution of non-neuronal cell types to the pathology, has changed the way we characterise the disease. It can no longer be thought of as a purely neuronal disorder as it is becoming clear that other body systems and cells are affected by the reduction in SMN levels (Hamilton and Gillingwater, 2013). It has been clearly shown that non-neuronal cell types, such as myelinating glia have intrinsic abnormalities in SMA (Hunter et al., 2014). The results from this chapter extend these findings by showing that axon-glia interactions are affected in some but not all peripheral nerves in SMA.

5.3.2 Disrupted axon-glia interactions in the sciatic nerve in a mouse model of spinal muscular atrophy

Paranodal junctions are known to first appear closest to the node of Ranvier and develop towards the juxtaparanode (Tao-Cheng and Rosenbluth, 1982). Paranodal length was found to be significantly smaller in the sciatic nerve of SMA mice at both pre/early and late symptomatic time-points, with a greater difference seen at late symptomatic stages. Paranodal proteins Nfasc155 and Caspr were always present closest to the node of Ranvier in the SMA mice indicating that although paranodal maturation was delayed, axon-glia interactions were still present. This delay in maturation could impact on neuronal function by slowing the conduction velocity in

the nerve. Paranodes act as diffusion barriers for ions (Robertson, 1959; Rios et al., 2003) and a shorter paranode could result in ions and current leaking out of the axonal membrane.

Paranodes function as barriers for ion channels by restricting Na_v channels to the node of Ranvier and K_v channels to the juxtaparanode, with mouse models of paranodal disruption exhibiting mislocalisation of nodal and juxtaparanodal components (Rios et al., 2003). Nodal measurements using ankyrin G and pan-Na_v channel labelling revealed normal nodes of Ranvier in the SMA mice. This result is not surprising as axon-glia interaction was present closest to the node, forming a barrier for the Na_v channels. It is also known that nodes of Ranvier can develop independently of paranodes (Jenkins and Bennett, 2002).

5.3.3 Normal axon-glia interactions in the intercostal nerve in a mouse model of spinal muscular atrophy

It was interesting to find that paranodal maturation was unaffected in the intercostal nerve, considering the more severe molecular and ultrastructural defects associated with this nerve compared to the sciatic nerve in the study by Hunter et al., 2014. One possible explanation for this might be found from studying the levels of key myelin proteins in these nerves. Hunter et al., 2014 found that PMP22 levels were downregulated in the intercostal nerve and massively upregulated in the sciatic nerve of late symptomatic SMA mice. A time-course of PMP22 expression in both nerves showed that PMP22 levels peak at P5 in the intercostal nerve and P14 in the sciatic

nerve. PMP22 is found in compact myelin in the CNS and PNS (Pareek et al., 1993). It has a specific carbohydrate epitope that is shared by a number of cell adhesion/recognition molecules (Schachner and Martini, 1995) and so it is thought that it could play a role in axon-glia interaction. Moreover, it has been shown that paranodes begin to develop at the very early stages of myelination (Rasband et al., 1999). If PMP22 levels peak 9 days earlier in the intercostal nerve compared to the sciatic nerve, then it is possible that axon-glia interaction is more stable and less vulnerable to disruption in the intercostal nerve, at the time-point when low SMN levels take effect.

It must also be noted that paranodes develop at different times and rates in different peripheral nerves due to varying onset of myelination (Schafer and Friede, 1988). The length of fully formed paranodes could also vary between nerves. It could therefore be possible that if a delay in paranodal development were present in the intercostal nerve, it would have not been observed at P8. Paranodes may develop faster in the intercostal nerve meaning that a delay would only be noticed if the nerves were taken at an earlier time-point. This is unfortunately not possible in these mice, as teasing intercostal nerves earlier than P8 proved to be too difficult and resulted in tissue damage.

5.3.4 Disruption of axon-glia interaction in SMA mice could be due to lack of SMN in other cell types

Axon-glia interactions were disrupted in SMA mice, manifesting as a delay in maturation. This delay could be caused by the intrinsic differences present in SMA Schwann cells, as the molecular make-up and function of these cells is altered (Hunter et al., 2014). The possibility that other affected systems and cells in SMA could be the cause for delayed paranodal development must also be considered. Recent studies have elucidated on the contribution of non-neuronal body systems and cells to the disease. A study by Somers et al., 2012 clearly showed how the vasculature in SMA mice is severely affected manifesting as a significant reduction in vascular density (Somers et al., 2012). We also know that a disruption in blood flow, induced by cerebral hypoperfusion, in turn affects paranodal integrity in the CNS (Reimer et al., 2011). It must therefore be acknowledged that the paranodal defects observed in the SMA mice could be due to a lack of blood flow from the capillaries surrounding the nerves.

We now know that SMA is a global body system disease, with significant pathology observed in many cell and tissue groups. Due to the widespread pathology, it can be difficult to tease apart the pathways downstream of SMN protein. It remains to be determined whether axon-glia interaction is disrupted as a direct consequence of loss of SMN in the Schwann cell, or in the axon, as both cell types express SMN and contribute protein components for formation of the paranode. It could also be the case that axon-glia interaction is disrupted due to downstream effects from other

systems such as the vasculature. What can be stated from the results of this chapter, however, is that reduced SMN levels are sufficient to delay maturation of axon-glial interaction at the paranode, which could be a contributory factor to the reduced conduction velocity observed in SMA patients (Krajewska and Hausmanowa-Petrusewicz, 2002).

Chapter 6

General Discussion

6.1 Overview of results

In this thesis, three main questions have been addressed and answered.

1. Is Nfasc155-mediated axon-glia interaction important for normal rates of synapse elimination at the mouse NMJ? If so, is this role dependent or independent of paranodal formation? (Chapter 3)

The experiments described in Chapter 3 were designed to address these questions. Using a mouse model of disrupted axon-glia interaction, the *Nfasc155*^{-/-} mouse, I showed that when axon-glia interaction at the paranode is disrupted, synapse elimination at the NMJ is significantly delayed. Further analysis using a second mouse model of paranodal disruption, the *Caspr*^{-/-} mouse, revealed that this delay was due to loss of Nfasc155 specifically from the myelinating glial cell rather than absence of paranodal junctions, as synapse elimination occurred normally in *Caspr*^{-/-} mice who display an identical paranodal phenotype but retain high levels of Nfasc155 in myelinating glia. This work highlights a novel role for Nfasc155, outside of its well-known canonical duties in paranodal formation. This work also uncovered a regulatory role for myelinating Schwann cells during synapse elimination in the PNS, providing the first evidence for such a role. The only

documented role for myelinating Schwann cells during synapse elimination prior to these results was in end-stage debris clearance, which is secondary to the elimination of inputs (Song et al., 2008).

2. How does glial *Nfasc155* modulate rates of synapse elimination? (Chapter 4)

The experiments undertaken in Chapter 4 were designed to provide molecular insight in to the mechanisms through which *Nfasc155* modulates rates of synapse elimination. iTRAQ proteomic analysis was performed on sciatic-tibial nerve from *Nfasc155*^{-/-}, *Caspr*^{-/-} and littermate controls at P12 in an attempt to tease apart the regulators of synapse elimination downstream of *Nfasc155*. Including the *Caspr*^{-/-} mice in this analysis and comparing these results with *Nfasc155*^{-/-} mice allowed me to produce a list of potential protein candidates involved in paranodal formation. This list was subtracted from the list of proteins changed in *Nfasc155*^{-/-} mice producing a list of altered proteins that directly correlated with delayed synapse elimination. This is the first known list of its kind, providing molecular insight in to how a fundamental developmental process at the NMJ is regulated, at the level of proteins and pathways.

iTRAQ and pathway analyses in *Nfasc155*^{-/-} mice revealed alterations to cytoskeletal organisation and transport systems in peripheral nerve. This correlated with a selective loss of NF-L in distal peripheral nerve and axon terminals, suggesting that NF-L was involved in the regulation of synapse elimination. Polyinnervation analysis in *NF-L*^{-/-} mice at P10 confirmed that this neurofilament subunit is essential

for normal rates of synapse elimination, with *NF-L*^{-/-} mice displaying higher levels of polyinnervation than littermate controls. These results suggest that NF-L specifically plays a role during synapse elimination. Further support for this role was strengthened by the finding that NF-L is the predominant neurofilament subunit at axon terminals and axon terminal protrusions of healthy neo-natal mice, the parts of the axon that are continuously remodelling and adapting to changes in innervation status during competition for sole innervation of the endplate (Keller-Peck et al., 2001; Walsh and Lichtman, 2003; Turney and Lichtman, 2012). This result implicates NF-L in axon stability/plasticity, and provides a plausible explanation for how loss of NF-L specifically from axon terminals of *Nfasc155*^{-/-} mice could be driving the delay in synapse elimination.

3. Is paranodal development/maturation compromised in a mouse model of SMA with known Schwann cell defects? (Chapter 5)

It is becoming increasingly clear that spinal muscular atrophy (SMA) is a global body system disorder, with reduced levels of SMN affecting a multitude of cells and organs (Hamilton and Gillingwater, 2013). Previous to the studies outlined in Chapter 5, Schwann cells were known to be defective in SMA mouse models, responding abnormally to myelination cues and displaying perturbations in myelin formation and compaction (Hunter et al., 2014). I sought to test whether abnormalities in axon-glia interactions were present in a mouse model of SMA, with known Schwann cell defects. This work showed that although paranodes developed, paranodal maturation was delayed in a mouse model of SMA, with shorter paranodes

present in the peripheral nerves of SMA mice compared to controls. This work indicates that loss of SMN is sufficient to disrupt paranodal maturation in peripheral nerve, providing further support for the characterisation of SMA as a multi-system disorder.

6.2 Insight in to the regulation of synapse elimination – an important role for myelinating Schwann cells

The work I have presented in this thesis reveals several novel findings. Firstly, I have discovered a novel role for Nfasc155, in the myelinating Schwann cell, in the modulation of synapse elimination. It is clear that Nfasc155 has a specific role during development of the mouse PNS, as it is required for normal rates of synapse elimination to occur across a range of skeletal muscles in the mouse without affecting other aspects of PNS development such as muscle fibre diameter or lower motor neuron number (Chapter 3). The only known role for Nfasc155 prior to the findings presented in this thesis was in paranodal assembly, acting in a complex with Caspr/contactin to form paranodal junctions and restrict Na_v and K_v channels to the node and juxtaparanode respectively (Charles et al., 2002; Sherman et al., 2005). I have discovered a new role for Nfasc155 outwith its canonical paranodal duties. This also raises the question of what axonal receptors Nfasc155 interacts with to alter rates of synapse elimination. Future studies will hopefully provide answers to this question.

Secondly, this work has also introduced a novel aspect to the regulation of synapse elimination, showing a clear role for myelinating glial cells in determining the outcome of synapse elimination at the NMJ. Although it is appreciated that myelinating Schwann cells are not passive during synapse elimination as they recycle/degrade unwanted axonal debris once axons have pruned away (Song et al., 2008), a primary, regulatory role for these cells has never before been shown. The

work presented in this thesis delivers an exciting finding and increases our understanding and appreciation for the role that myelinating glial cells play during developmental axonal remodelling in the PNS. This poses an interesting aspect to the regulation of developmental processes throughout the nervous system. For example, could myelinating oligodendrocytes be playing a similar regulatory role in developmental pruning in the CNS? Synapse elimination takes place throughout the CNS including in the retinogeniculate system (Chen and Regehr, 2000) and cerebellum (Hashimoto and Kano, 2005) so it is possible that oligodendrocytes, and possibly *Nfasc155*, could be playing a regulatory role during postnatal remodelling at synapses in these areas. It is hoped that this work will open up exciting research avenues with the goal to understand how developmental pruning in the nervous system is regulated. It is crucial that we understand the role that myelinating glia play during developmental synaptic remodelling of the nervous system before we can begin to fully comprehend synaptic function in health and disease, and develop successful treatments for nervous system disorders where the synapse is a target.

*The *Nfasc155*^{-/-} mouse model presented a unique opportunity to tease apart the regulators of synapse elimination at the mouse NMJ. Performing iTRAQ proteomic analysis on *Nfasc155*^{-/-}, *Caspr*^{-/-} and littermate controls allowed me to control for the proteomic results associated with paranodal disruption in *Nfasc155*^{-/-} mice, and formulate a list of protein changes that directly correlated with delayed synapse elimination. Such a dataset has never before been generated and provides us with a window in to the complex yet tightly controlled process of synapse elimination. The third novel finding in this thesis, is that loss of *Nfasc155* in the myelinating glial cell*

leads to disruption in cytoskeletal organisation and transport, as well as a selective reduction in NF-L levels in distal peripheral nerve and axon terminals at the NMJ, suggesting a link between NF-L levels and rates of synapse elimination. Indeed, analysis of synapse elimination in *NF-L*^{-/-} mice confirmed the importance of NF-L for developmental pruning at the NMJ. These findings provide important insights in to how Nfasc155 modulates synapse elimination and in to the cellular processes and proteins that are required for this process to occur normally. For example, transport proteins have never before been implicated in synapse elimination. Although neurofilament dynamics have previously been linked to synapse elimination, I have shown that NF-L specifically is important.

6.3 A novel role for NF-L in axon plasticity/stability

Such a selective role for NF-L during synapse elimination had never before been suggested, and so, to elucidate on this role further and determine the reasons for why NF-L specifically is important, the localisation and levels of NF-H, NF-M and NF-L were assessed at NMJs of healthy mice. This exposed a very interesting and fourth novel finding: that NF-L was present at higher levels than NF-H and NF-M in the most terminal parts of axons innervating NMJs and is present at high levels in axon terminal protrusions, the parts of the axon undergoing vast remodelling and adaptations during synapse elimination (Keller-Peck et al., 2001; Walsh and Lichtman, 2003; Turney and Lichtman, 2012), proposing a novel, specific role for NF-L in axon stability/plasticity. This is not so surprising considering that NF-L has previously been implicated in the dynamic growth and stability of motor neurons *in*

vivo and neurite processes *in vitro* (Zhu et al., 1997; Zhang et al., 2002; Chen et al., 2014).

Interestingly, previously published studies have implicated NF-L specifically in motor neuron diseases. Increased expression of *NF-L* in lower motor neurons resembles motor neuron disease, by resulting in axon degeneration, axon swelling and severe skeletal muscle atrophy (Xu et al., 1993). Mutations and altered expression of *NF-L* have also been implicated as causes in Charcot-Marie-Tooth disease (Mersiyanova et al., 2000; Georgiou et al., 2002) and ALS (Bergeron et al., 1994). In fact, antagonistic functions have been shown for NF-H/NF-M and NF-L in shaping dendritic arborisation in spinal motor neurons (Kong et al., 1998), in support of the view that neurofilament subunits, particularly NF-L, have specific individual roles outwith intermediate filament assembly. This is an important point to consider when assessing neurofilament dynamics during development, maturation, regeneration and disease throughout the nervous system, as it must not be presumed that the three neurofilament subunits will be playing similar roles at all stages of health and disease.

6.4 SMN and paranodal maturation

Paranodal abnormalities have previously been associated with neurological diseases, in models of multiple sclerosis (Howell et al., 2006; Pomicter et al., 2010) and Guillain Barré syndrome (Yuki and Kuwabara, 2007). SMA is now recognised as a multi-system disorder, with lack of SMN affecting multiple cell types and systems (Hamilton and Gillingwater, 2013). It was already known that Schwann cells are defective in SMA (Hunter et al., 2014), and I carried out experimental analysis to determine if this also resulted in a disruption to axon-glia interaction at the paranode. My results show that reduced SMN levels are sufficient to delay maturation of axon-glia interaction at the paranode, which could be a contributory factor to the reduced conduction velocity observed in SMA patients (Krajewska and Hausmanowa-Petrusewicz, 2002), as disrupted paranodes are known to affect the conductive properties along the nerve (Bhat et al., 2001; Pillai et al., 2009). This result emphasises the need to appreciate SMA as a multicellular disorder and also highlights the importance of SMN for physical axon-glia interactions, the fifth novel finding presented in this thesis.

6.5 Conclusion

In summary, with the results I have obtained throughout my PhD studies, I have furthered our understanding of how developmental synapse elimination at the mouse NMJ is controlled. In doing so, I have also discovered a novel role for a glial cell protein, Nfasc155, and provided clear evidence of a modulatory role for myelinating Schwann cells during synapse elimination. These new insights will hopefully lead on to further studies attempting to tease apart the complex mechanisms at play during synapse elimination, as well as further our understanding of and appreciation for the role that glial cells play during developmental axonal remodelling. I have also shown that paranodal maturation is delayed in a mouse model of SMA, supporting the notion that reduced levels of SMN affect a multitude of non-neuronal cell types and processes. This work contributes significantly to our understanding of the importance of axon-glial interactions for development of the PNS e.g. Synapse elimination, as well as the significance of these interactions in disease states of the PNS e.g. Spinal muscular atrophy.

Bibliography

- Adlkofer K, Martini R, Aguzzi A, Zielasek J, Toyka KV, Suter U (1995) Hypermyelination and demyelinating peripheral neuropathy in Pmp22-deficient mice. *Nat Genet* 11:274-280.
- Ali HH, Savarese JJ (1976) Monitoring of neuromuscular function. *Anesthesiology* 45:216-249.
- Allen NJ, Barres BA (2009) Neuroscience: Glia - more than just brain glue. *Nature* 457:675-677.
- Anderson MJ, Cohen MW (1974) Fluorescent staining of acetylcholine receptors in vertebrate skeletal muscle. *J Physiol* 237:385-400.
- Auld DS, Robitaille R (2003) Glial cells and neurotransmission: an inclusive view of synaptic function. *Neuron* 40:389-400.
- Azevedo FA, Carvalho LR, Grinberg LT, Farfel JM, Ferretti RE, Leite RE, Jacob Filho W, Lent R, Herculano-Houzel S (2009) Equal numbers of neuronal and nonneuronal cells make the human brain an isometrically scaled-up primate brain. *J Comp Neurol* 513:532-541.
- Balice-Gordon RJ, Lichtman JW (1993) In vivo observations of pre- and postsynaptic changes during the transition from multiple to single innervation at developing neuromuscular junctions. *J Neurosci* 13:834-855.
- Balice-Gordon RJ, Bone LJ, Scherer SS (1998) Functional gap junctions in the schwann cell myelin sheath. *J Cell Biol* 142:1095-1104.
- Banner LR, Patterson PH (1994) Major changes in the expression of the mRNAs for cholinergic differentiation factor/leukemia inhibitory factor and its receptor after injury to adult peripheral nerves and ganglia. *Proc Natl Acad Sci U S A* 91:7109-7113.
- Barres BA (2008) The mystery and magic of glia: a perspective on their roles in health and disease. *Neuron* 60:430-440.
- Bender AN, Ringel SP, Engel WK, Daniels MP, Vogel Z (1975) Myasthenia gravis: a serum factor blocking acetylcholine receptors of the human neuromuscular junction. *Lancet* 1:607-609.
- Bennett MR, Robinson J (1989) Growth and elimination of nerve terminals at synaptic sites during polyneuronal innervation of muscle cells: a trophic hypothesis. *Proc R Soc Lond B Biol Sci* 235:299-320.
- Bergeron C, Beric-Maskarel K, Muntasser S, Weyer L, Somerville MJ, Percy ME (1994) Neurofilament light and polyadenylated mRNA levels are decreased in amyotrophic lateral sclerosis motor neurons. *J Neuropathol Exp Neurol* 53:221-230.
- Beuche W, Friede RL (1984) The role of non-resident cells in Wallerian degeneration. *J Neurocytol* 13:767-796.
- Bhat MA, Rios JC, Lu Y, Garcia-Fresco GP, Ching W, St Martin M, Li J, Einheber S, Chesler M, Rosenbluth J, Salzer JL, Bellen HJ (2001) Axon-glia interactions and the domain organization of myelinated axons requires neurexin IV/Caspr/Paranodin. *Neuron* 30:369-383.
- Bird TD, Farrell DF, Sumi SM (1978) Brain lipid composition of the shiverer mouse: (genetic defect in myelin development). *J Neurochem* 31:387-391.

- Birks R, Huxley HE, Katz B (1960) The fine structure of the neuromuscular junction of the frog. *J Physiol* 150:134-144.
- Bishop DL, Misgeld T, Walsh MK, Gan WB, Lichtman JW (2004) Axon branch removal at developing synapses by axosome shedding. *Neuron* 44:651-661.
- Bixby JL (1981) Ultrastructural observations on synapse elimination in neonatal rabbit skeletal muscle. *J Neurocytol* 10:81-100.
- Black JA, Renganathan M, Waxman SG (2002) Sodium channel Na(v)1.6 is expressed along nonmyelinated axons and it contributes to conduction. *Brain Res Mol Brain Res* 105:19-28.
- Bolin LM, Verity AN, Silver JE, Shooter EM, Abrams JS (1995) Interleukin-6 production by Schwann cells and induction in sciatic nerve injury. *J Neurochem* 64:850-858.
- Bowerman M, Swoboda KJ, Michalski JP, Wang GS, Reeks C, Beauvais A, Murphy K, Woulfe J, Sreaton RA, Scott FW, Kothary R (2012) Glucose metabolism and pancreatic defects in spinal muscular atrophy. *Ann Neurol* 72:256-268.
- Boyle ME, Berglund EO, Murai KK, Weber L, Peles E, Ranscht B (2001) Contactin orchestrates assembly of the septate-like junctions at the paranode in myelinated peripheral nerve. *Neuron* 30:385-397.
- Brady ST, Witt AS, Kirkpatrick LL, de Waegh SM, Readhead C, Tu PH, Lee VM (1999) Formation of compact myelin is required for maturation of the axonal cytoskeleton. *J Neurosci* 19:7278-7288.
- Britsch S, Goerich DE, Riethmacher D, Peirano RI, Rossner M, Nave KA, Birchmeier C, Wegner M (2001) The transcription factor Sox10 is a key regulator of peripheral glial development. *Genes Dev* 15:66-78.
- Brophy PJ (2001) Axoglial junctions: separate the channels or scramble the message. *Curr Biol* 11:R555-557.
- Brophy PJ (2003) Myelinated Nerves: Filling in the Juxtaparanodal Gap. *Current Biology* 13:R956-R957.
- Brown MC, Jansen JK, Van Essen D (1976) Polyneuronal innervation of skeletal muscle in new-born rats and its elimination during maturation. *J Physiol* 261:387-422.
- Buffelli M, Burgess RW, Feng G, Lobe CG, Lichtman JW, Sanes JR (2003) Genetic evidence that relative synaptic efficacy biases the outcome of synaptic competition. *Nature* 424:430-434.
- Bullock TH, Moore JK, Fields RD (1984) Evolution of myelin sheaths: both lamprey and hagfish lack myelin. *Neurosci Lett* 48:145-148.
- Bunge RP (1968) Glial cells and the central myelin sheath. *Physiol Rev* 48:197-251.
- Bunge RP, Bunge MB, Bates M (1989) Movements of the Schwann cell nucleus implicate progression of the inner (axon-related) Schwann cell process during myelination. *J Cell Biol* 109:273-284.
- Burden SJ, DePalma RL, Gottesman GS (1983) Crosslinking of proteins in acetylcholine receptor-rich membranes: association between the beta-subunit and the 43 kd subsynaptic protein. *Cell* 35:687-692.
- Burghes AH, Beattie CE (2009) Spinal muscular atrophy: why do low levels of survival motor neuron protein make motor neurons sick? *Nat Rev Neurosci* 10:597-609.

- Caillol G, Vacher H, Musarella M, Bellouze S, Dargent B, Autillo-Touati A (2012) Motor endplate disease affects neuromuscular junction maturation. *Eur J Neurosci* 36:2400-2408.
- Cajal SR (1923) *Receurdos de mi vida*, in: *Historia de mi labor científica*, 3rd ed. Imprenta de Juan Pueyo, Madrid.
- Callaway EM, Soha JM, Van Essen DC (1987) Competition favouring inactive over active motor neurons during synapse elimination. *Nature* 328:422-426.
- Callaway EM, Soha JM, Van Essen DC (1989) Differential loss of neuromuscular connections according to activity level and spinal position of neonatal rabbit soleus motor neurons. *J Neurosci* 9:1806-1824.
- Carden MJ, Trojanowski JQ, Schlaepfer WW, Lee VM (1987) Two-stage expression of neurofilament polypeptides during rat neurogenesis with early establishment of adult phosphorylation patterns. *J Neurosci* 7:3489-3504.
- Chan JR, Cosgaya JM, Wu YJ, Shooter EM (2001) Neurotrophins are key mediators of the myelination program in the peripheral nervous system. *Proc Natl Acad Sci U S A* 98:14661-14668.
- Charles P, Tait S, Faivre-Sarrailh C, Barbin G, Gunn-Moore F, Denisenko-Nehrbass N, Guennoc AM, Girault JA, Brophy PJ, Lubetzki C (2002) Neurofascin is a glial receptor for the paranodin/Caspr-contactin axonal complex at the axoglial junction. *Curr Biol* 12:217-220.
- Chen C, Regehr WG (2000) Developmental remodeling of the retinogeniculate synapse. *Neuron* 28:955-966.
- Chen H, Qian K, Du Z, Cao J, Petersen A, Liu H, Blackburn LWt, Huang CL, Errigo A, Yin Y, Lu J, Ayala M, Zhang SC (2014) Modeling ALS with iPSCs Reveals that Mutant SOD1 Misregulates Neurofilament Balance in Motor Neurons. *Cell stem cell* 14:796-809.
- Chiu SY, Zhou L, Zhang CL, Messing A (1999) Analysis of potassium channel functions in mammalian axons by gene knockouts. *J Neurocytol* 28:349-364.
- Chung WS, Barres BA (2012) The role of glial cells in synapse elimination. *Curr Opin Neurobiol* 22:438-445.
- Chung WS, Clarke LE, Wang GX, Stafford BK, Sher A, Chakraborty C, Joung J, Foo LC, Thompson A, Chen C, Smith SJ, Barres BA (2013) Astrocytes mediate synapse elimination through MEGF10 and MERTK pathways. *Nature* 504:394-400.
- Cleveland DW, Monteiro MJ, Wong PC, Gill SR, Gearhart JD, Hoffman PN (1991) Involvement of neurofilaments in the radial growth of axons. *Journal of cell science Supplement* 15:85-95.
- Cohen MW, Godfrey EW (1992) Early appearance of and neuronal contribution to agrin-like molecules at embryonic frog nerve-muscle synapses formed in culture. *J Neurosci* 12:2982-2992.
- Cole JS, Messing A, Trojanowski JQ, Lee VM (1994) Modulation of axon diameter and neurofilaments by hypomyelinating Schwann cells in transgenic mice. *J Neurosci* 14:6956-6966.
- Collinson JM, Marshall D, Gillespie CS, Brophy PJ (1998) Transient expression of neurofascin by oligodendrocytes at the onset of

- myelinogenesis: implications for mechanisms of axon-glia interaction. *Glia* 23:11-23.
- Costanzo EM, Barry JA, Ribchester RR (1999) Co-regulation of synaptic efficacy at stable polyneuronally innervated neuromuscular junctions in reinnervated rat muscle. *J Physiol* 521 Pt 2:365-374.
- Costanzo EM, Barry JA, Ribchester RR (2000) Competition at silent synapses in reinnervated skeletal muscle. *Nat Neurosci* 3:694-700.
- Court FA, Sherman DL, Pratt T, Garry EM, Ribchester RR, Cottrell DF, Fleetwood-Walker SM, Brophy PJ (2004) Restricted growth of Schwann cells lacking Cajal bands slows conduction in myelinated nerves. *Nature* 431:191-195.
- Court FA, Gillingwater TH, Melrose S, Sherman DL, Greenshields KN, Morton AJ, Harris JB, Willison HJ, Ribchester RR (2008) Identity, developmental restriction and reactivity of extralaminar cells capping mammalian neuromuscular junctions. *J Cell Sci* 121:3901-3911.
- Culican SM, Nelson CC, Lichtman JW (1998) Axon withdrawal during synapse elimination at the neuromuscular junction is accompanied by disassembly of the postsynaptic specialization and withdrawal of Schwann cell processes. *J Neurosci* 18:4953-4965.
- Curtis R, Scherer SS, Somogyi R, Adryan KM, Ip NY, Zhu Y, Lindsay RM, DiStefano PS (1994) Retrograde axonal transport of LIF is increased by peripheral nerve injury: correlation with increased LIF expression in distal nerve. *Neuron* 12:191-204.
- Darabid H, Arbour D, Robitaille R (2013) Glial cells decipher synaptic competition at the mammalian neuromuscular junction. *J Neurosci* 33:1297-1313.
- Dashiell SM, Tanner SL, Pant HC, Quarles RH (2002) Myelin-associated glycoprotein modulates expression and phosphorylation of neuronal cytoskeletal elements and their associated kinases. *J Neurochem* 81:1263-1272.
- Davis AD, Weatherby TM, Hartline DK, Lenz PH (1999) Myelin-like sheaths in copepod axons. *Nature* 398:571.
- Davis JQ, Lambert S, Bennett V (1996) Molecular composition of the node of Ranvier: identification of ankyrin-binding cell adhesion molecules neurofascin (mucin+ /third FNIII domain-) and NrCAM at nodal axon segments. *J Cell Biol* 135:1355-1367.
- De Robertis ED, Bennett HS (1955) Some features of the submicroscopic morphology of synapses in frog and earthworm. *J Biophys Biochem Cytol* 1:47-58.
- de Waegh SM, Brady ST (1991) Local control of axonal properties by Schwann cells: neurofilaments and axonal transport in homologous and heterologous nerve grafts. *Journal of neuroscience research* 30:201-212.
- de Waegh SM, Lee VM, Brady ST (1992) Local modulation of neurofilament phosphorylation, axonal caliber, and slow axonal transport by myelinating Schwann cells. *Cell* 68:451-463.
- DeChiara TM, Bowen DC, Valenzuela DM, Simmons MV, Poueymirou WT, Thomas S, Kinetz E, Compton DL, Rojas E, Park JS, Smith C, DiStefano PS, Glass DJ, Burden SJ, Yancopoulos GD (1996) The

- receptor tyrosine kinase MuSK is required for neuromuscular junction formation in vivo. *Cell* 85:501-512.
- Duncan JE, Goldstein LS (2006) The genetics of axonal transport and axonal transport disorders. *PLoS Genet* 2:e124.
- Eccles JC, Katz B, Kuffler SW (1941) NATURE OF THE "ENDPLATE POTENTIAL" IN CURARIZED MUSCLE. 4:362-387.
- Ehrenberg CG (1836) Beobachtungeneiner auffallenden bisher unerkannten Struckfurder Seelenorgans bei Menschen und Thieren, Koniglichen Akademie der Wissenschaft, Berlin.
- Einheber S, Zanazzi G, Ching W, Scherer S, Milner TA, Peles E, Salzer JL (1997) The axonal membrane protein Caspr, a homologue of neurexin IV, is a component of the septate-like paranodal junctions that assemble during myelination. *J Cell Biol* 139:1495-1506.
- Emery DG, Ito H, Coggeshall RE (1977) Unmyelinated axons in thoracic ventral roots of the cat. *J Comp Neurol* 172:37-47.
- English AW, Schwartz G (1995) Both basic fibroblast growth factor and ciliary neurotrophic factor promote the retention of polyneuronal innervation of developing skeletal muscle fibers. *Dev Biol* 169:57-64.
- Eroglu C, Barres BA (2010) Regulation of synaptic connectivity by glia. *Nature* 468:223-231.
- Erzen I, Cvetko E, Obreza S, Angaut-Petit D (2000) Fiber types in the mouse levator auris longus muscle: a convenient preparation to study muscle and nerve plasticity. *Journal of neuroscience research* 59:692-697.
- Escurat M, Djabali K, Gumpel M, Gros F, Portier MM (1990) Differential expression of two neuronal intermediate-filament proteins, peripherin and the low-molecular-mass neurofilament protein (NF-L), during the development of the rat. *J Neurosci* 10:764-784.
- Eskelinen EL (2006) Roles of LAMP-1 and LAMP-2 in lysosome biogenesis and autophagy. *Molecular aspects of medicine* 27:495-502.
- Farrar MA, Vucic S, Lin CS, Park SB, Johnston HM, du Sart D, Bostock H, Kiernan MC (2011) Dysfunction of axonal membrane conductances in adolescents and young adults with spinal muscular atrophy. *Brain* 134:3185-3197.
- Favero M, Busetto G, Cangiano A (2012) Spike timing plays a key role in synapse elimination at the neuromuscular junction. *Proc Natl Acad Sci U S A* 109:E1667-1675.
- Favero M, Cangiano A, Busetto G (2014) Hebb-based rules of neural plasticity: are they ubiquitously important for the refinement of synaptic connections in development? *Neuroscientist* 20:8-14.
- Favero M, Massella O, Cangiano A, Buffelli M (2009) On the mechanism of action of muscle fibre activity in synapse competition and elimination at the mammalian neuromuscular junction. *Eur J Neurosci* 29:2327-2334.
- Favero M, Buffelli M, Cangiano A, Busetto G (2010) The timing of impulse activity shapes the process of synaptic competition at the neuromuscular junction. *Neuroscience* 167:343-353.
- Fernandez-Valle C, Bunge RP, Bunge MB (1995) Schwann cells degrade myelin and proliferate in the absence of macrophages: evidence from in vitro studies of Wallerian degeneration. *J Neurocytol* 24:667-679.

- Fertuck HC, Salpeter MM (1974) Localization of acetylcholine receptor by ¹²⁵I-labeled alpha-bungarotoxin binding at mouse motor endplates. *Proc Natl Acad Sci U S A* 71:1376-1378.
- Finzsch M, Schreiner S, Kichko T, Reeh P, Tamm ER, Bosl MR, Meijer D, Wegner M (2010) Sox10 is required for Schwann cell identity and progression beyond the immature Schwann cell stage. *J Cell Biol* 189:701-712.
- Fischer LR, Culver DG, Tennant P, Davis AA, Wang M, Castellano-Sanchez A, Khan J, Polak MA, Glass JD (2004) Amyotrophic lateral sclerosis is a distal axonopathy: evidence in mice and man. *Exp Neurol* 185:232-240.
- Fodstad H (2001) The neuron theory, *Stereotact. Funct Neurosurg* 77:20-24.
- Fontaine B, Klarsfeld A, Changeux JP (1987) Calcitonin gene-related peptide and muscle activity regulate acetylcholine receptor alpha-subunit mRNA levels by distinct intracellular pathways. *J Cell Biol* 105:1337-1342.
- Fontaine B, Klarsfeld A, Hokfelt T, Changeux JP (1986) Calcitonin gene-related peptide, a peptide present in spinal cord motoneurons, increases the number of acetylcholine receptors in primary cultures of chick embryo myotubes. *Neurosci Lett* 71:59-65.
- Fontana X, Hristova M, Da Costa C, Patodia S, Thei L, Makwana M, Spencer-Dene B, Latouche M, Mirsky R, Jessen KR, Klein R, Raivich G, Behrens A (2012) c-Jun in Schwann cells promotes axonal regeneration and motoneuron survival via paracrine signaling. *J Cell Biol* 198:127-141.
- Foster M (1897) *A Textbook of Physiology*. Part three: the Central Nervous System, 7th Ed. Macmillan and Co Ltd, London.
- Fox MA, Tapia JC, Kasthuri N, Lichtman JW (2011) Delayed synapse elimination in mouse levator palpebrae superioris muscle. *J Comp Neurol* 519:2907-2921.
- Frail DE, Mudd J, Shah V, Carr C, Cohen JB, Merlie JP (1987) cDNAs for the postsynaptic 43-kDa protein of Torpedo electric organ encode two proteins with different carboxyl termini. *Proc Natl Acad Sci U S A* 84:6302-6306.
- Freeman MR (2006) Sculpting the nervous system: glial control of neuronal development. *Curr Opin Neurobiol* 16:119-125.
- Froehner SC, Luetje CW, Scotland PB, Patrick J (1990) The postsynaptic 43K protein clusters muscle nicotinic acetylcholine receptors in *Xenopus* oocytes. *Neuron* 5:403-410.
- Frostick SP, Yin Q, Kemp GJ (1998) Schwann cells, neurotrophic factors, and peripheral nerve regeneration. *Microsurgery* 18:397-405.
- Fuentes-Medel Y, Logan MA, Ashley J, Ataman B, Budnik V, Freeman MR (2009) Glia and muscle sculpt neuromuscular arbors by engulfing destabilized synaptic boutons and shed presynaptic debris. *PLoS Biol* 7:e1000184.
- Gan WB, Lichtman JW (1998) Synaptic segregation at the developing neuromuscular junction. *Science* 282:1508-1511.
- Ganju P, Walls E, Brennan J, Reith AD (1995) Cloning and developmental expression of Nsk2, a novel receptor tyrosine kinase implicated in skeletal myogenesis. *Oncogene* 11:281-290.

- Garrison CJ, Dougherty PM, Kajander KC, Carlton SM (1991) Staining of glial fibrillary acidic protein (GFAP) in lumbar spinal cord increases following a sciatic nerve constriction injury. *Brain Res* 565:1-7.
- Gautam M, Noakes PG, Moscoso L, Rupp F, Scheller RH, Merlie JP, Sanes JR (1996) Defective neuromuscular synaptogenesis in agrin-deficient mutant mice. *Cell* 85:525-535.
- Geisler N, Weber K (1981) Self-assembly in Vitro of the 68,000 molecular weight component of the mammalian neurofilament triplet proteins into intermediate-sized filaments. *J Mol Biol* 151:565-571.
- Georgiou DM, Zidar J, Korosec M, Middleton LT, Kyriakides T, Christodoulou K (2002) A novel NF-L mutation Pro22Ser is associated with CMT2 in a large Slovenian family. *Neurogenetics* 4:93-96.
- Gerlach Jv (1871) Von den Ruckenmarke, in S. Stricker (Ed.). *Handbuch der Lehre von den Geweben*, Engelmann, Leipzig:665-693.
- Giese KP, Martini R, Lemke G, Soriano P, Schachner M (1992) Mouse P0 gene disruption leads to hypomyelination, abnormal expression of recognition molecules, and degeneration of myelin and axons. *Cell* 71:565-576.
- Gillespie CS, Sherman DL, Fleetwood-Walker SM, Cottrell DF, Tait S, Garry EM, Wallace VC, Ure J, Griffiths IR, Smith A, Brophy PJ (2000) Peripheral demyelination and neuropathic pain behavior in periaxin-deficient mice. *Neuron* 26:523-531.
- Gilmour DT, Maischein HM, Nusslein-Volhard C (2002) Migration and function of a glial subtype in the vertebrate peripheral nervous system. *Neuron* 34:577-588.
- Giulian D, Young DG, Woodward J, Brown DC, Lachman LB (1988) Interleukin-1 is an astroglial growth factor in the developing brain. *J Neurosci* 8:709-714.
- Glass DJ, Apel ED, Shah S, Bowen DC, DeChiara TM, Stitt TN, Sanes JR, Yancopoulos GD (1997) Kinase domain of the muscle-specific receptor tyrosine kinase (MuSK) is sufficient for phosphorylation but not clustering of acetylcholine receptors: required role for the MuSK ectodomain? *Proc Natl Acad Sci U S A* 94:8848-8853.
- Glass DJ, Bowen DC, Stitt TN, Radziejewski C, Bruno J, Ryan TE, Gies DR, Shah S, Mattsson K, Burden SJ, DiStefano PS, Valenzuela DM, DeChiara TM, Yancopoulos GD (1996) Agrin acts via a MuSK receptor complex. *Cell* 85:513-523.
- Glass JD, Brushart TM, George EB, Griffin JW (1993) Prolonged survival of transected nerve fibres in C57BL/Ola mice is an intrinsic characteristic of the axon. *J Neurocytol* 22:311-321.
- Goldman D, Staple J (1989) Spatial and temporal expression of acetylcholine receptor RNAs in innervated and denervated rat soleus muscle. *Neuron* 3:219-228.
- Gollan L, Salomon D, Salzer JL, Peles E (2003) Caspr regulates the processing of contactin and inhibits its binding to neurofascin. *J Cell Biol* 163:1213-1218.
- Goodearl AD, Yee AG, Sandrock AW, Jr., Corfas G, Fischbach GD (1995) ARIA is concentrated in the synaptic basal lamina of the developing chick neuromuscular junction. *J Cell Biol* 130:1423-1434.

- Gorio A, Carmignoto G, Finesso M, Polato P, Nunzi MG (1983) Muscle reinnervation--II. Sprouting, synapse formation and repression. *Neuroscience* 8:403-416.
- Grant P, Pant HC (2000) Neurofilament protein synthesis and phosphorylation. *J Neurocytol* 29:843-872.
- Grinspan JB, Marchionni MA, Reeves M, Coulaloglou M, Scherer SS (1996) Axonal interactions regulate Schwann cell apoptosis in developing peripheral nerve: neuregulin receptors and the role of neuregulins. *J Neurosci* 16:6107-6118.
- Grosse G, Draguhn A, Hohne L, Tapp R, Veh RW, Ahnert-Hilger G (2000) Expression of Kv1 potassium channels in mouse hippocampal primary cultures: development and activity-dependent regulation. *J Neurosci* 20:1869-1882.
- Gunther J (1976) Impulse conduction in the myelinated giant fibers of the earthworm. Structure and function of the dorsal nodes in the median giant fiber. *J Comp Neurol* 168:505-531.
- Haggmark T, Thorstensson A (1979) Fibre types in human abdominal muscles. *Acta Physiol Scand* 107:319-325.
- Hamilton G, Gillingwater TH (2013) Spinal muscular atrophy: going beyond the motor neuron. *Trends Mol Med* 19:40-50.
- Hansson HA, Dahlin LB, Danielsen N, Fryklund L, Nachemson AK, Polleryd P, Rozell B, Skottner A, Stemme S, Lundborg G (1986) Evidence indicating trophic importance of IGF-I in regenerating peripheral nerves. *Acta Physiol Scand* 126:609-614.
- Hartline DK, Colman DR (2007) Rapid conduction and the evolution of giant axons and myelinated fibers. *Curr Biol* 17:R29-35.
- Hashimoto K, Kano M (2005) Postnatal development and synapse elimination of climbing fiber to Purkinje cell projection in the cerebellum. *Neuroscience research* 53:221-228.
- Hirata K, Kawabuchi M (2002) Myelin phagocytosis by macrophages and nonmacrophages during Wallerian degeneration. *Microscopy research and technique* 57:541-547.
- Hirokawa N (1982) Cross-linker system between neurofilaments, microtubules, and membranous organelles in frog axons revealed by the quick-freeze, deep-etching method. *J Cell Biol* 94:129-142.
- Hoke A, Redett R, Hameed H, Jari R, Zhou C, Li ZB, Griffin JW, Brushart TM (2006) Schwann cells express motor and sensory phenotypes that regulate axon regeneration. *J Neurosci* 26:9646-9655.
- Hooks BM, Chen C (2006) Distinct roles for spontaneous and visual activity in remodeling of the retinogeniculate synapse. *Neuron* 52:281-291.
- Hopf C, Hoch W (1998a) Dimerization of the muscle-specific kinase induces tyrosine phosphorylation of acetylcholine receptors and their aggregation on the surface of myotubes. *J Biol Chem* 273:6467-6473.
- Hopf C, Hoch W (1998b) Tyrosine phosphorylation of the muscle-specific kinase is exclusively induced by acetylcholine receptor-aggregating agrin fragments. *Eur J Biochem* 253:382-389.
- Howell OW, Palser A, Polito A, Melrose S, Zonta B, Scheiermann C, Vora AJ, Brophy PJ, Reynolds R (2006) Disruption of neurofascin localization reveals early changes preceding demyelination and remyelination in multiple sclerosis. *Brain* 129:3173-3185.

- Hsieh-Li HM, Chang JG, Jong YJ, Wu MH, Wang NM, Tsai CH, Li H (2000) A mouse model for spinal muscular atrophy. *Nat Genet* 24:66-70.
- Hunter G, Aghamaleky Sarvestany A, Roche SL, Symes RC, Gillingwater TH (2014) SMN-dependent intrinsic defects in Schwann cells in mouse models of spinal muscular atrophy. *Hum Mol Genet* 23:2235-2250.
- Huxley AF, Stampfli R (1949) Evidence for saltatory conduction in peripheral myelinated nerve fibres. *J Physiol* 108:315-339.
- Ide C, Tohyama K, Yokota R, Nitatori T, Onodera S (1983) Schwann cell basal lamina and nerve regeneration. *Brain Res* 288:61-75.
- Ilyas AA, Willison HJ, Quarles RH, Jungalwala FB, Cornblath DR, Trapp BD, Griffin DE, Griffin JW, McKhann GM (1988) Serum antibodies to gangliosides in Guillain-Barre syndrome. *Ann Neurol* 23:440-447.
- Inglese M, Petracca M (2014) Therapeutic strategies in multiple sclerosis: A focus on neuroprotection and repair and relevance to schizophrenia. *Schizophrenia research*.
- Ip FC, Cheung J, Ip NY (2001) The expression profiles of neurotrophins and their receptors in rat and chicken tissues during development. *Neurosci Lett* 301:107-110.
- Jablonka S, Schrank B, Kralewski M, Rossoll W, Sendtner M (2000) Reduced survival motor neuron (Smn) gene dose in mice leads to motor neuron degeneration: an animal model for spinal muscular atrophy type III. *Hum Mol Genet* 9:341-346.
- Jacobs JR, Goodman CS (1989) Embryonic development of axon pathways in the Drosophila CNS. I. A glial scaffold appears before the first growth cones. *J Neurosci* 9:2402-2411.
- Je HS, Yang F, Ji Y, Potluri S, Fu XQ, Luo ZG, Nagappan G, Chan JP, Hempstead B, Son YJ, Lu B (2013) ProBDNF and mature BDNF as punishment and reward signals for synapse elimination at mouse neuromuscular junctions. *J Neurosci* 33:9957-9962.
- Jenkins SM, Bennett V (2002) Developing nodes of Ranvier are defined by ankyrin-G clustering and are independent of paranodal axoglial adhesion. *Proc Natl Acad Sci U S A* 99:2303-2308.
- Jessen KR, Mirsky R (2005) The origin and development of glial cells in peripheral nerves. *Nat Rev Neurosci* 6:671-682.
- Jessen KR, Mirsky R (2010) Control of Schwann cell myelination. *F1000 Biol Rep* 2.
- Jiang YQ, Oblinger MM (1992) Differential regulation of beta III and other tubulin genes during peripheral and central neuron development. *J Cell Sci* 103 (Pt 3):643-651.
- Jordan CL (1996) Morphological effects of ciliary neurotrophic factor treatment during neuromuscular synapse elimination. *J Neurobiol* 31:29-40.
- Kamal A, Almenar-Queralt A, LeBlanc JF, Roberts EA, Goldstein LS (2001) Kinesin-mediated axonal transport of a membrane compartment containing beta-secretase and presenilin-1 requires APP. *Nature* 414:643-648.
- Kano M, Hashimoto K (2009) Synapse elimination in the central nervous system. *Curr Opin Neurobiol* 19:154-161.
- Kaplan MP, Chin SS, Fliegner KH, Liem RK (1990) Alpha-internexin, a novel neuronal intermediate filament protein, precedes the low molecular

- weight neurofilament protein (NF-L) in the developing rat brain. *J Neurosci* 10:2735-2748.
- Karch CM, Cruchaga C, Goate AM (2014) Alzheimer's Disease Genetics: From the Bench to the Clinic. *Neuron* 83:11-26.
- Kasthuri N, Lichtman JW (2003) The role of neuronal identity in synaptic competition. *Nature* 424:426-430.
- Katz B (1966) *Nerve, Muscle and Synapse*. New York: McGraw Hill.
- Keller-Peck CR, Walsh MK, Gan WB, Feng G, Sanes JR, Lichtman JW (2001) Asynchronous synapse elimination in neonatal motor units: studies using GFP transgenic mice. *Neuron* 31:381-394.
- Kiernan MC, Vucic S, Cheah BC, Turner MR, Eisen A, Hardiman O, Burrell JR, Zoing MC (2011) Amyotrophic lateral sclerosis. *Lancet* 377:942-955.
- Komada M, Soriano P (2002) [Beta]IV-spectrin regulates sodium channel clustering through ankyrin-G at axon initial segments and nodes of Ranvier. *J Cell Biol* 156:337-348.
- Kong J, Tung VW, Aghajanian J, Xu Z (1998) Antagonistic roles of neurofilament subunits NF-H and NF-M against NF-L in shaping dendritic arborization in spinal motor neurons. *J Cell Biol* 140:1167-1176.
- Kordeli E, Lambert S, Bennett V (1995) AnkyrinG. A new ankyrin gene with neural-specific isoforms localized at the axonal initial segment and node of Ranvier. *J Biol Chem* 270:2352-2359.
- Krajewska G, Hausmanowa-Petrusewicz I (2002) Abnormal nerve conduction velocity as a marker of immaturity in childhood muscle spinal atrophy. *Folia Neuropathol* 40:67-74.
- Kühne W (1862) *Über die peripherischen Endorgane der Motorischen Nerve*, Engelmann, Leipzig.
- Kühne W (1871) *Nerv- und Muskelfaser*, 1869. Contenido en: Stricker S *Handbuch der Lehre von den Geweben*, Engelmann, Leipzig.
- Kummer TT, Misgeld T, Sanes JR (2006) Assembly of the postsynaptic membrane at the neuromuscular junction: paradigm lost. *Curr Opin Neurobiol* 16:74-82.
- Kwon YW, Abbondanzo SJ, Stewart CL, Gurney ME (1995) Leukemia inhibitory factor influences the timing of programmed synapses withdrawal from neonatal muscles. *J Neurobiol* 28:35-50.
- Lantermann AJ (1877) *Arch mikr Anat* 13.
- Lappe-Siefke C, Goebbels S, Gravel M, Nicksch E, Lee J, Braun PE, Griffiths IR, Nave KA (2003) Disruption of *Cnp1* uncouples oligodendroglial functions in axonal support and myelination. *Nat Genet* 33:366-374.
- Lawrence CJ et al. (2004) A standardized kinesin nomenclature. *J Cell Biol* 167:19-22.
- Lee S, Sunil N, Tejada JM, Shea TB (2011) Differential roles of kinesin and dynein in translocation of neurofilaments into axonal neurites. *J Cell Sci* 124:1022-1031.
- Lefebvre S, Burglen L, Reboullet S, Clermont O, Burlet P, Viollet L, Benichou B, Cruaud C, Millasseau P, Zeviani M, et al. (1995) Identification and characterization of a spinal muscular atrophy-determining gene. *Cell* 80:155-165.
- Lemke G, Chao M (1988) Axons regulate Schwann cell expression of the major myelin and NGF receptor genes. *Development* 102:499-504.

- Leung CL, Liem RK (1996) Characterization of interactions between the neurofilament triplet proteins by the yeast two-hybrid system. *J Biol Chem* 271:14041-14044.
- Lichtman JW, Colman H (2000) Synapse elimination and indelible memory. *Neuron* 25:269-278.
- Liem RK, Hutchison SB (1982) Purification of individual components of the neurofilament triplet: filament assembly from the 70 000-dalton subunit. *Biochemistry* 21:3221-3226.
- Lin W, Burgess RW, Dominguez B, Pfaff SL, Sanes JR, Lee KF (2001) Distinct roles of nerve and muscle in postsynaptic differentiation of the neuromuscular synapse. *Nature* 410:1057-1064.
- Ling KK, Gibbs RM, Feng Z, Ko CP (2012) Severe neuromuscular denervation of clinically relevant muscles in a mouse model of spinal muscular atrophy. *Hum Mol Genet* 21:185-195.
- Liuzzi FJ, Tedeschi B (1992) Axo-glial interactions at the dorsal root transitional zone regulate neurofilament protein synthesis in axotomized sensory neurons. *J Neurosci* 12:4783-4792.
- Loeb JA, Fischbach GD (1995) ARIA can be released from extracellular matrix through cleavage of a heparin-binding domain. *J Cell Biol* 130:127-135.
- Long DM, Bodenheimer TS, Hartmann JF, Klatzo I (1968) Ultrastructural features of the shark brain. *Am J Anat* 122:209-236.
- Lorson CL, Rindt H, Shababi M (2010) Spinal muscular atrophy: mechanisms and therapeutic strategies. *Hum Mol Genet* 19:R111-118.
- Low PA (1976a) Hereditary hypertrophic neuropathy in the trembler mouse. Part 2. Histopathological studies: electron microscopy. *Journal of the neurological sciences* 30:343-368.
- Low PA (1976b) Hereditary hypertrophic neuropathy in the trembler mouse. Part 1. Histopathological studies: light microscopy. *Journal of the neurological sciences* 30:327-341.
- Lowry K, Quach H, Wreford N, Cheema SS (2001) There is no loss of motor neurons in the rat spinal cord during postnatal maturation. *Journal of anatomy* 198:473-479.
- Lubke T, Lobel P, Sleat DE (2009) Proteomics of the lysosome. *Biochim Biophys Acta* 1793:625-635.
- Mandich P, Mancardi GL, Varese A, Soriani S, Di Maria E, Bellone E, Bado M, Gross L, Windebank AJ, Ajmar F, Schenone A (1999) Congenital hypomyelination due to myelin protein zero Q215X mutation. *Ann Neurol* 45:676-678.
- Marcus J, Dupree JL, Popko B (2002) Myelin-associated glycoprotein and myelin galactolipids stabilize developing axo-glial interactions. *J Cell Biol* 156:567-577.
- Marrosu MG, Vaccargiu S, Marrosu G, Vannelli A, Cianchetti C, Muntoni F (1998) Charcot-Marie-Tooth disease type 2 associated with mutation of the myelin protein zero gene. *Neurology* 50:1397-1401.
- Martini R (1994) Expression and functional roles of neural cell surface molecules and extracellular matrix components during development and regeneration of peripheral nerves. *J Neurocytol* 23:1-28.

- Martini R, Zielasek J, Toyka KV, Giese KP, Schachner M (1995a) Protein zero (P0)-deficient mice show myelin degeneration in peripheral nerves characteristic of inherited human neuropathies. *Nat Genet* 11:281-286.
- Martini R, Mohajeri MH, Kasper S, Giese KP, Schachner M (1995b) Mice doubly deficient in the genes for P0 and myelin basic protein show that both proteins contribute to the formation of the major dense line in peripheral nerve myelin. *J Neurosci* 15:4488-4495.
- McArdle JJ (1975) Complex end-plate potentials at the regenerating neuromuscular junction of the rat. *Exp Neurol* 49:629-638.
- McCann CM, Nguyen QT, Santo Neto H, Lichtman JW (2007) Rapid synapse elimination after postsynaptic protein synthesis inhibition in vivo. *J Neurosci* 27:6064-6067.
- Meier C, Dermietzel R, Davidson KG, Yasumura T, Rash JE (2004) Connexin32-containing gap junctions in Schwann cells at the internodal zone of partial myelin compaction and in Schmidt-Lanterman incisures. *J Neurosci* 24:3186-3198.
- Meier T, Gesemann M, Cavalli V, Ruegg MA, Wallace BG (1996) AChR phosphorylation and aggregation induced by an agrin fragment that lacks the binding domain for alpha-dystroglycan. *Embo J* 15:2625-2631.
- Menke LA, Poll-The BT, Clur SA, Bilardo CM, van der Wal AC, Lemmink HH, Cobben JM (2008) Congenital heart defects in spinal muscular atrophy type I: a clinical report of two siblings and a review of the literature. *Am J Med Genet A* 146A:740-744.
- Merlie JP, Sanes JR (1985) Concentration of acetylcholine receptor mRNA in synaptic regions of adult muscle fibres. *Nature* 317:66-68.
- Mersiyanova IV, Perepelov AV, Polyakov AV, Sitnikov VF, Dadali EL, Oparin RB, Petrin AN, Evgrafov OV (2000) A new variant of Charcot-Marie-Tooth disease type 2 is probably the result of a mutation in the neurofilament-light gene. *American journal of human genetics* 67:37-46.
- Metuzals J, Mushynski WE (1974) Electron microscope and experimental investigations of the neurofilamentous network in Deiters' neurons. Relationship with the cell surface and nuclear pores. *J Cell Biol* 61:701-722.
- Metuzals J, Montpetit V, Clapin DF (1981) Organization of the neurofilamentous network. *Cell Tissue Res* 214:455-482.
- Meyer M, Matsuoka I, Wetmore C, Olson L, Thoenen H (1992) Enhanced synthesis of brain-derived neurotrophic factor in the lesioned peripheral nerve: different mechanisms are responsible for the regulation of BDNF and NGF mRNA. *J Cell Biol* 119:45-54.
- Mirsky R, Jessen KR, Brennan A, Parkinson D, Dong Z, Meier C, Parmantier E, Lawson D (2002) Schwann cells as regulators of nerve development. *J Physiol Paris* 96:17-24.
- Misgeld T, Kummer TT, Lichtman JW, Sanes JR (2005) Agrin promotes synaptic differentiation by counteracting an inhibitory effect of neurotransmitter. *Proc Natl Acad Sci U S A* 102:11088-11093.
- Monsma PC, Li Y, Fenn JD, Jung P, Brown A (2014) Local regulation of neurofilament transport by myelinating cells. *J Neurosci* 34:2979-2988.
- Monteiro MJ, Hoffman PN, Gearhart JD, Cleveland DW (1990) Expression of NF-L in both neuronal and nonneuronal cells of transgenic mice:

- increased neurofilament density in axons without affecting caliber. *J Cell Biol* 111:1543-1557.
- Moore RL, Stull JT (1984) Myosin light chain phosphorylation in fast and slow skeletal muscles in situ. *Am J Physiol* 247:C462-471.
- Morris JK, Lin W, Hauser C, Marchuk Y, Getman D, Lee KF (1999) Rescue of the cardiac defect in ErbB2 mutant mice reveals essential roles of ErbB2 in peripheral nervous system development. *Neuron* 23:273-283.
- Moscoso LM, Sanes JR (1995) Expression of four immunoglobulin superfamily adhesion molecules (L1, Nr-CAM/Bravo, neurofascin/ABGP, and N-CAM) in the developing mouse spinal cord. *J Comp Neurol* 352:321-334.
- Motil J, Chan WK, Dubey M, Chaudhury P, Pimenta A, Chylinski TM, Ortiz DT, Shea TB (2006) Dynein mediates retrograde neurofilament transport within axons and anterograde delivery of NFs from perikarya into axons: regulation by multiple phosphorylation events. *Cell Motil Cytoskeleton* 63:266-286.
- Murray LM, Gillingwater TH, Parson SH (2010) Using mouse cranial muscles to investigate neuromuscular pathology in vivo. *Neuromuscul Disord* 20:740-743.
- Murray LM, Comley LH, Thomson D, Parkinson N, Talbot K, Gillingwater TH (2008) Selective vulnerability of motor neurons and dissociation of pre- and post-synaptic pathology at the neuromuscular junction in mouse models of spinal muscular atrophy. *Hum Mol Genet* 17:949-962.
- Mutsaers CA, Wishart TM, Lamont DJ, Riessland M, Schreml J, Comley LH, Murray LM, Parson SH, Lochmuller H, Wirth B, Talbot K, Gillingwater TH (2011) Reversible molecular pathology of skeletal muscle in spinal muscular atrophy. *Hum Mol Genet* 20:4334-4344.
- Nadim W, Anderson PN, Turmaine M (1990) The role of Schwann cells and basal lamina tubes in the regeneration of axons through long lengths of freeze-killed nerve grafts. *Neuropathol Appl Neurobiol* 16:411-421.
- Nave KA, Salzer JL (2006) Axonal regulation of myelination by neuregulin 1. *Curr Opin Neurobiol* 16:492-500.
- Nave KA, Trapp BD (2008) Axon-glia signaling and the glial support of axon function. *Annu Rev Neurosci* 31:535-561.
- New HV, Mudge AW (1986) Calcitonin gene-related peptide regulates muscle acetylcholine receptor synthesis. *Nature* 323:809-811.
- Newsom-Davis J, Pinching AJ, Vincent A, Wilson SG (1978) Function of circulating antibody to acetylcholine receptor in myasthenia gravis: investigation by plasma exchange. *Neurology* 28:266-272.
- Nguyen QT, Parsadanian AS, Snider WD, Lichtman JW (1998) Hyperinnervation of neuromuscular junctions caused by GDNF overexpression in muscle. *Science* 279:1725-1729.
- Nicholson GA, Valentijn LJ, Cherryson AK, Kennerson ML, Bragg TL, DeKroon RM, Ross DA, Pollard JD, McLeod JG, Bolhuis PA, et al. (1994) A frame shift mutation in the PMP22 gene in hereditary neuropathy with liability to pressure palsies. *Nat Genet* 6:263-266.
- Nicolopoulos-Stournaras S, Iles JF (1983) Motor neuron columns in the lumbar spinal cord of the rat. *J Comp Neurol* 217:75-85.

- Noakes PG, Phillips WD, Hanley TA, Sanes JR, Merlie JP (1993) 43K protein and acetylcholine receptors colocalize during the initial stages of neuromuscular synapse formation in vivo. *Dev Biol* 155:275-280.
- Ota K, Matsui M, Milford EL, Mackin GA, Weiner HL, Hafler DA (1990) T-cell recognition of an immunodominant myelin basic protein epitope in multiple sclerosis. *Nature* 346:183-187.
- Palade GE (1954) Electron microscope observations of interneuronal and neuromuscular synapses. *Anat Rec* 118:335-336.
- Pareek S, Suter U, Snipes GJ, Welcher AA, Shooter EM, Murphy RA (1993) Detection and processing of peripheral myelin protein PMP22 in cultured Schwann cells. *J Biol Chem* 268:10372-10379.
- Patten SA, Armstrong GA, Lissouba A, Kabashi E, Parker JA, Drapeau P (2014) Fishing for causes and cures of motor neuron disorders. *Disease models & mechanisms* 7:799-809.
- Peper K, Dreyer F, Sandri C, Akert K, Moor H (1974) Structure and ultrastructure of the frog motor endplate. A freeze-etching study. *Cell Tissue Res* 149:437-455.
- Personius KE, Chang Q, Mentis GZ, O'Donovan MJ, Balice-Gordon RJ (2007) Reduced gap junctional coupling leads to uncorrelated motor neuron firing and precocious neuromuscular synapse elimination. *Proc Natl Acad Sci U S A* 104:11808-11813.
- Pette D, Schnez U (1977) Myosin light chain patterns of individual fast and slow-twitch fibres of rabbit muscles. *Histochemistry* 54:97-107.
- Pette D, Muller W, Leisner E, Vrbova G (1976) Time dependent effects on contractile properties, fibre population, myosin light chains and enzymes of energy metabolism in intermittently and continuously stimulated fast twitch muscles of the rabbit. *Pflugers Arch* 364:103-112.
- Pfrieger FW (2010) Role of glial cells in the formation and maintenance of synapses. *Brain Res Rev* 63:39-46.
- Phillips WD, Kopta C, Blount P, Gardner PD, Steinbach JH, Merlie JP (1991) ACh receptor-rich membrane domains organized in fibroblasts by recombinant 43-kilodalton protein. *Science* 251:568-570.
- Piirsoo M, Kaljas A, Tamm K, Timmusk T (2010) Expression of NGF and GDNF family members and their receptors during peripheral nerve development and differentiation of Schwann cells in vitro. *Neurosci Lett* 469:135-140.
- Pillai AM, Thaxton C, Pribisko AL, Cheng JG, Dupree JL, Bhat MA (2009) Spatiotemporal ablation of myelinating glia-specific neurofascin (Nfasc NF155) in mice reveals gradual loss of paranodal axoglial junctions and concomitant disorganization of axonal domains. *Journal of neuroscience research* 87:1773-1793.
- Poliak S, Peles E (2003) The local differentiation of myelinated axons at nodes of Ranvier. *Nat Rev Neurosci* 4:968-980.
- Poliak S, Salomon D, Elhanany H, Sabanay H, Kiernan B, Pevny L, Stewart CL, Xu X, Chiu SY, Shrager P, Furley AJ, Peles E (2003) Juxtaparanodal clustering of Shaker-like K⁺ channels in myelinated axons depends on Caspr2 and TAG-1. *J Cell Biol* 162:1149-1160.
- Pomicter AD, Shroff SM, Fuss B, Sato-Bigbee C, Brophy PJ, Rasband MN, Bhat MA, Dupree JL (2010) Novel forms of neurofascin 155 in the

- central nervous system: alterations in paranodal disruption models and multiple sclerosis. *Brain* 133:389-405.
- Portier MM, de Nechaud B, Gros F (1983) Peripherin, a new member of the intermediate filament protein family. *Dev Neurosci* 6:335-344.
- Pun S, Sigrist M, Santos AF, Ruegg MA, Sanes JR, Jessell TM, Arber S, Caroni P (2002) An intrinsic distinction in neuromuscular junction assembly and maintenance in different skeletal muscles. *Neuron* 34:357-370.
- Purkinje JE (1837) *Neueste, Untersuchungen aus der Nerven-und Hirnanatomie*. Opera Omnia 3:45-49.
- Qiu J, Cai D, Filbin MT (2000) Glial inhibition of nerve regeneration in the mature mammalian CNS. *Glia* 29:166-174.
- Quarles RH (2007) Myelin-associated glycoprotein (MAG): past, present and beyond. *J Neurochem* 100:1431-1448.
- Raff MC, Lillien LE, Richardson WD, Burne JF, Noble MD (1988) Platelet-derived growth factor from astrocytes drives the clock that times oligodendrocyte development in culture. *Nature* 333:562-565.
- Rasband MN, Peles E, Trimmer JS, Levinson SR, Lux SE, Shrager P (1999) Dependence of nodal sodium channel clustering on paranodal axoglial contact in the developing CNS. *J Neurosci* 19:7516-7528.
- Ratcliffe CF, Westenbroek RE, Curtis R, Catterall WA (2001) Sodium channel beta1 and beta3 subunits associate with neurofascin through their extracellular immunoglobulin-like domain. *J Cell Biol* 154:427-434.
- Rathjen FG, Wolff JM, Chang S, Bonhoeffer F, Raper JA (1987) Neurofascin: a novel chick cell-surface glycoprotein involved in neurite-neurite interactions. *Cell* 51:841-849.
- Rautenstrauss B, Nelis E, Grehl H, Pfeiffer RA, Van Broeckhoven C (1994) Identification of a de novo insertional mutation in P0 in a patient with a Dejerine-Sottas syndrome (DSS) phenotype. *Hum Mol Genet* 3:1701-1702.
- Readhead C, Popko B, Takahashi N, Shine HD, Saavedra RA, Sidman RL, Hood L (1987) Expression of a myelin basic protein gene in transgenic shiverer mice: correction of the dysmyelinating phenotype. *Cell* 48:703-712.
- Reddy LV, Koirala S, Sugiura Y, Herrera AA, Ko CP (2003) Glial cells maintain synaptic structure and function and promote development of the neuromuscular junction in vivo. *Neuron* 40:563-580.
- Redfern PA (1970) Neuromuscular transmission in new-born rats. *J Physiol* 209:701-709.
- Reid B, Slater CR, Bewick GS (1999) Synaptic vesicle dynamics in rat fast and slow motor nerve terminals. *J Neurosci* 19:2511-2521.
- Reimer MM, McQueen J, Searcy L, Scullion G, Zonta B, Desmazieres A, Holland PR, Smith J, Gliddon C, Wood ER, Herzyk P, Brophy PJ, McCulloch J, Horsburgh K (2011) Rapid disruption of axon-glial integrity in response to mild cerebral hypoperfusion. *J Neurosci* 31:18185-18194.
- Reindl M, Linington C, Brehm U, Egg R, Dilitz E, Deisenhammer F, Poewe W, Berger T (1999) Antibodies against the myelin oligodendrocyte glycoprotein and the myelin basic protein in multiple sclerosis and other neurological diseases: a comparative study. *Brain* 122 (Pt 11):2047-2056.

- Reist NE, Werle MJ, McMahan UJ (1992) Agrin released by motor neurons induces the aggregation of acetylcholine receptors at neuromuscular junctions. *Neuron* 8:865-868.
- Ribchester RR, Thomson D, Wood NI, Hinks T, Gillingwater TH, Wishart TM, Court FA, Morton AJ (2004) Progressive abnormalities in skeletal muscle and neuromuscular junctions of transgenic mice expressing the Huntington's disease mutation. *Eur J Neurosci* 20:3092-3114.
- Rich MM, Lichtman JW (1989) In vivo visualization of pre- and postsynaptic changes during synapse elimination in reinnervated mouse muscle. *J Neurosci* 9:1781-1805.
- Richmond FJ, Singh K, Corneil BD (2001) Neck muscles in the rhesus monkey. I. Muscle morphometry and histochemistry. *J Neurophysiol* 86:1717-1728.
- Ridge RM, Betz WJ (1984) The effect of selective, chronic stimulation on motor unit size in developing rat muscle. *J Neurosci* 4:2614-2620.
- Riessland M, Ackermann B, Forster A, Jakubik M, Hauke J, Garbes L, Fritzsche I, Mende Y, Blumcke I, Hahnen E, Wirth B (2010) SAHA ameliorates the SMA phenotype in two mouse models for spinal muscular atrophy. *Hum Mol Genet* 19:1492-1506.
- Riley DA (1981) Ultrastructural evidence for axon retraction during the spontaneous elimination of polyneuronal innervation of the rat soleus muscle. *J Neurocytol* 10:425-440.
- Rios JC, Melendez-Vasquez CV, Einheber S, Lustig M, Grumet M, Hemperly J, Peles E, Salzer JL (2000) Contactin-associated protein (Caspr) and contactin form a complex that is targeted to the paranodal junctions during myelination. *J Neurosci* 20:8354-8364.
- Rios JC, Rubin M, St Martin M, Downey RT, Einheber S, Rosenbluth J, Levinson SR, Bhat M, Salzer JL (2003) Paranodal interactions regulate expression of sodium channel subtypes and provide a diffusion barrier for the node of Ranvier. *J Neurosci* 23:7001-7011.
- Ritchie JM, Rogart RB (1977) Density of sodium channels in mammalian myelinated nerve fibers and nature of the axonal membrane under the myelin sheath. *Proc Natl Acad Sci U S A* 74:211-215.
- Roa BB, Garcia CA, Pentao L, Killian JM, Trask BJ, Suter U, Snipes GJ, Ortiz-Lopez R, Shooter EM, Patel PI, Lupski JR (1993a) Evidence for a recessive PMP22 point mutation in Charcot-Marie-Tooth disease type 1A. *Nat Genet* 5:189-194.
- Roa BB, Garcia CA, Suter U, Kulpa DA, Wise CA, Mueller J, Welcher AA, Snipes GJ, Shooter EM, Patel PI, Lupski JR (1993b) Charcot-Marie-Tooth disease type 1A. Association with a spontaneous point mutation in the PMP22 gene. *N Engl J Med* 329:96-101.
- Robertson JD (1957) New observations on the ultrastructure of the membranes of frog peripheral nerve fibers. *J Biophys Biochem Cytol* 3:1043-1048.
- Robertson JD (1958) The ultrastructure of Schmidt-Lanterman clefts and related shearing defects of the myelin sheath. *J Biophys Biochem Cytol* 4:39-46.
- Robertson JD (1959) Preliminary observations on the ultrastructure of nodes of ranvier. *Zeitschrift fur Zellforschung* 50:553-560.

- Robinson D, Galasko CS, Delaney C, Williamson JB, Barrie JL (1995) Scoliosis and lung function in spinal muscular atrophy. *Eur Spine J* 4:268-273.
- Roden RL, Donahue SP, Schwartz GA, Wood JG, English AW (1991) 200 kD neurofilament protein and synapse elimination in the rat soleus muscle. *Synapse* 9:239-243.
- Rosen DR, Siddique T, Patterson D, Figlewicz DA, Sapp P, Hentati A, Donaldson D, Goto J, O'Regan JP, Deng HX, et al. (1993) Mutations in Cu/Zn superoxide dismutase gene are associated with familial amyotrophic lateral sclerosis. *Nature* 362:59-62.
- Rosenbluth J (1976) Intramembranous particle distribution at the node of Ranvier and adjacent axolemma in myelinated axons of the frog brain. *J Neurocytol* 5:731-745.
- Rosenthal JL, Taraskevich PS (1977) Reduction of multi-axonal innervation at the neuromuscular junction of the rat during development. *J Physiol* 270:299-310.
- Rubinstein NA, Kelly AM (1978) Myogenic and neurogenic contributions to the development of fast and slow twitch muscles in rat. *Dev Biol* 62:473-485.
- Rudnik-Schoneborn S, Heller R, Berg C, Betzler C, Grimm T, Eggermann T, Eggermann K, Wirth R, Wirth B, Zerres K (2008) Congenital heart disease is a feature of severe infantile spinal muscular atrophy. *J Med Genet* 45:635-638.
- Saftig P, Klumperman J (2009) Lysosome biogenesis and lysosomal membrane proteins: trafficking meets function. *Nat Rev Mol Cell Biol* 10:623-635.
- Salzer JL, Brophy PJ, Peles E (2008) Molecular domains of myelinated axons in the peripheral nervous system. *Glia* 56:1532-1540.
- Sanchez I, Hassinger L, Paskevich PA, Shine HD, Nixon RA (1996) Oligodendroglia regulate the regional expansion of axon caliber and local accumulation of neurofilaments during development independently of myelin formation. *J Neurosci* 16:5095-5105.
- Sanchez I, Hassinger L, Sihag RK, Cleveland DW, Mohan P, Nixon RA (2000) Local control of neurofilament accumulation during radial growth of myelinating axons in vivo. Selective role of site-specific phosphorylation. *J Cell Biol* 151:1013-1024.
- Sanes JR, Lichtman JW (1999) Development of the vertebrate neuromuscular junction. *Annu Rev Neurosci* 22:389-442.
- Schachner M, Martini R (1995) Glycans and the modulation of neural-recognition molecule function. *Trends Neurosci* 18:183-191.
- Schafer K, Friede RL (1988) The onset and rate of myelination in six peripheral and autonomic nerves of the rat. *Journal of anatomy* 159:181-195.
- Schapira AH, Olanow CW, Greenamyre JT, Bezdard E (2014) Slowing of neurodegeneration in Parkinson's disease and Huntington's disease: future therapeutic perspectives. *Lancet* 384:545-555.
- Schmidt HD (1874) *Monthly Micr J* 11.
- Schmidt I, Thomas S, Kain P, Risse B, Naffin E, Klambt C (2012) Kinesin heavy chain function in Drosophila glial cells controls neuronal activity. *J Neurosci* 32:7466-7476.

- Schnaar RL, Lopez PH (2009) Myelin-associated glycoprotein and its axonal receptors. *Journal of neuroscience research* 87:3267-3276.
- Schnapp BJ, Reese TS (1982) Cytoplasmic structure in rapid-frozen axons. *J Cell Biol* 94:667-669.
- Schreml J, Riessland M, Paterno M, Garbes L, Rossbach K, Ackermann B, Kramer J, Somers E, Parson SH, Heller R, Berkessel A, Sterner-Kock A, Wirth B (2013) Severe SMA mice show organ impairment that cannot be rescued by therapy with the HDACi JNJ-26481585. *Eur J Hum Genet* 21:643-652.
- Schroder JM, Bohl J, von Bardeleben U (1988) Changes of the ratio between myelin thickness and axon diameter in human developing sural, femoral, ulnar, facial, and trochlear nerves. *Acta neuropathologica* 76:471-483.
- Sealock R, Wray BE, Froehner SC (1984) Ultrastructural localization of the Mr 43,000 protein and the acetylcholine receptor in Torpedo postsynaptic membranes using monoclonal antibodies. *J Cell Biol* 98:2239-2244.
- Sepp KJ, Auld VJ (2003) Reciprocal interactions between neurons and glia are required for Drosophila peripheral nervous system development. *J Neurosci* 23:8221-8230.
- Sepp KJ, Schulte J, Auld VJ (2001) Peripheral glia direct axon guidance across the CNS/PNS transition zone. *Dev Biol* 238:47-63.
- Shah JV, Cleveland DW (2002) Slow axonal transport: fast motors in the slow lane. *Curr Opin Cell Biol* 14:58-62.
- Shah JV, Flanagan LA, Janmey PA, Leterrier JF (2000) Bidirectional translocation of neurofilaments along microtubules mediated in part by dynein/dynactin. *Mol Biol Cell* 11:3495-3508.
- Shea TB, Flanagan LA (2001) Kinesin, dynein and neurofilament transport. *Trends Neurosci* 24:644-648.
- Shepard GM (1991) *Foundations of the Neuron Doctrine*. Oxford University Press, New York.
- Sheremata W, Colby S, Karkhanis Y, Eylar EH (1975) Cellular hypersensitivity to basic myelin (P2) protein in the Guillain-Barre syndrome. *The Canadian journal of neurological sciences Le journal canadien des sciences neurologiques* 2:87-90.
- Sherman DL, Brophy PJ (2005) Mechanisms of axon ensheathment and myelin growth. *Nat Rev Neurosci* 6:683-690.
- Sherman DL, Krols M, Wu LM, Grove M, Nave KA, Gangloff YG, Brophy PJ (2012) Arrest of myelination and reduced axon growth when Schwann cells lack mTOR. *J Neurosci* 32:1817-1825.
- Sherman DL, Tait S, Melrose S, Johnson R, Zonta B, Court FA, Macklin WB, Meek S, Smith AJ, Cottrell DF, Brophy PJ (2005) Neurofascins are required to establish axonal domains for saltatory conduction. *Neuron* 48:737-742.
- Sjostrand J (1965) Proliferative changes in glial cells during nerve regeneration. *Z Zellforsch Mikrosk Anat* 68:481-493.
- Slater CR (1982) Postnatal maturation of nerve-muscle junctions in hindlimb muscles of the mouse. *Dev Biol* 94:11-22.
- Smith IW, Mikesch M, Lee Y, Thompson WJ (2013) Terminal Schwann cells participate in the competition underlying neuromuscular synapse elimination. *J Neurosci* 33:17724-17736.

- Somers E, Stencel Z, Wishart TM, Gillingwater TH, Parson SH (2012) Density, calibre and ramification of muscle capillaries are altered in a mouse model of severe spinal muscular atrophy. *Neuromuscul Disord* 22:435-442.
- Son YJ, Thompson WJ (1995) Schwann cell processes guide regeneration of peripheral axons. *Neuron* 14:125-132.
- Song JW, Misgeld T, Kang H, Knecht S, Lu J, Cao Y, Cotman SL, Bishop DL, Lichtman JW (2008) Lysosomal activity associated with developmental axon pruning. *J Neurosci* 28:8993-9001.
- Sretavan D, Shatz CJ (1984) Prenatal development of individual retinogeniculate axons during the period of segregation. *Nature* 308:845-848.
- Standaert FG (1982) Release of transmitter at the neuromuscular junction. *British journal of anaesthesia* 54:131-145.
- Sternberger NH, Itoyama Y, Kies MW, Webster HD (1978) Myelin basic protein demonstrated immunocytochemically in oligodendroglia prior to myelin sheath formation. *Proc Natl Acad Sci U S A* 75:2521-2524.
- Stevens B, Allen NJ, Vazquez LE, Howell GR, Christopherson KS, Nouri N, Micheva KD, Mehalow AK, Huberman AD, Stafford B, Sher A, Litke AM, Lambris JD, Smith SJ, John SW, Barres BA (2007) The classical complement cascade mediates CNS synapse elimination. *Cell* 131:1164-1178.
- Stoll G, Muller HW (1999) Nerve injury, axonal degeneration and neural regeneration: basic insights. *Brain pathology* 9:313-325.
- Stoll G, Griffin JW, Li CY, Trapp BD (1989) Wallerian degeneration in the peripheral nervous system: participation of both Schwann cells and macrophages in myelin degradation. *J Neurocytol* 18:671-683.
- Su Y, Brooks DG, Li L, Lepercq J, Trofatter JA, Ravetch JV, Lebo RV (1993) Myelin protein zero gene mutated in Charcot-Marie-tooth type 1B patients. *Proc Natl Acad Sci U S A* 90:10856-10860.
- Sugiyama I, Tanaka K, Akita M, Yoshida K, Kawase T, Asou H (2002) Ultrastructural analysis of the paranodal junction of myelinated fibers in 31-month-old-rats. *J Neurosci Res* 70:309-317.
- Suresh S, Wang C, Nanekar R, Kursula P, Edwardson JM (2010) Myelin basic protein and myelin protein 2 act synergistically to cause stacking of lipid bilayers. *Biochemistry* 49:3456-3463.
- Swoboda KJ, Prior TW, Scott CB, McNaught TP, Wride MC, Reyna SP, Bromberg MB (2005) Natural history of denervation in SMA: relation to age, SMN2 copy number, and function. *Ann Neurol* 57:704-712.
- Tait S, Gunn-Moore F, Collinson JM, Huang J, Lubetzki C, Pedraza L, Sherman DL, Colman DR, Brophy PJ (2000) An oligodendrocyte cell adhesion molecule at the site of assembly of the paranodal axo-glial junction. *J Cell Biol* 150:657-666.
- Taniuchi M, Clark HB, Johnson EM, Jr. (1986) Induction of nerve growth factor receptor in Schwann cells after axotomy. *Proc Natl Acad Sci U S A* 83:4094-4098.
- Tao-Cheng JH, Rosenbluth J (1982) Development of nodal and paranodal membrane specializations in amphibian peripheral nerves. *Brain Res* 255:577-594.

- Tao-Cheng JH, Rosenbluth J (1983) Axolemmal differentiation in myelinated fibers of rat peripheral nerves. *Brain Res* 285:251-263.
- Tapia JC, Wylie JD, Kasthuri N, Hayworth KJ, Schalek R, Berger DR, Guatimosim C, Seung HS, Lichtman JW (2012) Pervasive synaptic branch removal in the mammalian neuromuscular system at birth. *Neuron* 74:816-829.
- Terenghi G (1999) Peripheral nerve regeneration and neurotrophic factors. *Journal of anatomy* 194 (Pt 1):1-14.
- Tofaris GK, Patterson PH, Jessen KR, Mirsky R (2002) Denervated Schwann cells attract macrophages by secretion of leukemia inhibitory factor (LIF) and monocyte chemoattractant protein-1 in a process regulated by interleukin-6 and LIF. *J Neurosci* 22:6696-6703.
- Topilko P, Schneider-Maunoury S, Levi G, Baron-Van Evercooren A, Chennoufi AB, Seitanidou T, Babinet C, Charnay P (1994) Krox-20 controls myelination in the peripheral nervous system. *Nature* 371:796-799.
- Trapp BD (1990) Myelin-associated glycoprotein. Location and potential functions. *Ann N Y Acad Sci* 605:29-43.
- Trapp BD, McIntyre LJ, Quarles RH, Sternberger NH, Webster HD (1979) Immunocytochemical localization of rat peripheral nervous system myelin proteins: P2 protein is not a component of all peripheral nervous system myelin sheaths. *Proc Natl Acad Sci U S A* 76:3552-3556.
- Triolo D, Dina G, Lorenzetti I, Malaguti M, Morana P, Del Carro U, Comi G, Messing A, Quattrini A, Previtalli SC (2006) Loss of glial fibrillary acidic protein (GFAP) impairs Schwann cell proliferation and delays nerve regeneration after damage. *J Cell Sci* 119:3981-3993.
- Tsukita S, Usukura J, Tsukita S, Ishikawa H (1982) The cytoskeleton in myelinated axons: a freeze-etch replica study. *Neuroscience* 7:2135-2147.
- Turney SG, Lichtman JW (2012) Reversing the outcome of synapse elimination at developing neuromuscular junctions in vivo: evidence for synaptic competition and its mechanism. *PLoS Biol* 10:e1001352.
- Turney SG, Walsh MK, Lichtman JW (2012) In vivo imaging of the developing neuromuscular junction in neonatal mice. *Cold Spring Harb Protoc* 2012:1166-1176.
- Uchida A, Alami NH, Brown A (2009) Tight functional coupling of kinesin-1A and dynein motors in the bidirectional transport of neurofilaments. *Mol Biol Cell* 20:4997-5006.
- Uchida S, Yamamoto H, Iio S, Matsumoto N, Wang XB, Yonehara N, Imai Y, Inoki R, Yoshida H (1990) Release of calcitonin gene-related peptide-like immunoreactive substance from neuromuscular junction by nerve excitation and its action on striated muscle. *J Neurochem* 54:1000-1003.
- Ullian EM, Sapperstein SK, Christopherson KS, Barres BA (2001) Control of synapse number by glia. *Science* 291:657-661.
- Usdin TB, Fischbach GD (1986) Purification and characterization of a polypeptide from chick brain that promotes the accumulation of acetylcholine receptors in chick myotubes. *J Cell Biol* 103:493-507.

- Vabnick I, Novakovic SD, Levinson SR, Schachner M, Shrager P (1996) The clustering of axonal sodium channels during development of the peripheral nervous system. *J Neurosci* 16:4914-4922.
- Valentin GG (1836) *Über den Verlauf und die letzten Enden der Nerven.* Nova Acta Phys-Med Acad Leopoldina (Breslau) 18:51-240.
- Valenzuela DM, Stitt TN, DiStefano PS, Rojas E, Mattsson K, Compton DL, Nunez L, Park JS, Stark JL, Gies DR, et al. (1995) Receptor tyrosine kinase specific for the skeletal muscle lineage: expression in embryonic muscle, at the neuromuscular junction, and after injury. *Neuron* 15:573-584.
- Vanacker G, del RMJ, Lew E, Ferrez PW, Moles FG, Philips J, Van Brussel H, Nuttin M (2007) Context-based filtering for assisted brain-actuated wheelchair driving. *Computational intelligence and neuroscience*:25130.
- Vinson M, Rausch O, Maycox PR, Prinjha RK, Chapman D, Morrow R, Harper AJ, Dingwall C, Walsh FS, Burbidge SA, Riddell DR (2003) Lipid rafts mediate the interaction between myelin-associated glycoprotein (MAG) on myelin and MAG-receptors on neurons. *Mol Cell Neurosci* 22:344-352.
- Vizoso AD (1950) The relationship between internodal length and growth in human nerves. *J Anat* 84:342-353.
- Vizoso AD, Young JZ (1948) Internode length and fibre diameter in developing and regenerating nerves. *J Anat* 82:110-134.
- Volkmer H, Hassel B, Wolff JM, Frank R, Rathjen FG (1992) Structure of the axonal surface recognition molecule neurofascin and its relationship to a neural subgroup of the immunoglobulin superfamily. *J Cell Biol* 118:149-161.
- Walsh MK, Lichtman JW (2003) In vivo time-lapse imaging of synaptic takeover associated with naturally occurring synapse elimination. *Neuron* 37:67-73.
- Wang GY, Hirai K, Shimada H (1992) The role of laminin, a component of Schwann cell basal lamina, in rat sciatic nerve regeneration within antiserum-treated nerve grafts. *Brain Res* 570:116-125.
- White R, Kramer-Albers EM (2014) Axon-glia interaction and membrane traffic in myelin formation. *Front Cell Neurosci* 7:284.
- Willard M, Simon C (1983) Modulations of neurofilament axonal transport during the development of rabbit retinal ganglion cells. *Cell* 35:551-559.
- Wishart TM, Rooney TM, Lamont DJ, Wright AK, Morton AJ, Jackson M, Freeman MR, Gillingwater TH (2012) Combining comparative proteomics and molecular genetics uncovers regulators of synaptic and axonal stability and degeneration in vivo. *PLoS Genet* 8:e1002936.
- Wishart TM, Huang JP, Murray LM, Lamont DJ, Mutsaers CA, Ross J, Geldsetzer P, Ansorge O, Talbot K, Parson SH, Gillingwater TH (2010) SMN deficiency disrupts brain development in a mouse model of severe spinal muscular atrophy. *Hum Mol Genet* 19:4216-4228.
- Wishart TM et al. (2014) Dysregulation of ubiquitin homeostasis and beta-catenin signaling promote spinal muscular atrophy. *J Clin Invest* 124:1821-1834.

- Wuerker RB, Palay SL (1969) Neurofilaments and microtubules in anterior horn cells of the rat. *Tissue & cell* 1:387-402.
- Xia C, Rahman A, Yang Z, Goldstein LS (1998) Chromosomal localization reveals three kinesin heavy chain genes in mouse. *Genomics* 52:209-213.
- Xia CH, Roberts EA, Her LS, Liu X, Williams DS, Cleveland DW, Goldstein LS (2003) Abnormal neurofilament transport caused by targeted disruption of neuronal kinesin heavy chain KIF5A. *J Cell Biol* 161:55-66.
- Xu K, Terakawa S (1999) Fenestration nodes and the wide submyelinic space form the basis for the unusually fast impulse conduction of shrimp myelinated axons. *J Exp Biol* 202:1979-1989.
- Xu Z, Cork LC, Griffin JW, Cleveland DW (1993) Increased expression of neurofilament subunit NF-L produces morphological alterations that resemble the pathology of human motor neuron disease. *Cell* 73:23-33.
- Yamada KM, Spooner BS, Wessells NK (1970) Axon growth: roles of microfilaments and microtubules. *Proc Natl Acad Sci U S A* 66:1206-1212.
- Yamada KM, Spooner BS, Wessells NK (1971) Ultrastructure and function of growth cones and axons of cultured nerve cells. *J Cell Biol* 49:614-635.
- Yang DP, Kim J, Syed N, Tung YJ, Bhaskaran A, Mindos T, Mirsky R, Jessen KR, Maurel P, Parkinson DB, Kim HA (2012) p38 MAPK activation promotes denervated Schwann cell phenotype and functions as a negative regulator of Schwann cell differentiation and myelination. *J Neurosci* 32:7158-7168.
- Yang LJ, Zeller CB, Shaper NL, Kiso M, Hasegawa A, Shapiro RE, Schnaar RL (1996) Gangliosides are neuronal ligands for myelin-associated glycoprotein. *Proc Natl Acad Sci U S A* 93:814-818.
- Yellin H (1969) A histochemical study of muscle spindles and their relationship to extrafusil fiber types in the rat. *Am J Anat* 125:31-45.
- Yiu G, He Z (2006) Glial inhibition of CNS axon regeneration. *Nat Rev Neurosci* 7:617-627.
- Yu WP, Collarini EJ, Pringle NP, Richardson WD (1994) Embryonic expression of myelin genes: evidence for a focal source of oligodendrocyte precursors in the ventricular zone of the neural tube. *Neuron* 12:1353-1362.
- Yuki N, Kuwabara S (2007) Axonal Guillain-Barre syndrome: carbohydrate mimicry and pathophysiology. *J Peripher Nerv Syst* 12:238-249.
- Zalc B, Goujet D, Colman D (2008) The origin of the myelination program in vertebrates. *Curr Biol* 18:R511-512.
- Zenker J, Stettner M, Ruskamo S, Domenech-Estevéz E, Baloui H, Medard JJ, Verheijen MH, Brouwers JF, Kursula P, Kieseier BC, Chrast R (2014) A role of peripheral myelin protein 2 in lipid homeostasis of myelinating schwann cells. *Glia*.
- Zhang Z, Guth L (1997) Experimental spinal cord injury: Wallerian degeneration in the dorsal column is followed by revascularization, glial proliferation, and nerve regeneration. *Exp Neurol* 147:159-171.
- Zhang Z, Casey DM, Julien JP, Xu Z (2002) Normal dendritic arborization in spinal motoneurons requires neurofilament subunit L. *J Comp Neurol* 450:144-152.

- Zhu Q, Couillard-Despres S, Julien JP (1997) Delayed maturation of regenerating myelinated axons in mice lacking neurofilaments. *Exp Neurol* 148:299-316.
- Zonta B, Desmazieres A, Rinaldi A, Tait S, Sherman DL, Nolan MF, Brophy PJ (2011) A critical role for Neurofascin in regulating action potential initiation through maintenance of the axon initial segment. *Neuron* 69:945-956.

Appendices

Appendix 1: Papers published

** Publications of the work presented in this thesis*

* **Roche SL**, Sherman DL, Dissanayake KN, Soucy G, Desmazieres A, Peles E, Julien JP, Ribchester RR, Brophy PJ & Gillingwater TH, 2014. Glial neurofascin155 mediates neuronal remodelling during developmental synapse elimination. *In press at Journal of Neuroscience*.

Hunter G, **Roche SL**, Somers E, Fuller HR, Gillingwater TH, 2014. The influence of storage parameters on measurement of survival of motor neuron (SMN) protein levels: implications for pre-clinical studies and clinical trials for spinal muscular atrophy. *Neuromuscular disorders*. doi: 10.1016/j.nmd.2014.05.013

Carpanini SM, McKie L, Thomson D, Wright AK, Gordon SL, **Roche SL**, Handley MT, Morrison H, Wishart TM, Cousin MA, Gillingwater TH, Aligianis IA & Jackson I, 2014. A Novel Mouse Model of Warburg Micro Syndrome Reveals Roles for RAB18 in Eye Development and Organisation of the Neuronal Cytoskeleton. *Disease Models and Mechanisms*. doi:10.1242/dmm.015222

Hegarty SV, Collins LM, Gavin AM, **Roche SL**, Wyatt SL, Sullivan AM, 2014. Canonical BMP-Smad signalling promotes neurite outgrowth in rat midbrain dopaminergic neurons. *Neuromolecular Medicine*. doi:10.1007/s12017-014-8296-8.

Wishart TW, Mutsaers CA, Riessland M, Reimer M, Hunter G, Hannam M, Eaton S, Fuller H, **Roche SL**, Somers E, Morse R, Young P, Lamont D, Hammerschmidt M, Joshi A, Hohenstein P, Morris G, Parson S, Skehel P, Becker T, Robinson I, Becker C, Wirth B & Gillingwater TH, 2014. Dysregulation of ubiquitin homeostasis and β -catenin signalling promote spinal muscular atrophy. *Journal of Clinical Investigation*. doi:10.1172/JCI71318

* Hunter G, Aghamaleky Sarvestany A, **Roche SL**, Symes RC & Gillingwater TH, 2014. SMN-dependent intrinsic defects in Schwann cells in mouse models of spinal muscular atrophy. *Human Molecular Genetics*. doi:10.1093/hmg/ddt612

Eaton SL, **Roche SL**, Llaverro Hurtado M, Oldknow KJ, Farquharson, Gillingwater TH & Wishart TM, 2013. Total protein analysis as a reliable loading control for quantitative fluorescent Western blotting. *Plos One*. Vol. 8, Issue 8, e72457.